Archives

SEP 23 1963

LIBRARIES

HEAT TRANSFER TO A VAPORIZING IMMISCIBLE DROP

by

David H. Klipstein

B.S. in E., Princeton University
(1952)

Submitted in Partial Fulfillment
of the Requirements for the
Degree of Doctor of Science

at the

MASSACHUSETTS INSTITUTE OF TECHNOLOGY

June, 1963

Signature of Author: _____
Department of Chemical Engineering
May 10, 1963

Certified by: _____
Thesis Supervisor

Accepted by: _____
Chairman,
Departmental Committee on Graduate Theses

UNION CARBIDE CHEMICALS COMPANY
DIVISION OF UNION CARBIDE CORPORATION
270 PARK AVENUE, NEW YORK 17, N. Y.

September 9, 1963

Professor William N. Locke, Director
Massachusetts Institute of Technology
Library
Cambridge 39, Massachusetts

Dear Professor Locke:

Here is the library copy of my thesis revised in accordance with the comments and suggestions made by members of your department. I trust that it will now be fully acceptable but if any difficulties still remain you may expect my prompt cooperation.

Very truly yours,

David H. Klipstein

DHK/ch

Attachment

Department of Chemical Engineering
Massachusetts Institute of Technology
Cambridge 39, Massachusetts

May 10, 1963

Professor Philip Franklin
Secretary of the Faculty
Massachusetts Institute of Technology
Cambridge 39, Massachusetts

Dear Professor Franklin:

In accordance with the regulations of the Faculty, I herewith submit a thesis, entitled, "Heat Transfer to a Vaporizing Immiscible Drop," in partial fulfillment of the requirements for the Degree of Doctor of Science in Chemical Engineering at the Massachusetts Institute of Technology.

Respectfully submitted,

David H. Klipstein

ACKNOWLEDGMENT

The execution of this thesis was an extended and sometimes hectic undertaking. Delayed by an unusual collection of dilemmas, snags and distractions it has been only through the sustained and patient urging of Prof. E. R. Gilliland, my understanding advisor, Dr. Ernest A. Harvey, my close friend and often midnight laboratory companion, and my infinitely forgiving wife, Gay, that the job is finally done.

To them and to the myriad of friends, artists and craftsmen who have made their special contributions when the need arose I am forever grateful.

In addition, I am in debt to The American Cyanamid Company and the Union Carbide Corporation at whose locations portions of this work was done, for allowing me generous access to the many specialized services and facilities which they have available.

TABLE OF CONTENTS

		Page
Abstract		2
Prologue	Thesis Motivation and Statement of Objective	3
Chapter 1	Previous Work	5
	I. Flow Past a Rigid Body	5
	II. Flow Past a Fluid Body	9
	III. Drop Distortion and Oscillation	14
	IV. Effect of Acceleration	17
	V. Effect of Multiparticle Interaction	18
	VI. Movement Within Particles	20
	VII. Transport Studies	24
	VIII. Nucleation and Boiling Heat Transfer	31
Chapter 2	Preliminary Decisions	39
Chapter 3	Equipment and Procedure	46
	A. Equipment	46
	B. Experimental Procedure	49
Chapter 4	Experimental Results	54
	A. Qualitative Observations	54
	B. Quantitative Observations	57
Chapter 5	Analysis of Differential Data - Study of Mechanism	69
	A. Temperature Driving Force	69
	B. Area	70
	C. Heat Transfer Coefficient	80
	D. Growth Model	85
Chapter 6	Large Scale Potential	87
Chapter 7	Conclusion and Recommendation	89

APPENDIX

Section		Page
A. 1	Supplementary Details	A1
A. 2	Tables of Data	A3
A. 3	Sample Calculations	A30
A. 4	Table of Nomenclature	A37
A. 5	Literature Citations	A44
A. 6	Location of the Original Data	A49

TABLE OF TABLES

Table No.		Page
3.1	Summary of Experimental Conditions	50
4.1	Drop size data, Ethyl chloride - Distilled water	58
4.2	Drop size data, Ethyl chloride - Distilled water plus Aerosol 22	58
4.3	Accuracy of data; drop sizes Vs. terminal velocities	59
4.4	Empirical Overall Coefficient, Ethyl choride - Distilled water	68
5.1	Importance of gas phase transfer	71
5.2	Reported ranges of index number for modes of bubble behavior	75
5.3	Observed ranges of index numbers for modes of bubble behavior: Ethyl chloride water	75
5.4	Correlating power of various index numbers for observed bubble behavior, Ethyl chloride - Water	75
5.5	Observed ranges of index numbers for modes of bubble behavior, Ethyl chloride water plus Aerosol 22	79
5.6	Observed ranges of index numbers for modes of bubble behavior, Ethyl chloride - 65% glycerine	79A
A.1	Physical Properties of Systems studied	A3
A.2	Summary of Bubble Data and calculated values	A4
A.3	Summary of Run Data	A28

LIST OF ILLUSTRATIONS

Figure

3.1 Flow Diagram of Equipment

3.2 Details of Droplet Feed System

3.3 Hot Wire Nucleation System

3.4 Lighting System

4.1 Sample Drop Oscillation Pattern

4.2 Bubble and Liquid Puddle Shapes

4.3 Heat Content vs. Time, EtCl - Distilled Water

4.4 Heat Content vs. Time, EtCl - Water Plus Aerosol 22

4.5 Heat Content vs. Time, EtCl - 65% Glycerine - Water

4.6 Velocity of Rise, EtCl in Various Continuous Phases

4.7 Velocity of Rise, EtCl - Water, With and Without Surfactant

4.8 Heat Transfer Rate vs. Drop Size, EtCl - Water

4.9 Heat Transfer Rate vs. ΔT, EtCl - Distilled Water

4.10 Heat Transfer Rate vs. Drop Size, EtCl - 65% Glycerine

4.11 Heat Transfer Rate vs. ΔT, EtCl - 65% Glycerine

4.12 Average Coefficient of Heat Transfer vs. Prandtl No.

4.13 Average Transfer Rate vs. Surfactant Concentration

4.14 Average Transfer Rate Vs. Surface Pressure

4.15 Average Transfer Rate vs. Interfacial Pressure

5.1 Area Development - 3 Basic Drop Shapes

5.2 Bubble Behavior Vs. Eötvos No., EtCl - Distilled Water

5.3 Bubble Behavior Vs. Equiv. Spherical Diameter, EtCl - Distilled Water

5.4 Bubble Behavior Vs. Re_d, EtCl - Distilled Water

5.5 Bubble Behavior Vs. Re_A, EtCl - Distilled Water

5.6 Area Development Vs. Frac. Vaporized and Drop Size

5.7 Bubble Behavior Vs. Eötvos No., EtCl - Water plus Aerosol 22

5.8 Bubble Behavior Vs. Re_d, EtCl Water plus Aerosol 22

LIST OF ILLUSTRATIONS (Cont'd)

Figure

5.9 Area Vs. Frac. Vaporized, Large Drop With and Without Surfactant

5.10 Area Vs. Frac. Vaporized, Medium Drop With and Without Surfactant

5.11 Bubble Behavior Vs. Eötvos No., EtCl - 65% Glycerine

5.12 Bubble Behavior Vs. Re_d, EtCl - 65% Glycerine

5.13 Heat Flux Vs. ΔT for Various Systems

5.14 Heat Transfer Coefficient Vs. Fraction Vaporized

5.15 Test of Ranz Marshall Correlation

5.16 Test of Handlos Baron Model

5.17 Growth Rate Model, Size vs. Time

HEAT TRANSFER FROM A CONTINUOUS LIQUID TO A VAPORIZING IMMISCIBLE DROP

by

David H. Klipstein

Submitted to the Department of Chemical Engineering in May, 1963, in partial fulfillment of the requirements for the degree of Doctor of Science.

ABSTRACT

A study of heat transfer to vaporizing immiscible drops has been conducted by nucleating single drops with a hot wire and photographically recording their growth. The results have shown that average heat transfer rate is directly proportional to the temperature driving force and the initial diameter squared. Analysis of differential rates has shown that heat is transferred to the vaporizing liquid primarily from the wake region. Correlation of observed heat transfer coefficients has been accomplished by the equation,

$$Nu = 2 + .094\, Re^{.93} Pr^{1/3}.$$

This dependence of Reynolds number agrees closely with data for heat transfer to cylinders from the wake region at high Reynolds numbers.

The effect of surfactant additions on heat transfer was also examined. Results showed that surfactants improve transfer rate for small drops by enhancing oscillation tendencies while reducing transfer rates to large drops by surpressing interfacial rippling tendencies.

Estimates of peak flux potentials for this system show that direct contact vaporization is capable of rates about two times those reported for comparable systems undergoing boiling in contact with submerged heaters.

Thesis Supervisor: E. R. Gilliland,
Professor of Chemical Engineering

PROLOGUE - THESIS MOTIVATION AND STATEMENT OF THESIS OBJECTIVE

The need to alter rapidly and efficiently the temperature of a process stream is so basic to modern process technology that shell and tube heat exchangers are today among the most commonly encountered working tools of the process plant. This is true in spite of their high initial cost and expensive upkeep requirements. It is not uncommon to pay $35/sq. ft. for heat exchanger area and then face the necessity of yearly overhaul to clean fouled surfaces and restore degraded heat transfer efficiencies. Beyond this, the very nature of the concept carries with it inefficiencies stemming from the solid tube wall which separates the exchanging phases. Laminar layers which form on each side of the tube wall almost always offer the limiting resistance to heat transfer and frictional resistance offered by these same tube walls further inflates operating expenses by causing pressure losses in the moving fluids.

Where heating is required, many of these shortcomings can sometimes be overcome by a direct contact process, using steam or flue gases. For cooling, direct introduction of dry ice or flake ice is sometimes used, but is rarely justifiable except where unusual economic restraints prevail.

On the other hand, since commonly used refrigerants are almost completely immiscible with water, there seems no reason why efficient direct contact cooling cannot be achieved by simply allowing the refrigerant to vaporize in direct contact with the liquid to be cooled, instead of containing it in coils during this process. By collecting the vapors at the top of the space and recompressing them, all the advantages of direct contact could be obtained at a minimum operating cost. Since no data were available in the literature on such a process, exploitation of the idea required that work be performed to answer three basic questions:

1) Does such a system offer significant advantages ?
2) Will it be stable and controllable ?
3) What is the nature of the design equations required ?

Since such studies could have great value by providing means for the desalination of water, the shock cooling of chemical reactions and the dehydration of sensitive materials as well as providing useful information on the heat transfer aspects of steam distillation and emulsion polymerization, it seemed a highly rewarding area for thesis work.

Thus, the objective for this thesis was chosen as follows:

To examine the basic mechanism by which heat is transferred from a hot continuous phase to a vaporizing immiscible drop rising through it and to identify quantitatively the variables which have a bearing on the process.

CHAPTER I - PREVIOUS WORK

Although there have been many papers published in recent years which discuss the transfer of heat to drops and also the behavior of vaporizing liquids, only the thesis work of **Kavesh** (49), of Berinstein and Khetani (5), and of Katz and Schroeder (48) have dealt with the two phenomenon together. Even these studies, however, were mainly concerned with bulk effects and shed little light on the mechanism of transfer. Nevertheless, there is much that is pertinent in past work on fluid flow, on interfacial phenomenon and on mass and heat transfer. This material will now be summarized in the belief that a better understanding of the several separate mechanisms involved will aid in analyzing the more complex situation which results from their combination.

I. FLOW PAST A RIGID BODY

A. Drag and Boundary Layer Concepts

Let us begin with an examination of the forces which control the behavior of the internal and external boundary layers. For the continuous phase, we may consult the extensive work on flow around submerg objects, drops and bubbles.

Early work in this field was largely theoretical being restricted by the simplifying assumption that the continuous phase was an ideal, incompressible, non-viscous fluid. Predictions based on this approach gave good descriptions of pressure distributions and flow patterns for laminary flow at very low viscosity, but due to the assumption of no viscosity, this approach was of little practical utility; it predicted zero drag which is untrue even for low viscosity materials.

As a next step, a rigorous differential equation for flow behavior was developed in the form of the Navier Stokes equation. For an incompressible fluid flowing past a sphere, this gave:

$$\frac{\delta u}{\delta t} + u\nabla u = \frac{2}{Re}\nabla^2 u - 1/2\,p;\ \nabla u = 0 \qquad (25)$$

(time) (inertia) (viscosity) (pressure)

where the properties u, t and p have been made dimensionless.

Although no general solution for this equation has yet been developed, several special solutions have been achieved. In addition, consideration of the terms has led to a better understanding of the nature of drag, particularly in distinction between its two basic components:

a) viscous drag - due to tangential forces and surface shear (viscosity term)

b) form drag - due to inertial energy losses experienced in acceleration and declaration (inertia term)

Both forms of drag must still be subject to the first law of thermodynamics so that all work done by the body on the stream must always increase the energy of the fluid. It may take several intermediate forms, but ultimately the work needed to overcome drag must always end up as heat.

One of the most important special cases for which Navier Stokes' solutions have been achieved is the condition of creeping motion. At low Reynolds numbers inertial forces drop out and for a sphere Drag = $3\pi\mu du_\infty$ Under these conditions, 1/3 of the drag is due to pressure differences and 2/3 to shear. Flow patterns in the approach zone and wake are similar.

For large Reynolds numbers on the other hand, direct simplification is not possible since both inertia and viscosity effects are important. To get around this, Prandtl (58A) showed that the analysis could be simplified by separating the flow into two regions:

a) the bulk fluid where free stream velocity prevails throughout and ideal fluid behavior can be assumed.

b) the boundary layer which extends from the interface out to a point where the velocity is 99% of the free steam. Here frictional effects predominate and Stokes assumptions become valid.

Most analysis of flow around drops and bubbles is built upon this boundary layer concept. Still, even with this simplification direct prediction of drag from fundamental considerations is not yet possible and working calculations often depend upon empirically developed charts of drag coefficients, C_D, vs. Re for various shapes.

Once the drag coefficient is selected, the universal drag law:

$$F_D = \frac{C_D \rho S u^2}{2g_c}$$

can then be used to calculate total drag force. Factors which determine the behavior of C_D with increasing Re will now be discussed.

B. Flow Past a Rigid Sphere

As a fluid is started moving slowly past a rigid sphere, a thin boundary layer is formed where the fluid moves away from the forward stagnation point. The fluid is steadily accelerated as it moves toward the equator. This results in a pressure decrease and in a thickening of the boundary layer. Proceeding toward the rear, the fluid again slows down and the initial pressure is recovered. Up to Re = .2 viscous drag predominates. Above this point, form drag begins to have significance. With increasing free stream velocity, losses become significant and pressure recovery at the rear stagnation point is no longer complete. When the Reynolds number reaches a value of about 17 to 20 (25) field fluid under the external pressure begins to flow forward from the rear to divert the boundary layer fluid which no longer has the momentum or pressure required to complete its journey. At this point, flow at the interface is reversed and the boundary layer separates from the solid surface in the form of a weak toroidal eddy (25). Separation first occurs at a point very near the rear stagnation point and then moves forward with increasing Reynolds number until at Re = 450 separation occurs at a point 104^o back from the forward stagnation point. From this point on, only form drag is significant and the drag coefficient for this remains fairly constant up to Re = 300,000.

Between Re = 450 and Re = 2500 (42, 25) the now well-developed toroidal eddies break loose from the sphere and move away with the fluid stream. The point of release moves successively around the separation ring, resulting in a wake consisting of a helical string of eddies, a form of Karman street. The frequency of release can be calculated from $\frac{nd}{V_A}$ = Str (64) where the Strouhal Number, Str, rises from a value of .12 at Re = 50 to a constant value of .21 at Re >500. Release frequency continues to increase up to Re = 5000 where the wake goes turbulent. At Re = 300, 000, the drag coefficient drops sharply as the boundary layer over the leading surface goes turbulent (64). Due to the greater efficiency of momentum transfer across a turbulent boundary, separation is deferred resulting in a lower overall drag (14). In addition, a standing eddy is formed at the rear of the sphere causing the free stream to see the rigid object as a streamlined shape (8).

C. Boundary Layer Thickness

Of major importance in studying heat transfer behavior is a knowledge of boundary layer thickness. Some attempts have been made to estimate boundary layer thickness for flat plates. The following formulas have been developed: (42)

For laminary conditions ($Re_x < 300,000$) $\quad \frac{\delta}{x} = \frac{5}{(Re_x)^{1/2}}$

For turbulent conditions $\quad \frac{\delta}{x} = \frac{.37}{(Re_x)^{1/5}}$

These formulas can be applied to spheres using path length as the characteristic dimension, but this is a crude approximation applicable only upstream of separation. No means is available for estimating effective boundary layer thickness downstream of the separation point.

D. Terminal Velocity

Terminal velocity is defined as the velocity at which drag forces and gravitational forces exactly balance each other. This condition is described by the equation:

$$v\,(\Delta\rho)\,g + C_D \rho A^2 V_A^2 = 0$$

assuming that:

a) there is no hindering effect due to wall proximity

b) the object is settling freely without interference from other dispersed phase bodies.

c) the object is large compared to the mean free path of molecules of the bulk fluid.

For a rigid sphere at high Reynolds number, this equation can be simplified to give

$$V = 1.74\sqrt{\frac{g\,\Delta\rho\,d}{\rho_c}}$$

When confining walls are present, free movement in the bulk fluid is inhibited and corrections must be made. Ladenberg (52A) has suggested an equation for correcting terminal velocities when wall effects are significant.

for walls $\quad V_t = \left(1 + 2.4\,\frac{d}{D_v}\right) V$

for bottom $\quad V_t = \left(1 + 1.7\,\frac{d}{L}\right) V$

where D_v = diameter of container

L = distance to the bottom.

Molecular scale effects are insignificant for most practical interphase transfer systems; the question of interaction in multibody systems is covered in detail in later sections.

II. FLOW PAST A FLUID BODY: A MOVING INTERFACE

When a fluid sphere is substituted for a solid sphere in a flowing stream, one of the most important changes to occur is the ability of the fluid to move under shear making possible a finite velocity at the interface. In this section, we will examine the extent to which shear forces are transmitted through the interface and the effect which this has on external phase flow behavior.

A. Circulation and Interfacial Shear

Although the replacement of a solid by a fluid boundary does permit some shear energy to pass into the drop the extent to which this occurs is still limited by surface tension and dispersed phase viscosity. On small drops surface forces can so effectively resist shear transmission that flow behavior will be identical with that for a rigid body. With a highly viscous dispersed phase shear resistance within the drop can be so great that deviations from rigid body behavior are insignificant. However, under most conditions of interest in this work drop sizes are large enough and the dispersed phase fluid thin enough for extensive circulation to develop even to the extreme of vigorous turbulence.

When circulation does take place, energy must be supplied to the front of the drop to create fresh surface. Most of this is recovered at the rear of the drop although some losses do occur through what Garner and Hammerton (24) have called a relaxation effect. A more significant loss occurs, however, due to viscous shear within the drop (41). Much of the recovered energy is dissipated in fluid friction as it moves from the point of surface recovery at the rear to the point of surface generation at the front. Thus fully developed circulation can only be achieved when skin friction is sufficient to supply all the energy needed to overcome surface forces at the point where new surface is formed. This requirement can be estimated as $P = 2\pi r\gamma_i u$ where P is the rate of energy input required to sustain fully developed circulation, r is the drop radius and u is the tangential velocity at the radius (24). From this formula we can see why fluids with low interfacial tensions circulate more easily than those with high interfacial tensions.

Many attempts have been made to formulate these concepts into equations which could predict the degree to which circulation would take place under a given set of circumstances. Bond and Newton (6) tried to define a threshold size above which well established circulation would always be found. They proposed the relationship:

$$d_c = 3\sqrt{\frac{\sigma}{g|\rho_d - \rho_c|}}$$

stating that transition begins at $d = .1d_c$. This, however, was inadequate due to the omission of any viscosity term. Others have tried correlating the degree of circulation with the Reynolds number (62), but this has proved unreliable due to insensitivity to surface tension effects. The most recent proposal (15) attempts to define the degree to which circulation is fully developed as a "% circulation."

$$\text{"\% circulation"} = \frac{100}{1 + 1.5\,(\mu_d/\mu_c)} - \frac{32\,C_s^{-1}}{r^2 g\,\Delta\rho}$$

This equation attaches little importance to drop size except as it is involved in surface contamination term. This is in agreement with the findings of many that even very small drops can circulate freely if their surface is clean enough which implies that the so-called critical drop size is entirely a function of interfacial contamination.

The degree to which the fluid in the drop can circulate has a major influence on drag and boundary layer behavior. Whereas a solid body totally resists shear requiring that velocity at the interface be zero, a fluid body which offers no shear resistance will experience full stream velocity at the interface and will not develop any boundary layer. Since this leads to a complete elimination of viscous drag effects the situation will closely approximate that of pure potential flow. Experiments (16) have shown that this can frequently be the case near the forward stagnation point of a rising spherical cap bubble. Conkie and Savic (12) showed that the degree of approach to these conditions could be approximated by postulating that the work done by skin friction is equal to the work dissipated in viscous friction within the drop. By their formula

$$\frac{\text{boundary layer velocity at the interface}}{\text{adjacent free stream velocity}} = 0.0094\,\mathrm{Re}\left(\frac{\mu_c}{\mu_d}\right)^2\left(\sqrt{1+\frac{213}{\mathrm{Re}\left(\frac{\mu_c}{\mu_d}\right)^2}} - 1\right)$$

where Re = Reynolds number

μ_c = continuous fluid viscosity

μ_d = droplet viscosity

In the extreme, drops with an excess of circulation energy have been observed (45) to "swim" downstream at greater than their terminal velocity implying that an excess of internal circulation energy (e.g. as acquired in drop release) causes fluid velocity at the interface to exceed that of the adjacent free stream.

In addition to reducing skin friction, circulation has the effect of postponing boundary layer separation, thereby further reducing drag. At low Reynolds Numbers, pictures have shown that separation occurs quite close to the rear of a circulating drop (22, 31). At high Reynolds numbers, this effect is greatly reduced (12); Elzinga and Banchero (18) estimate that the pressure of circulation can shift the separation point to the rear by 6^{o}, which is nevertheless still a 14.6% change in boundary layer area. For low to moderate Reynolds numbers, it is estimated that the reduction of skin drag can reduce overall drag by about 10% and total drag reduction from both effects can be as high as 40% (18). At high Reynolds numbers skin drag becomes very much less important so that total drag reduction is also much less pronounced.

B. Predicting Terminal Velocities

Much of the work done on the behavior of drops and bubbles has been aimed at developing predictive correlations for terminal velocities under a wide variety of conditions. This has usually been done semi-empirically by building up correlations from force analyses and experimental data.

Early attempts were based upon finding a correction factor for the Stokes law equation. The Hadamard-Rybczynski equation (34, 62B), for instance, was built on the presumption that in the presence of fully developed circulation tangential stresses on both sides of the interface were equal.

$$V = V_{STOKES} \times \frac{3\mu_d + 3\mu_c}{3\mu_d + 2\mu_c}$$

where μ_d = drop liquid viscosity

μ_c = continuous phase viscosity

Boussinesq (6A) sought to refine this model by allowing for the effect of dynamic surface tension

$$V = V_{STOKES} \times \frac{e + 2_r(\mu_c + \mu_d)}{e + r\,(2\mu_c + 3\mu_d)}$$

where e is the coefficient or surface viscosity. Real bubbles follow Stokes equation until they reach Re = .6 to 40. They then exhibit a higher velocity than that predicted by the Stokes equation rising slowly to the line for the Hademard-Rybczynski equation which predicts velocities about 50% higher than those for rigid spheres.

It will be noted that as size decreases and surface viscosity rises, Boussinesq's law reduces to Stokes law. As bubble size increases, surface viscosity decreases and Boussinesq's law reduces to the Hadamard-Rybczynski equation.

Spanning a much broader range of Reynolds numbers, Haberman and Morton (33) took quite a different approach and were able to obtain a good correlation for drag coefficient against the Weber number. In their work, drag coefficients for gas bubbles were seen to reach a minimum value at Weber No. = 2.0 and then to approach an assymptote of about 2.6 at We = 32. Hu and Kintner (40) working with liquid-liquid systems achieved a correlation based on Weber Number, Reynolds Number and a friction factor. Their correlation $C_D W_e N_p^{\cdot 15}$ vs. $Re/N_p^{\cdot 15}$ gave a straight line on log-log coordinates. Johnson and Braida (45) improved upon this correlation by dividing the ordinate by $(\mu_c/\mu_w)^{\cdot 14}$. In their curves, a sharp break was observed where maximum velocity was reached and oscillation drag began to become significant.

C. Effects of Interfacial Contaminents

Numerous investigations have reported data which indicate that circulation and drag is strongly influenced by interfacial contamination.

Circulation which is normally fully developed by Re = 10 for air in water can be delayed to Re = 400 (33). Under these circumstances, drops and bubbles will continue to behave as rigid spheres until circulation begins. Garner and Hale (23) have shown that concentrations of surfactant too small to effect interfacial tension can double the critical diameter at which drops of nitrobenzene are observed to begin circulating in water. Similarly, small quantities of detergent by inhibiting circulation in the Re range 200 - 4000 can reduce the rate of rise of a drop by as much as 12% (15) over that of an uncontaminated drop.

Not all surface active materials have the same degree of effect; the nature of the disperse phase fluid, the nature of the surfactant and the pH of the continuous phase are all important factors. Polar solvents circulate easily because surfactants have a low energy of absorption on their surfaces (15). When water is the continuous phase surfactants with long hydrophobic groups are strong inhibitors, those predominated by hydrophilic groups are weak inhibitors (23). Davies and Rideal (15) comment that the ability of a surfactant saturated surface to resist shear depends mainly on the reciprocal compressibility modulus, C_s^{-1} and the density of molecular packing at the interface, although interfacial viscosity may also be important. Based upon this contention, they have developed a tentative formula, which defines the degree of approach to fully developed circulation:

$$\% \text{ circulation} = \frac{100}{1 + 1.5(\mu_d/\mu_c)} - \frac{32\, C_s^{-1}}{r^2 g \Delta\rho}$$

This equation should have considerably greater utility than any of the others currently proposed since both surfactant and viscosity properties are included.

III. DROP DISTORTION AND OSCILLATION

The second major difference between rigid and fluid spheres is the ability of fluid spheres to distort under the influence of hydraulic and dynamic pressure gradients. Significant distortion radically changes drag

coefficients and terminal velocities and can ultimately lead to oscillation and drop breakup.

A. Drop Distortion

The major factors contributing to drop and bubble distortion are (18):

a) differences in hydraulic head
b) external and internal fluid motion
c) interfacial tension
d) surface drag (where the interface behaves as a rigid film)

These forces act in the following way: hydraulic and impact pressures tend to flatten the drop, viscous drag tends to elongate it and surface tension acts in opposition to both these effects by trying to retain a spherical shape. The result is that small drops are spherical because of the predominance of surface tension. Medium size drops are ellipsoids representing a balance between all of the forces. Saito's (see ref. 41) derivation of Stokes equation which carries drag on a sphere to a second approximation predicts a prolate sphere for mercury due to drag predominating and oblate spheroid for water or organic drops due to hydraulic and impact pressures predominating. Shape eccentricity increases with increasing size until drop size is so large that surface tension effects become negligible. At this point, a spherical cap shape is assumed and eccentricity becomes constant at 4.02. Davies and Taylor (16) established that the perfect spherical form assumed by the top surface of a spherical cap can be fully explained in terms of balanced hydraulic and dynamic forces at all points on the surface.

Several approaches have been taken in attempting to predict shape as a function of size and measurable system properties. Some workers have tabulated behavior for air bubbles in water as a function of equivalent radius (62, 24) or Reynolds number (62). These methods are limited, however, due to their failure to include surface tension. Others (37, 15) have worked with the Eötvos number, $\frac{g\Delta\rho d^2}{\sigma}$, but due to the omission of viscosity from this group, its generalized utility is limited to the region

of high Reynolds numbers where viscosity effects are insignificant.

B. Drop Oscillation

In low viscosity fields, the behavior of medium sized drops and bubbles is complicated considerably by their tendency to undergo shape oscillation and to travel a zig-zag or helical path. In water, this behavior is usually observed over the Reynolds Number range 300-3000. Johnson and Braida (45) cite functional variables as follows:

a) drop diameter
b) drop velocity
c) physical properties of the system

Eddies within the drop tend to damp out oscillations due to a high rate of internal energy dissipation; a highly viscous field fluid has the same effect externally.

The magnitude of the oscillation effect has been reported by Licht and Narasimhammurty (53A) showing that for a given bubble maximum A/B can be as much as three times minimum A/B with liquid systems of low internal and external viscosity.

Gunn (32A) has noted that extreme drop oscillation can lead to the breakup of liquid drops. He predicts that this is most likely to occur when the natural frequency of drop oscillation, $\sqrt{\frac{192\sigma}{(3\rho_d + 2\rho_c)}}\, d^3$ equals the frequency of vortex discharge. On this basis, the critical diameter for breakup in liquid-liquid systems can be defined by solving the following equations simultaneously with the one above:

for $Re < 2000$, $\frac{nd}{V} = 3.12 \times 10^{-6}\ Re^{1.8}$

for $Re > 2000$, $\frac{nd}{V} = 1.9$

C. Effect of Distortion and Oscillation on Drag and Terminal Velocity

Both distortion and oscillation tend to increase drag and reduce the terminal velocity over that for a rigid sphere. Oscillation in particular is accompanied by a sharp rise in drag.

Brown (8) recommends that distortion effects be allowed for by calculating the spherecity ratio = $\frac{\text{surface area of sphere of the same vol.}}{\text{surface area of shape}}$

Drag coefficients can then be calculated and used as usual.

Harmathy (37) has successfully correlated drag coefficient vs. Eötvos number with a $\pm 20\%$ confidence for behavior above $Re_d = 500$, taking into account both distortion and oscillation effects.

Rosenberg (62) and Davies and Taylor (16) have studied spherical caps of air in water and have concluded that all spherical caps have geometric similitude and a constant drag coefficient of 2.6 independent of field fluid properties.

IV. EFFECT OF ACCELERATION

Hughes and Gilliland in 1954 reviewed work up to that time on the degree to which acceleration affected drag coefficients for solid spheres and drops. Of particular pertinence were the following:

a) drag coefficients for bodies being accelerated are much larger than those for bodies in steady motion (10 to 20% higher at $V/V_t = .65$)

b) As Reynolds numbers approach the turbulent range, C_D/C_{Do}, the ratio of true drag to that for steady motion grows still larger for a given V/V_t.

c) Charts developed by Cook are given from which a first approximation of C_D/C_{Do} can be achieved for various V/V_t and ρ_d/ρ_c values.

Work on the effects of acceleration since then has not been extensive and for the most part has coincided with the comments already made. Shlichting (64) has noted that a steadily accelerated cylinder can experience boundary layer separation after traveling only .5r. Elzinga and Banchero (18) in studying liquid-liquid systems noted that drops accelerated from a standstill in low viscosity fluids reach 95% of their terminal velocity within the first 5 cm. of travel. In addition, Pearcy and Hill (58B) and Ingebo (43) have studied the motion of drops during acceleration through a gas phase.

The only piece of new work to draw major issue with past findings was that of Torobin and Gauvin (69A). Working with spherical particles

in a turbulent gas phase they concluded that drag coefficients were a function of Reynolds numbers and relative turbulent intensity but not of acceleration. This finding is, of course, in direct conflict with the comments of the workers already cited. Since it has not, however, been tested on liquid-liquid systems thus far, the drag response described in Hughes and Gilliland will be chosen in preference at least until a more precise definition of the limitations on this new hypothesis becomes available.

V. EFFECT OF MULTIPARTICLE INTERACTION

Drops and bubbles in high concentrations behave differently from the same bodies rising individually. This effect begins to become significant whenever bubbles move along the same path with a spacing of less than 24. inches (33).

The main source of this interaction behavior stems from the tendency of each body to draw along with it a certain portion of fluid. As these portions combine, they form a channel of moving fluid which serves to add an additional component of motion to all bodies involved. As a result the apparent terminal velocity can increase by up to 55% (36A) even though the relative "slip" velocity between phases is probably less improved. In addition at higher Reynolds numbers a leading drop can pass along sufficient turbulence with its wake to affect the boundary layer behavior in the next drop, improving momentum transfer efficiency and reducing drag. This is appreciable even at Re = .27 where Happel and Pfeffer (36A) have proposed drag equations for a pair of spheres as follows:

$$F_1 = F_{Stokes} \times \left(1 - \tfrac{3}{4}\frac{d}{s} + .11\,Re\right)$$

$$F_2 = F_{Stokes} \times \left(1 - \tfrac{3}{4}\frac{d}{s}\right)$$

Two important conclusions can be drawn from these equations:

1) The degree of mutual drag reduction is linearly dependent on the separation distance, and
2) The follower will have less drag than the leader, and thus will have a tendency (increasing with increasing Re) to catch up to the leader thereby decreasing the drag of both.

From these facts we conclude that there is an appreciable tendency for bubbles in a stream to:

1) have a shorter residence time by virtue of being carried along by bulk fluid movement
2) have a lower drag and a somewhat different boundary layer behavior by virtue of turbulence induced in the approach fluid by the passage of preceding drops.

Work by Benzing (4) and Bowman and Johnson (7) show that these same tendencies are present at higher Reynolds numbers in bulk systems.

A. Effect of Bubble Size

At high feed rates Benzing found that velocity of rise for large drops was proportional to $r^{.82}$; for small drops Bowman and Johnson reported a linear correlation of velocity with size similar to that found by Garner and Hammerton but about 25% higher for a feed rate of 340 bubbles/min.

B. Effect of Bubble Velocity

Studying small uniform bubbles Bowman and Johnson observed a 55% increase in rate of rise for a feed rate of 645 bubbles compared with terminal velocity for a single bubble. Similarly Benzing recommended a correlation of terminal velocity with mass flow rate, $G^{.22}$. Data in both studies imply that still higher bubble rates would lead to further velocity increases right up to the point of flooding.

C. Flooding Limitations

Although flooding is usually defined as a condition which brings about rejection of one or the other of the phase fed, a more appropriate limit to particle density for this study is reached when the continuous liquid phase is entrained to a significant degree in the upflowing gas phase. For prediction of this point, Brown (8) gives the relationship $G = C\sqrt{\rho_d(\rho_c - \rho_d)}$ where C is a function of interfacial tension and free space over the liquid. A chart given on p. 348 of ref. 8 allows estimation of C.

By this equation, a maximum flow rate for air through a column of water would be 2300 lbs./hr./ft.^{2}. Parallel calculations using empirical correlations for packed towers (8, p. 362) yielded the same value.

VI. MOVEMENT WITHIN PARTICLES

In any interphase transfer process the resistance offered by the dispersed phase is largely dependent on the degree of movement which occurs within the bubbles or drops. There are a number of separate processes which can contribute: shear induced circulation, oscillation induced eddies, and interfacial instability. In the present situation where the bubble contains a liquid puddle, liquid-upon-liquid spreading must also be considered. In the sections which follow we will explore each process in greater detail.

A. Shear-induced Circulation:

As stated earlier, when drag forces are sufficient to overbalance surface forces and internal viscosity, internal circulation is initiated. Movement first appears at the forward stagnation point, working its way back through the drop during a two-fold growth in drop diameter. Hadamard (34) pictured a toroidal pattern of circulation concentric with the axis of the drop and possessing a ring of stagnation on the equatorial plane. Hadamard's descriptive equation was

$$r^2 (r_o^2 - r^2) \sin^2 \theta = \text{const.}$$

When r and θ are the polar coordinates of any point in the sphere taken from the sphere center and the axis of travel, r_o is the radius of the drop.

Spells (66) later proved photographically that the circulation patterns conjectured by Hadamard actually exist at low Reynolds Numbers. As the Reynolds number increases, however, the initial vortex ring moves forward and a stagnant cap forms at the rear of the drop. When separation occurs in the external flow, the stagnant cap at the rear becomes a second vortex ring (35). With fluid drops, high Reynolds numbers are accompanied by deformation which in turn reduces the size of the rear vortex, increases the assymmetry of flow and ultimately moves the stagnation ring of the forward vortex well back of the equator. For

increased values of μ_d/μ_c these same effects occur at lower values of Reynolds No.

Most workers have talked of circulation as a condition which is either present or absent making little effort to give it quantitative character. Exceptions are Hughes and Gilliland who define the rate of circulation as the rate of flow through the equitorial stagnant ring equal to

$$\frac{\pi d^2}{32} \frac{V}{(1+\mu_d/\mu_c)}$$

and Davies and Rideal who as already noted define a % of maximum circulation as equal to

$$\frac{100}{1+1.5(\mu_d/\mu_c)} - \frac{32C_s^{-1}}{r^2 g \Delta\rho}$$

Both equations clearly imply that maximum circulation is achieved by a bubble rising through a viscous liquid; Hughes and Gilliland note that under such conditions a bubble can achieve nearly complete surface renewal for every diameter of distance travelled. For fluids of equal viscosity circulation rate would be reduced to about 40% of this rate.

Kronig and Brink (52) refined Hadamard's picture in their mass transfer model by assuming that the circulation lines were lines of constant concentration exchanging mass with each other by diffusion only. This amounts to an assumption that drop circulation is purely viscous in nature.

Kronig and Brink compared times for equivalent transport by circulation and by diffusion, t_c and t_d, and drew the following conclusions:

1) Circulation becomes more important with increasing drop size. This derives from the fact that t_c is proportional to r_o and t_d is proportional to r_o^2 making $t_c/t_d \sim 1/r_o$.

2) The time required to reduce the concentration of solute in the drop to 1/e of its original value by the combined action of diffusion and circulation can be estimated as $t'd = .022 \frac{r^2}{D_d}$.

3) Comparing t'_d to a comparable extraction by diffusion alone, $t_d = .056\frac{r^2}{D_d}$, we see that the presence of circulation decreases transfer time 2.5 fold.

B. Oscillation Induced Eddies:

As the Reynolds number of the drop rises, eddy activity within the drop becomes significant. Hughes and Gilliland (41) noted that oscillations of a 5% amplitude can produce streamline velocities in a 3mm water drop of 37 cms/sec. For Re >1000, Handlos and Baron (36) proclaimed that turbulent eddy movement dominated drop circulation and that Hadamard's model must be replaced by one which allows for appreciable random bulk flow between streamlines. They developed such a model and used it to derive dimensionless equations for heat and mass transfer which will be reviewed in a later section.

C. Liquid Upon Liquid Spreading:

Unique to the present situation where a puddle of partially vaporized liquid lies in the bottom of a bubble is the importance of spreading to internal movement. The tendency of one liquid to spread upon another is measured by the spreading coefficient:

$$S_p = \gamma_{W/G} - \gamma_{O/G} - \gamma_{O/W}$$

where

$\gamma_{W/G}$ is the interfacial tension of the water phase against vapor

$\gamma_{O/G}$ is the interfacial tension of the oil phase against vapor

$\gamma_{O/W}$ is the interfacial tension of the oil phase against the water phase.

A tendency to spread is indicated by a positive spreading coefficient. Tables of spreading coefficients (15, 1) list polar compounds (e.g., short chain paraffinic alcohols) with high positive values and non polar compounds (e.g., aromatic iodides) with negative values. The spreading velocity of polar oils on water is about 10 cm/sec.

D. Interfacial Turbulence Effects:

The development of gradients in temperature, concentration or interfacial tension between two points on an interface can lead to intense

interfacial turbulence as the system works to equilibrate these differences. Movement of mass along the interface can become vigorous enough to generate visible eddies and in the extreme to spontaneously emulsify two liquid phases. Dominating variables are:

a) the extent of surface pressure gradient built up by the inequality
b) the surface viscosity resisting the flow of material resulting from the surface pressure gradient.

A discussion of how these forces act on droplets of disperse phase in a mass transfer system is given by Davies and Rideal (15) on pages 322-325. Cited in their discussion are cases of interfacial instability brought on by surface pressure differences of as little as 0.25 dynes/cm. Unfortunately, none of the systems described were sufficiently similar to the system of the present work to yield directly pertinent data.

The importance of surface viscosity is effectively demonstrated by experiments which show that instability in an evaporating surface is nearly eliminated by the presence of an insoluble monolayer which increases surface viscosity.

In a mathematical treatment of the hydrodynamics of surface and interfacial turbulence, Sternling and Scriven (66A) predict that surface eddying will be promoted during mass transfer if:

1) solute transfers from the phase of higher viscosity and lower diffusivity
2) there are large differences in diffusivity and in kinematic viscosity between the two phases
3) there are steep concentration differences near the interface
4) $\Delta\gamma/\Delta c$ is large and negative
5) surface active agents are absent
6) the interface is large in extent

It is likely that a parallel set of statements could be made substituting thermal variables for concentration variables throughout although the authors have estimated that turbulence induced by thermal imbalance is only about one one-thousandth as intense as that due to concentration effects.

VII. TRANSPORT STUDIES

The large amount of work done on mass transfer in fluid systems has established the nature and pattern of response for most of the variables involved. Much of this is also applicable to heat transfer through the substitution of appropriate dimensionless groups in the correlation equations. In both cases analysis is usually simplified by dividing the overall resistance into three parts; outer phase, interface and inner phase. This approach will also be used here.

A. Outer Phase Resistance

Following the pattern of previous sections, we will begin by reviewing the classic situation of transfer to a solid sphere at low Reynolds number and then see what happens when Reynolds numbers are increased and a fluid sphere is used.

1. Transfer to a solid sphere at Re <1000:

As already noted a moving sphere is separated from the bulk continuous phase by a laminar boundary layer over the forward half of the body and, above Re = 17, a turbulent wake region over the rear half. A value for total heat flow must be built up by summing over both sections.

Transfer coefficients for the forward half can be estimated from any of the various forms of the Frossling equation, $Nu = b(Re)^{\frac{1}{2}}(Pr)^{\frac{1}{3}}$. However, this equation cannot be applied beyond the point of separation and corresponding equations for the wake region have not yet been developed.

Fortunately, at low Reynolds numbers a small portion of the overall heat transfer takes place in the wake region; Baird and Hamielec (2) show that less than 10% of the transfer to a solid sphere occurs in the wake region at Re = 100. Thus, fairly successful estimates of overall transfer coefficients have been achieved by merely adjusting the constants of the Frossling equation to compensate for wake region transfer. A widely used equation which does this quite well over the Reynolds Number region 0 - 1000 is that developed by Ranz and Marshall (60).

2. Transfer to Solid spheres at Reynolds Numbers $\geq$1000.

As Reynolds numbers increase the boundary layer becomes thinner and turbulence in the wake region grows. Transfer coefficients over the whole surface grow and the wake region takes on increasingly greater importance.

For Re = 40,000 Drew and Ryan(16B) have shown that equally high rates of heat transfer occur at front and rear stagnation points while rates at the sides fall to about 40 per cent of these levels. A recent attempt (66B) to use a modified Frossling equation in this region (1 - 30,000) reflects this effect by assigning a .62 exponent to the Reynolds number instead of .5. Extending this trend, Harriott (38) has suggested that at very high Reynolds numbers transfer in the wake region might be almost directly proportional to the Reynolds number. And indeed, local coefficients (44) in the wake of a cylinder show a linear dependence for a Re_d above 20,000.

3. Transfer to a circulating drop

If a fluid drop is substituted for a solid sphere, the circulation and oscillation effects already described can cause major changes in transfer behavior. The ability of the interface to take on a finite velocity reduces shear and defers separation so that boundary layer covers more of the sphere surface and is also thinner. In the extreme potential flow is established and the boundary layer disappears. Harriott (38) noted that Boussinesq (6A) and Ruckenstein (62A) analyzed the concentration gradients for the flow lines of potential flow and gave their equation for average Nusselt number as:

$$Nu = 1.13\sqrt{Pe}$$

This is identical with the equation proposed by Handlos and Baron for the external film coefficient in heat transfer to drops in a liquid-liquid system at high Reynolds numbers (36).

Several workers (12) have argued that the point of separation is unaltered by the presence of circulation making the above approach invalid.

However, photographs of external flow patterns show that separation occurs very close to the rear of circulating drops for systems with low disperse phase viscosity so that the assumption of potential flow is fully reasonable and indeed correlation of results with the above equation has usually been successful to ±20% with systems for which $(\mu_c/\mu_d)\sqrt{Re} > 10$. (38)

The effect of drop oscillation on external film coefficient has not been closely examined. The only comments found in previous work are mainly speculative:

1) Calderbank and Korchinski (9) note that the coefficient of heat transfer to drops in a liquid-liquid system rises sharply coincidental with the onset of oscillation but whether the effect is one acting primarily on the external or on the internal film also is not clear.

2) Harriott (38) speculates that oscillations would probably increase the heat transfer coefficient and suggests that the penetration theory be applied using equal contact time for both phases.

B. Inner Phase Resistance

As already noted, the transfer resistance offered by the dispersed phase is strongly dependent on the degree of motion present. Resistance is at a maximum when internal motion is absent and undergoes proportionate decrease as mixing intensity grows. Details are given in the following sections.

1. Diffusion: Conductive heat flow obeys the basic Fourier equation $q = \frac{k}{l} S \Delta T$. To use this for predicting heat flow into a drop requires that a function for S and for l be defined which appropriately acknowledges the changing contours of the transfer path. This has been done for the case of a solid sphere suddenly exposed to a step temperature change in the surroundings and the results charted for varying outside phase resistances (55). Several workers (52, 56) have used these charts successfully to predict the rate of heat absorption by a noncirculating drop.

Vermeulen (70) achieved a more practical solution to this problem, however, by developing an empirical equation for estimating the fractional approach to equilibrium. This was later modified by Johnson and Hamielec (46) to yield

$$E = 1 - 6 \sum_{n=1}^{\infty} B_n \exp \left(\frac{-\lambda_n^2 X Dt}{r^2} \right)$$

X in this equation is called the diffusion or conductivity ratio and represents an empirical multiplier which allows internal transfer rates collected under any set of conditions to be evaluated in terms of multiples of the rate for pure conduction. If only pure conduction were operating in a drop X would = 1. Experimental data seldom achieve this low a value since other forces are almost always present to stimulate some movement. Nevertheless, very viscous drops moving slowly in a low viscosity field fluid should yield values close to 1.

2. Laminar Circulation

In an effort to explain why transfer rates in most real drops should exceed conduction levels, Kronig and Brink (52) developed equations for predicted transfer rates in the presence of the internal laminar circulation currents proposed by Hadamard. They concluded that the presence of circulation would increase X in the diffusion equation of section 1 to 2.25 resulting in an increase in transfer coefficient of 1.5 fold. McDowell and Myers (56) developed experimental data in their study of heat transfer from hot water to organic drops which coincided closely with Kronig and Brinks prediction.

3. Turbulent Mixing

At higher Reynolds numbers (>200) increased shear and the presence of oscillation causes eddy diffusion to occur between circulating stream lines so that transfer rates rise sharply. Calderbank and Korchinski (9) report experimental X values of 7 to 70 for systems where oscillations are present. Handlos and Baron (36) derived an equation based on the assumption that turbulent motion dominated the fluid within the drop. Their model, $Nu: = .00375\ Pe'_d$ can be written in terms

of the diffusivity multiplier factor by setting $X = Pe'_d/2048$.

4. Liquid-upon-liquid Spreading

The main effect of spreading on transfer rates is to increase interfacial area. There is some doubt, however, about the equivalence of film area with that over the main puddle. Measurements of vapor diffusivity by the Stefan method (rate of evaporation from a partially filled liquid tube) are unaffected by any tendency of the vaporizing liquid to climb the wall. In fact, correct diffusivity values are arrived at only if the capillary film is ignored (27A). Thus the question of spreading tendencies of the liquid may be largely academic having little effect on observed rates.

5. Interfacial Instability

Since the motion produced by interfacial instability in the dispersed phase is matched by corresponding action in the continuous phase, its effect on transfer rate will be treated in terms of overall resistance in a later section.

C. End Effects

In mass transfer studies of droplet extraction, data have shown that up to 50 per cent of the total extraction can occur during drop formation (15). The most important variables involved are set forth in Heertjes' (39B) equation for the degree of approach to equilibrium achieved by entrance effects:

$$E_f \doteq \frac{20.6}{d}\sqrt{\frac{Dt_f}{\pi}}$$

Although a similar behavior should prevail in heat transfer systems, attempts at experimental verification have produced conflicting results. Garwin and Smith (26) in their study of spray column heat transfer, found an end effect for heat flowing into the disperse phase which disappeared when the direction of heat flow was reversed. McDowell and Meyers (56) studying transfer to single drops saw no evidence of end effects.

Harriot (38) has noted that drop coefficients for mass transfer usually decrease with time from release and he suggested that this was

due to the gradual damping out of release vibrations. Calderbank and Korchinski (9), however, found no evidence of this type of entrance effect in their work on heat transfer. Possibly the damping which Harriot comments on is due to progressive interfacial fouling or merely interfacial aging. This would account for its greater prominence in mass transfer situations.

D. Interfacial Effects

Normally the interface itself offers only a minor resistance to mass transfer between liquids and no resistance to the flow of heat. Interfacial resistance to mass transfer increases sharply, however, in the presence of even minute amounts of surfactant. This is due primarily to the accumulation at the interface of an oriented layer of tightly packed surfactant molecules. An actual physical film is established which resists mass transfer in either direction. The film is much too thin, however, to offer any direct resistance to heat transfer.

As already noted absorbed surfactants also reduce transfer indirectly by supressing mixing motion in the adjacent boundary layers. This effect will be treated in the next section.

E. Overall Resistance

Component resistances and interfacial effects combine to yield the overall coefficients usually reported for experiments. The following results are pertinent:

1. Controlling Resistance

McDowell and Meyers (56) studied heat transfer from a continuous water phase to rising drops of various organic liquids. For high viscosity oil drops which did not circulate continuous phase resistance was found to account for less than 4% of the overall resistance.

When circulation occurred using drops of kerosene and xylene dispersed phase resistance was appreciably reduced but remained controlling. Transfer coefficients for both of these cases were in the vicinity of .011 cal/(cm.)^2(°C)(sec.) [81. B.t.u./(hr.)(ft.^{2})(°F)]. When a circulating drop of water was heated by a mixed kerosene -trichloro ethylene continuous

phase, however, the continuous phase resistance increased becoming nearly equal in importance to that of the dispersed phase. Overall coefficients were somewhat reduced.

Calderbank and Moo-Young (10) have pointed out that the density differences between the continuous and discontinuous phases is one of the prime factors determining transfer rate. The exterior film effect is shown through the Reynolds number where both velocity and density are involved. In addition, oscillation effects and interfacial rippling which can occur at high drop velocities, i.e., >3 cm./sec. lead to additional transfer rate improvements not wholly anticipated by Reynolds number correlations.

2. Effect of Surfactants

As previously mentioned overall resistance is strongly effected by the presence of surface contaminents. Garner and Hale (23) report that only a .015% addition of Teepol to water reduced the rate of extraction of diethylamine from toluene drops to 45% of its original value. They attributed this change mainly to a damping of internal circulation in the drop. However, other work (18, 38) already discussed in this review suggests that important changes in the exterior film resistance are also involved.

At higher Reynolds numbers (>300) where oscillation becomes important, the presence of surfactants can enhance transfer rates by lowering the surface and interfacial tension that normally restrain the oscillation tendency. This is particularly true in the equivalent spherical radius range .077 to .35 cm.

When Reynolds numbers exceed 5000 bubbles take on the spherical cap shape and surfactants again act to reduce transfer rates by repressing surface ripples which are normally present on the flat underside. Baird and Davidson (2A) observed that these ripples when present acted to increase rates of absorption of CO_2 bubbles in tap water to 50% higher than predicted by theory; the suppresion of the ripples by n-hexanol totally neutralized this increase.

3. Interfacial Turbulence

As previously mentioned the presence of sufficient interfacial gradients in concentrations or surfactant contamination can cause pronounced interfacial turbulence. Precise prediction of the importance of this effect is not yet possible although a simplified mathematical model has been presented by Sternling and Scriven (66A). Experimental studies (53C, 53D, 73A) have shown that mass transfer rates are increased several fold.

F. Particle Density Effect

As population density increases, interaction between drops becomes greater. Transfer rates are enhanced since all but the first drops must pass through a continuous phase in which some turbulence has already been generated by preceeding drops. Under these circumstances, the density difference begins to assume less importance. Johnson and Minard (47) found that the density of the dispersed phase in a spray column had little effect over a wide range of operating conditions. However, where extreme density differences and high feed rates exist in combination there is always the risk of a loss of transfer efficiency through channeling as observed in the mercury-water study of Pierce, Dwyer, et al (58).

Bubble size also becomes less important at high particle densities. Both Bowman and Johnson (7) and Johnson and Minard (47) found that drop size had little effect on transfer coefficients in spray towers.

Short of flooding conditions, flow rate has only a minor effect on transfer efficiency. Bowman and Johnson (7) found that a tenfold increase in rate caused only a 35 per cent increase in transfer coefficient. Garwin and Smith found that efficiency dropped off as dispersed phase flow rate increased (26). Pierce et al (58) found that heat transfer coefficients varied only slightly with increased dispersed phase flow rate.

VIII. NUCLEATION AND BOILING HEAT TRANSFER

A. Nucleation

When a gas phase first nucleates in a pure liquid, the pressure

in the bubble will be higher than the system pressure because of surface tension forces and the effect of surface curvature on vapor pressure:

$$p_v(r) = p_v + \frac{2\sigma}{r} \cdot \frac{\rho_v}{\rho_l - \rho_v}$$

where $p_v(r)$ is the pressure inside the bubble and p_v is the system pressure. From this equation it is apparent that a nucleus will form only if the equilibrium vapor pressure of the liquid at the given temperature is sufficiently elevated above the system pressure to overcome the surface tension and curvature effects. In proof of this experiments have shown that pure liquids can exist at pressure of more than 100 atmospheres below their equilibrium vapor pressure and not nucleate. Specifically, Moore (57) has described a series of experiments on Freon 12 droplets undergoing spontaneous nucleation while suspended in an aqueous continuous phase. His results show that liquids can superheat to 1.35 times their absolute boiling points before nucleation begins. The presence of surfactants or of low frequency random vibration did not increase nucleation tendencies.

Nucleation by ionizing radiation has also been proposed but would seem to offer only a minor improvement. Experience with cloud chambers has shown that the comparable process of ion nucleation in a supersaturated vapor still requires a considerable departure from equilibrium conditions (14). The only process by which high superheating can be effectively avoided is hetergeneous nucleation. Thus, any dissolved gas or solid surfaces which are easily wet by the vaporizing liquid can provide active nucleation sites (21). In practice, traces of dust and dissolved gases are so routinely present in all but specially refined liquids that appreciable superheating is seldom observed.

B. Boiling Heat Transfer - Submerged Heater

Once the problem of nucleation is overcome, any attempt to transfer heat to liquid at its boiling point results in some vaporization. As the temperature driving force is increased, vaporization becomes more vigorous until vapor generation rate exceeds the rate at which vapor leaves the heating surface and either the heating element burns out or a vapor flooding condition sets in.

When heat is being supplied by a submerged hot surface, the process of vaporization will take on different forms as ΔT increases:

At low ΔT (0 - 10°F)	Surface Evaporation	- Heat travels by conduction and convection to the free liquid surface where evaporation occurs.
At medium ΔT (10 - 50°F)	Nucleate Boiling	- Vapor bubbles nucleate at the heater and grow by gathering additional vapor from the surrounding liquid as they rise.
At high ΔT (>50°F)	Film Boiling	- As above, with greatly increased turbulence and much more of the heating surface covered with vapor phase.

McAdams (55) has reported on this behavior as follows:

1) In surface evaporation the natural convection mechanism causes flux to be proportional to $\Delta T^{5/4}$. For nucleate boiling and film boiling still higher ΔT exponents prevail.
2) If forced convection is imposed, work by Beecher (3) has shown that flux becomes linear to ΔT for 0 - 10°F with only a slightly higher power dependence at ΔT = 20°F.
3) Peak flux for a submerged heater system may be estimated from the critical pressure by the formula

$$\frac{(q/S)p}{P_c} = 380$$

where q/S is flux is Btu/(ft.^{2})(hr.) and P_c is the critical pressure in lbs./sq. in. abs. Peak values for boiling organics usually fall below 9.5 cal/(sec.)(°C.)(cm.)^2 [125,000 Btu/(hr.)(°F)(ft.)^2] and peak values for boiling water are usually less than 30 cal/(sec.)(°C)(cm)^2 [400,000 Btu/(hr.)(°F)(ft.)^2].
4) These fluxes can be exceeded, however, if the liquid being heated is subcooled. For water, a flux of 4.7 million Btu/hr.(ft.^{2}) has been measured. This gain is attributed to major boundary layer

disturbances resulting from rapid bubble growth and collapse. More recently, an alternate approach to peak flux based upon vapor flooding limitations has been presented by Zuber, Tribus and Westwater (74). They proposed the equation:

$$(q/S)\ crit = .131\lambda_v\rho_v\left[\frac{\sigma g(\rho_l - \rho_r)}{\rho_v^2}\right]^{1/4}$$

and demonstrated its utility for water and five organic liquids.

C. Evaporation From a Shallow Pool

As with all vaporization processes the rate of evaporation from a pool surface can be limited either by the rate of heat transfer to the surface or the rate of escape of vaporizing molecules.

1. Heat Transfer

If a liquid and its vapor are both at saturation temperature, evaporation and condensation rates will be equal and no net vaporization will occur. If the temperature of the heat source is raised slightly, heat will flow through the liquid by conduction to the surface until surface molecules acquire sufficient excess energy to begin escaping in greater numbers than are simultaneously condensing. As the ΔT between source and surface grows rates will increase proportionately until density differences within the liquid become excessive and convection currents are initiated. Spangenburg and Rowland (65) studied this situation by exposing a shallow pool of warm water to still dry air. They reported that convection began when the ΔT between the bulk of the liquid and its surface exceeded $0.2^{\circ}C$. Once convection currents had begun a temperature difference of $.056^{\circ}C$ was sufficient to maintain them.

Container depth did not effect the rate of convective circulation as long as it exceeded the minimum needed for a given thermal gradient. This minimum depth was a function of thermal gradient. Spangenberg and Rowland confirmed Rayleigh's contention that circulation will be initiated whenever the Rayleigh number for an infinite layer of liquid

with uniform gradient and top and bottom boundaries conducting exceeds $(27\pi^4)/4$. In equation form they give this condition as:

$$\alpha g \Delta T l^4/\beta\nu > 27\pi^4/4$$

where α is the coefficient of cubic expansion, l is the depth, β is thermal diffusivity and ν is the kinematic viscosity. They further demonstrated that circulation once started will be maintained as long as the Rayleigh number exceeds nine per cent of this value.

2. Mass Transfer

In general as heat transfer to the surface increases, net mass transfer of vaporizing molecules through the interface will increase accordingly. However, for every liquid there is an upper limit to the rate of evaporation imposed by the maximum escape rate of the molecules. This has been defined from theory by Langmuir (see ref. 61) as being equal to

$$m = p\sqrt{\frac{M}{2\pi RT}}$$

where p is the system pressure, M the molecular weight, T the absolute temperature and R, the gas constant. Some liquids have approximated this rate under very high vacuum, but others have exhibited much lower limiting values. Recent work (39A) indicates that steric effects can impose rate restrictions which will reduce limiting levels to only a few per cent of those predicted by Langmuir.

The presence of surfactant films on an evaporating surface can further restrict mass transfer through the liquid surface to a marked degree. Thus whereas for evaporation into a still atmosphere the main resistance to evaporation is normally in the vapor phase with negligible resistance elsewhere, Davies and Rideal (15) have shown that a highly compressed surface film can raise interfacial resistance up to a place of equal importance. Adamson (1) reports that surface films can decrease overall evaporation rate by as much as 90 per cent depending upon the surfactant used. Films of organic esters being poor packers

offer a low resistance, whereas highly linear fatty acid films are strong inhibitors. For most compounds, the effect is linear in surface pressure.

E. Evaporation of a Floating Immiscible Layer

A type of boiling heat transfer between immiscibles which has already received some attention is that which occurs when a low-boiling layer is floated on a heated liquid substrate. Kavesch (49) studied the systems water-pentane, water-ether and water-2,2-dimethyl butane with the following results:

1) Only moderate fluxes were obtained [maximum was

$$.45 \frac{\text{cal}}{(\text{sec.})(\text{cm.}^2)}, \ (6000 \text{ Btu}/(\text{hr.})(\text{ft.}^2) \text{ for } \Delta T = 37.7]$$

based upon interfacial area of the initial drop.

2) No unusual interfacial turbulence was observed.

3) Layer depth had no observable effect on rate.

4) Temperature responses were as follows:

Water to pentane - $q/S \sim \Delta T^{1.9}$

Water to 2,2 dimethyl Butane - $q/S \sim \Delta T^{2.1}$

Water to ether - $q/S \sim \Delta T^{\infty}$ - system unstable, heater burned out.

In a more carefully controlled study, Gordan et al (29) examined the same type of arrangement with the systems mercury-water, mercury-methanol and mercury-ethanol. Here some interfacial contamination with solds was present and violent interfacial turbulence was observed. The flux rates were still lower than those observed for submerged heaters at the same ΔT but were about five fold higher than those reported by Kavesch. This was probably due to the observed interfacial turbulence as well as the very low thermal resistance of the mercury layer compared to that of water.

For mercury to water $q/S \sim \Delta T^{1.7}$

For mercury to methanol $q/S \sim \Delta T^{.7}$

For mercury to ethanol $q/S \sim \Delta T^{1.0}$

Maximum values of the heat transfer coefficient for methanol and ethanol were about .12 cal/(sec.)(cm.^{2})($^\circ$C) [880 Btu/(hr.)(ft.^{2})($^\circ$C)]. Water at $\Delta T = 33^\circ C$ showed a coefficient of .25 cal/(sec.)(cm.^{2})($^\circ$F) [1800 Btu/(hr.)(ft.^{2})($^\circ$F)] which appeared to be still rising.

F. Heat Transfer to an Evaporating Dispersed Phase

1. Studies on Bulk Systems

Kavesch also tried to measure heat transfer rates from water to boiling drops of pentane and ethyl ether. Inconsistent nucleation caused wide variability in the results, but in spite of this, estimates were developed for the US product. These were found to be an order of magnitude higher than for layered boiling. Values for US of 13.6 to 25.7 $\frac{cal}{sec.\ ^\circ C}$ [114 to 215 Btu/(hr.)($^\circ$F.)] were measured in the boiling drop system compared with .5 to 4.3 [4.2 to 36 Btu/(hr.)($^\circ$F)] for the separate layer arrangement. Dispersed phase flow rate did not appear to have any major influence.

Katz and Shroader (48) later extended this work by studying pentane and a saturated aqueous solution of lithium chloride. In their system reproducible nucleation was achieved by dissolving an inert gas in the dispersed phase feed. US products of 7.6 to 58.2 cal/(sec.)($^\circ$C) [61 to 460 Btu/(hr.)($^\circ$F.)] were achieved by using finer nozzles and higher flow rates than those used by Kavesch. A linear dependence of total heat transferred upon depth demonstrated that end effects were insignificant. The US product had only a mild dependence upon flow rate (80 per cent rate increase for a threefold rise in feed rate) although excessive channeling occurred when high flow rates were used with shallow depths.

Further refinements of this approach were made by Berinstein and Khetani (5). Using greater continuous phase depths and a set of thermocouples for measuring a continuous phase temperature profile, they found a maximum heat transfer coefficient of 2.3 cal/(sec.)(cm.^{2})($^\circ$C) [17,000 Btu/(hr.)($^\circ$F.)(ft.^{2})] based upon the interfacial area of the starting droplet.

2. Studies of Transfer to Individual Bubbles

There has been no work reported to date on the specific subject matter of this thesis although work on bubble growth in superheated liquids is certainly closely parallel. Representative of these studies is the recent work of Strenge, Orell and Westwater (67) who examined the rate of bubble growth for boiling pentane and ether and concluded that all bubbles whose radius is a power function of time will obey

$$Nu = Re\,Pr\,\frac{(\rho_v \lambda_v)}{C_p \rho_l \Delta T}$$

Vapor bubble growth rate is apparently uneffected by oscillations. It was at this point, armed with the knowledge of the previous work and the many questions which it raised that the present study was begun.

CHAPTER II - PRELIMINARY DECISIONS

On the basis of questions raised by previous studies (5, 48, 49), it was felt that an inquiry into the mechanism of heat transfer was the most important next step. Because of the uniquely heterogeneous nature of the system, a new experimental technique had to be selected and the conditions of its use precisely defined.

1. A Dropwise Approach

The behavior of single drops was chosen as the prime focus for this study so that maximum advantage could be taken of previous work without the need for a detailed analysis of particle interaction.

Important additional advantages were the following:

a) A laboratory scale tank of continuous phase can be treated as an infinite and invariant heat sink, since only a small amount of heat is required to vaporize a single drop, thereby simplifying the problems of both temperature control and analysis of results.

b) Wall effects can be safely avoided even in a continuous phase tank of modest volume. Thus, the results are independent of the specific equipment used.

c) Using estimates of interfacial area made from photographic analysis of drop size and shape, heat transfer coefficients can be calculated for direct comparison with other basic types of heat transfer systems.

d) By controlling the release of individual drops it becomes possible to separate the phenomenon of vapor phase nucleation from vapor phase growth. This is particularly pertinent to the utility of the results since previous work (44, 57) has shown that the temperature driving force required for spontaneous nucleation is about tenfold larger than that required to sustain the operation of a spray column exchanger (48, 49) Vapor phase growth was selected for study with nucleation being accomplished artificially.

2. Data Collection

Photography was chosen as the main tool for data collection because it provided a means of collecting data on both instantaneous conditions and rate relationships without physically interfering with any of the processes involved. The principle techniques now in use for drop and bubble study are high-speed motion picture and multiple exposure strobe light photography. The former offers a complete dynamic picture with freedom to provide lighting which will record internal and external liquid motion as well as instantaneous size and shape. The latter, however, is much more economical and through the use of Polaroid film, allows immediate evaluation of results. The exploratory nature of this study made the latter a more suitable choice.

3. Elimination of Side Effects

a) Wall Effects - The degree to which nearby walls reduce the terminal velocities of drops and bubbles is almost always expressed as some fraction of a free rise or free fall value. Since no such values were available for heterogeneous accelerating bubbles of continuously changing density, an oversized vessel was chosen so that any potential wall effects would be safely avoided.

b) Mass Transfer - The decision was made to presaturate the continuous phase with the discontinuous phase to avoid complicating observations on heat transfer rates with simultaneous mass transfer effects. Since it would not be practical to tolerate absorbtion of more than trace quantities on a commercial scale, the elimination of mass transfer effects should not seriously detract from the utility of the results.

c) Non-stationary Continuous Phase - Assuming that the normal commercial equipment for this type of heat transfer would be a spray column, it is natural to suppose that the two components would flow past each other countercurrently. In this work, however, the continuous phase was held stationary so that the entire phase might be assumed to have a constant temperature and so that stray eddies might be held to a minimum.

d) Dissolved Air - It is no doubt true that dissolved gases would be routinely present in both liquid components of any commercial system built on the direct contact concept. In this work, however, it was necessary to deaerate the feed in order to achieve controlled release of the partially superheated drops. In preliminary tests the presence of dissolved gas here was seen to cause premature nucleation making control of drop size and synchronization with the camera impossible.

4. Selection of Immiscible Liquids

Because of the exploratory nature of this study, the immiscible liquids were chosen to provide the simplest and most tractible system for study.

(1) Dispersed Phase - The following criteria were used for choosing the dispersed phase.

a) lighter than water - a lighter than water material separates more cleanly from the nozzle, requires less nucleation energy to achieve release, has less tendency to separate from its vapor phase and shows less tendency toward hard-to-analyze high inertia oscillations.

b) high purity - a high purity material will have identical physical properties from lot to lot, a very narrow boiling point range, and little likelihood of any surface active contaminents.

c) boiling point near room temperature - a close to ambient boiling point reduces the amount of heating and cooling needed to reach appropriate continuous phase temperatures and minimizes problems of heat loss or gain and temperature control

d) very low solubility in continuous phase - low solubility is necessary to achieve presaturation of the large volume of continuous phase with a reasonable amount of dispersed phase.

Ethyl chloride was chosen for the continuous phase because it offered all of the above properties at a low cost.

Ideally, several dispersed phase liquids with different Prandtl numbers should have been chosen, but the range of Pr numbers for various liquids at their boiling point is quite limited. Denbigh (16A) gives a correlation for estimating Pr

$$\log \quad Pr = .10 \frac{\Delta H_{Vb}}{T_b} \quad \frac{T_b}{T} - 1.8$$

But for vaporizing organic liquids with a reasonable boiling point, $T = T_b$ and $\Delta H_V/T_b \cong 21$ so that little variation is possible. Typical of the range of variation are the Pr of ethyl chloride and water at their boiling points, 3.17 and 1.5 respectively. Additives cannot be used here to modify the Prandtl number artificially since their effect will be constantly changing as the drop evaporates.

(2) Continuous Phase - The following criteria were used for choosing the continuous phase.

a) transparency - a transparent continuous phase is essential to any photographic study.

b) low vapor pressure at ambient temperature - the lower the continuous phase vapor pressure, the less complicated will be the partial pressure effects in the system.

c) low solubility in the discontinuous phase - this is necessary to avoid excessive mass transfer and an unpredictable boiling point.

d) high purity - high purity material is less likely to contain interfacial contaminants or contaminants that might be absorbed into the dispersed phase.

e) capacity for simple modification of Prandtl number - the means of easily altering physical properties is a prerequisite for building any heat exchange correlations along conventional lines.

Distilled water was chosen as the continuous phase since it is inexpensive, satisfies requirements a, b, c and d, and can easily be modified with

glycerine to meet requirement e.

(3) Interaction - In addition to the above properties required of phases individually, the following criteria were applied to the system as a whole.

a) chemically inert - although ethyl chloride does hydrolize in water, the rate is slow, relative to the time of a set of experimental runs so that this was not considered a major drawback of the ethyl chloride - water system.

b) scope for interfacial tension adjustment - the pure system has initially a fairly high interfacial tension value providing ample margin for depression with a surfactant.

(4) Choice of Surfactant - A surfactant was chosen with the following characteristics:

a) high water solubility, low organic solubility - this was required to avoid the possibility of an effect which would vary as droplet evaporation proceeded.

b) minimal depression of interfacial tension at the critical micelle concentration - in order to detect rate effects (e.g. film renewal at the interface) it was desired to be able to exceed critical micelle concentration without depressing the interfacial tension so far that drop release could no longer be controlled and drop breakup would become excessive.

A summary of the physical properties of each of the systems used is given in Table A-1 of the Appendix.

5. Selection of Operating Variables

(1) Variables Included - Drop size, ΔT driving force, continuous phase Pr number, and surfactant concentration were included as operating variables for the following reasons:

a) drop size - basic to any heat transfer study is the concept of flux, rate per unit area. As a basic design parameter for this system, drop diameter takes the place of the pipe

diameter of the normal heat exchanger. It not only occurs directly in both the Reynolds and Nusselt number of the usual transfer coefficient equations, but also indirectly controls the velocity of rise term.

b) ΔT driving force - in all heat transfer studies, the power dependence of rate upon ΔT is a prime indication of the mechanism involved. It can be used to identify the boiling regime which prevails as well as to distinguish the dominance of natural or forced convection. In addition, it is the design parameter most directly indicative of maximum rate potential.

c) continuous phase Prandtl Number - the Pr number is a controlling parameter for the resistance offered by the external phase boundary layer. By manipulating it, we can gain some indication of the relative importance of the inner and outer phase resistances.

d) surfactant concentration - a major difference between laboratory and plant conditions is that interfaces in plant work are seldom free of contaminants. Artificially adding them to this system helps to identify their importance as it relates to not only transfer coefficient, but also to liquid spreading and drop breakup.

(2) Variables Excluded - Continuous phase depth, system pressure, release temperature, mechanical agitation, nozzle material, nozzle shape and direction of injection were excluded for the following reasons.

a) depth - previous studies (5, 48) had shown that the major effect of varying depth was the effect on residence time. The possibility of achieving minor refinements for this conclusion was judged an inappropriate goal for this study.

b) pressure - it was expected that the major influence of any moderate pressure change would be to vary bubble size and

with it the rate of rise. Since some understanding of this effect was certain to accrue from experiments dealing with initial drop size, it was believed unnecessary to dilute the present work by including the pressure variable. Later studies should certainly be planned to examine this response more directly, particularly at the higher pressures.

c) release temperature - no provision was made for controlling the release temperature since this provision would have greatly complicated the equipment needed to conduct a single drop study. As the ratio of specific heat to latent heat for ethyl chloride is only .0043, this elaboration did not seem justified.

d) mechanical agitation - the presence of mechanical agitation in the system would have caused undefined turbulence and excessive droplet breakup, both of which are antagonistic to the basic objective of defining the transfer mechanism. Later studies can more easily study the effect of agitation, once the role played by ΔT, area and the resistance offered by each of the phases has been better defined.

e) nozzle material; nozzle shape - A previous study (39) has determined that a sharp edged orifice is preferable for clean drop release. Preliminary experimentation demonstrated that a teflon lined brass nozzle gave the most reproducible troublefree performance. Since greater than 99 per cent of the process being studied takes place after droplet release, no major gains could be expected from any detailed examination of these variables.

f) direction of injection - although this may certainly be regarded as an important variable in any working design, it was incompatible with the experimental procedures chosen for this study. It would be highly appropriate for any future bulk flow study.

CHAPTER 3 - EQUIPMENT AND PROCEDURE

The basic function of the experimental scheme was to:

1. Measure out a drop of chosen size
2. Start it vaporizing at a desired time into an environment of carefully controlled and accurately known temperature
3. Generate detailed information on the rate of vaporization of the drop liquid and all conditions and phenomenon which might affect it.

To do this within the scope of the restrictions developed in Chapter 2 the following equipment and procedures were evolved.

A. Equipment:

The equipment used in this work was arranged as shown schematically in Fig. 3.1. It consisted of three major sections: the continuous phase column, the dispersed phase feed system and the photographic system.

1. The Continuous Phase System

The continuous phase was placed in a stainless steel tank, with a stainless steel bottom and an open top. A depth of 4 feet was chosen on the basis of preliminary tests to allow observation of the complete vaporization process for temperature driving forces down to 2°C. An inside diameter of 15 in. was selected to avoid wall effects for the largest drop size in its fully vaporized state. To avoid contamination all metal joints were welded or silver soldered and glass observation windows were cemented in with an epoxy polyamide cement, chosen for its inertness to water, ethyl chloride, hydrochloric acid, and ethyl alcohol. A single packing gland used in the tank bottom was packed with unimpregnated asbestos packing.

The temperature adjustment of the continuous phase was accomplished through the use of a heating and cooling coil welded into the tank bottom and an electrical immersion heater submerged at the free liquid

Fig. 3.1 - Flow Diagram of Equipment Legend

A 50 ml. EtCl. supply syringe

B 2 ml. EtCl. metering syringe with micrometer drive

C Constant temperature bath with distilled water kept at $+5^{o}C$.

D Main coolant resevoir filled with 50-50 methanol-water at $-10^{o}C$.

E Resevoir for supplying coolant to feed tube jacket at $+5^{o}C$.

F Continuous phase tank. 4 feet deep by 15 inches diam. made of stainless steel and glass

G High speed mixer with long shaft and two 4 inch impellers (removed during runs)

H "Strobolume", multiple flash strobe light

I "Strobotac", to control flashing frequency of Strobolume

J Hot wire positioning stand

K 500 mfd. condenser for pulsing hot wire

L Relay which acts to fire hot wire circuit as camera lens opens

M Milltown controller set to actuate coolant pump as needed to maintain temperature

N 2 KW electrical, immersion heater

P Speed Graphic camera with Polaroid back

T Mercury in glass thermometer for monitoring temperature and actuating Milltown control circuit.

Figure 3-1 FLOW DIAGRAM OF EQUIPMENT

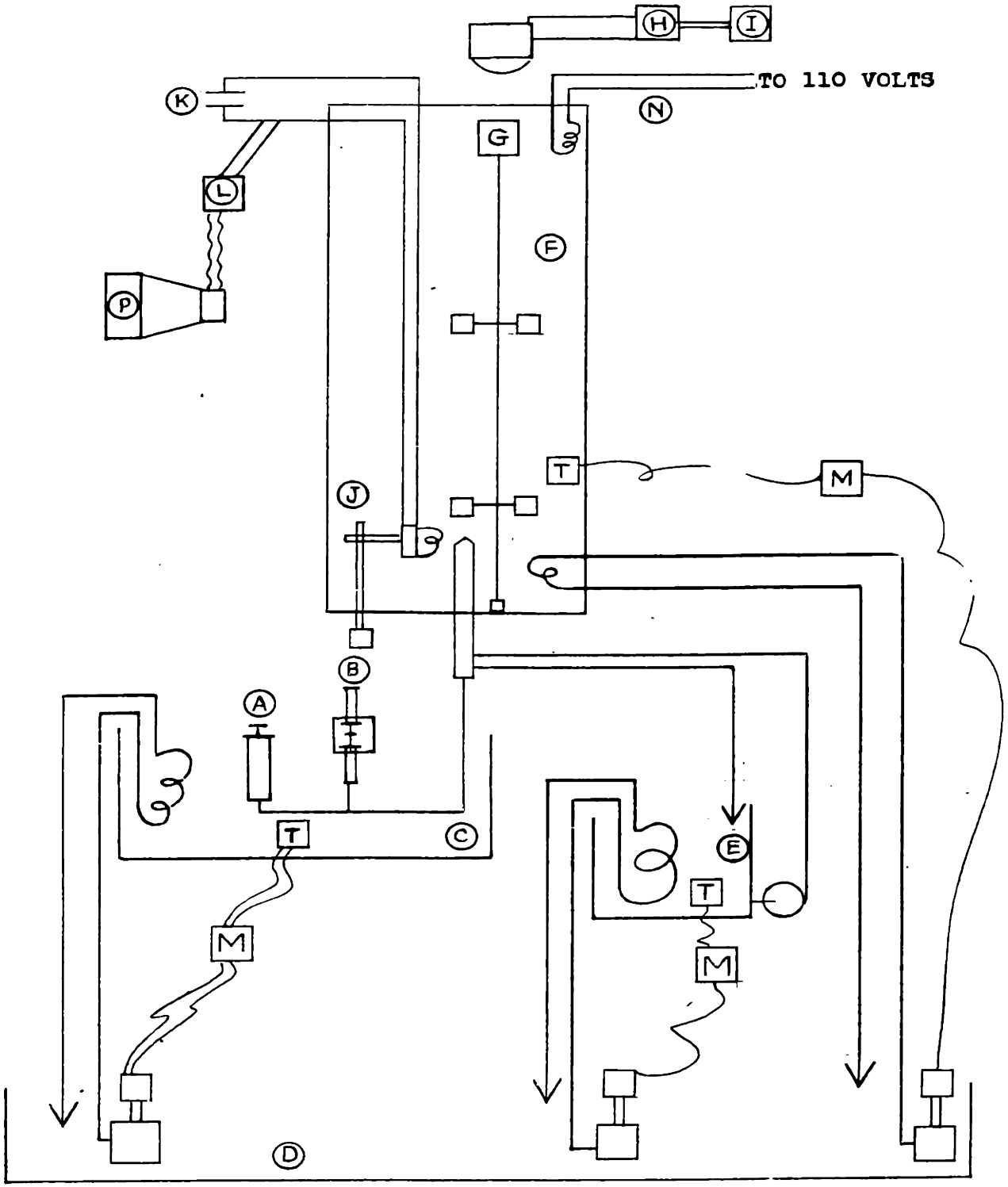

surface through the open tank top. The operation of these devices was controlled from a thermometer set point by a Milltown Model 301A proportional mode controller. Thorough mixing of the tank contents during temperature adjustment was insured by use of two 4" turbine agitators mounted on the tank centerline at 8" and 24" from the tank bottom. The use of an external pumping circuit for mixing and temperature adjustment was tried but discarded; the danger of fluid contamination was increased and the pump impeller action caused desorption of dissolved EtCl with an accompanying fogging of the continuous phase fluid. Temperature drift during the runs (when the control system was shut off) was minimized by insulating the bottom and sides of the tank with two 1-1/2" layers of foam glass.

2. Dispersed Phase Feed System

The dispersed phase feed system consisted of 3 elements: a metering section, a temperature control section and an apparatus for nucleating metered drops. These are shown schematically in Fig. 3.2 and 3.3.

(a) Metering section - The heart of the metering section was a two milliliter syringe driven by a micrometer screw. This was filled from a 50 milliliter supply syringe connected to the feed line through a gas tight needle valve which was closed to prevent backleaking during drop extrusion. 1/8" stainless steel tubing connected the meter syringe to the main feed tube which led up through the tank bottom to the release nozzle. Essential to the success of this system was the assumption that the amount displaced by the metering syringe piston caused an exactly equivalent extrusion of organic liquid at the nozzle tip. The worst hazard faced in trying to assure this was found to be backleaking of continuous phase through the nozzle tip. This caused additional organic fluid to be displaced beyond that metered in. This problem was effectively minimized by installing a small ball check in the feed tube just under the nozzle and by coating the inside walls of the nozzle tip with teflon to enhance its preference for organic phase wetting.

Fig. 3.2 - Details of Droplet Feed System Legend

A 50 ml. glass supply syringe with Luer Lock tip

B Manual screw drive for supply syringe

C Needle Valve

D 2 ml ground glass metering syringe with Luer Lock tip

E Micrometer feed screw (1 turn = .07 ml)

F Jacketed feed tube

G Axial baffle to divide jacket into separate supply and return channels

H Teflon insulating jacket 1/2" thick

I Teflon insulating cap used to hold nozzle in place

J Brass nozzle with 60^{o} outside bevel and Teflon coated inner channel

K Stainless Steel 1/4" ball check spring loaded to 5 lbs. pressure by stainless steel spring L

Figure 3-2

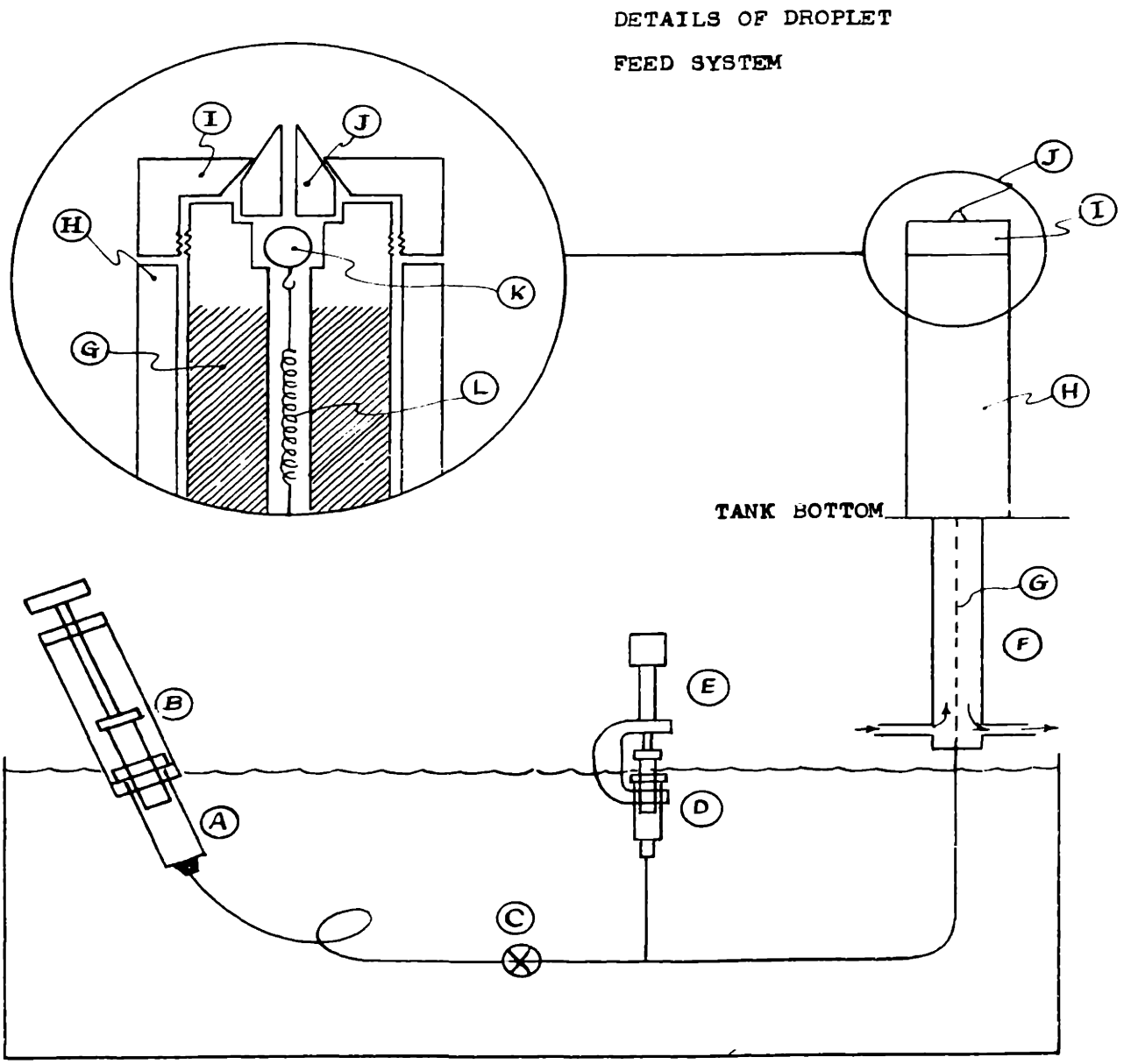
DETAILS OF DROPLET
FEED SYSTEM
I
J
H
K
G
L
J
I
H
TANK BOTTOM
G
F
E
B
A
D
C

Fig. 3.3 - Hot Wire Nucleation System Legend

A Handwheel
B Packing Gland and Bearing
C Threaded post for height adjustment
D Rider bar which holds positioning head
E Stabilizer post on which rider slides
F Teflon positioning head
G .019 inch diameter nichrome nucleating wire
H Extruded drop awaiting nucleation
I Teflon insulated jacketed feed tube
J Screw clamp to hold lead wires in place on positioning head
K No. 10 copper lead wires

Figure 3-3

HOT WIRE NUCLEATION SYSTEM

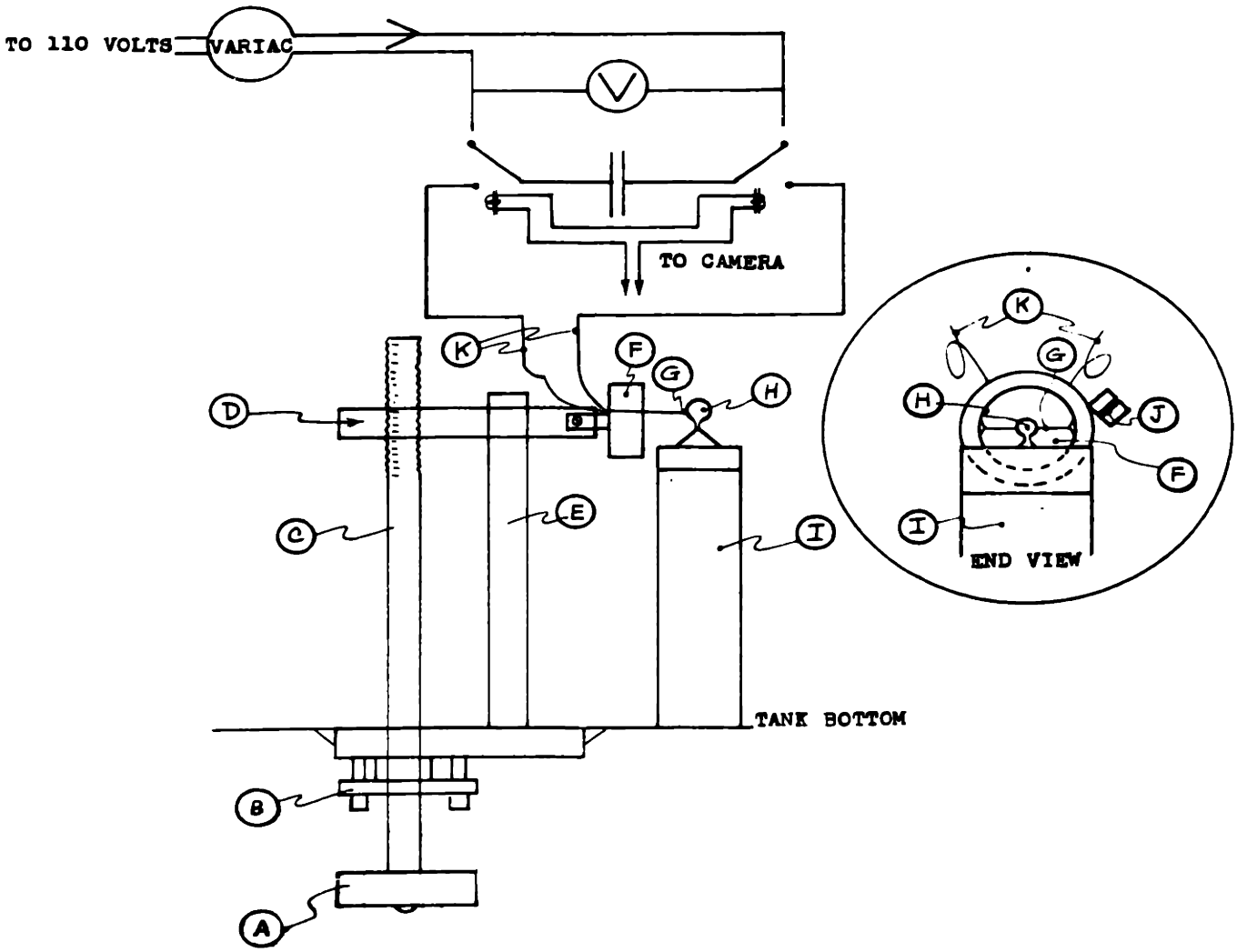

(b) Temperature Control Section - The temperature of the organic phase was controlled in two ways. The supply syringe, the metering syringe and much of the connecting tubing was submersed in a water bath held at $+5^{o}C$. In addition, the vertical rise section of the feed tube leading through the tank bottom to the nozzle was jacketed. Cooling water flowing to this jacket was circulated from a separate thermostatically controlled reservoir so that the temperature of the organic liquid could be separately adjusted to provide a minimum of subcooling consistent with the avoidance of premature drop vaporization. All parts of this jacketed tube inside the tank were insulated from the hot continuous phase by a teflon sleeve. Details of this portion of the feed assembly are shown in the insert of Fig. 3.2.

(c) Nucleating Section - To provide a controlled and reproducible nucleation of the drops an adjustable mounting bracket was built to hold a .019 cm diameter nichrome heating wire in contact with a poised drop. This wire was connected through No. 10 copper leads to a relay which supplied a single short duration power pulse in synchronization with the camera shutter. The pulse was created by discharging a 500 mfd. condenser through the hot-wire circuit. Its energy content was controlled by the size of the DC potential used to charge the condenser between pulses. In general a potential of about 12 volts was used yielding a pulse of .0086 cal (3.4×10^{-5} Btu). Details of the hot wire positioning head are shown in Fig. 3.3 along with the circuitry of the pulsing system.

3. The Photographic System

The most difficult part of the experimental program lay in developing a satisfactory lighting scheme for the bubble photographs. Problems of uneven image lighting and inadequate contrast between image and background frustrated early attempts to collect adequate data. These problems were ultimately solved using the system illustrated in Fig. 3.4 and described below.

The camera was positioned at a mid-height level on an axis normal to the viewing window. A General Radio Strobolume flash lamp was mounted

Fig. 3.4 - LIGHTING SYSTEM

A Camera

B Standard window shade mounted upside down with 6" x 7" window cut as shown

C Flat plate glass viewing window

D Strobolume flash head

E 1" x 48" plate glass mirror strips arranged to provide light reflection from all planes except those seen directly from the camera

F Furane coated stainless steel plate serving as a dead black backdrop

LIGHTING SYSTEM

Figure 3-4

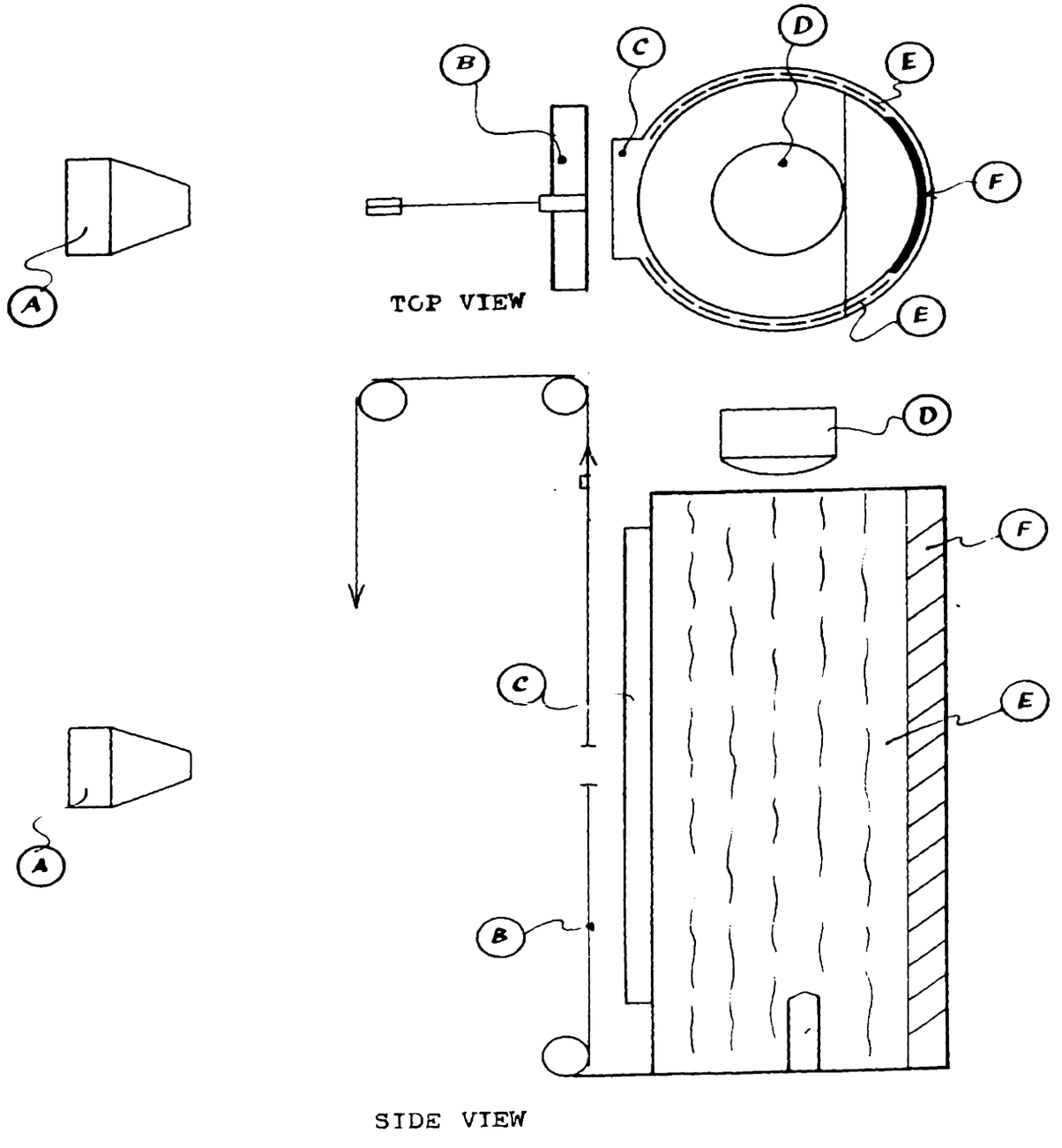

about one foot above the open tank top and concentric with it. The rate of flashing was regulated by a General Radio Strobotac set to provide either 10 or 20 flashes per second. Light from the strobe lamp was reflected onto the curved bubble surface by twenty-one 1" wide strip mirrors, arranged along the tank walls. To improve contrast a stainless steel plate painted with dull black furane resin was positioned in the tank on the back wall directly across from the viewing window. To further increase contrast on the negative, an ordinary window shade through which a ho le had been cut was mounted upside down between the tank and the camera. By moving the hole in the shade in such a way as to have the camera always viewing only that section of the tank through which the bubble was passing, unnecessary overexposure of the whole negative was minimized and an unusually large number of clear images were captured (in excess of 40 compared to maximums of 6 claimed for conventional multi-exposure work (50)).

Polaroid Type 46L film was used in an overexposure underdevelopment scheme which effectively extended its already superior shade separation properties. Additional details of exposure conditions together with a summary of the unsuccessful approaches which were tried is given in Section A3 of the Appendix.

The camera was usually positioned about 6 feet from the viewing window, far enough away to minimize parallex while still close enough to capture a reasonably large bubble image on the negative. For each camera position used one picture was taken of a stainless steel scale placed in the vertical plane of the feed nozzle and set normal to the camera. This provided a dimensional reference standard from which scale factors for the bubble images were later calculated.

B. Experimental Procedure

The experimental procedure can be described most easily in two sections, Run Preparation and Run Execution.

1. Run Preparation:

To obtain dependable results it was found necessary to draw

up a detailed formal procedure for the preparation of both contacting phases and all portions of the equipment.

(a) Equipment

(1) Tank and Feed System: Preparations were begun in every case by disassembling and cleaning all portions of the equipment which came in contact with either phase during the experiments. Trichloroethylene, acetone and distilled water in that order were used as cleansing solvents. Final flushing with the distilled water was continued until no odor of the prior solvents remained. The continuous phase tank was then repositioned and the baffle and mirrors set into place. The metering system was reassembled, tested for air leaks under water and reconnected to the jacketed nozzle line in the tank bottom. Run conditions were selected for the run being undertaken (see Table 3. 1) and filling operations begun.

(2) Hot Wire Pulsing System - Prior to each run the nichrome pulsing wire was checked by resistance measurement to see that it was intact and securely connected. Fresh wire, when needed, was prepared by cleaning it with emery paper before soldering it into place. Each freshly installed wire was deaerated by passing a steady 6 volt DC current through it for about 2 minutes.

(3) Photographic System - While the continuous phase was being saturated and brought to temperature the camera was set up, focused and its distance from the tank recorded. A separate record photograph was taken of the stainless steel scale for each new camera position used. The Strobolume head was mounted in its proper position over the tank and the desired flashing frequency set on the Strobotac. In final preparation for a run several test firings were executed to insure smooth operation of the camera, the lighting system and the hot wire pulsing system.

(b) Continuous Phase - The continuous phase liquid was added to the tank in the required volume and the depth measured and recorded. The tank agitator was installed and the temperature control

Table 3.1

Summary of Experimental Conditions

Run No.	Cont. phase	Disc. Phase	T_c °C	Drop size Initial Diam.
1 - 3	Distilled water	Ethyl chloride	24.6	.301
4 - 5	" "	" "	"	.239
6 - 7	" "	" "	"	.379
8 - 10	" "	" "	32.6	.301
11 - 12	" "	" "	"	.239
13 - 14	" "	" "	"	.379
64 - 67	65% Glycerine 35% Distilled water	" "	24.1	.239
68 - 71	" "	" "	"	.301
72 - 74	" "	" "	31.7	.301
75 - 81	" "	" "	"	.239
82 - 85	Distilled water	" "	18.1	.239
86 - 89	" "	" "	"	.301
90 - 92	" "	" "	"	.379
93 - 95	Distilled water plus .00575 wt. % Aerosol 22	" "	24.5	.379
96 - 98	" "	" "	"	.301
99 - 102	" "	" "	"	.239
103 - 106	Distilled water plus .074 wt. % Aerosol 22	" "	"	.239
107 - 109	" "	" "	"	.301
110 - 113	Distilled water plus .135 wt. % Aerosol 22	" "	"	.301
114 - 118	" "	" "	"	.239

Table 3.1

Summary of Experimental Conditions

Run No.	Cont. phase	Disc. Phase	T_c °C	Drop size Initial Diam.
1 - 3	Distilled water	Ethyl chloride	24.6	.301
4 - 5	" "	" "	"	.239
6 - 7	" "	" "	"	.379
8 - 10	" "	" "	32.6	.301
11 - 12	" "	" "	"	.239
13 - 14	" "	" "	"	.379
64 - 67	65% Glycerine 35% Distilled water	" "	24.1	.239
68 - 71	" "	" "	"	.301
72 - 74	" "	" "	31.7	.301
75 - 81	" "	" "	"	.239
82 - 85	Distilled water	" "	18.1	.239
86 - 89	" "	" "	"	.301
90 - 92	" "	" "	"	.379
93 - 95	Distilled water plus .00575 wt. % Aerosol 22	" "	24.5	.379
96 - 98	" "	" "	"	.301
99 - 102	" "	" "	"	.239
103 - 106	Distilled water plus .074 wt. % Aerosol 22	" "	"	.239
107 - 109	" "	" "	"	.301
110 - 113	Distilled water plus .135 wt. % Aerosol 22	" "	"	.301
114 - 118	" "	" "	"	.239

system set to bring the temperature to the required value. To minimize ethyl chloride absorption during the runs gaseous ethyl chloride was fed through the feed nozzle into the eye of the lower impeller for about four hours. An amount equivalent to one to two times the weight required for full saturation was fed and adequacy of saturation tested by careful observation of the rising bubbles for any signs of shrinkage.

After saturation was complete, the entire metering system was filled with distilled water, all air bubbles carefully removed and final connection to the jacketed feed line made. The water bath which surrounded the feed system was then filled with distilled water to the bottom of the feed tube jacket and set to cool to $+5^{\circ}C$.

When the continuous phase temperature had stabilized at the proper value, samples of the continuous phase were removed and measurements made of significant physical properties (i.e. surface tension for runs with Aerosol 22 added, density and viscosity for runs with glycerin added). Any major deviations from desired levels were corrected by enriching the tank contents in the deficient component.

After all preparations and adjustments had been carried out, the tank temperature was noted and the agitator removed just prior to run execution.

(c) Dispersed Phase Preparation - Liquid ethyl chloride was obtained in 150 ml. aliquots by withdrawing it from an inverted storage cylinder into a dry ice - methanol trap. This cold liquid was filtered through silica gel and aluminum oxide powder to remove solid particle which might cause uncontrolled nucleation and to absorb any traces of dissolved surfactants.

In some of the early runs (1-14) the ethyl chloride was vigorously shaken with distilled water to presaturate the dispersed phase. This was later abandoned (run 15 on) because crystals (presumably a hydrate of ethyl chloride) began forming in the feed lines and syringes, causing

severe plugging problems. Since the solubility of water in boiling ethyl chloride is only .12% by weight it was assumed that experimental behavior would be unaffected by this change.

Next the feed sample was refluxed under high vacuum for ten minutes to remove all dissolved air.

Lastly, the feed was packed in ice to await charging to the feed system.

When the feed system and surrounding bath had cooled to the set point of $+5^{o}C$, the 50 ml supply syringe was disconnected from the feed line and filled with the prepared ethyl chloride. The smoothest filling was achieved when the ethyl chloride temperature was between 0 and $8^{o}C$. Material colder than 0^{o} caused the syringe plunger to stick and material hotter than $8^{o}C$ caused vapor to form in the syringe so that a full load could not be drawn in.

The full syringe was reconnected and about 20 ml of ethyl chloride forced through the feed lines to clear them of distilled water. Finally, the metering syringe was loaded from the supply syringe and the needle valve between them closed.

2. Run Execution

With all equipment readied run execution followed the following sequence:

a) The nozzle was flushed with about half a cc of ethyl chloride to clear out any water and bring fresh solvent up to the tip.

b) A preliminary drop was extruded to properly establish the point of release.

c) The test drop was extruded into poised position on the tip of the nozzle touching the nucleating wire.

d) The window in the moving shade was positioned so as to give the camera a clear view of the poised drop.

e) Room lights were extinguished and the strobe light turned on.

f) The camera shutter was opened pulsing the nucleating wire and releasing the drop.

g) The camera shutter was held open and the window in the shade moved to follow the rising drop to the surface.

h) The shutter was closed and the film developed for 40 sec. (normal time, 2 min.).

i) The film was evaluated, coated and stored.

In addition to the photographic record, notation was made of barometric pressure, feed tube jacket water temperature, flashing frequency, capacitor charging voltage, metering plunger displacement and continuous phase temperature before and after the run.

C. Data Processing

Each record film was made into a projection slide and projected onto millimeter graph paper. The outline of each bubble was traced onto the paper and the nozzle tip outline marked as a reference point.

From the graphs measurements were made of bubble width, bubble height and bubble distance from the nozzle tip. These constituted the main experimental data. Scale values for each image were assigned by comparing measured dimensions with the dimensions of an image of the stainless steel standard photographed from the same camera position. A computer program was developed from the methods of calculation presented in the appendix which converted the raw data into the calculated values presented in Chapter 4 and Table A-2 of the Appendix.

CHAPTER 4 - EXPERIMENTAL RESULTS

Because of the exploratory nature of this study, both qualitative and quantitative results represent important products of the experimental work. These are presented in the two separate sections which follow.

A. Qualitative Observations

For the purposes of this section, the experimental event will be divided into three sections. The release step, the vaporization step and the post-vaporization step. In each section, generalized behavior will be described followed by comments on behavior differences noted with changes in the experimental conditions.

1. Release Step

(a) General - In general a clean and instantaneous release was achieved when the nucleating hot wire was pulsed. A tiny vapor nucleus was formed on the side of the drop tangential to the liquid-liquid interface at the point where the wire touched the drop surface. This nucleus began growing immediately while simultaneously moving along the interface toward the top of the drop and lifting the drop clear of the nozzle. Although the positioning of the nucleating wire was frequently such as to displace the drop slightly sideways from its equilibrium vertical position, the rising drop did not make any excursions from the vertical axis which could be directly attributed to this displacement. Controlled release of single drops without fracture was easily achieved under most conditions. Observations of liquid left on the nozzle after release showed that separation occurred reproducibly approximately in the plane of the nozzle tip.

(b) Effect of Drop Size - No differences in release behavior were observed between the various drop sizes. All released with equal smoothness requiring about the same nucleation energy.

(c) Effect of Temperature - The main influence of temperature on drop release was seen in a trend toward a lowered nucleation energy requirement for higher temperature driving forces. The energy

required ranged from a low of .001 calories for the highest driving force to .016 for the lowest driving force.

This amount of energy is small compared to the energy required for total drop vaporization. Visual observations and photographs show that the drop is well clear of the wire before even .3% of the contained liquid is vaporized.

For runs at the lowest ΔT, excursions from a vertical path were noted in the range of .12 to .58 cm. from the nozzle axis line with a mean of .4 cm. These occurred in the first 5 cm. of drop rise. In most cases the drops returned about 3/4 of the way to the vertical axis of the nozzle. In some cases recovery was less complete and in the case where large drops were used a second counter excursion to the opposite side usually occured before the rising drop stabilized on its original path. (See Fig. 4.1 for an example).

(d) Effect of Continuous Phase Properties - Drop release in 65% and 86% glycerine solutions though similar, differed from behavior in plain water as follows: The maximum drop size which could be held on the nozzle tip was reduced to less than half that for plain water because of greater drop buoyancy resulting from increased continuous phase density. The rate of departure and early rise was slowed down considerably because of a much greater continuous phase viscosity. No oscillations or vertical excursion in the early rise period were observed at any level of ΔT.

(e) Effect of Surfactant - The addition of a surface active agent to the plain water external phase reduced the maximum size of drops which could be held on the nozzle tip and caused some drops to break up upon release. After separation no differences were noted in the early stages of rise. At low ΔT's, an excursion effect was noted which was quite similar to that observed in plain water.

2. Vaporization Step

(a) General - Most of the vaporizing drops rose smoothly up the column with only minor random excursions from a stable vertical

Figure 4-1

SAMPLE OF DROP OSCILLATION PATTERN OBSERVED FOR LARGE DROP AT LOW Δ T.

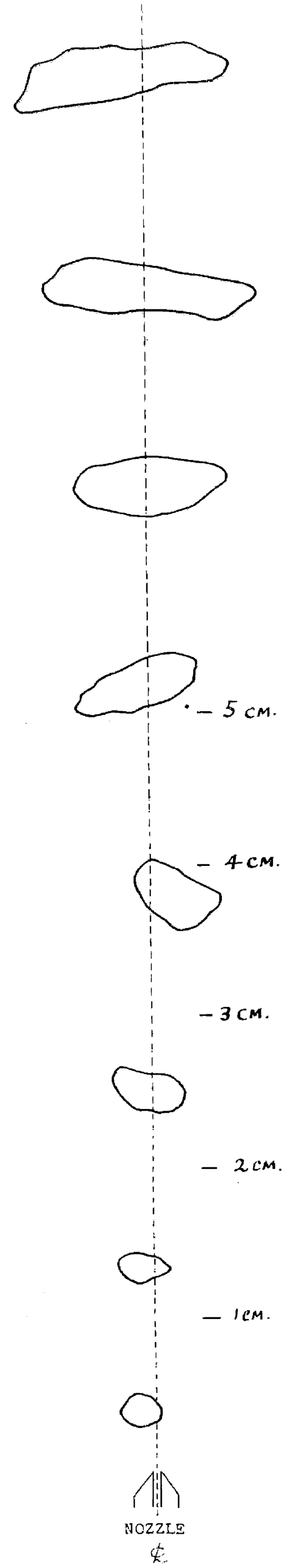

path. As vapor generation caused the bubble-drop size to grow, its shape changed gradually from spherical through ellipsoidal to spherical cap. At no stage was there any sign that the presence of liquid was causing any unusual surface distention or distortion of the basic shape. All shapes were oblate in form as predicted from work by Saito cited in Hughes & Gilliland (41). (See Fig. 4.2 for visualisation of the basic shape and hypothetical disposition of unvaporized liquid). There was some shape oscillation around these basic forms under most conditions. Visual observations indicated that turbulence along the path of the drop was localized to a region extending to less than twice the projected radius from the axis of travel. It died out within a few seconds after each bubble passed.

(b) Effect of Drop Size - The only noticable effect of drop size on vaporization behavior was a slight increase in shape oscillation with decreasing drop size.

(c) Effect of Temperature Driving Force - Greater shape oscillation was seen at the lowest level of ΔT. A clear increase in heat transfer with increasing ΔT was apparent.

(d) Effect of Continuous Phase Properties - Drop behavior during vaporization in 65% and 86% glycerine solutions was quite different from that in plain water. There was no sign of either shape or path oscillation.

All the drops studied in glycerine solutions suffered from unexpectedly high absorption losses so that direct cross comparison on an absolute basis was not possible. Nevertheless, some drops showed only slight losses so that rate comparisons referred to observed peak sizes can still be used.

(e) Effect of Surfactant - The only obvious effect of surfactants was to make possible greater shape oscillation leading occasionally to bubble breakup or split before the end of its rise.

3. Post-Vaporization Step

Motion of each fully vaporized bubble followed the pattern

TYPICAL BUBBLE SHAPES
WITH HYPOTHESIZED DISPOSITION
OF THE UNVAPORIZED LIQUID

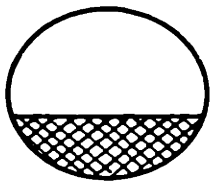

SPHERE

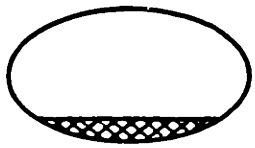

ELLIPSOID

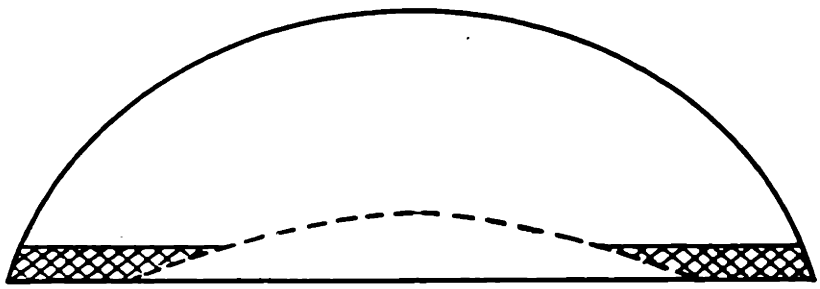

SPHERICAL CAP

established by the corresponding vaporizing drop. The extent of shape and path oscillation was about the same; the same decreased stability in the presence of surfactants and increased stability with a more viscous continuous phase was observed. Behavior of these bubbles was fully consistent with descriptions given in the literature for single normal gas bubbles of the same size (33, 62).

B. Quantitative Observations

There are two basic types of data available from the experimental measurements. These are the heat transfer data and the hydrodynamic data. To generate the former, rates of vaporization are calculated from successive bubble volume measurements. Bubble position and shape measurements are used to develop the latter. A plot of heat content versus time is presented for all the plain water runs in Fig. 4.3. Fig. 4.4 presents the same data for runs where surface active agents were added. Fig. 4.5 shows the results of selected runs using 65% glycerine as the continuous phase. Rates of rise for all three conditions are compared in Fig. 4.6 and 4.7.

1. Reproducibility, Precision and Accuracy

Before quantitative conclusions can be drawn evaluations of data precision and accuracy must be made together with some demonstration that differences shown for contrasted experimental conditions significantly exceed the range of experimental error.

(a) Reproducibility - Although a nominal value of drop size and temperature driving force was selected for each run, variations in the functioning of the equipment caused actual experimental conditions to vary somewhat from the selected values. Because of the comparitively large volume of continuous phase, temperature variations were slight within a given experimental set and cannot be considered to have effected reproducibility. Variation in drop size appears to have been substantial, however, as seen from differences in the asymptotic heat content values achieved by nominally duplicate runs. A tabulation of nominal and observed values for the plain water-EtCl runs and the runs in which a surfactant

Figure 4-3 BUBBLE HEAT CONTENT V^s TIME FOR DROP SIZES AND ΔT'S SYSTEM: Et-Cl - WATER

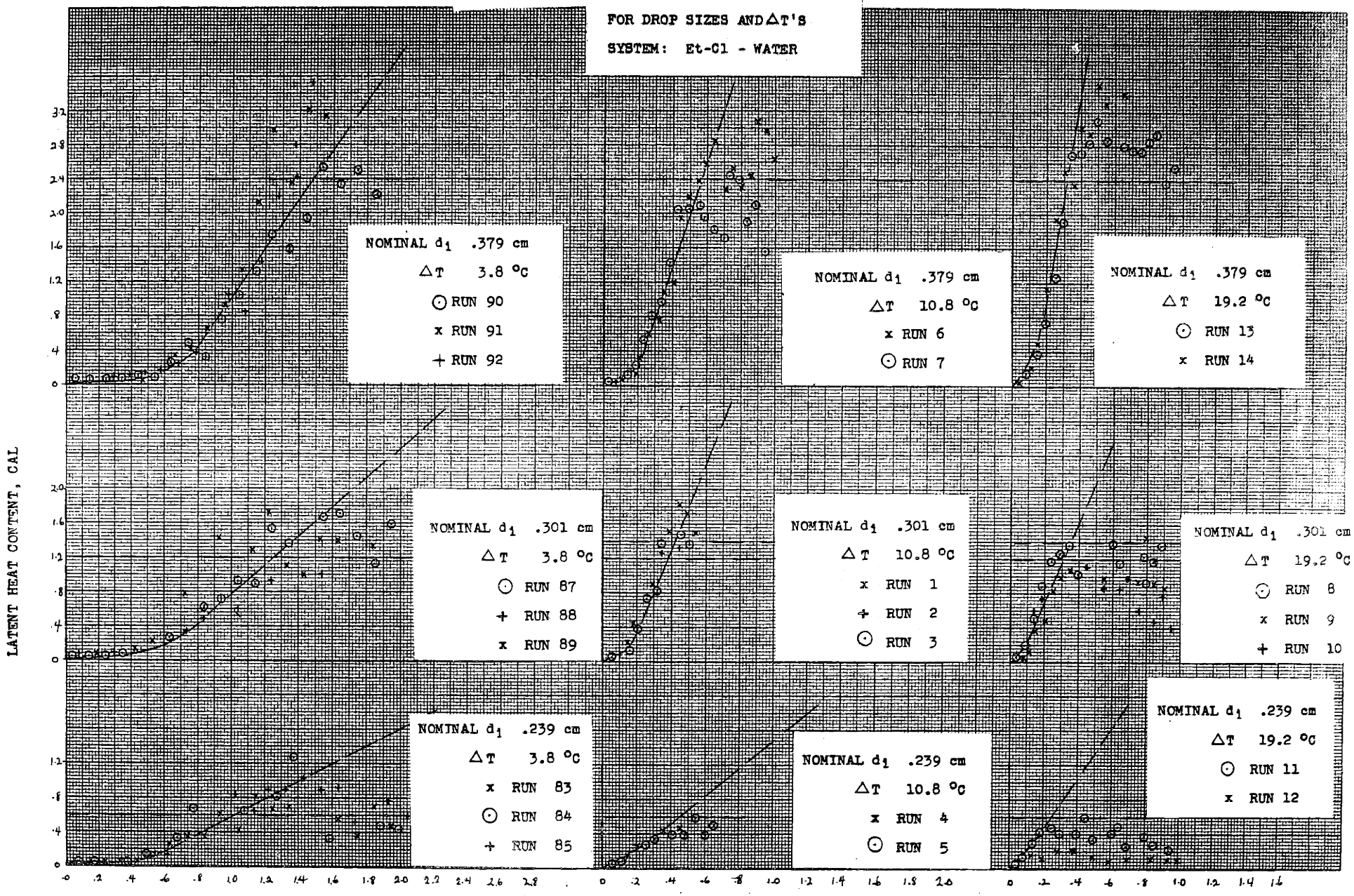

Figure 4-4

BUBBLE HEAT CONTENT V^s TIME

FOR VARIOUS DROP SIZES AND SURFACTANT CONCENTRATIONS (WEIGHT % IN WATER)

SYSTEM: ETHYLCl - WATER WITH AEROSOL 22

TEMPERATURE DRIVING FORCE 10.8 °C

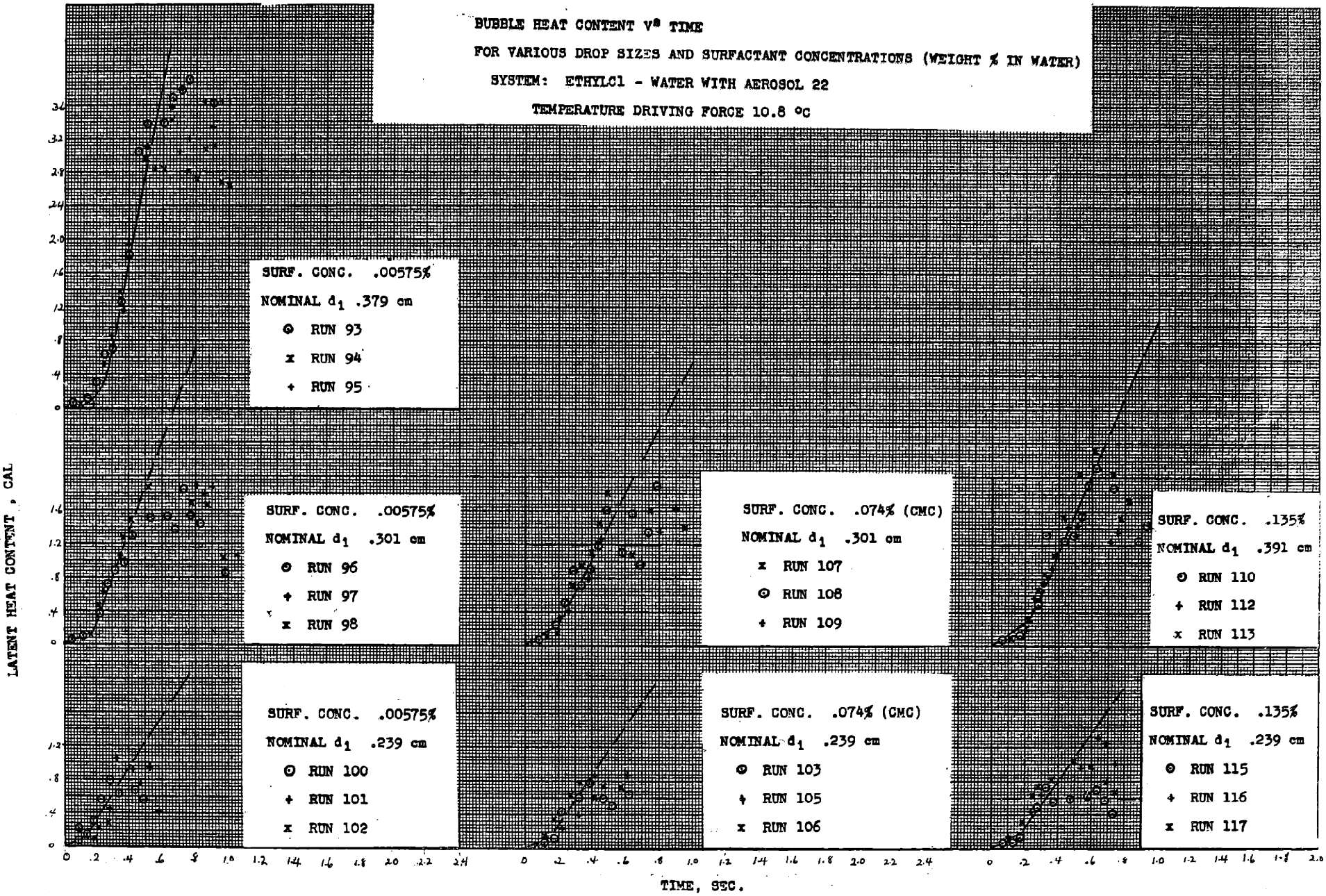

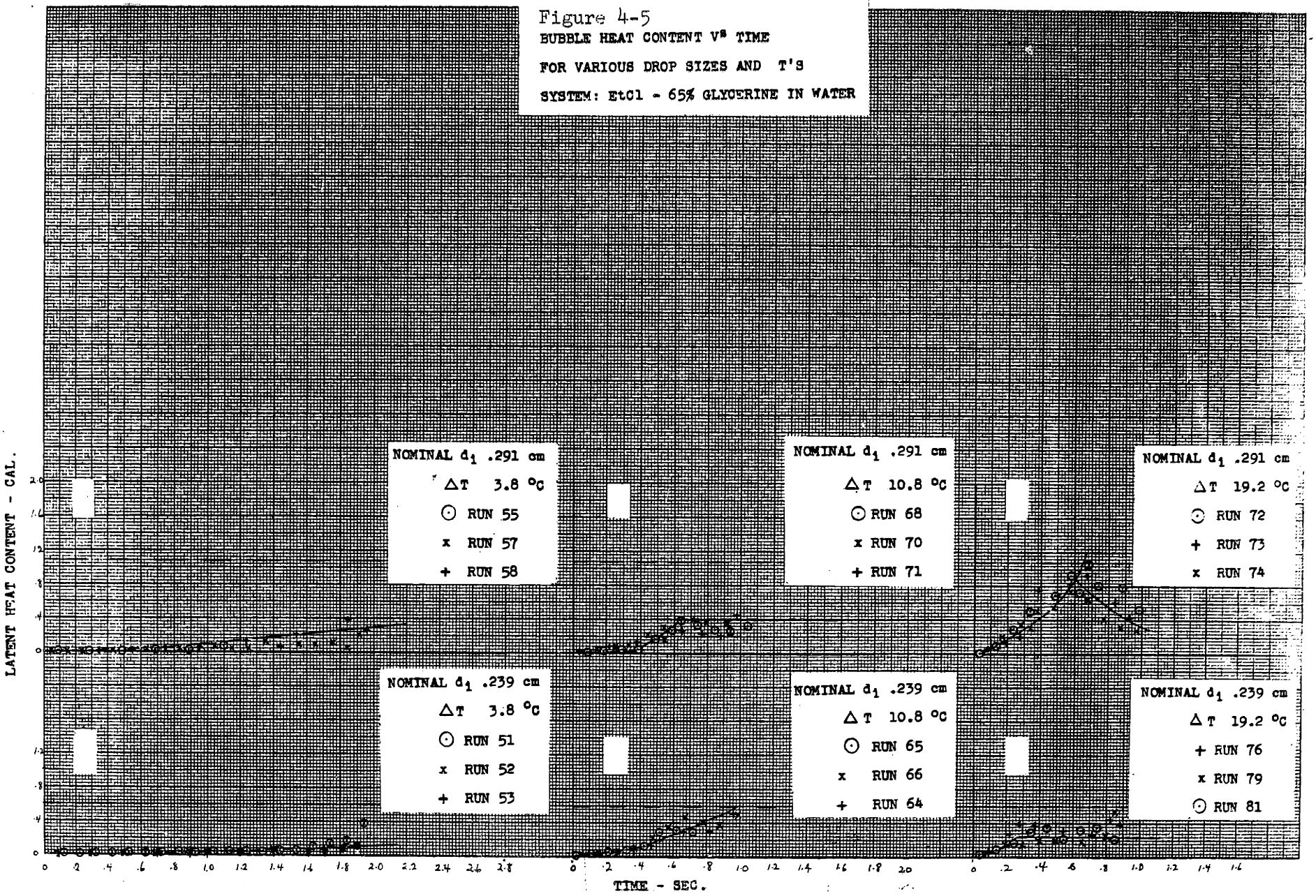

Figure 4-5
BUBBLE HEAT CONTENT V^s TIME
FOR VARIOUS DROP SIZES AND T'S
SYSTEM: EtCl - 65% GLYCERINE IN WATER

Figure 4-6

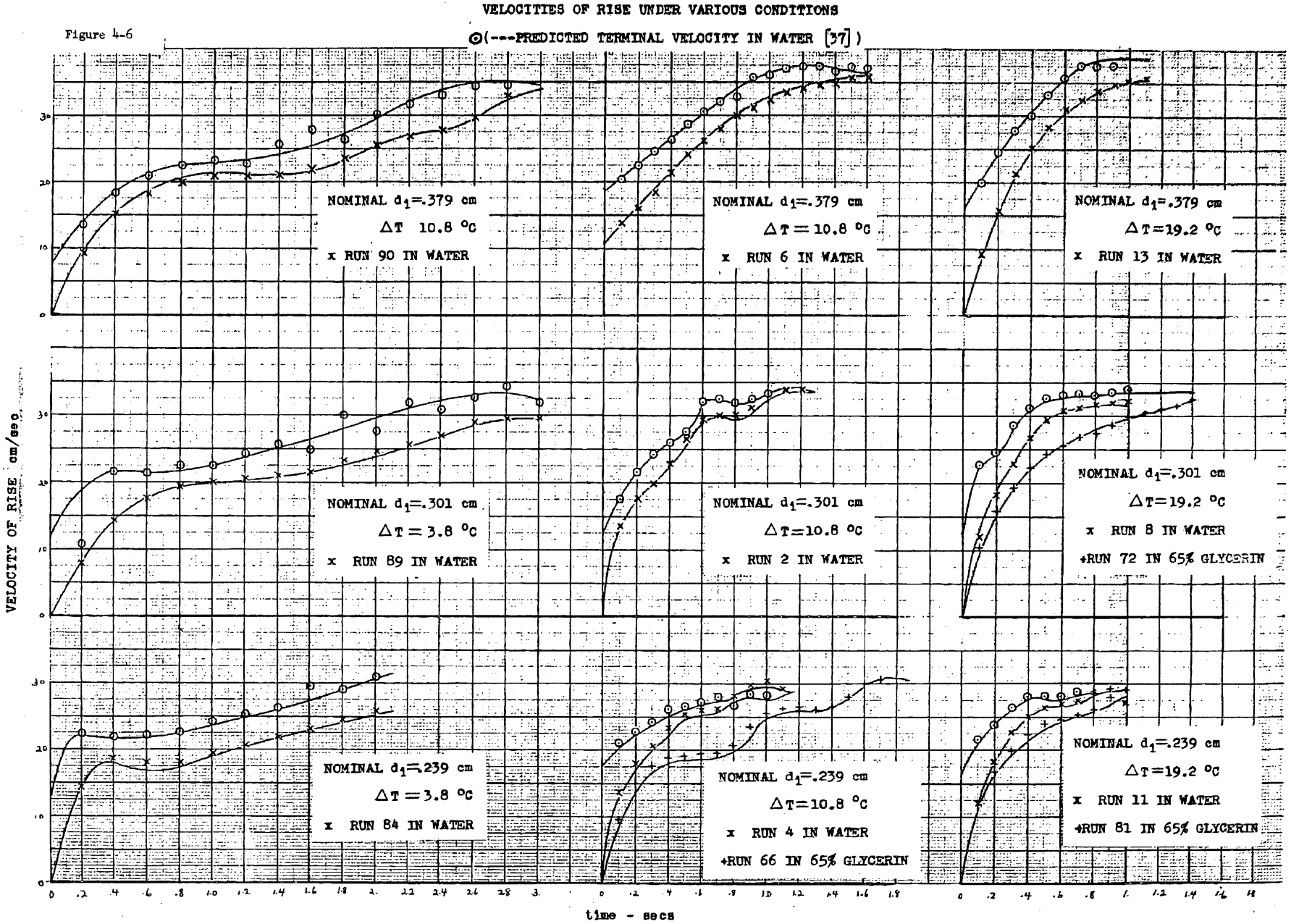
VELOCITIES OF RISE UNDER VARIOUS CONDITIONS
⊙(---PREDICTED TERMINAL VELOCITY IN WATER [37])
NOMINAL d_1=.379 cm
ΔT 10.8 °C
x RUN 90 IN WATER
NOMINAL d_1=.379 cm
ΔT = 10.8 °C
x RUN 6 IN WATER
NOMINAL d_1=.379 cm
ΔT=19.2 °C
x RUN 13 IN WATER
NOMINAL d_1=.301 cm
ΔT = 3.8 °C
x RUN 89 IN WATER
NOMINAL d_1=.301 cm
ΔT=10.8 °C
x RUN 2 IN WATER
NOMINAL d_1=.301 cm
ΔT=19.2 °C
x RUN 8 IN WATER
+RUN 72 IN 65% GLYCERIN
NOMINAL d_1=.239 cm
ΔT = 3.8 °C
x RUN 84 IN WATER
NOMINAL d_1=.239 cm
ΔT=10.8 °C
x RUN 4 IN WATER
+RUN 66 IN 65% GLYCERIN
NOMINAL d_1=.239 cm
ΔT=19.2 °C
x RUN 11 IN WATER
+RUN 81 IN 65% GLYCERIN
VELOCITY OF RISE cm/sec
time - secs

Figure 4-7

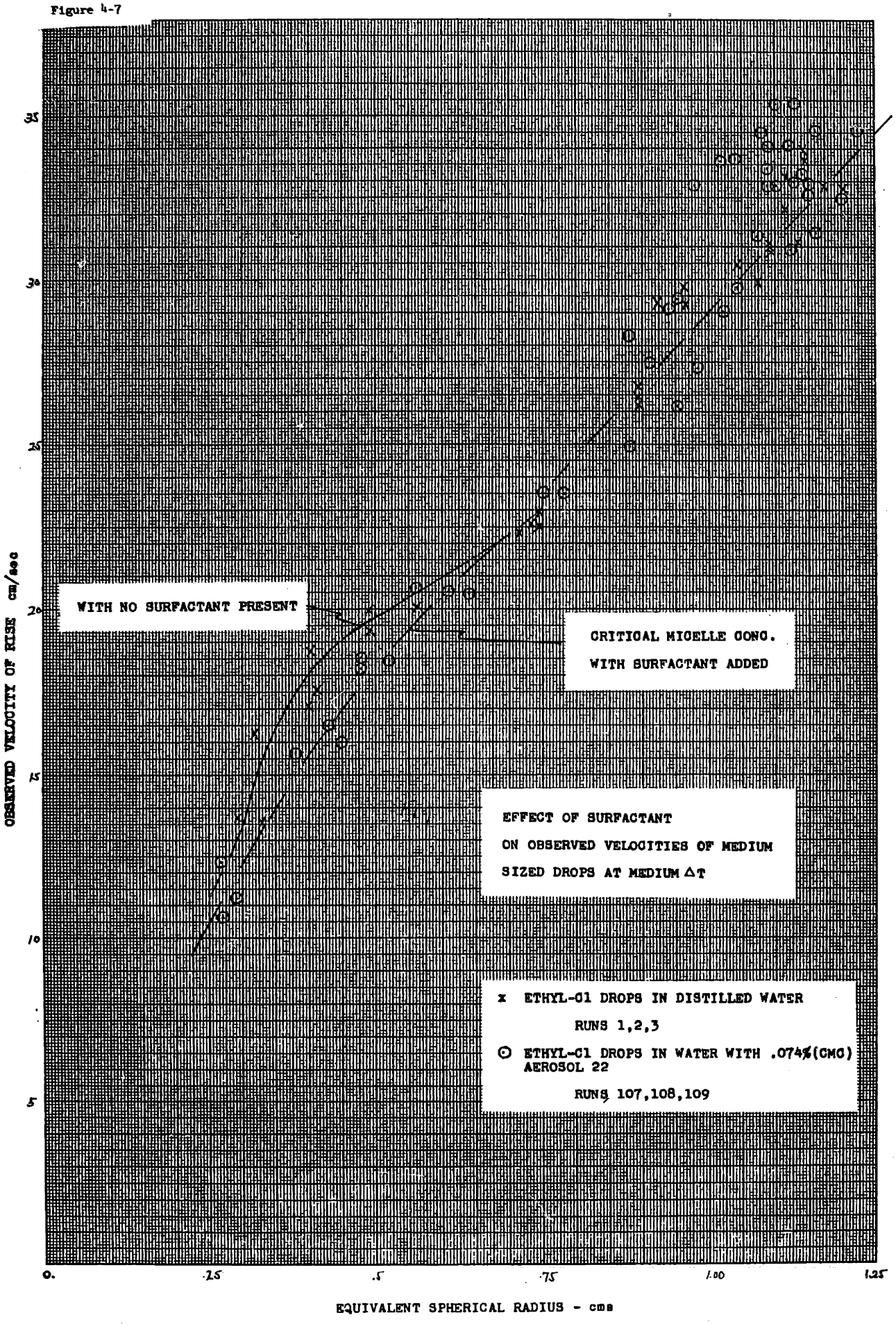
OBSERVED VELOCITY OF RISE cm/sec
35
30
25
20
15
10
5
0.
.25
.5
.75
1.00
1.25
EQUIVALENT SPHERICAL RADIUS - cms
WITH NO SURFACTANT PRESENT
CRITICAL MICELLE CONC.
WITH SURFACTANT ADDED
EFFECT OF SURFACTANT
ON OBSERVED VELOCITIES OF MEDIUM
SIZED DROPS AT MEDIUM ΔT
x ETHYL-Cl DROPS IN DISTILLED WATER
RUNS 1,2,3
⊙ ETHYL-Cl DROPS IN WATER WITH .074%(CMC) AEROSOL 22
RUNS 107,108,109

was added are given in Tables 4.1 and 4.2. In the system involving plain water, a random pattern of deviation from the nominal values is observed while results from the surfactant runs show a pattern of deviations consistently on the high side. It is reasonable to expect such a difference since the surface forces involved in drop release would certainly be altered by the presence of a surfactant. This deviation to the larger rather than smaller side though is somewhat unexpected. However, if the surfactant served to reduce the contact angle of ethyl chloride with the teflon coating in the nozzle, this could have caused the drop separation plane to recede further into the nozzle orifice thereby resulting in a larger drop than was released when the surfactant was not present.

(b) Precision - The main measurements which could contain appreciable error are those of position, drop size, and temperature. By comparison, errors in measuring such background data as depth, barometric pressure, concentrations and system physical properties play a sufficiently minor role in the data reduction scheme to be safely ignored.

Because of the interdependance of linear and volumetric measurements within the data analysis, deviation in linear measurement will simply be considered to be the equivalent of the cube root of volumetric deviation. The latter can be evaluated from measurements made on successive photographic images of each fully vaporized drop. Tabulation of error estimates from the individual runs may be found in Tables 4.1 and 4.2. As these tables show, average volumetric deviation is calculated as $\pm 15.7\%$ for the runs with EtCl and plain water and $\pm 12.5\%$ for runs with surfactant added. These errors show no correlation with temperature and only a mild correlation with drop size. This suggests that mass and volumetric comparisons of groups of data, e.g. averages of runs or regression coefficients, will be meaningful in any direction through the experimental region whenever the average deviations quoted above are

TABLE 4.1

Nominal Vs. Observed Values for Experimental Drop Sizes

System: EtCl - Distilled Water

Nominal Size	ΔT, °C					
	3.8 (low)		10.8 (med.)		19.2 (high)	
Latent Heat Cont., Cals.	Run No.	Obs. Size	Run No.	Obs. Size	Run No.	Obs. Size
.6 (low)	83	.56± .11	4	.47± .06	11	.39± .06
	84	.66± .20	5	.46± .17	12	.14± .04
	85	.78± .12				
1.2 (med.)	87	1.45± .17	1	1.59± .30	8	1.28± .05
	88	1.07± .18	2	1.40± .12	9	.98± .14
	89	1.30± .16	3	1.36± .20	10	.95± .13
2.4 (high)	90	2.37± .23	6	2.63± .22	13	2.84± .08
	91	3.31± .58	7	1.95± .26	14	3.03± .35
	92	4.05± 1.09				

Average % Confidence Interval ± 15.7%

TABLE 4.2

Nominal Vs. Observed Values for Experimental Drop Sizes

System: EtCl - Water + Aerosol 22

Nominal Size Latent Heat Content, Cal.	Weight % - Surfactant .00575 Run No.	.00575 Obs. Size	.074 (CMC) Run No.	.074 (CMC) Obs. Size	.135 Run No.	.135 Obs. Size
.6	100	.71 ± .09	103	.64 ± .06	115	.84 ± .10
	101	.83 ± .20	105	.71 ± .13	116	1.10 ± .17
	102	1.01 ± .16	106	.71 ± .07	117	.61 ± .07
1.2	96	1.43 ± .18	107	1.42 ± .21	110	1.60 ± .23
	97	1.64 ± .22	108	1.47 ± .20	112	1.50 ± .24
	98	1.58 ± .16	109	1.41 ± .07	113	1.73 ± .26
2.4	93	3.99 ± .39				
	94	2.95 ± .18				
	95	3.50 ± .19				

Average % Confidence Interval ±12.5%

TABLE 4.2

Nominal Vs. Observed Values for Experimental Drop Sizes

System: EtCl - Water + Aerosol 22

Nominal Size Latent Heat Content, Cal.	Weight % - Surfactant .00575 Run No.	.00575 Obs. Size	.074 (CMC) Run No.	.074 (CMC) Obs. Size	.135 Run No.	.135 Obs. Size
.6	100	.71 ± .09	103	.64 ± .06	115	.84 ± .10
	101	.83 ± .20	105	.71 ± .13	116	1.10 ± .17
	102	1.01 ± .16	106	.71 ± .07	117	.61 ± .07
1.2	96	1.43 ± .18	107	1.42 ± .21	110	1.60 ± .23
	97	1.64 ± .22	108	1.47 ± .20	112	1.50 ± .24
	98	1.58 ± .16	109	1.41 ± .07	113	1.73 ± .26
2.4	93	3.99 ± .39				
	94	2.95 ± .18				
	95	3.50 ± .19				

Average % Confidence Interval ±12.5%

appreciably exceeded. Correspondingly linear deviations due to experimental error are estimated as ±4.8% and ±3.9% respectively.

Precision in time measurements depends upon the reliability of the strobotac flash frequency. An estimate of error in time measurement will be taken as ±1.% based upon manufacturer's specifications for the instrument used (27). Since appreciable deviation in this measurement is unlikely when the unit is calibrated according to the instructions, it will be treated as a primary standard.

The precision in reading temperature is affected in two ways: by fineness of scale divisions on the thermometer and by the degree to which a spot temperature at the beginning of the run may fail to represent the true water phase temperature along the path as a given bubble rises. The second factor is by far the most important since reading precision could have caused no more than a 1.4% error in the lowest temperature runs. At the beginning of each run water temperature was made effectively uniform by intensive mixing prior to measurement. Thus the major source of error was a temperature drift during operation. This may be estimated, from temperature readings taken before and after each run, to be approximately .4 degree Centigrade. This is a minor contribution to all runs except those runs at the lowest ΔT's. Even there, however, the maximum effect is less than ±12% or roughly the same magnitude of error as for the volumetric measurements.

(c) Accuracy - Again, as above, the major area of uncertainty is in the linear and volumetric measurements both because of the use of reflective photography of curved surfaces and the use of empirical estimating procedures in the data reduction scheme. To gain some indication of data accuracy sizes calculated for fully vaporized bubbles were compared with size estimates made from the measured terminal velocities through the correlations of Haberman and Morton (33). These comparisons are shown in Table 4.3. The data for runs 1-14 show a random scatter of ratios with a mean ratio of 1.03. Comparing the observed velocity of rise with that predicted for the observed size

Table 4.3

Measure of Data Accuracy. Comparison of Observed Terminal Sizes Vs. Those Predicted from Terminal Velocity of Rise Data

Run No.	Nom. Size	Obs. Size	Predict. Size	Ratio Obs. Size / Pred. Size	Obs. Term Vel.	ΔT	Term Vel. of Obs. Size	Ratio Pred. Vel. / Obs. Vel
1	1.2	1.59		-		10.8		
2	1.2	1.40	1.38	1.01	32.8	10.8	32.9	1.00
3	1.2	1.36	1.44	.94	33.0	10.8	32.7	.99
4	.6	.47	.64	.90	29.7	10.8	27.9	.94
5	.6	.46	-	-		10.8		-
6	2.4	2.63	2.30	1.14	35.6	10.8	35.9	1.01
7	2.4	1.95	1.93	1.01	34.4	10.8	34.6	1.01
8	1.2	1.28	1.16	1.10	32.0	19.2	32.2	1.01
9	1.2	.98	.91	1.08	30.7	19.2	31.1	1.01
10	1.2	.95	1.13	.84	31.6	19.2	30.9	.98
11	.6	.39	.45	.87	27.7	19.2	27.3	.99
12	.6	.14	-	-	-	19.2	-	-
13	2.4	2.84	2.13	1.33	35.1	19.2	36.8	1.05
14	2.4	3.03	2.80	1.08	36.6	19.2	37.1	1.01
			Av.	1.03			Av.	1.00
83	.6	.56	.27	2.07	26.0	3.8	28.6	1.10
84	.6	.66	.37	1.78	27.1	3.8	29.3	1.08
85	.6	.78	.22	3.58	25.4	3.8	30.0	1.18
87	1.2	1.45	.96	1.51	31.0	3.8	33.0	1.06
88	1.2	1.07	.69	1.55	29.5	3.8	31.4	1.06
89	1.2	1.30	.75	1.73	29.8	3.8	32.4	1.09
90	2.4	2.37	1.62	1.46	33.5	3.8	35.7	1.07
91	2.4	3.31	1.64	2.02	33.6	3.8	37.7	1.12
92	2.4	4.05	1.54	2.63	33.2	3.8	39.0	1.17
			Av.	2.03			Av.	1.09

by Haberman and Morton gives an average ratio of predicted velocity to observed velocity of 1.00. In view of the strong sensitivity of velocity measurements to small errors in the time interval and linear displacement measurements, this degree of consistency indicates that a high order of accuracy had been achieved.

Runs 83-92 show indications of a much larger discrepancy in that the ratio of observed to predicted size is 2.03. However, since the companion ratio of predicted to observed velocity of rise in only 1.09, it is clear that a fairly minor error in velocity measurement or in the assumptions on which the velocity-size correlation was built could be responsible for almost all of the inaccuracy implied. Although interfacial contamination might have significantly increased the drag, it is unlikely that any single error could have caused all observed bubble velocities to be 9% too low. In addition, the use of a colder more viscous continuous phase, less effective lighting and slight timing light errors were probably all involved. However, it is unlikely that the results from runs 83-92 are sufficiently biased to restrict their utility in this study.

Reasonable accuracy in the measurement of temperature was insured by the use of a thermometer calibrated to $\pm .03^{\circ}$ centigrade.

2. Direct Observations - Heat Transfer

Quantitative comparison of the basic data given in Figs. 4.3, 4.4 and 4.5, allow us to examine directly the form of dependence which heat transfer rate has upon drop size, temperature driving force, continuous phase properties and the presence of surfactant. Because the drop size was hardest to control, we must first correlate heat transfer data against drop size so that cross correlation at standard drop sizes may be used in the other comparisons.

Average vaporization rate is selected as the main correlating response since this has the greatest utility for practical applications. This value can be extracted from the data for each run by estimating the time at which vaporization is essentially complete, and dividing it

into the assymptotic terminal size. The resulting rate values are tabulated in Table A-3 of the appendix.

(a) Effect of Drop Size - The effect of drop size on over-all heat transfer rates is shown in Fig. 4.8.

Least squares regression coefficients were developed from the three sets of data shown for the model,

$$\text{Log (Rate)} = \text{Log } a + b \text{ Log (Latent Heat Content)}.$$

These are:

ΔT	b, Slope Coeff.	a, Intercept Coeff.
Low (3.9°C)	.64 ± .14	.95 ± .09
Med (10.9°C)	.78 ± .20	2.48 ± .30
Large (19.2°C)	.66 ± .12	4.17 ± .52

To explore the implications of these results, let us examine them in the context of the conventional heat transfer equations.

$$q_A = US\Delta T; Nu = a + b\, Re^y Pr^z$$

For a single system at Re >500 with invarient temperatures in each phase these equations become

$$q_A \sim US; \frac{hd}{k} \sim \left(\frac{dV\rho}{\mu}\right)^y$$

For geometrically similar spherical shapes

$$S \sim (\text{size})^{2/3} \quad d \sim (\text{size})^{1/3}$$

If we assume that transfer resistance lies predominantly in one phase then U = h and

$$U \sim (\text{size})^{(y-1)/3} \quad (V)^y$$

Data has shown that average velocity is fairly insensitive to size in the range of experimentation so that by substitution

$$q_A \sim (\text{size})^{2/3 + y/3 - 1/3} \quad \text{or} \quad q_A \sim (\text{size})^{(y+1)/3}$$

As noted in Chapter 1, most versions of the Frossling equation including the Handlos Baron model for external phase resistance in a liquid-liquid system set y = .5.

Figure 4-8 EFFECT OF DROP SIZE ON AVERAGE HEAT TRANSFER RATES

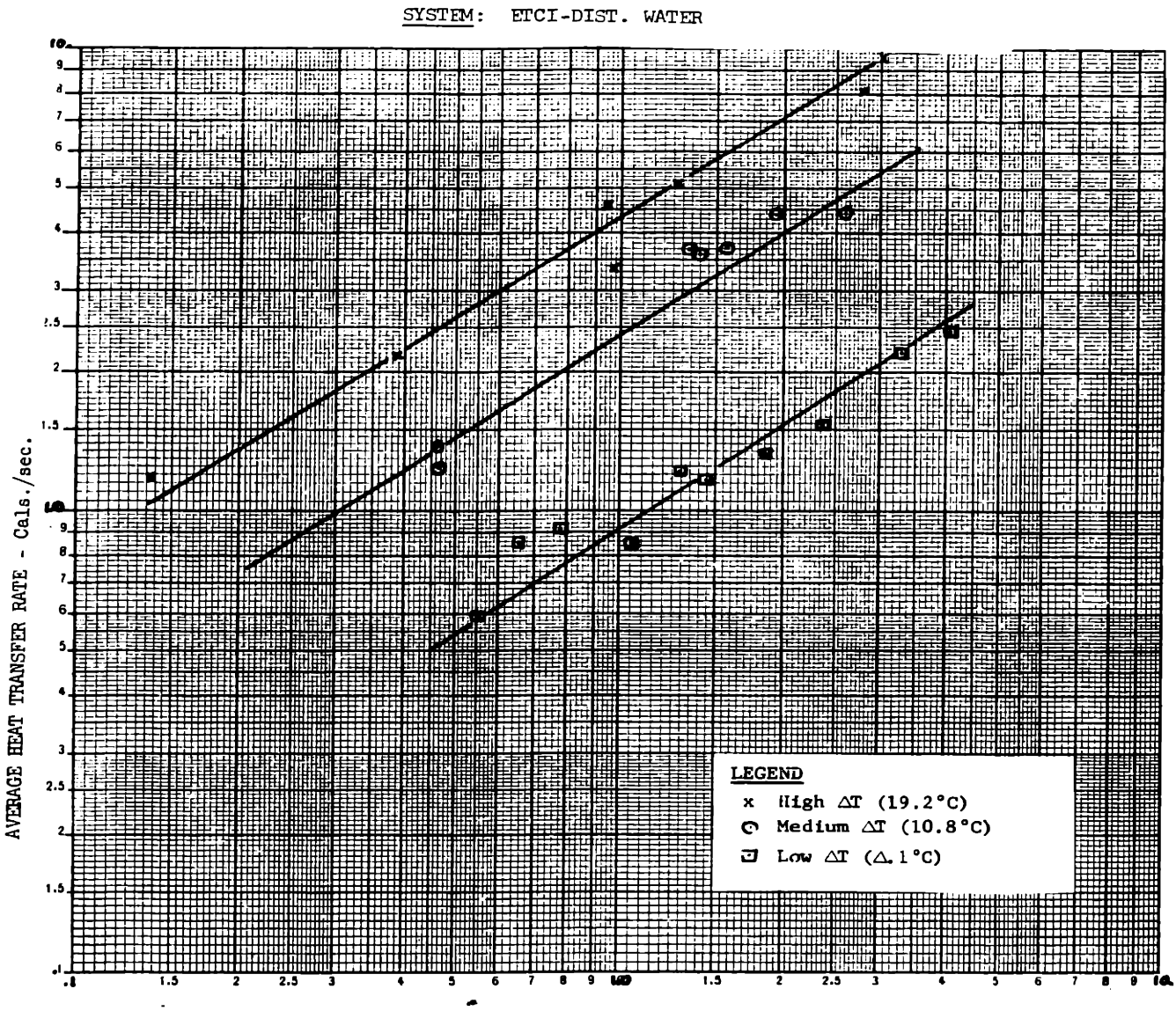

Accordingly, $q_A \sim (\text{size})^{.50}$

This, however, is inconsistent with the exponents derived from Fig. 4.8 whose true value cannot reasonably be expected to be lower than .58.

Working the same problem backward, y would have to = 1.09 in order for the size term to have an exponent equal to the average slope from Fig. 4.8, .69.

$$q_A \sim (\text{size})^{.69}$$

Since a value of greater that 1.0 for y is most unlikely, it is reasonable to accept a Reynolds number exponent of 1.0 as being consistent with the data. Veiwed against past work this leads to the conclusion that either the internal film controls as in the Handlos and Baron correlation (36) $Nu = .000375\ Re\ Pr/(1 + \mu_d/\mu_c)$ or that all transfer in taking place in a turbulent backflow region where Nu~Re as noted by Harriott (38). To distinguish between these cases an examination must be made of how instantaneous rate varies with instantaneous Reynolds number. This will be undertaken in Chapter V.

(b) Effect of ΔT Driving Force - In non-boiling situations involving forced convection the usual form of dependence of temperature driving force is that of a simple proportionality. When natural convection predominates the rate equation involves ΔT to the 5/4 power. When the heated liquid is boiling, temperature driving force is usually raised to some larger power in the rate equation, each of the various regimes of boiling having its own characteristic exponent value. To judge the data in this context, values taken from Fig. 4.8 are cross plotted in Fig. 4.9 as rate versus ΔT for the three nominal sizes. Least square linear regression slopes and intercepts of the log-log equation, Log Rate = Log a + b Log (ΔT) are as follows:

Size	b, Slope	a, Intercept
Small (.6 Cal.)	.943	.17
Med. (1.2 Cal.)	.963	.28
Large (2.4 Cal.)	.979	.45

Figure 4-9 EFFECT OF TEMPERATURE DRIVING FORCE ON AVERAGE HEAT TRANSFER RATES

SYSTEM: ETCI- DIST. WATER

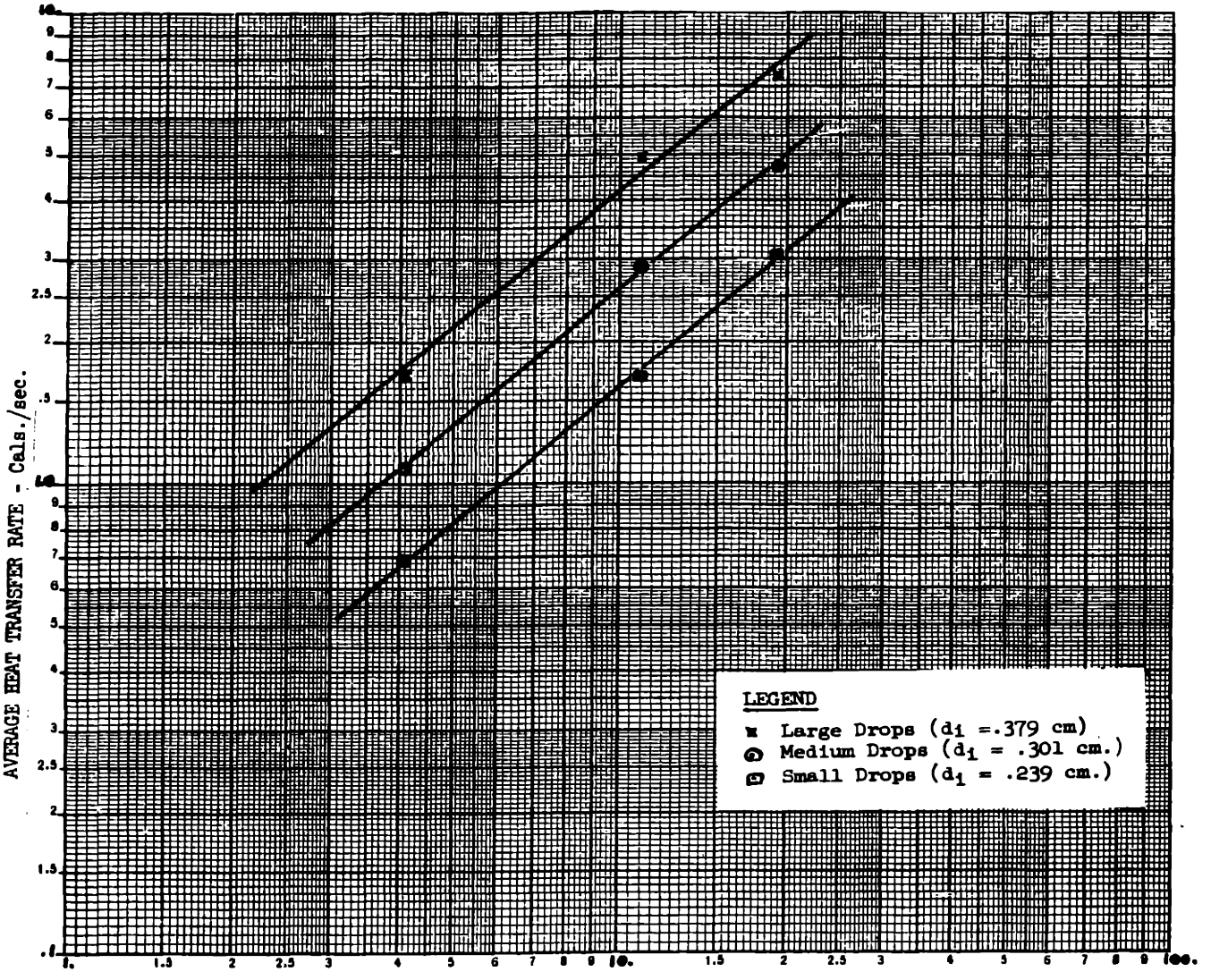

The fact that the rate slopes very closely approximate 1.0 in all three cases strongly supports a simple linear dependence of rate on temperature driving force. It is perhaps meaningful, however, that in all three cases the slope is slightly less than 1.0 although no reason for this is immediately apparent.

(c) Effect of Continuous Phase Properties - The overall rate of heat transfer may now be expressed in the general form, rate = $U' d_i^2 \Delta T$ with the U' being similar to the usual overall heat transfer coeff. Because of the dynamic nature of the system, it seems likely that momentum transport properties and interfacial properties may both act strongly to determine the value of U' under different conditions. Attempts to explore the effect of differences in continuous phase properties on the overall heat transfer rate were partially frustrated by the unexpectedly high solubility of ethyl chloride in the glycerine-water solutions used. Data from a few of these runs appear to be reliable, however, and plots of rate versus size and rate versus ΔT for 65% Glycerine - EtCl system are presented in Figures 4.10 and 4.11. Coefficients for the log-log rate model comparable to those given for plain water are as follows:

For rate versus size

ΔT	b, Slope	a, Intercept
Med. (10.7°C)	.59 ± .10	1.16 ± .003
High (18.8°C)	.65	1.73

This is additional evidence of a consistent linear rate dependence on area since the hypothesis that the true slope is .67 is still tenable. As before, cross plotting is used to determine dependence on driving force (See Fig. 4.11). Slopes for these lines both are approximately .75. This shows again the tendency for the ΔT exponent to be less than 1, although now to a much greater extent. The most likely explanation is that increased temperatures also lead to increased absorption rates. Thus observed bubble growth rates which would be low by the rate at which EtCl is lost from the bubble by absorption would be proportionately lower

EFFECT OF DROP SIZE ON AVERAGE

HEAT TRANSFER RATE

SYSTEM · EtCl - 65% GLYCERINE WATER

Figure 4-10

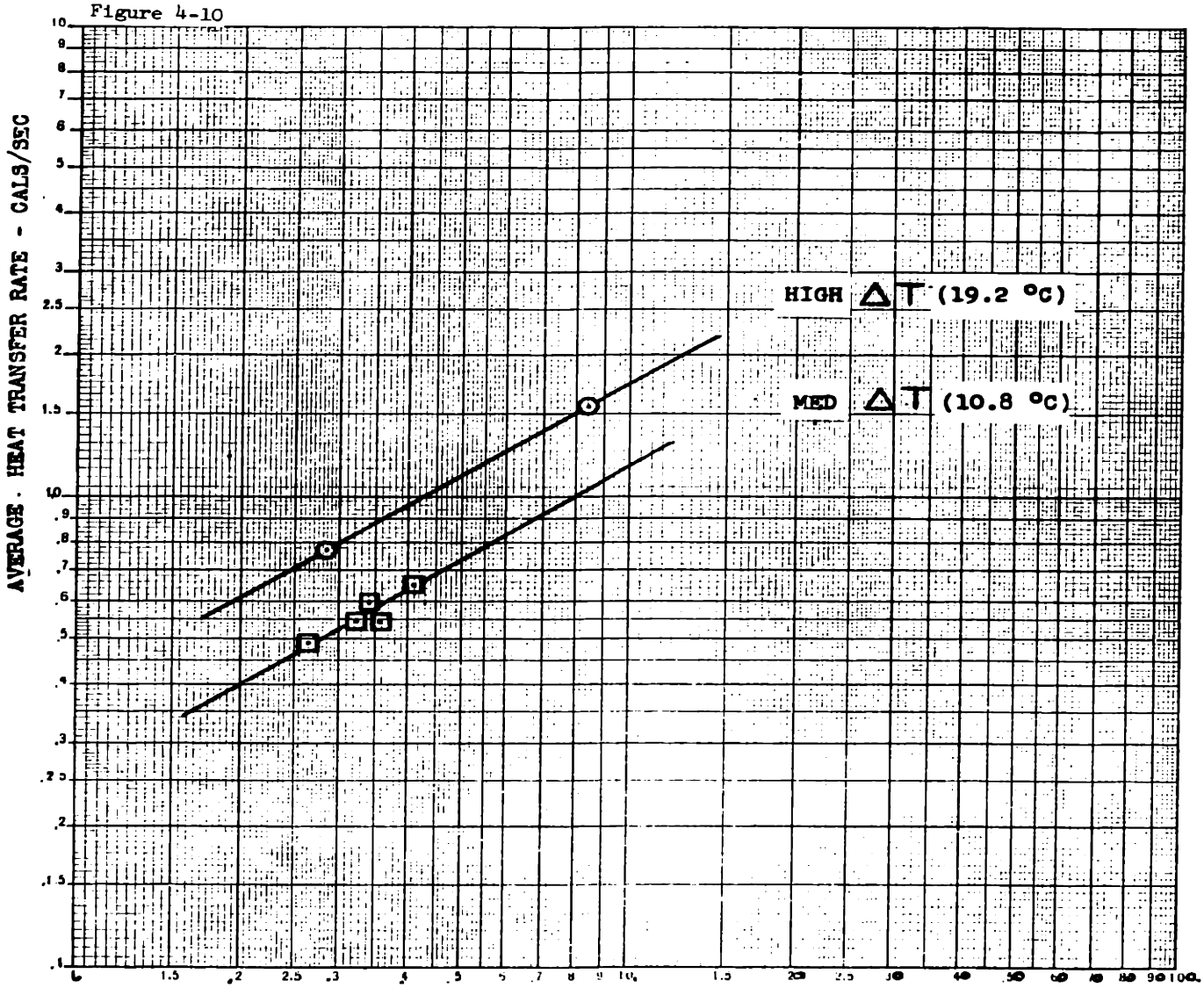

EFFECT OF TEMPERATURE DRIVING

FORCE ON AVERAGE HEAT TRANSFER RATES

SYSTEM: EtCl - 65% GLYCERINE WATER

Figure 4-11

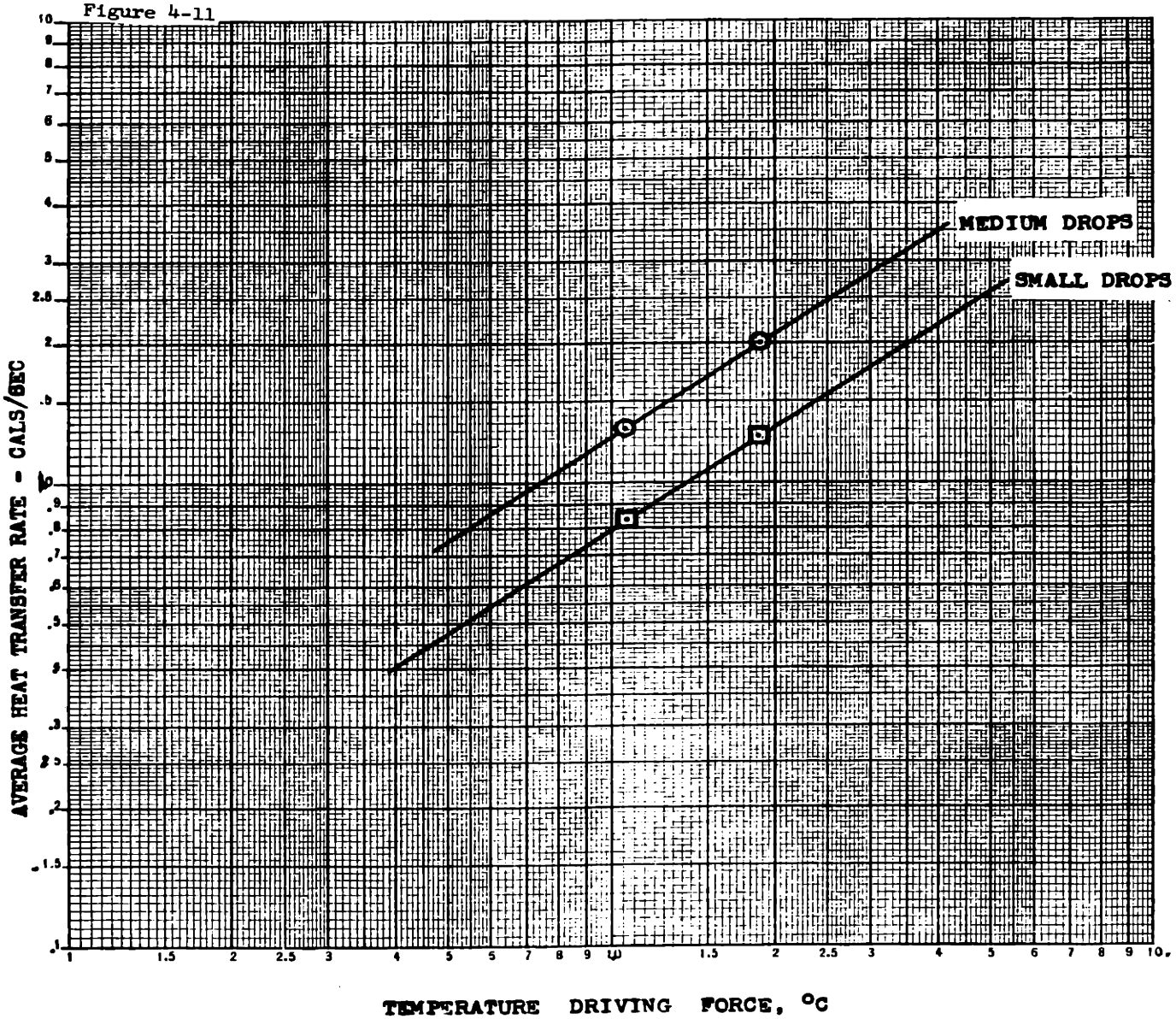

with increasing continuous phase temperature. This portion of the data should certainly be re-run as a part of future work.

As noted previously the most commonly used way to correlate heat transfer coefficients with continuous phase properties is via equations of the Frossling type $Nu \sim Re^{y} Pr^{z}$. Such an approach cannot be applied to this terminal state correlation directly because the absence of an appropriate bubble velocity value makes it impossible to calculate a Reynolds number. A plot of $\frac{\text{rate}}{d_i^2 \Delta T}$ versus Pr for the three ΔT levels given in Fig. 4.12 shows that the Prandlt Number alone is insufficient for correlating average rates. Although a line could be drawn between the two groups of data, it would place a negative exponent on the Prandlt number which would be in conflict with the positive slopes suggested by the position of data points within each group. Further examination of these effects will be undertaken on instantaneous rate data in later sections.

(d) Effect of Surfactant Concentrations - The effect which various concentrations of a surfactant might have was studied by comparing overall heat transfer rates using four levels of concentration and three different drop sizes at the middle temperature level. The results are shown in Fig. 4.13.

The results show that surfactants have a decided influence whose direction and magnitude vary with initial drop size. The reversal of the surfactant influence on vaporization rate from positive to negative with increasing drop size indicates that two separate phenomenon are involved which respond in opposite ways to drop size changes. The following observations drawn from earlier work (23, 72) on surfactant action in bubble systems are helpful in understanding what is involved:

When surface active molecules are present in a gas-liquid or liquid-liquid system, they rapidly orient across the two phase interface with two effects:

1) The interface begins to resist shear thereby absorbing forces which would otherwise transmit through the interface to sustain circulation in the internal fluid. By increasing shear resistance the surfactant molecules

Figure 4-12

HEAT TRANSFER COEFFICIENT VS PRANDTL NUMBER FOR TWO CONTINUOUS PHASE FLUIDS AT SEVERAL TEMP. LEVELS

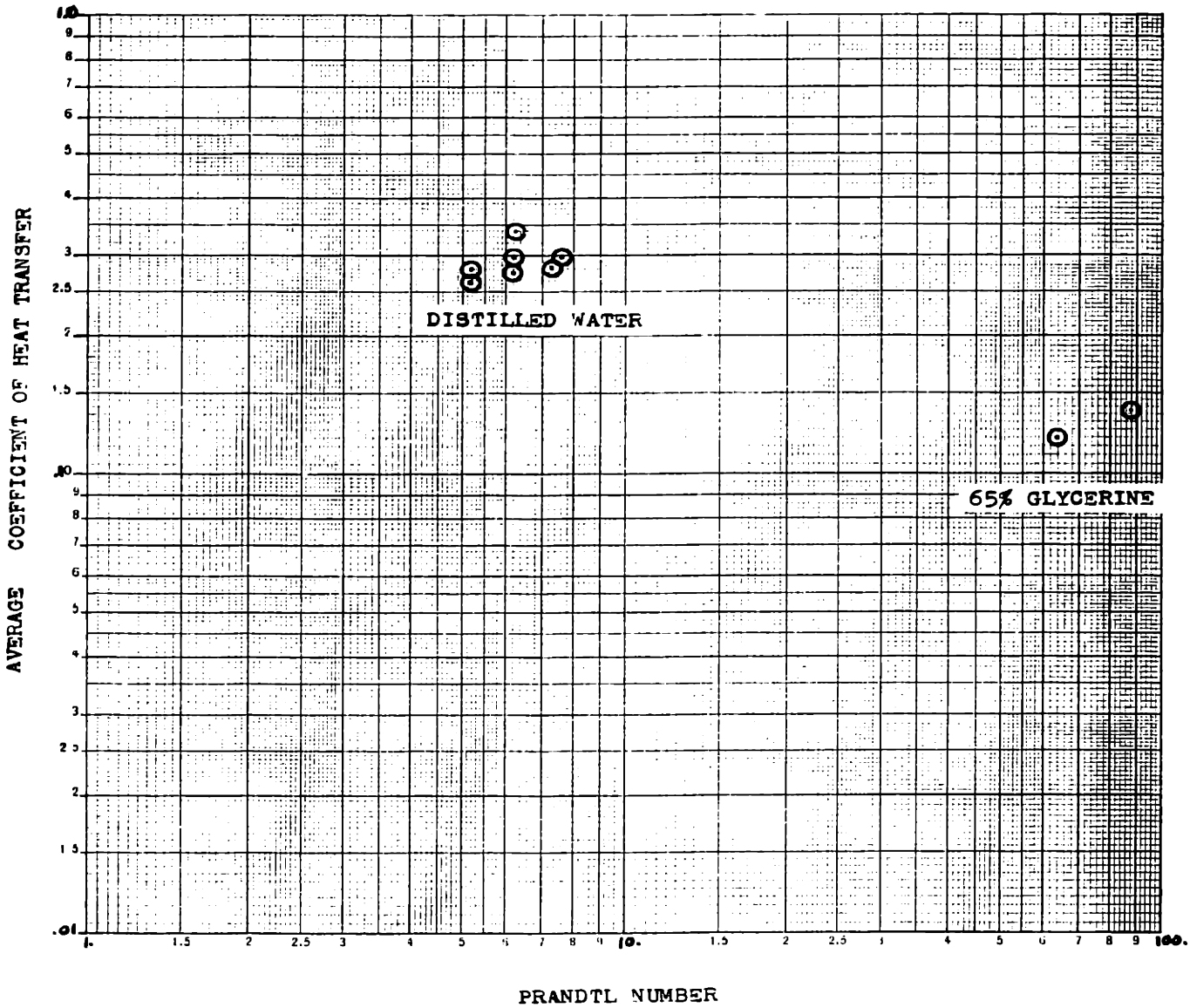

also cause thickening of the external boundary layer. These effects can combine to reduce overall transfer rates by up to 60%.

2) The presence of surfactants will also strongly depress interfacial tensions. This can cause changes in the equilibrium shape of rising drops or bubbles. Where shape oscillation tendencies already exist reduced interfacial tension will permit more extreme oscillations with an attendant increase of interfacial area and internal fluid mixing.

If through the action described in 1) the thickness of the exterior film is increased and internal circulation is damped, a reduction in heat transfer would certainly result. This would explain the 14% rate reduction exhibited by the large drop size. One might then imagine that this effect is exactly balanced by area increases and oscillation mixing in the medium size drops which remain as irregular ellipsoids for a longer period. Extending this we can reason that area increases and oscillation mixing predominate for the case of the more unstable small drop resulting in a net rate increase.

The magnitude of both of these effects is thought to relate to the degree to which the interface is saturated with surfactant. One measure of the interfacial saturation is the so-called surface pressure defined as the amount of change of interfacial tension caused by the presence of the surfactant in any given concentration. Replotting the observed overall heat transfer rates against surface pressure for the vapor-water and for ethyl chloride liquid-water interfaces (Figs. 4.14 & 4.15) does indeed produce simpler correlations for concentrations lower than the critical micelle concentration. Although several curves show that small changes are continuing to occur at concentrations higher than the CMC, the curves are all nearly asymptotic showing that the rate of surfactant diffusion to a growing bubble interface is not an important variable.

The divergence of effect for low and high drop sizes makes it impossible to develop an empirical relationship from these data which

Figure 4-14

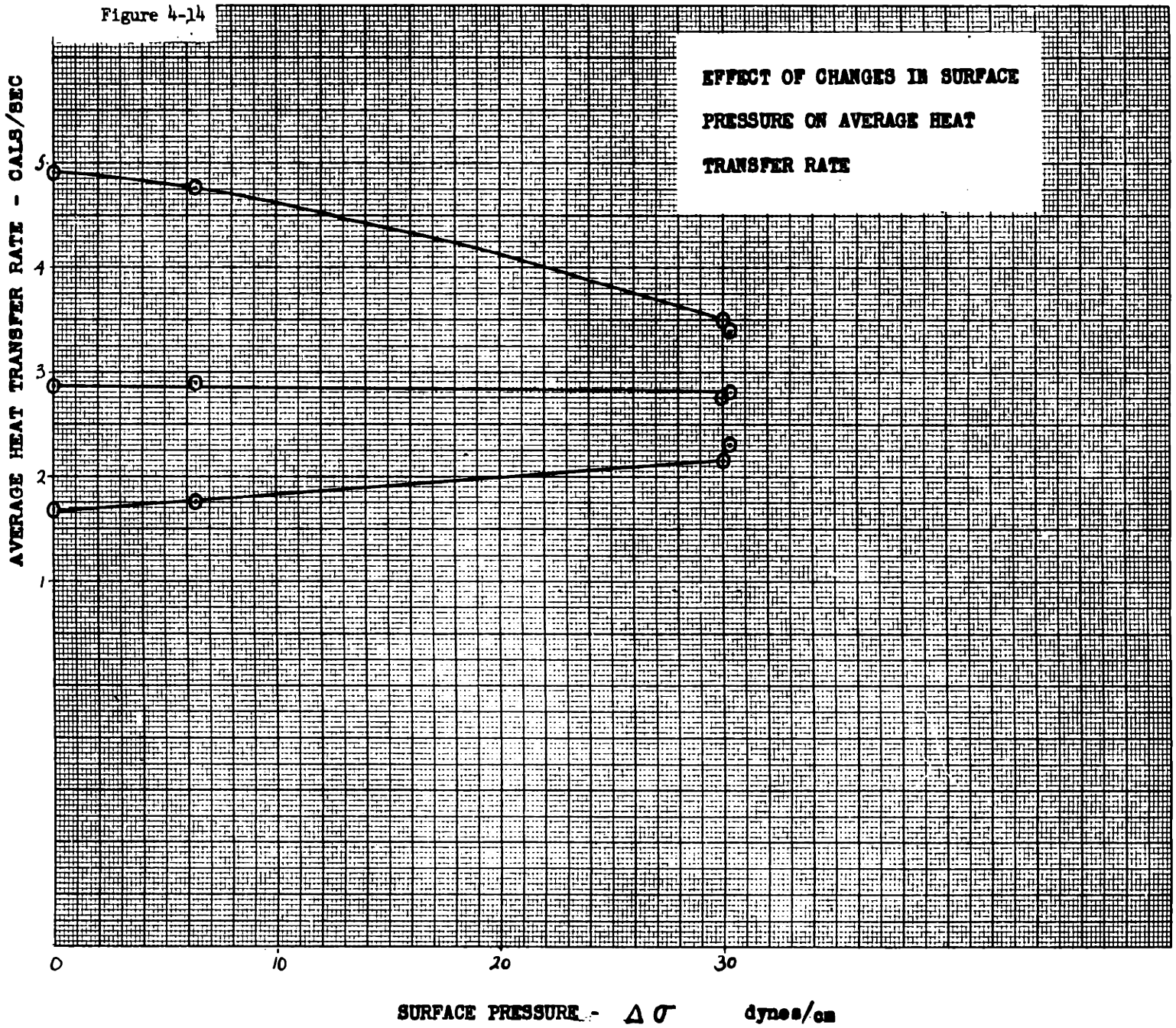
EFFECT OF CHANGES IN SURFACE PRESSURE ON AVERAGE HEAT TRANSFER RATE
AVERAGE HEAT TRANSFER RATE - CALS/SEC
5
4
3
2
1
0
10
20
30
SURFACE PRESSURE - Δ σ dynes/cm

Figure 4-15

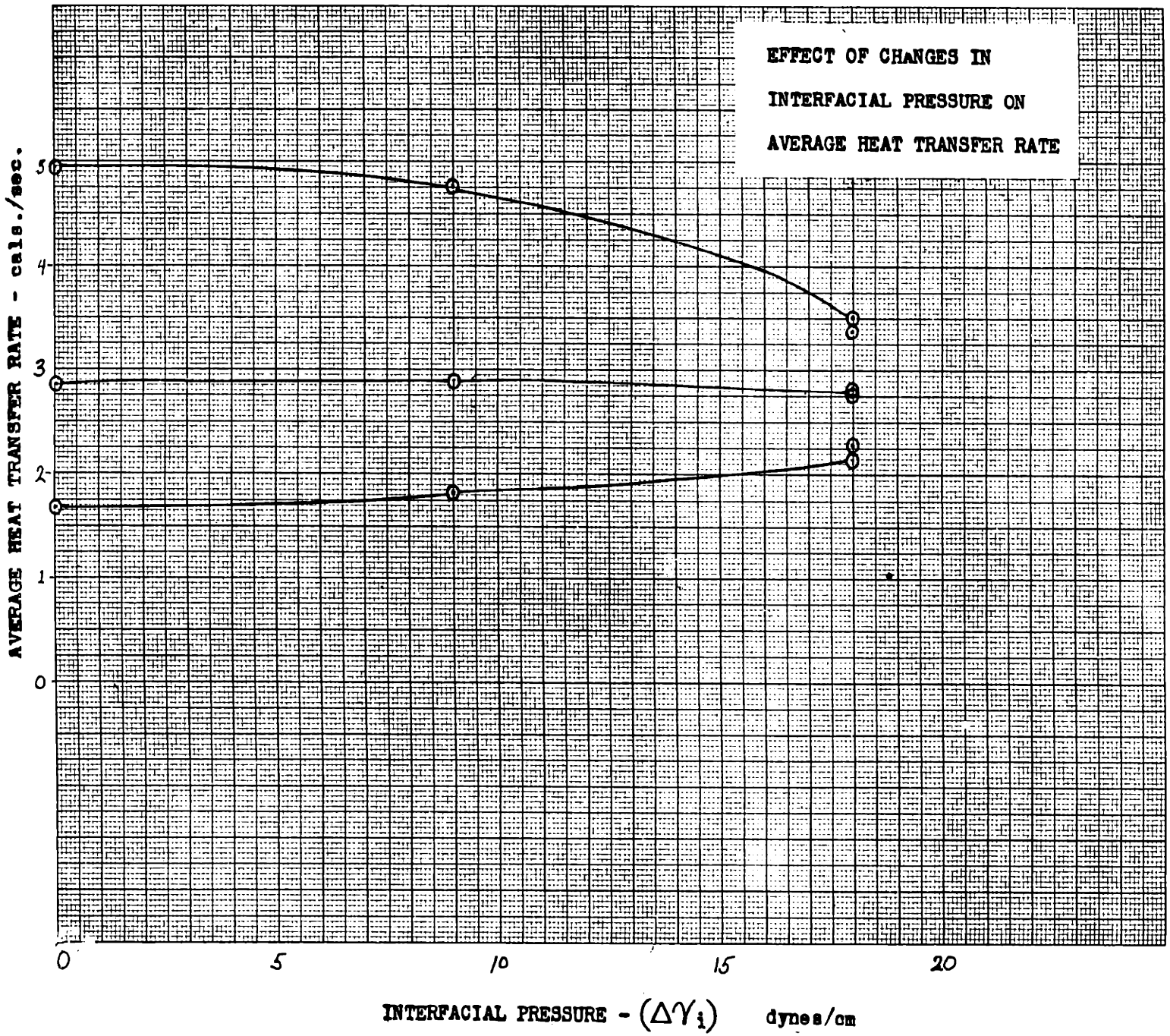
EFFECT OF CHANGES IN
INTERFACIAL PRESSURE ON
AVERAGE HEAT TRANSFER RATE
AVERAGE HEAT TRANSFER RATE - cals./sec.
0
1
2
3
4
5
0
5
10
15
20
INTERFACIAL PRESSURE - $(\Delta\gamma_i)$ dynes/cm

would have any general utility. Thus these graphs alone will be used to represent the nature and degree of the effect as it has operated in this work and no attempt will be made to incorporate these dependencies into the overall rate equation presente earlier. Further consideration will be given to these data in the chapter on mechanism which follows.

3. Velocity of Rise Behavior

Curves for observed velocity of rise vs. time are given for selected runs in water together with corresponding curves of terminal velocity as predicted from work by Harmathy (37) and by Haberman and Morton (33). Curves built on observed values for drops of a comparable size in 65% glycerin are also given. The following observations can be made.

(a) General - Shapes of the curves are similar for all conditions differing only to a fairly minor degree in shape and magnitude through the whole experimental region. Many of the curves resemble the curves of Haberman and Morton for terminal velocity of air bubbles versus size by showing a mild decrease in velocity with increasing size for intermediate sizes (d_e = .16 to .6 cm).

(b) Effect of drop size - As expected the asymptotic value for terminal velocity at full vaporization increases with increasing drop size. The deceleration effect mentioned above is most apparent for small sizes and does not show up at all in the curves for large sized drops. This is reasonable since small size drops spend most of their growth period in the critical size region. Large size drops grow through this region very quickly during a period when their decreasing density is exerting a major influence on their velocity of rise behavior.

It is also apparent that the observed velocity of rise lags the terminal velocity to a greater degree as size increases. This is presumably an inertial effect.

(c) Effect of ΔT driving force - The effect of increasing ΔT is similar to that for increasing size. Although the velocities of fully

vaporized bubbles are the same for any given size at all ΔT's, plateauing in the curves of observed velocity of rise are more pronounced under milder conditions (low ΔT). In spite of the faster growth rate which prevails at higher ΔT's the degree to which actual velocity is depressed below the expected terminal values appears unchanged. Apparently mass alone is the dominant factor in determining the degree of lag.

(d) Effect of continuous phase properties - Although the velocity of rise for all drops in 65% glycerine falls well below that in plain water during the growth period it is significant to note that in both situations velocities for fully vaporized drops take on the same asymptotic value. This indicates that fully vaporized drops in all cases have grown to a sufficient size to approach the spherical cap region ($d_e > 1.8$ cms) where the velocity of rise ceases to be influenced by the physical properties of the continuous phase. And in fact the smallest drop used in these curves when fully vaporized has a $d_e = 1.4$ at which level velocities in the two environments should differ by only 4%.

The lag during growth could be attributed to any of three effects or a combination thereof:

1. The depression of terminal velocities by increased continuous phase viscosity,
2. The retardation of the rate of approach to equilibrium by increased continuous phase viscosity, and
3. the reduction in growth rate as a consequence of reduced heat transfer rate.

The fact that lag increases with decreasing ΔT (i.e. decreasing continuous phase temperature) shows that viscosity effects are involved suggesting that all three of the above effects are important. However, without more data no distinction of relative importance can be made.

(e) Effect of Surfactant - In Fig. 4.7 a comparison is given of typical runs with and without a surfactant. The effect of the

surfactant on velocity of rise though not pronounced does correspond closely to the behavior of other dispersed phased systems as reviewed in Chapter I. Maximum reduction in terminal velocity is 11% which corresponds closely to the 12% reduction reported by Davies & Rideal (15) for a similar system. In addition the Reynolds number ranges for this behavior are nearly identical being 440 - 3840 for this work and 400 - 4000 for the data of Davies and Rideal (15).

4. An Empirical Coefficient

For the system EtCl-Distilled Water without a surfactant an empirical overall coefficient may now be estimated by combining the conclusions reached in the above sections. Thus if the basic form, rate = $U' d_i^2 \Delta T$, is assumed and applied to the data, a mean value of U' can be calculated and confidence limits placed upon it. This is done in Table 4.7. The mean value results in an overall rate equation for this system of rate = $2.84\ d_i^2 \Delta T$ or $.904 S_i \Delta T$. The coefficient, .904,* may be compared with the results of Gordon et al (29) for heat transfer between liquid layers where the maximum coefficient obtained was .244,* to the work of Garwin and Smith (26) where .009* was the maximum, to the work of McDowell and Myers (56) where maximum film coefficients were estimated at .011,* and to Kramer's correlation for transfer from solid spheres where at comparable Reynolds numbers (1000 - 10,000) a coefficient of .063* is predicted (51). Certainly this is not meant to imply that transfer coefficients for vaporizing drops based on an actual liquid-liquid interfacial area would show this much advantage but these comparisons do clearly demonstrate that a given volume of coolant achieves a considerably higher rate effectiveness when it is made to vaporize.

* Cal/(sec.)(cm.^{2})($^\circ$C.)

Table 4.4

Calculation of an Empirical Rate Constant
Ethyl Chloride-Water Runs

Run	Size	d_i^3	ΔT	Rate	d_i^2	U'	average U'
	cals.	cm^3	°C	cal/sec	cm^2	$\frac{cal}{(sec)(cm^2)(°C)}$	
1.	1.591	.03674	10.8	3.68	.110	3.10	
2.	1.403	.03240	10.8	3.57	.102	3.24	
3.	1.355	.03129	10.8	3.66	.099	3.43	
4.	.466	.01076	10.8	1.236	.049	2.34	2.92
5.	.464	.01071	10.8	1.358	.049	2.57	
6.	2.672	.06066	10.8	4.328	.154	2.60	
7.	1.950	.04503	10.8	4.305	.127	3.14	
8.	1.284	.02965	19.2	5.016	.096	2.72	
9.	.977	.02256	19.2	3.301	.0795	2.16	
10.	.947	.02187	19.2	4.553	.078	3.04	
11.	.389	.00898	19.2	2.161	.043	2.62	2.70
12.	.139	.00320	19.2	1.188	.0217	2.85	
13.	2.835	.06546	19.2	8.147	.162	2.62	
14.	3.031	.06999	19.2	9.442	.170	2.89	
83.	.557	.01286	4.0	.590	.055	2.68	
84.	.657	.01517	3.9	.848	.061	3.56	
85.	.780	.01801	4.0	.905	.0685	3.30	
87.	1.449	.03346	4.1	1.116	.104	2.62	2.88
88.	1.070	.02471	4.1	.842	.085	2.42	
89.	1.301	.03004	4.0	1.205	.0965	3.12	
90.	2.372	.05477	4.2	1.517	.144	2.51	
92.	4.047	.09345	4.2	2.427	.206	2.81	
91.	3.310	.07643	4.2	2.163	.180	2.86	

Overall average U 2.84

Table 4.4

Calculation of an Empirical Rate Constant
Ethyl Chloride-Water Runs

Run	Size	d_i^3	ΔT	Rate	d_i^2	U'	average U'
	cals.	cm^3	°C	cal/sec	cm^2	$\frac{cal}{(sec)(cm^2)(°C)}$	
1.	1.591	.03674	10.8	3.68	.110	3.10	
2.	1.403	.03240	10.8	3.57	.102	3.24	
3.	1.355	.03129	10.8	3.66	.099	3.43	
4.	.466	.01076	10.8	1.236	.049	2.34	2.92
5.	.464	.01071	10.8	1.358	.049	2.57	
6.	2.672	.06066	10.8	4.328	.154	2.60	
7.	1.950	.04503	10.8	4.305	.127	3.14	
8.	1.284	.02965	19.2	5.016	.096	2.72	
9.	.977	.02256	19.2	3.301	.0795	2.16	
10.	.947	.02187	19.2	4.553	.078	3.04	
11.	.389	.00898	19.2	2.161	.043	2.62	2.70
12.	.139	.00320	19.2	1.188	.0217	2.85	
13.	2.835	.06546	19.2	8.147	.162	2.62	
14.	3.031	.06999	19.2	9.442	.170	2.89	
83.	.557	.01286	4.0	.590	.055	2.68	
84.	.657	.01517	3.9	.848	.061	3.56	
85.	.780	.01801	4.0	.905	.0685	3.30	
87.	1.449	.03346	4.1	1.116	.104	2.62	2.88
88.	1.070	.02471	4.1	.842	.085	2.42	
89.	1.301	.03004	4.0	1.205	.0965	3.12	
90.	2.372	.05477	4.2	1.517	.144	2.51	
92.	4.047	.09345	4.2	2.427	.206	2.81	
91.	3.310	.07643	4.2	2.163	.180	2.86	
					Overall average U		2.84

CHAPTER 5 - ANALYSIS OF DIFFERENTIAL DATA - STUDY OF MECHANISM

In attempting to refine the empirical model given in Chapter 4, it is necessary to examine in detail the way in which vaporization behavior was effected by contrasting experimental conditions. Combining these observations with the fluid dynamic data also contained in the photographs should provide a reasonable base for mechanistic conjectures of considerable utility.

In view of the adequacy with which a simple Fourier model was used to correlate the overall heat transfer rates in Chapter 4, it seems proper to continue building on this general form.

If we redefine the variables of the Fourier equation in terms of their dynamic rather than their terminal state, we have the equation.

$q = US\Delta T$ where now

U = instantaneous rate coefficient at time, t
S = liquid-liquid interfacial area at time, t
ΔT = actual T bulk - T boiling under total pressure p_t, on the bubble at time, t

Let us examine separately the behavior of these individual components as vaporization proceeds.

A. Temperature Driving Force

It has already been shown (Sec. 4B1b) that the Bulk phase temperature stays relatively constant at any given value chosen for it. The disperse phase temperature on the other hand, is dependent on the the local pressure within a bubble at any given time. Since this is continuously changing as the bubble rises, an estimate of this temperature must be made for each bubble image. A saturated liquid boiling point can be calculated from photographic data on bubble position and knowledge of the systems hydraulic head equation. These

values show that the maximum change in temperature driving force from start to finish of vaporization (that for the low temperature runs) is about $1^{o}C$. This represents a ±15% variation around the average ΔT for the low temperature runs but a variation of less than ±5% for the 11° and 19° driving force runs. Thus for the higher temperature levels average ΔT's will be adequate even for calculations on a differential basis. In analysis of the low temperature runs the individual image values must be used.

B. Area

The part played by interfacial area in determining rate behavior is the most critical and at the same time the most elusive aspect of the vaporization process. To more easily attack the problem, several sub-questions may be posed.

1. Does heat reach the vaporizing liquid through both the vapor and liquid phases in the bubble or only through the liquid?
2. What portion of the total bubble surface represents vapor-liquid interface and what portion liquid-liquid interface?

1. Prefered Transfer Route - To answer the first question let us begin by visualizing a spherical bubble with heat traveling through the vapor phase by route B and through the unvaporized liquid by route A.

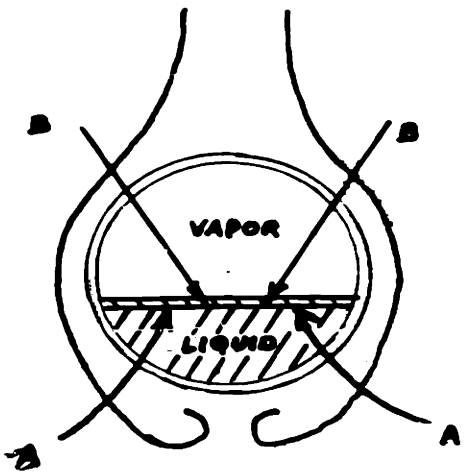

There is obviously an external film resistance present over the whole surface of the drop. Presumably the film is thinner offering less

values show that the maximum change in temperature driving force from start to finish of vaporization (that for the low temperature runs) is about $1^{o}C$. This represents a ±15% variation around the average ΔT for the low temperature runs but a variation of less than ±5% for the 11° and 19° driving force runs. Thus for the higher temperature levels average ΔT's will be adequate even for calculations on a differential basis. In analysis of the low temperature runs the individual image values must be used.

B. Area

The part played by interfacial area in determining rate behavior is the most critical and at the same time the most elusive aspect of the vaporization process. To more easily attack the problem, several sub-questions may be posed.

1. Does heat reach the vaporizing liquid through both the vapor and liquid phases in the bubble or only through the liquid?
2. What portion of the total bubble surface represents vapor-liquid interface and what portion liquid-liquid interface?

1. Prefered Transfer Route - To answer the first question let us begin by visualizing a spherical bubble with heat traveling through the vapor phase by route B and through the unvaporized liquid by route A.

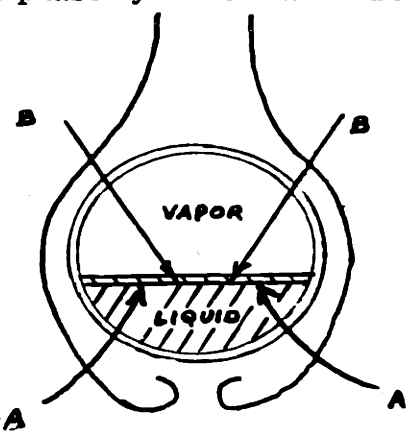

There is obviously an external film resistance present over the whole surface of the drop. Presumably the film is thinner offering less

resistance on the front and rear surfaces of the bubble than on the sides where the boundary layer is thickest. However, this difference cannot reasonably be assessed quantitatively so as a first approximation the film will be assumed to offer uniform resistance over the whole surface. Now, it is improbable that transfer through the vapor phase via path B accounts for a major portion of the total heat transferred. But to test this hypothesis let us assume that the most favorable conditions for this to happen do prevail, namely: that heat passes freely into the vapor phase maintaining the vapor at the same temperature as the continuous phase. Under these conditions the major resistance for path B would be at the ethyl chloride vapor-liquid interface: the transfer area involved may be taken as approximately equal to that at the ethyl chloride-water interface. (The methods by which this area can be estimated are given later in this section.) Using the Handlos-Baron equation (36) for an internal film, $Nu_d = .00375\ Re_d Pr_d/(1+\mu_d/\mu_c)$ the rate of heat transfer for this route is calculated at various stages in the vaporization cycle and compared in Table 5.1 with the observed overall rate as estimated from the slopes of curves given in Fig. 4.3. According to these results, transfer through the vapor phase accounts for less than .1% of the total heat transfer over the whole vaporization process. Thus even if the Handlos-Baron model gives a prediction which is an order of magnitude low, we may still safely assume that the only important transfer is through the liquid-liquid interface.

2. Area Distribution - In attempting to find out how much of the total bubble surface is liquid-liquid interface we may now pose some further questions:

a. What form does the unvaporized liquid take in a partly vaporized bubble?

b. Is there an appreciable tendency for liquid to climb the walls of the bubble?

Table 5-1

Comparison of Estimated Heat Transfer Rates Through the Vapor Phase with Overall Rates for the EtCl - Plain Water System Run #1 (Med. ΔT, Med. Drop Size)

Fraction Vaporized	q_v	q	q_v/q_l
.03	$.43 \times 10^{-3}$	.63	.00069
.06	$.83 \times 10^{-3}$	1.71	.00051
.17	1.22×10^{-3}	3.76	.00033
.37	2.14×10^{-3}	4.90	.00044
.58	2.09×10^{-3}	5.03	.00042
.77	$.79 \times 10^{-3}$	5.76	.00014

Table 5-1

Comparison of Estimated Heat Transfer Rates Through the Vapor Phase with Overall Rates for the EtCl - Plain Water System
Run #1 (Med. ΔT, Med. Drop Size)

Fraction Vaporized	q_v	q	q_v/q_l
.03	$.43 \times 10^{-3}$	.63	.00069
.06	$.83 \times 10^{-3}$	1.71	.00051
.17	1.22×10^{-3}	3.76	.00033
.37	2.14×10^{-3}	4.90	.00044
.58	2.09×10^{-3}	5.03	.00042
.77	$.79 \times 10^{-3}$	5.76	.00014

c. How do changes in size and shape effect liquid disposition?

None of these questions can be answered precisely since no observations were made by transmitted light and no separate measure of interfacial area is available. However, by studying contrasting runs and examining the dynamic drop behavior as recorded in the photographs some important conclusions can be drawn.

a. Liquid Disposition

Photographs of the bubbles show that the unvaporized liquid has no tendency to split off from the gas phase nor does it have any tendency to concentrate in pendant form on the bubble bottom. Instead the exterior profile suggests that the remaining liquid collects as a shallow puddle on the bubble bottom. The basic equilibrium positions would be as already shown in Fig. 4.2. The upward concave shape illustrated for the bottom of the spherical cap is similar to that described by Rosenberg (62) in his paper on air bubbles moving in liquids. Observation of rising bubbles from beneath during experimental runs showed that this feature was consistently present even though it cannot be seen in the photographs.

The only comparable description of a drop vaporizing in a two phase system is that presented by Moore (57) in his paper on superheating in two phase liquid system. He, too, observed that a vapor nucleus formed first at the top of the drop with the subsequent movement of a flat horizontal vapor-liquid interface downward as the remaining liquid vaporized. This behavior was qualitatively the same even when spontaneous nucleation was so rapid as to form a mist of vapor bubbles within the unvaporized puddle. Moore's description coincides well with the behavior noted in the present study and lends support to the conclusion that the artificial nucleation used in this study does not radically affect the basic vaporization process.

It is not possible to assume from these results, however, that the vapor and liquid phases will stay together in all systems. For EtCl-water the dispersed phase has the lower surface tension so that

by staying together the two organic phases act to minimize surface energy. If water were dispersed in an organic phase, however, a lowering of surface energy would be achieved by separation of the vapor and unvaporized liquid. In this case quite different overall heat transfer rates might result.

b. Spreading Tendencies and Liquid Splashing

The concept of a simple puddle represents only the minimum surface area available for a given geometric form. This may be appreciably augmented by spreading tendencies or by liquid splashing. Let us further examine these two possibilities.

If spreading tendencies are significant they would have their greatest effect in causing the liquid to spread over the concave bottom of spherical cap bubbles, completely covering the surface until vaporization is complete. Spreading would be most likely here because the inclination of the interface is shallow and interfacial shear opposing the spreading tendencies is at a minimum. If this thin film behaved in the same way as the rest of the heat transfer area, the resulting total coverage of the bottom surface would lead to a total área which would be continually growing up to the very end of the vaporization process. [$S = 1.64(\text{bubble vol.})^{.67}$] Since overall rate is a product of this area and a heat transfer coefficient which would logically also always be growing, heat transfer must exhibit an ever increasing rate to support the contention that spreading significantly augments the working area. Fig. 5.6 shows how the rate is actually observed to vary as vaporization proceeds for a typical case. In contrast to the above hypothesis, actual rate is seen to fall off steadily after 40% vaporized. Thus we conclude that spreading effects may be safely ignored. Such a conclusion is fully consistent with measurements of vapor diffusion by the Stefan method which have shown that even where the surface of a vaporizing liquid is considerably extended by capillary rise on the container walls no major increase in vaporization rate is observed. Apparently vaporization

from these films occurs at a much lower rate than it does from the bulk liquid so that the net effect is small whether spreading occurs or not.

The possibility that liquid splashing substantially adds to the area can only be examined by qualitative surmise. In most runs shape oscillation was slight and rise occurred smoothly along a stable vertical axis. In these runs splashing was probably insignificant because there was not much motion which could cause it. When runs in which some oscillation was observed (notably 11, 12), are examined in context with the nonoscillating runs, the measured rates do not appear to be unusually high. It is thus reasonable to conclude for pure water runs at least that splashing is unimportant, having negligible effect on rate measurement even when drop motion may cause it to occur.

c. Size and Shape Effects

The problem of characterizing area then may be resolved into examining how a flat pool of liquid might change in interfacial liquid-liquid area as vaporization procedes. The rate of area change per unit vaporized will depend both on the size and on which of the three basic shapes: spherical, ellipsoidal or spherical cap prevails at the time. Area histories for these three separate models are shown in Fig. 5.1. A real drop would probably begin as a sphere, soon evolve to an ellipsoidal shape and finally end up as a spherical cap. The pattern would be general for all drops with behavior differences showing up as shifts in the bubble size, at which transfer from shape to shape occur. Note that all three slopes yield qualitatively the same pattern of area development: area increases sharply as the bubble grows. Area increase slows down as growth continues finally ceasing at 40% vaporized where area gain due to puddle flattening can no longer outway area losses which occur as the liquid vaporized. Beyond 40% vaporized bubble growth becomes less important and transfer area falls as the covering power of the unvaporized liquid. Where a spherical cap with the flat bottom is assumed

Figure 5-1 LIQUID-LIQUID INTERFACIAL AREA FOR 3 BASIC DROP SHAPES MEDIUM DROP SIZE

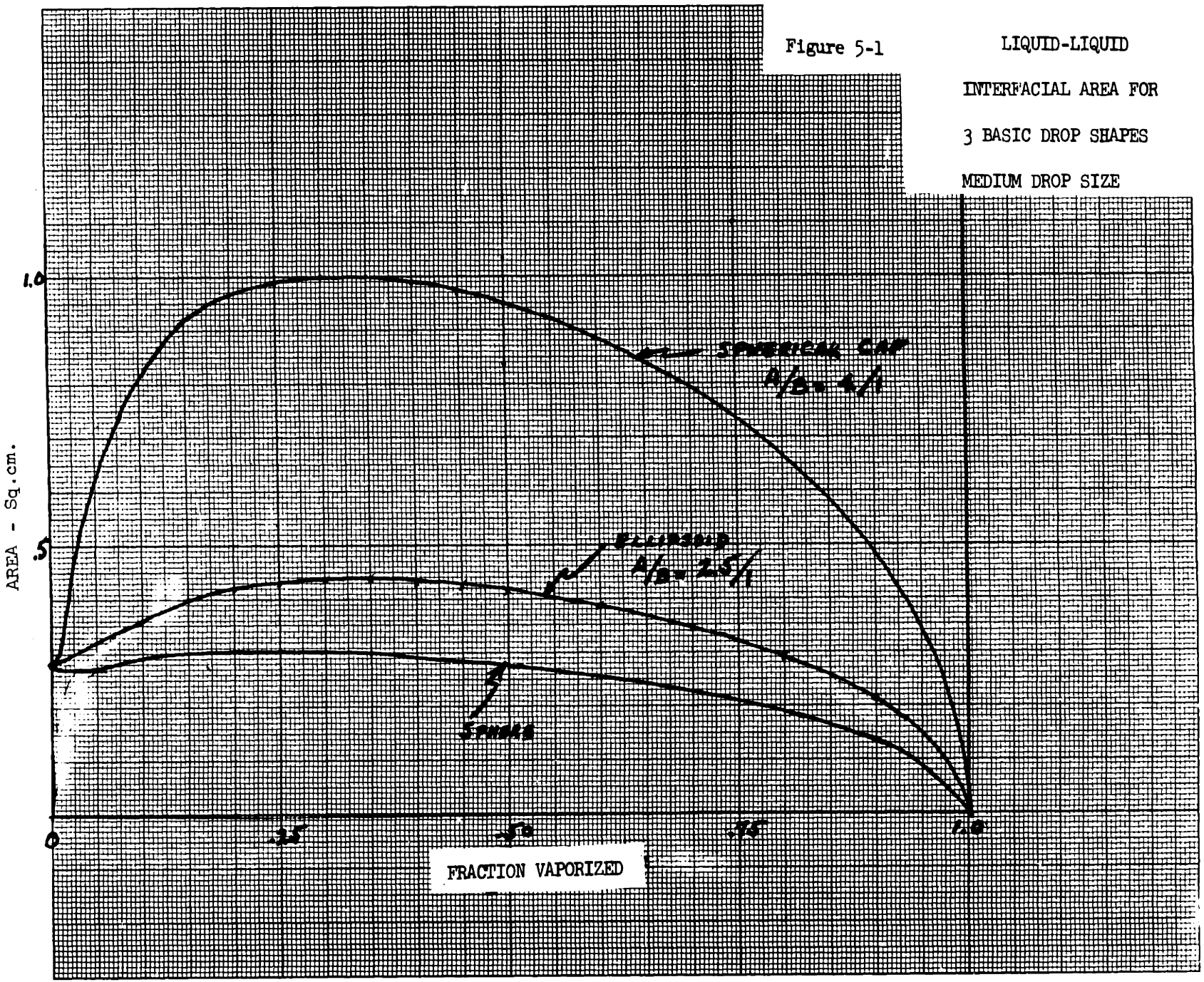

area continues to grow until vaporization is complete because on a flat surface (as opposed to surface with low points) the covering power of unvaporized liquid is undiminished until puddle thickness falls to monomolecular levels.

For predicting transitions between the various shapes, three indexes have been proposed: equivalent radius, the Reynolds No., $\frac{dV\rho}{\mu}$, and the Eötvos No., $\frac{g\Delta\rho d^2}{\sigma}$. Index number ranges characteristic of the several important patterns of behavior are given in Table 5.2. In addition to the standard indexes, recent work on liquid drops (30) has suggested that a better Reynolds number correlation may be obtained by using the projected shape diameter instead of the conventional equivalent spherical diameter as a characteristic dimension.

(1) Ethyl Chloride - Distilled Water System

To test the utility of these indexes in characterizing the behavior of vaporizing drops, the photographic images in each of the plain water runs were classified using the behavior mode numbers given in Table 5.2 and then were correlated against each of the four number indexes. The results are shown in Figs. 5.2 through 5.5. From these figures ranges for the various indexes were selected to correspond most appropriately with the modes of behavior observed. These are presented in Table 5.3. Lastly the utility of each index was evaluated by determining what percentage of images exhibited behavior deviating one, two or three modes from the one predicted for it. These results are given in Table 5.4.

Several important observations can be made:

1. Although none of the indexes gives a highly precise segregation, there is sufficient consistency to demonstrate that the index approach has value here. Actually, much of the lack of precision may be due to errors in classifying the images. Still photographs are more difficult to interpret than high speed motion pictures in this area and some of the modes are at best only short lived transients in the growth process.

Table 5.2

Modes of Behavior for Moving Drops and Bubbles

Equivalent Spherical Diameter r_e	Reynolds No. Re	Eötvos No. Eö	Description	Mode
$< .04$	< 70	$< 1.$	Spherical bubbles traveling in rectilinear paths	1
.04 - .062	70 - 400		Spherical bubbles traveling in rectilinear paths	
.062 - .077	400 - 500	1 - 13	Oblate spheroid, rectilinear motion	2
.077 - .24	500 - 1000		Oblate spheroid, helical motion	3
.24 - .35	1100 - 1600		Oblate spheroid but shape becomes increasingly irregular with increasing Re	4
.35 - .88	1600 - 5000	13 - 40	Transition - oblate spheroid to spherical cap. Shape is very irregular and fluctuates continuously. Motion is almost rectilinear	5
> 0.88	> 5000	> 40	Spherical caps, rectilinear motion	6

Table 5.3

Ranges of Behavior Indexes Corresponding to
Observed Fluid Dynamic Modes of Vaporizing Drops

EtCl - Water System

Behavior Indexes	Fluid Dynamic Modes 1	2	3	4	5	6
Eötvos No.						
Bubbles	< 1	1		13	13 - 40	> 40
Small drops		< 4	4 - 6.4	6.4 - 11	>11	
Med. drops	< 1	1 - 4	4 - 6	6 - 28	28 - 60	> 60
Large drops		< 1	1 - 3	3 - 11	11 - 45	> 45
Equivalent Spherical Diameter						
Bubbles	< .06	.06 - .08	.08 - .24	.24 - .35	.35 - .88	> .88
Small drops		< .3	.3 - .4	.4 - .53	.53 - 1.+	
Med. drops	< .15	.15 - .3	.3 - .4	.4 - .7	.7 - 1.05	> 1.05
Large drops		< .2	.2 - .3	.3 - .6	.6 - 1.1	> 1.1
Reynolds No. Eq. Sph. Diam.						
Bubbles	< 400	400 - 500	500 - 1100	1100 - 1600	1600 - 5000	>5000
Small drops		350 - 1000	1000 - 1400	1400 - 3000	3000 - 5400	>5400
Med. drops	< 300	300 - 950	950 - 1100	1100 - 3000	3000 - 7000	>7000
Large drops		340 - 850	850 - 1200	1200 - 3000	3000 - 6500	>6500
Reynolds No. Proj. Sph. Diam						
Bubbles		No Data Available				
Small drops		450 - 1300	1300 - 2000	2000 - 4300	4300 - 8000+	
Med. drops	<250	250 - 1100	1100 - 2100	2100 - 5000	5000 - 10500	>10, 500
Large drops		350 - 1100	1100 - 2000	2000 - 4500	4500 - 10000	>10, 000

Table 5.3

Ranges of Behavior Indexes Corresponding to
Observed Fluid Dynamic Modes of Vaporizing Drops

EtCl - Water System

Behavior Indexes	Fluid Dynamic Modes 1	2	3	4	5	6
Eötvos No.						
Bubbles	< 1	1		13	13 - 40	> 40
Small drops		< 4	4 - 6.4	6.4 - 11	>11	
Med. drops	< 1	1 - 4	4 - 6	6 - 28	28 - 60	> 60
Large drops		< 1	1 - 3	3 - 11	11 - 45	> 45
Equivalent Spherical Diameter						
Bubbles	< .06	.06 - .08	.08 - .24	.24 - .35	.35 - .88	> .88
Small drops		< .3	.3 - .4	.4 - .53	.53 - 1.+	
Med. drops	< .15	.15 - .3	.3 - .4	.4 - .7	.7 - 1.05	> 1.05
Large drops		< .2	.2 - .3	.3 - .6	.6 - 1.1	> 1.1
Reynolds No. Eq. Sph. Diam.						
Bubbles	< 400	400 - 500	500 - 1100	1100 - 1600	1600 - 5000	>5000
Small drops		350 - 1000	1000 - 1400	1400 - 3000	3000 - 5400	>5400
Med. drops	< 300	300 - 950	950 - 1100	1100 - 3000	3000 - 7000	>7000
Large drops		340 - 850	850 - 1200	1200 - 3000	3000 - 6500	>6500
Reynolds No. Proj. Sph. Diam						
Bubbles		No Data Available				
Small drops		450 - 1300	1300 - 2000	2000 - 4300	4300 - 8000+	
Med. drops	<250	250 - 1100	1100 - 2100	2100 - 5000	5000 - 10500	>10, 500
Large drops		350 - 1100	1100 - 2000	2000 - 4500	4500 - 10000	>10, 000

Table 5.4

Precision of Fluid Dynamic Indexes
in Classifying Behavior of Vaporizing Drops

EtCl - Water System

Characteristic No.	% falling 1 mode outside of prediction	% falling 2 modes outside of prediction	% falling 3 modes outside of prediction
Eötvos No.	32.8%	6.3%	.5%
Equivalent Spherical Diameter	32.1%	4.3%	0%
Reynolds No. on Equivalent Spherical Diameter	25.0%	4.8%	.5%
Reynolds No. on Projected Spherical Diameter	24.6%	4.8%	.9%

Table 5.4

Precision of Fluid Dynamic Indexes
in Classifying Behavior of Vaporizing Drops

EtCl - Water System

Characteristic No.	% falling 1 mode outside of prediction	% falling 2 modes outside of prediction	% falling 3 modes outside of prediction
Eötvos No.	32.8%	6.3%	.5%
Equivalent Spherical Diameter	32.1%	4.3%	0%
Reynolds No. on Equivalent Spherical Diameter	25.0%	4.8%	.5%
Reynolds No. on Projected Spherical Diameter	24.6%	4.8%	.9%

Figure 5-2

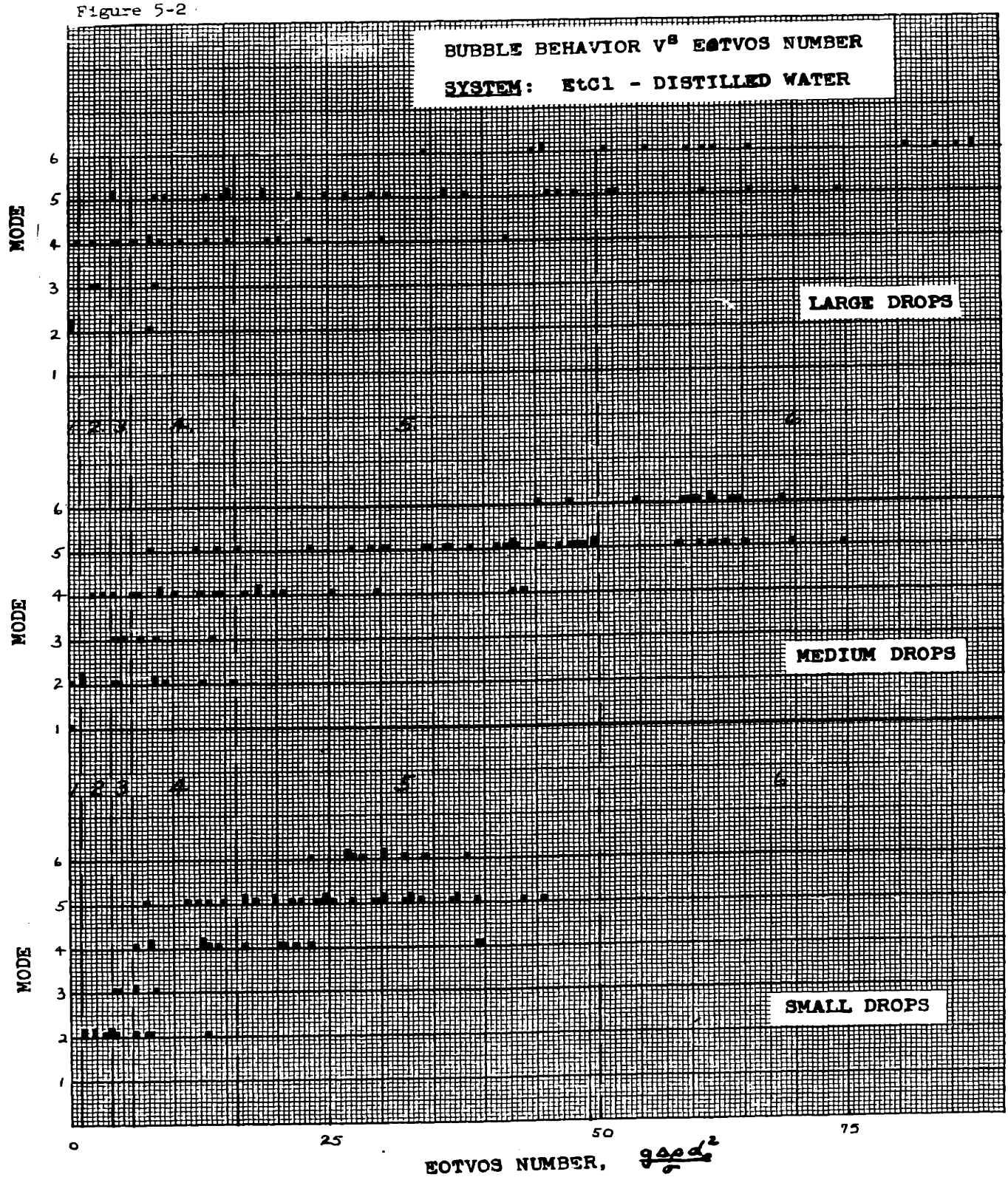
BUBBLE BEHAVIOR VS EOTVOS NUMBER
SYSTEM: EtCl - DISTILLED WATER
LARGE DROPS
MEDIUM DROPS
SMALL DROPS
MODE
MODE
MODE
1 2 3 4 5 6
1 2 3 4 5 6
1 2 3 4 5 6
0
25
50
75
EOTVOS NUMBER, $\frac{g\Delta\rho d_e^2}{\sigma}$

Figure 5-3

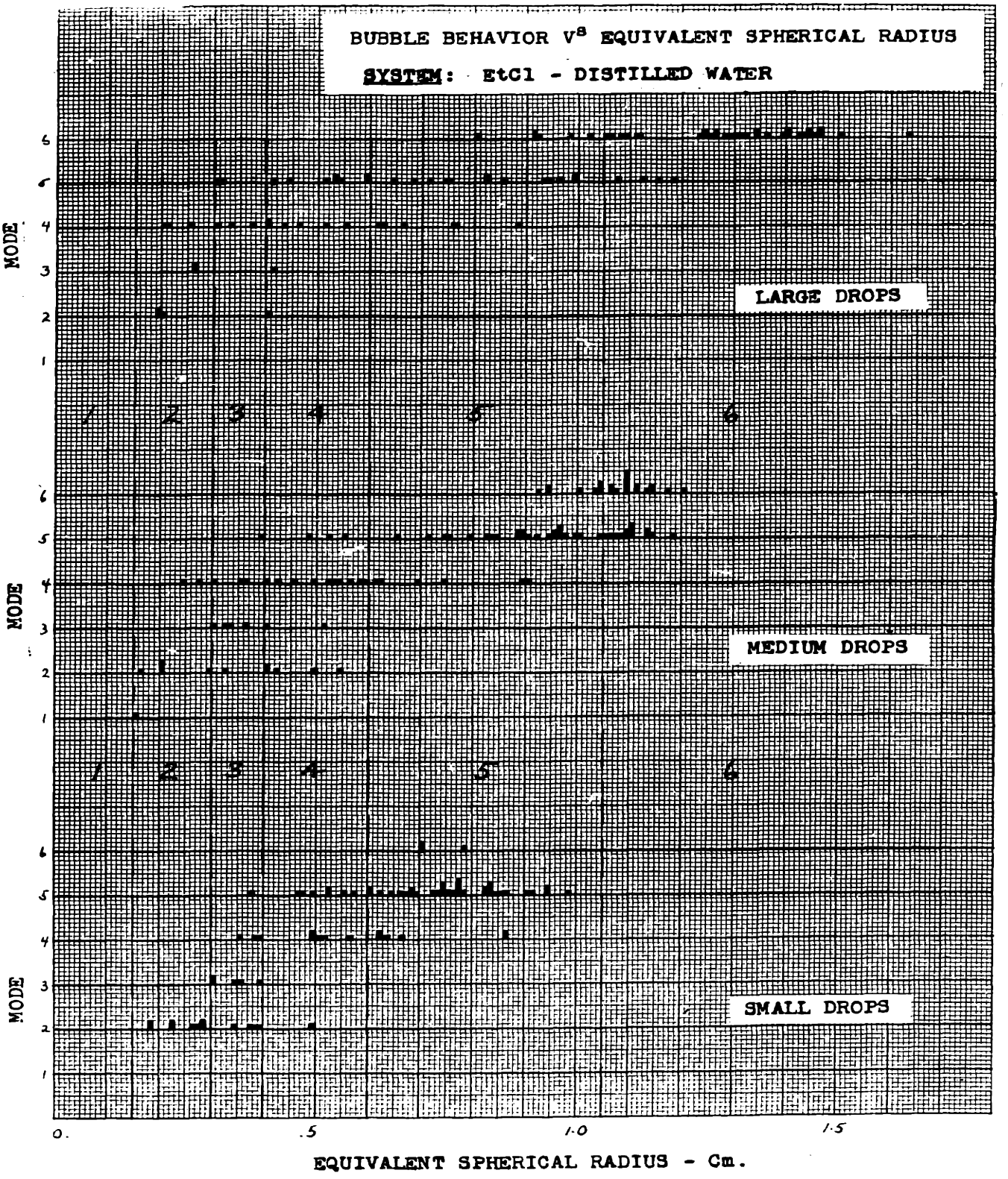
BUBBLE BEHAVIOR V^S EQUIVALENT SPHERICAL RADIUS
SYSTEM: EtCl - DISTILLED WATER
MODE
LARGE DROPS
MEDIUM DROPS
SMALL DROPS
1 2 3 4 5 6
0. .5 1.0 1.5
EQUIVALENT SPHERICAL RADIUS - Cm.

Figure 5-4

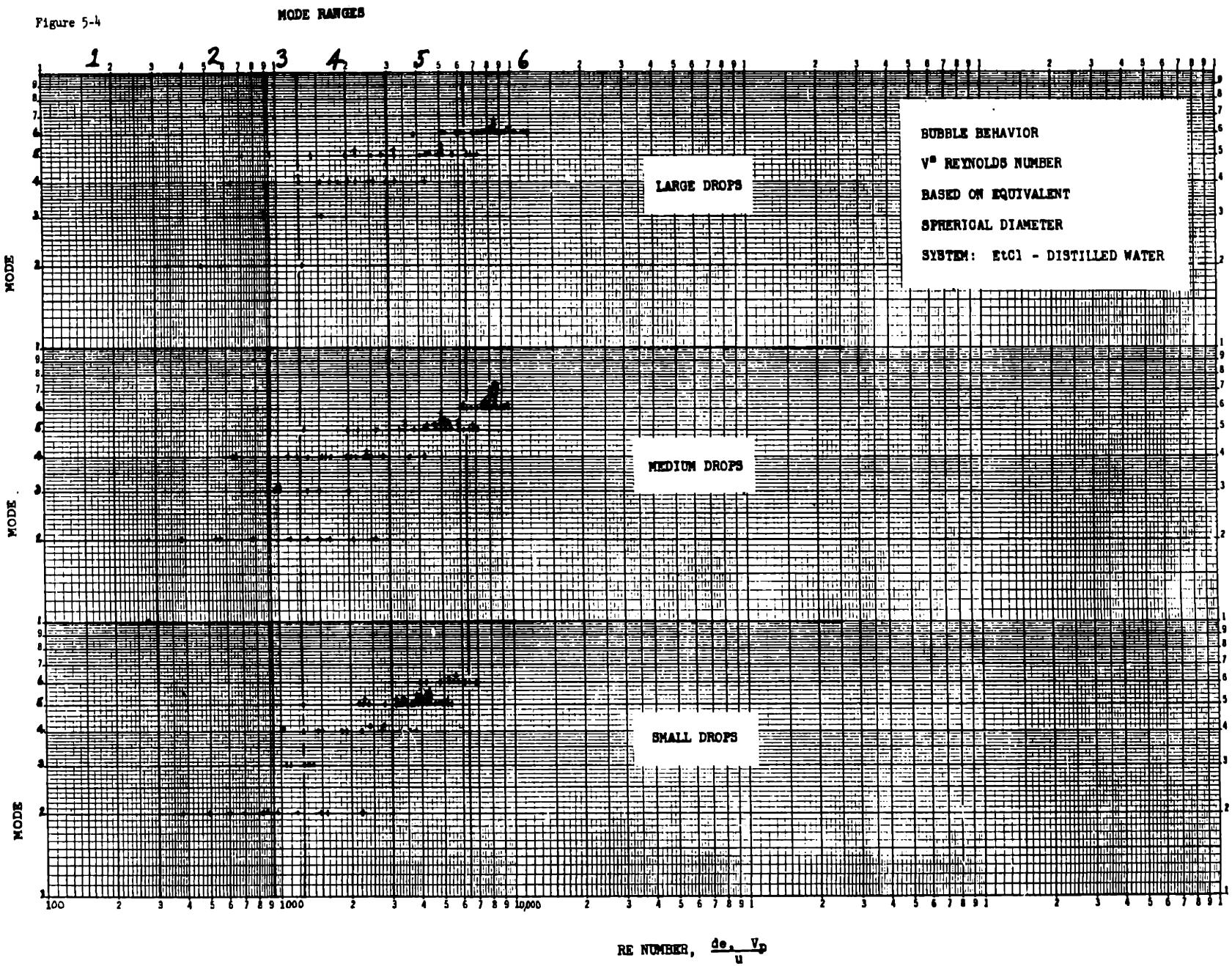
MODE RANGES
1
2
3
4
5
6
LARGE DROPS
MEDIUM DROPS
SMALL DROPS
BUBBLE BEHAVIOR
V^B REYNOLDS NUMBER
BASED ON EQUIVALENT
SPHERICAL DIAMETER
SYSTEM: EtCl - DISTILLED WATER
MODE
MODE
MODE
100
1000
10,000
RE NUMBER, de. Vp / u

Figure 5-5

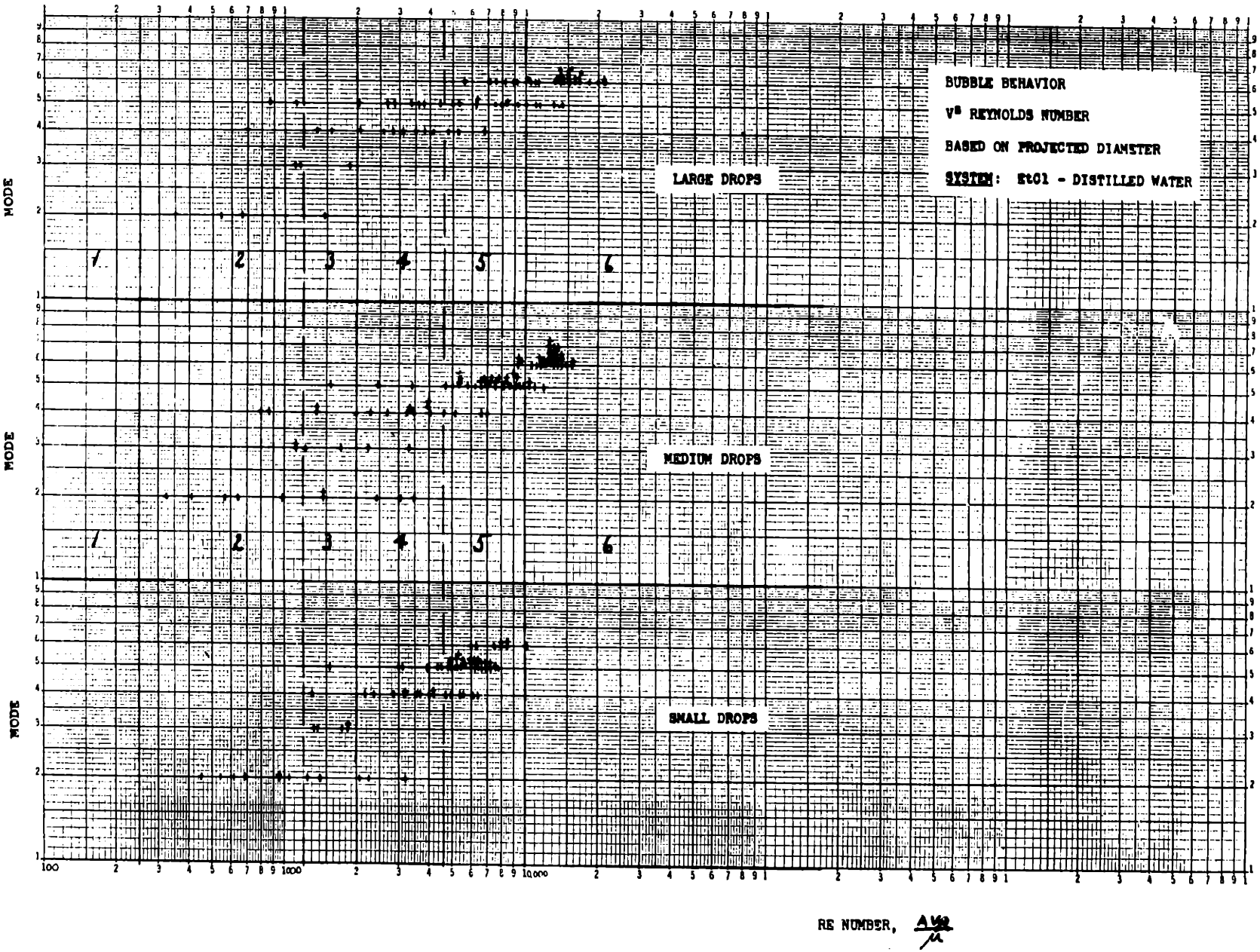
BUBBLE BEHAVIOR
V^B REYNOLDS NUMBER
BASED ON PROJECTED DIAMETER
SYSTEM: EtOl - DISTILLED WATER
LARGE DROPS
MEDIUM DROPS
SMALL DROPS
MODE
MODE
MODE
1
2
3
4
5
6
100
1000
10,000
RE NUMBER, $\frac{A V_B \rho}{\mu}$

2. The Reynolds Number index appears to be the most dependable of the indexes for the EtCl-water system. The results show no reason, however, to prefer the projected diameter basis or the equivalent spherical diameter basis. The latter is probably the better choice, if only because it is more widely used.
3. The Eötvos number is the only one for which the ranges correspond with previously reported values (37). The other index ranges run somewhat higher (62). This is to be expected since the Eötvos number through the $\Delta\rho$ component is the only one in which any compensation is possible for the presence of unvaporized liquid.
4. There seems to be no clear indication that the amount of unvaporized liquid present affects the pattern of bubble progression through the various modes. The transitions occur at roughly the same index value regardless of initial drop size.
5. The oscillations which were observed in the early phases of many of the runs are now seen to be a normal fluid dynamic response to eddy sheading which occurs when the drop is passing through a critical index range. This range, mode 3, is seen to be narrow from Table 5.4, and in fact, the photographs indicate that this zone prevails over no more than about 15% of the vaporization period and usually in the lower-rate early portion of the vaporization curve.

Having established the utility of classifying shapes we now have a basis for estimating liquid interfacial area from the dimensions of the photographic profiles. We must next derive area and volume formulas for each of the basic shapes. This is done as follows:

Interfacial Area Formulas:

For a sphere: (5 images out of 193)

Interfacial area $S, = 2\pi rl$

Liquid Volume $v_l, = \frac{1}{3}\pi l^2 (3r - l)$

where r is the radius of the sphere and l is the depth of the puddle.

For a ellipsoid (71 images out of 193)

To provide a reasonable but simple formula for a puddle in the bottom of an ellipsoid its shape was approximated by that of an inverse cone. The resulting formulas are:

Interfacial area $= \pi r' \sqrt{r'^2 + l^2}$ Where r' is the radius

Liquid Volume $= \frac{1}{3}\pi r'^2 l$ of the base of the cone.

For a spherical cap with a dimpled bottom (117 images out or 193)

A spherical cap of this shape can best be approximated by the model of a spherical segment whose normal volume is reduced 25% by a conical bottom having the same base dimensions as the cap itself. The most likely form for a liquid layer in this configuration is that of an annulus surrounding a truncated cone core. The corresponding formulas would be:

$$\text{Interfacial Area} = \pi A l + \pi\left(\frac{A}{2} + \frac{A'}{2}\right)\sqrt{\left(\frac{A}{2} - \frac{A'}{2}\right)^2 + l^2}$$

$$\text{Liquid Volume} \quad \frac{\pi A^2}{4l'}\left(l^2 - l^3/_{3l'}\right)$$

Where A is the diameter of the cap and cone base, A' is the diameter of the cone at the top of the frustrum and l' is the total height of the base cone.

In actually applying this approach it was found preferable to use the Eötvos number as a classifying index and to treat a liquid puddle in a sphere using the same inverse cone model as used for the ellipsoid. Converting the formulas to ones including only directly measurable quantities gave the following:

For Eo < 13 (spheres and Ellipsoids)

$$\frac{12 v_l}{\pi l A^2} - 4\frac{l}{B} + 4\frac{l^2}{B^2} = 0 \qquad S = \frac{1}{l}\sqrt{9 v_l^2 + 3\pi v_l l^3}$$

For Eo >13 (spherical caps)

$$v_l = \frac{\pi A^2 l^2}{.48B^2}(.6B - l) \qquad S = \pi A l \left[2 - \frac{2.5l}{B}\sqrt{1 + \frac{A^2}{.6B^2}}\right]$$

Where B is the height of the bubble measured from the photographs and A is its width.

In each case the first equation can be solved for h by Newton's method and the second can then be solved in turn for interfacial area.

These approximations will, of course, operate most satisfactorily when the puddle is thin i.e. when the vaporization process is more than 20% to 30% complete. It is least satisfactory in the very early stages. For example, when a bubble is half-liquid half-vapor (approximately .32% vaporized), its shape is that of a sphere but the estimating formula gives a value which is 22.8% too high. Since only six of the more than four hundred images used in analysis are less than half vapor, 22.8% may be taken as the maximum error introduced by the geometric approximation with the average error having a much lower value.

Using these approximations formulas liquid-liquid transfer areas were calculated for all the data images (See Appendix Table A-2). Plots of estimated area values versus fraction vaporized are given in Fig. 5.6 for drops representative of the three drop sizes. The figure shows that all three drop sizes have a similar area history. The positions of the curves relative to each other show that the dependence of area on initial diameter which was demonstrated on an average basis in Fig. 4.8 continues to hold on a differential basis, i.e., instantaneous area values for the three drop sizes are related to each other according to the relation $S = ad_i^2$ where a is a function of fraction vaporized.

Fig. 5.6 is marked to indicate where bubble shapes pass from one form to another as growth proceeds. Using the Eötvos number and the transition values of 13 for sphere to ellipsoid and 40 for ellipsoid to spherical cap, it is seen that

Figure 5-6

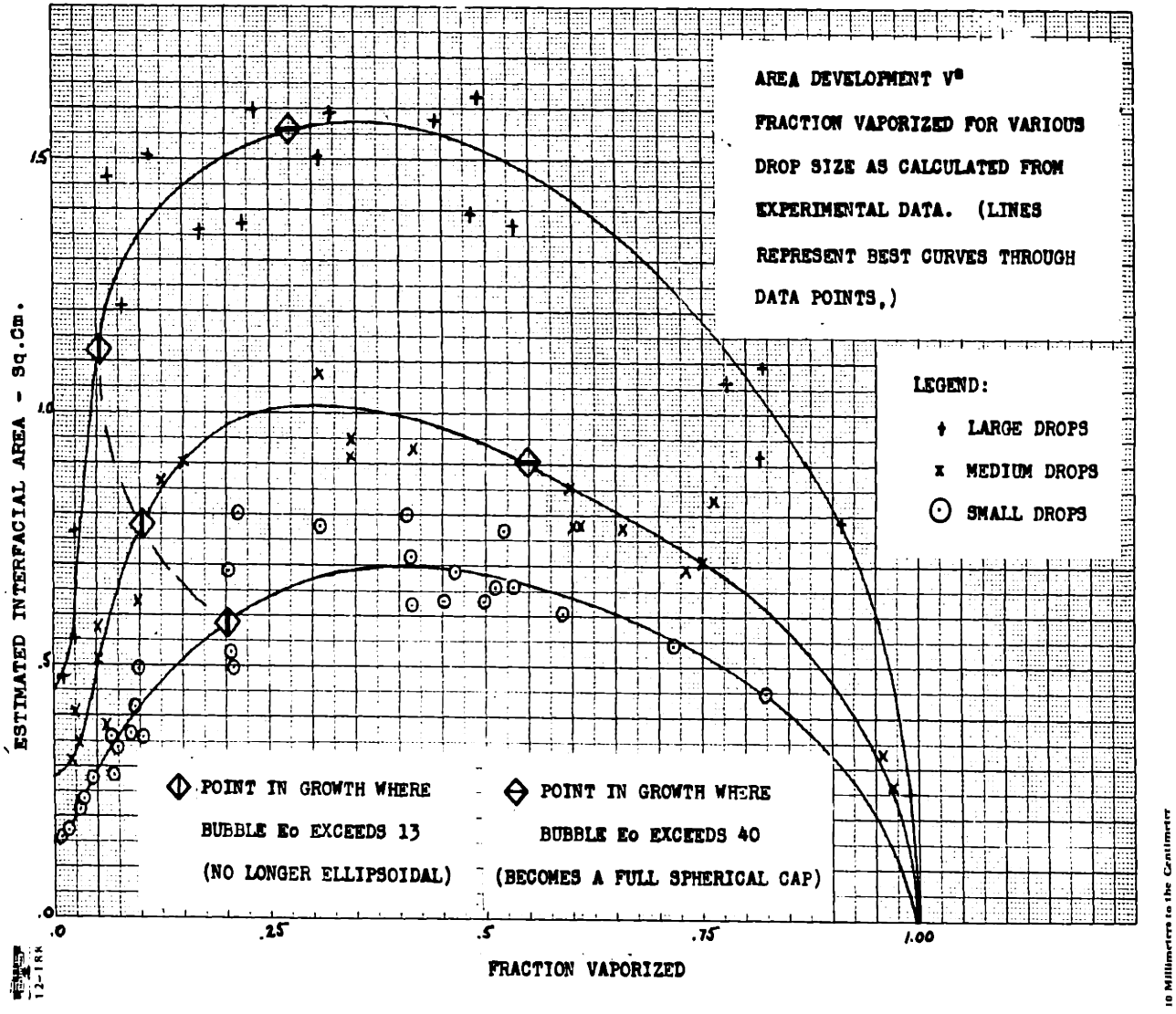
AREA DEVELOPMENT V^B
FRACTION VAPORIZED FOR VARIOUS DROP SIZE AS CALCULATED FROM EXPERIMENTAL DATA. (LINES REPRESENT BEST CURVES THROUGH DATA POINTS,)
LEGEND:
LARGE DROPS
MEDIUM DROPS
SMALL DROPS
POINT IN GROWTH WHERE BUBBLE Eo EXCEEDS 13 (NO LONGER ELLIPSOIDAL)
POINT IN GROWTH WHERE BUBBLE Eo EXCEEDS 40 (BECOMES A FULL SPHERICAL CAP)
ESTIMATED INTERFACIAL AREA - Sq.Cm.
1.5
1.0
.5
.0
.0
.25
.5
.75
1.00
FRACTION VAPORIZED
12-IRK
10 Millimeters to the Centimeter

a) large drops receive 75% of their heat as spherical caps

b) small drops never do become spherical caps. They have the form of an oscillating ellipsoid for most of their growth history.

In view of this it is surprising that both area (Fig. 5.6) and average transfer rates (Fig. 4.8) show such a simple dependence on initial diameter. Apparently for the ethyl chloride - distilled water system under the conditions studied drop shape and oscillation tendencies exert only minor influences on heat transfer rates.

(2) Effect of Surfactant

To discover whether the presence of a surfactant strongly altered the shape of the bubbles or their interfacial area, plots of Fluid Dynamic Mode vs. Reynolds Number (Fig. 5.8) and Eötvos Number (Fig. 5.7) were drawn up. These were augmented by plots of Interfacial Area vs. Fraction Vaporized (Fig. 5.9 and 5.10). Comparisons with similar data from the EtCl - distilled water system are presented on the plots and in Table 5.5. Based on these comparisons, the following observations may be made.

1) Where surfactants are present characteristic Eötvos number ranges are strongly displaced to the high side. Apparently the presence of surfactants does not change mode behavior to the degree that surface tension lowering would indicate. This is probably due to the formation of a surfactant film at the interface which is not present in systems having lower surface tensions naturally. Such films are known to inhibit rippling tendencies on a surface and a similar action here would probably defer the shape transitions just as observed.

2) The Reynolds number acts as a more reliable correlating index for surfactant containing systems although here too there is evidence of the effect of an interfacial film. Table 5-5 shows that modes are aligned with the same Reynolds number ranges as for plain water except for mode 2 where observed Reynolds numbers are somewhat high. Following the same reasoning used above, we can explain the shift by the presence of a "rigid" film of oriented

Table 5.5

Ranges of Eotvos Number
for Fluid Dynamic Modes
as a Function of Surfactant Concentration

Mode	Surfactant Concentration Wt% No. Surf.	.00575%	.079%	.135%
1	< 1	< 5.2	< 5.2	< 5.2
2	1-4	5.2-11.5	5.2-22	5.2-22
3	4-6	-	-	-
4	6-16	11.5-22	22-52	22-42
5	17-52	22-198+	52-120	42-110
6	> 52		> 120	> 110

Ranges of Reynolds Numbers for Fluid
Dynamic Modes as a Function of Surfactant Concentration

Mode	Surfactant Concentration Wt% No. Surf.	.00575%	.074%	.135%
1	< 300	< 900	< 670	< 670
2	300-950	900-1800	670-2000	670-2000
3	950-1250			
4	1250-3000	1800-3000	2000-4000	2000-4000
5	3000-6300	> 3000	4000-8200	3400-6000
6	> 6300		> 8200	> 6000

Table 5.6
Ranges of Eo Number for Fluid
Dynamic Modes as a Function of Viscosity

Mode	Plain Water	Hot 65% Gly. (μ=100cp)	Cold 65% Gly. (μ-137.5cp)
1	<1	<8.6	<2.5
2	1-4	8.6 - 22	2.5 - 10.5
3	4-6		
4	6-16		
5	17-52	22 - 42.5	20 - 52.5+
6	> 52	> 42.5	

Ranges of Reynolds Numbers for Fluid
Dynamic Modes as a Function of Viscosity (65% Gly.)

Mode	Plain Water	Hot 65% Gly. (μ=100cp)	Cold 65% Gly. (μ-137.5cp)
1	< 300	<115	< 38
2	300 - 950	115 - 300	38 - 130
3	950 - 1250	300 - 400	130 - 150
4	1250 - 3000		150 - 240
5	3000 - 6300	400 - 800	> 240
6	>6300	> 800	

Figure 5-7

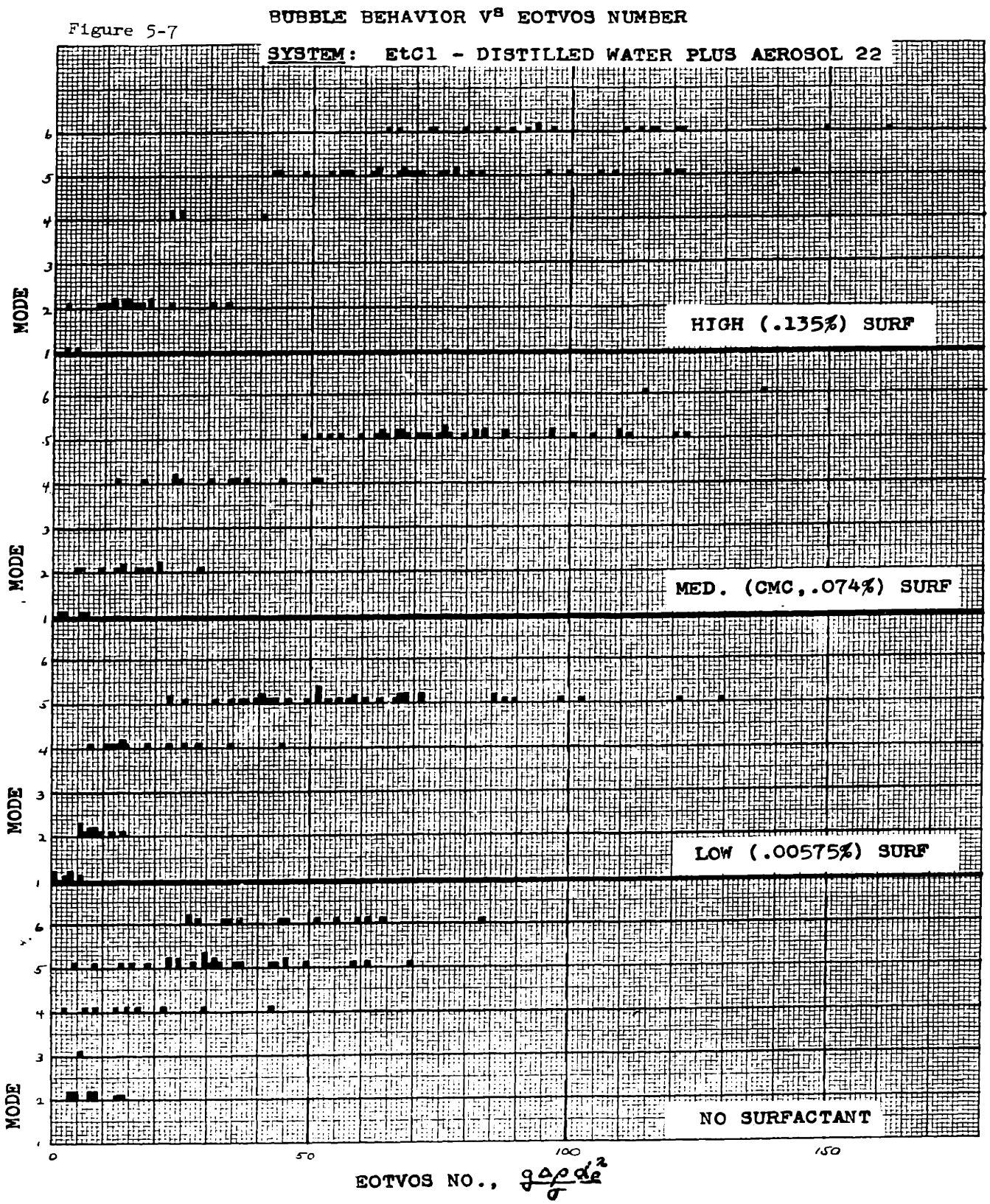
BUBBLE BEHAVIOR Vs EOTVOS NUMBER
SYSTEM: EtCl - DISTILLED WATER PLUS AEROSOL 22
MODE
HIGH (.135%) SURF
MED. (CMC, .074%) SURF
LOW (.00575%) SURF
NO SURFACTANT
0
50
100
150
EOTVOS NO., $\frac{g\Delta\rho d_e^2}{\sigma}$

Figure 5-8

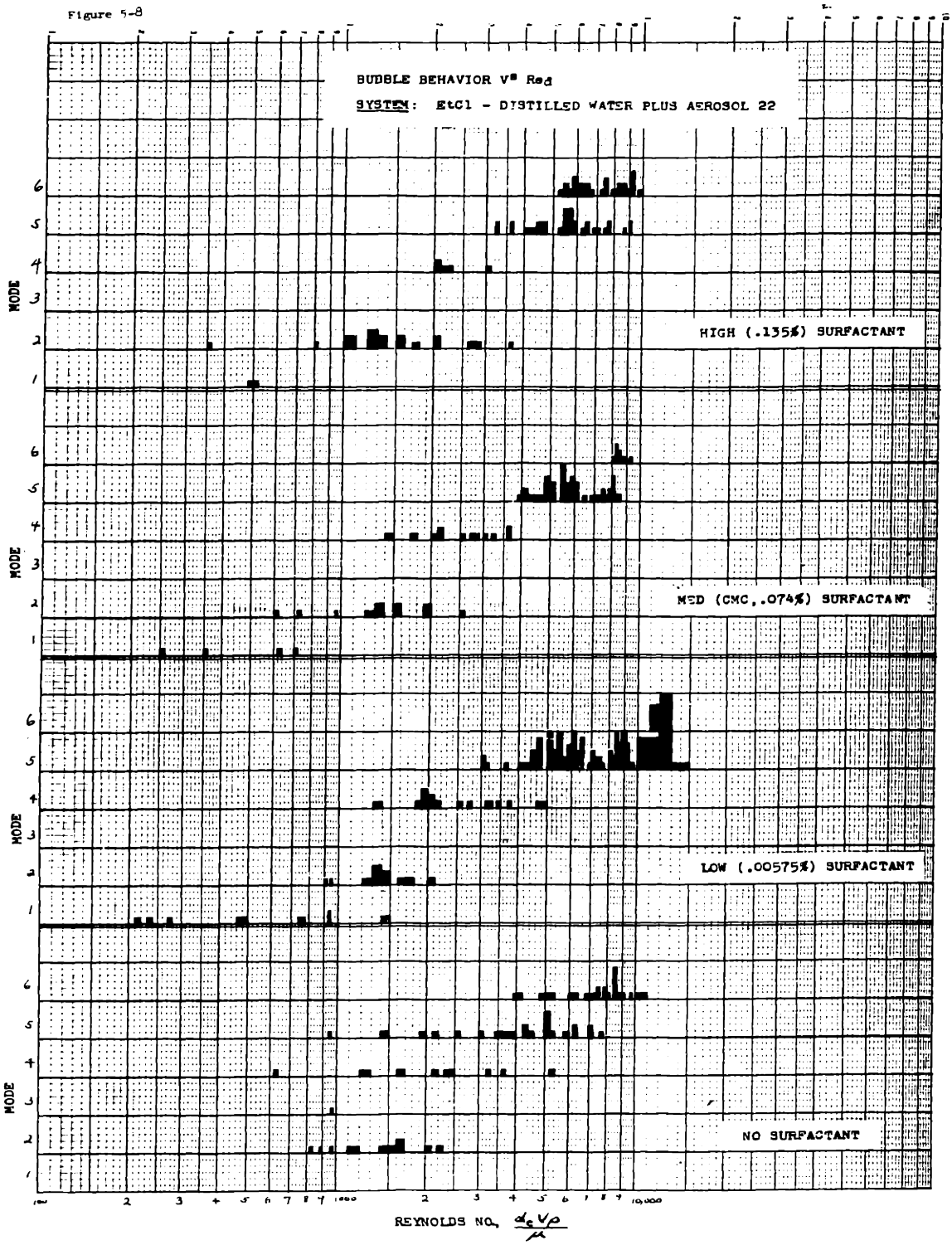
BUBBLE BEHAVIOR V^B Rad
SYSTEM: EtCl - DISTILLED WATER PLUS AEROSOL 22
MODE
HIGH (.135%) SURFACTANT
MED (CMC, .074%) SURFACTANT
LOW (.00575%) SURFACTANT
NO SURFACTANT
REYNOLDS NO. $\frac{d_e V \rho}{\mu}$

Figure 5.9

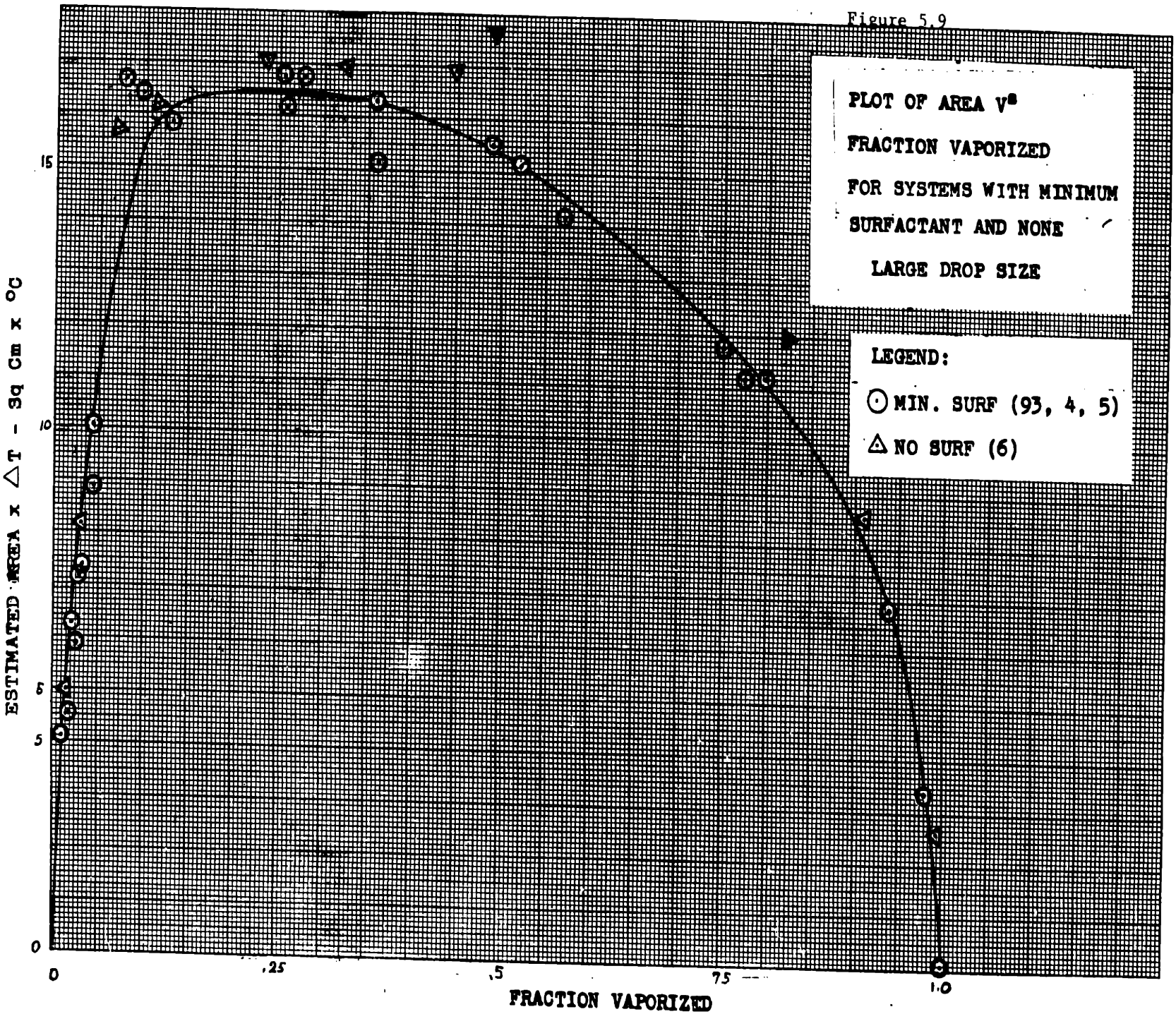
PLOT OF AREA V^s
FRACTION VAPORIZED
FOR SYSTEMS WITH MINIMUM
SURFACTANT AND NONE
LARGE DROP SIZE
LEGEND:
MIN. SURF (93, 4, 5)
NO SURF (6)
ESTIMATED AREA x ΔT - Sq Cm x °C
FRACTION VAPORIZED
0
5
10
15
.25
.5
.75
1.0

Figure 5-9

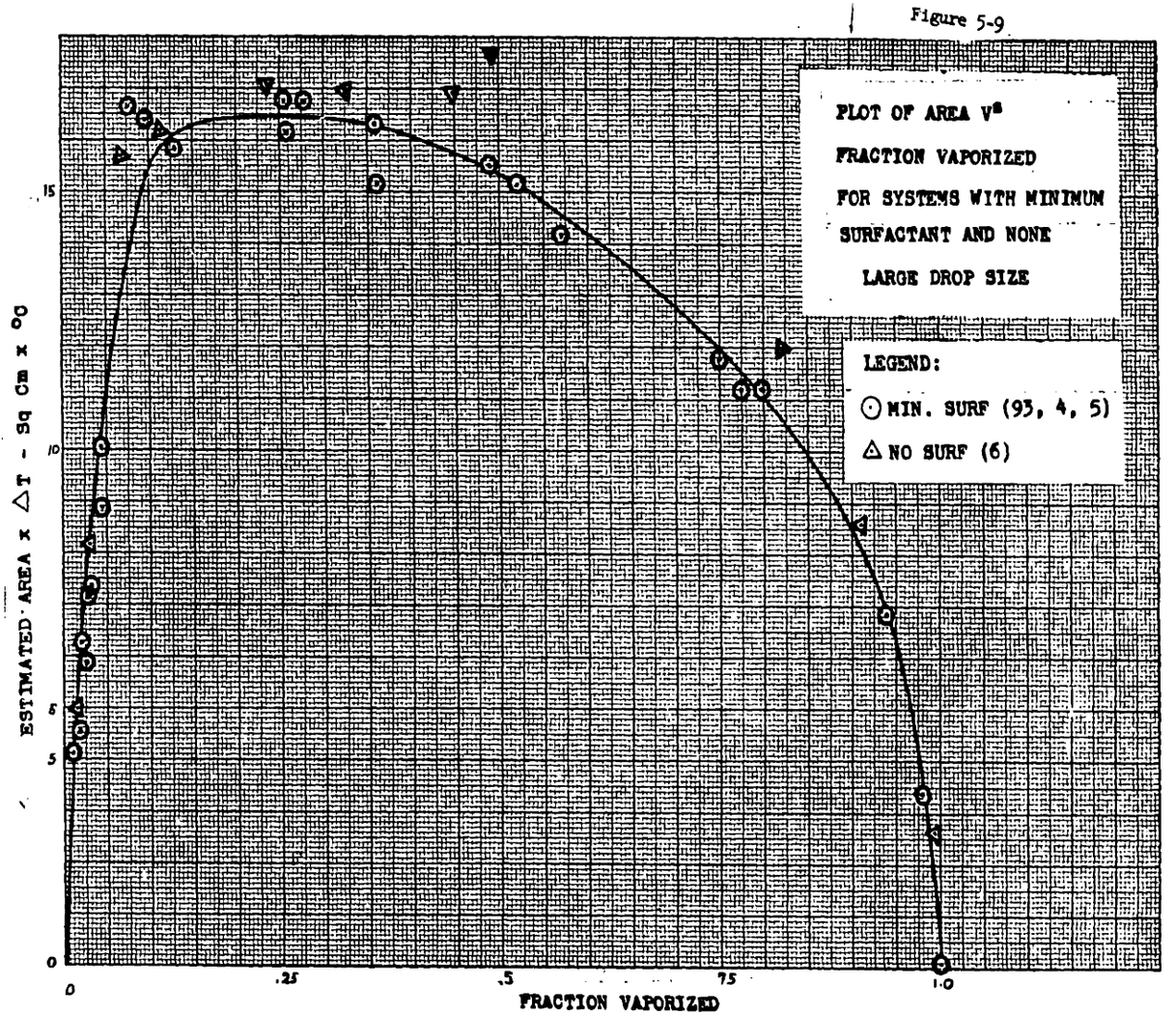
PLOT OF AREA V^B
FRACTION VAPORIZED
FOR SYSTEMS WITH MINIMUM
SURFACTANT AND NONE
LARGE DROP SIZE
LEGEND:
⊙ MIN. SURF (93, 4, 5)
△ NO SURF (6)
ESTIMATED AREA x △T - Sq Cm x °C
FRACTION VAPORIZED
0
5
10
15
.25
.5
.75
1.0

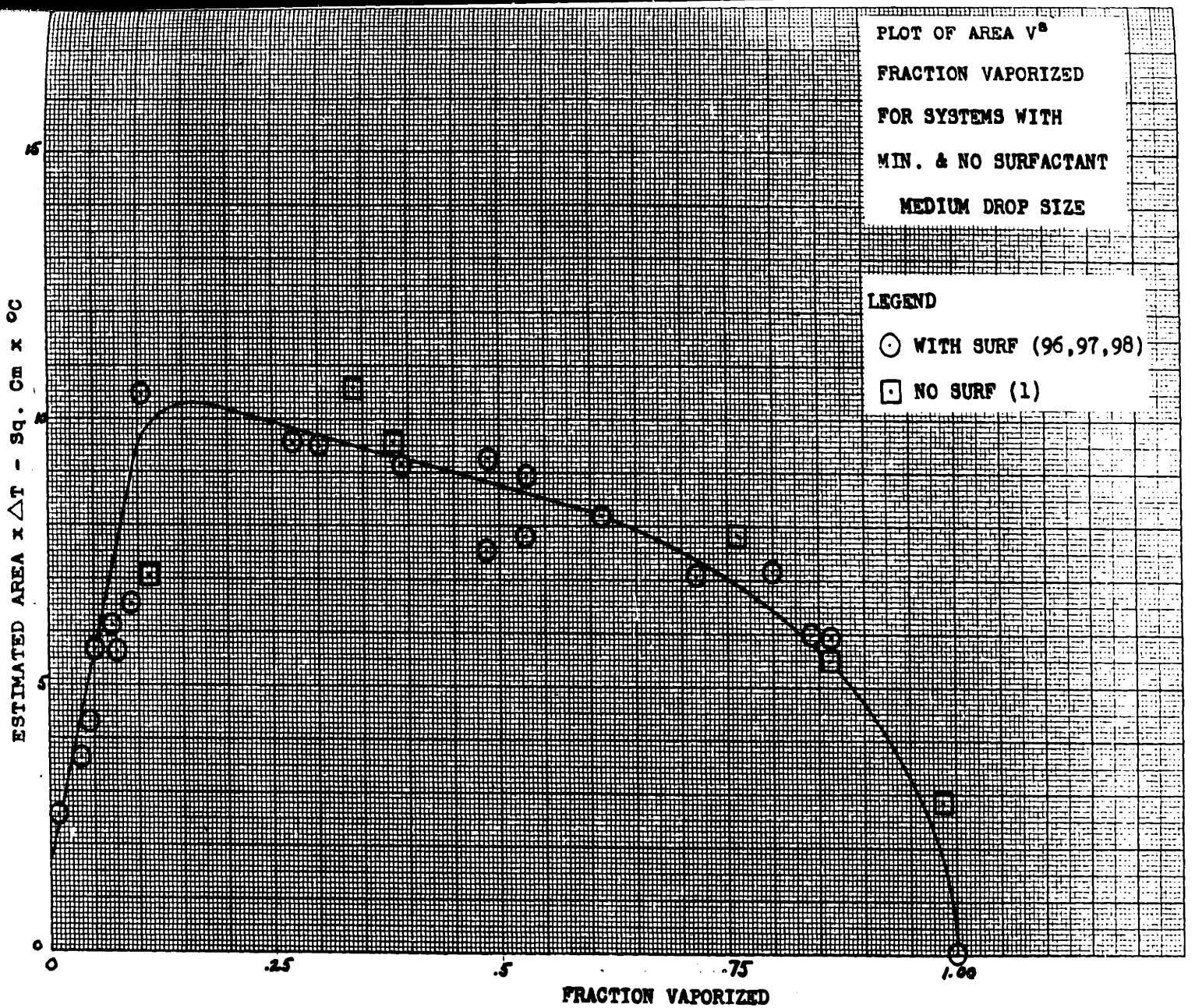
PLOT OF AREA V^B
FRACTION VAPORIZED
FOR SYSTEMS WITH
MIN. & NO SURFACTANT
MEDIUM DROP SIZE
LEGEND
WITH SURF (96,97,98)
NO SURF (1)
ESTIMATED AREA x ΔT - Sq. Cm x °C
FRACTION VAPORIZED
0
.25
.5
.75
1.00

Figure 5-10

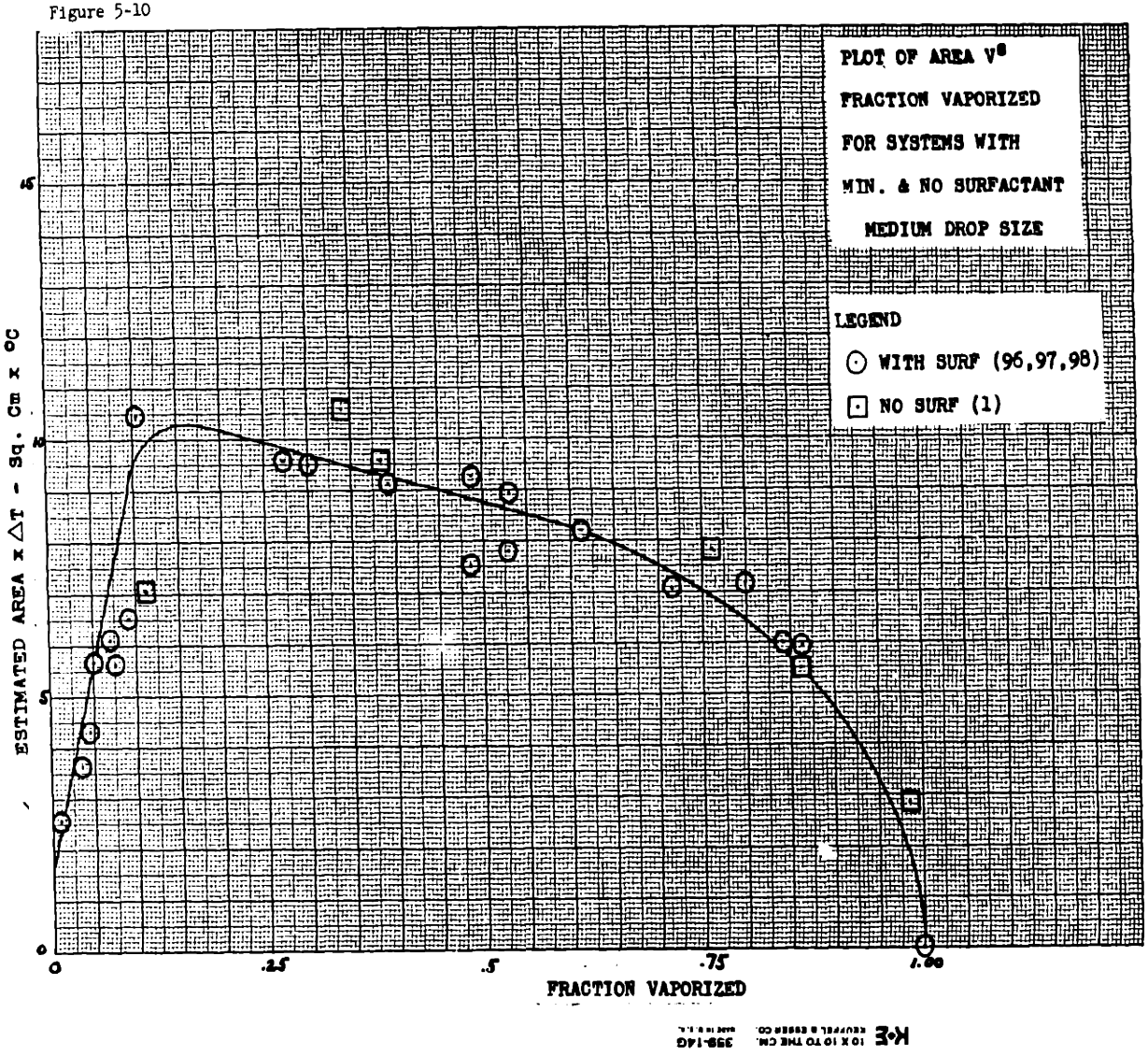
PLOT OF AREA V$^{\theta}$
FRACTION VAPORIZED
FOR SYSTEMS WITH
MIN. & NO SURFACTANT
MEDIUM DROP SIZE
LEGEND
WITH SURF (96,97,98)
NO SURF (1)
ESTIMATED AREA x ΔT - Sq. Cm x °C
FRACTION VAPORIZED
0
.25
.5
.75
1.00
5
10
15

Figure 5-11

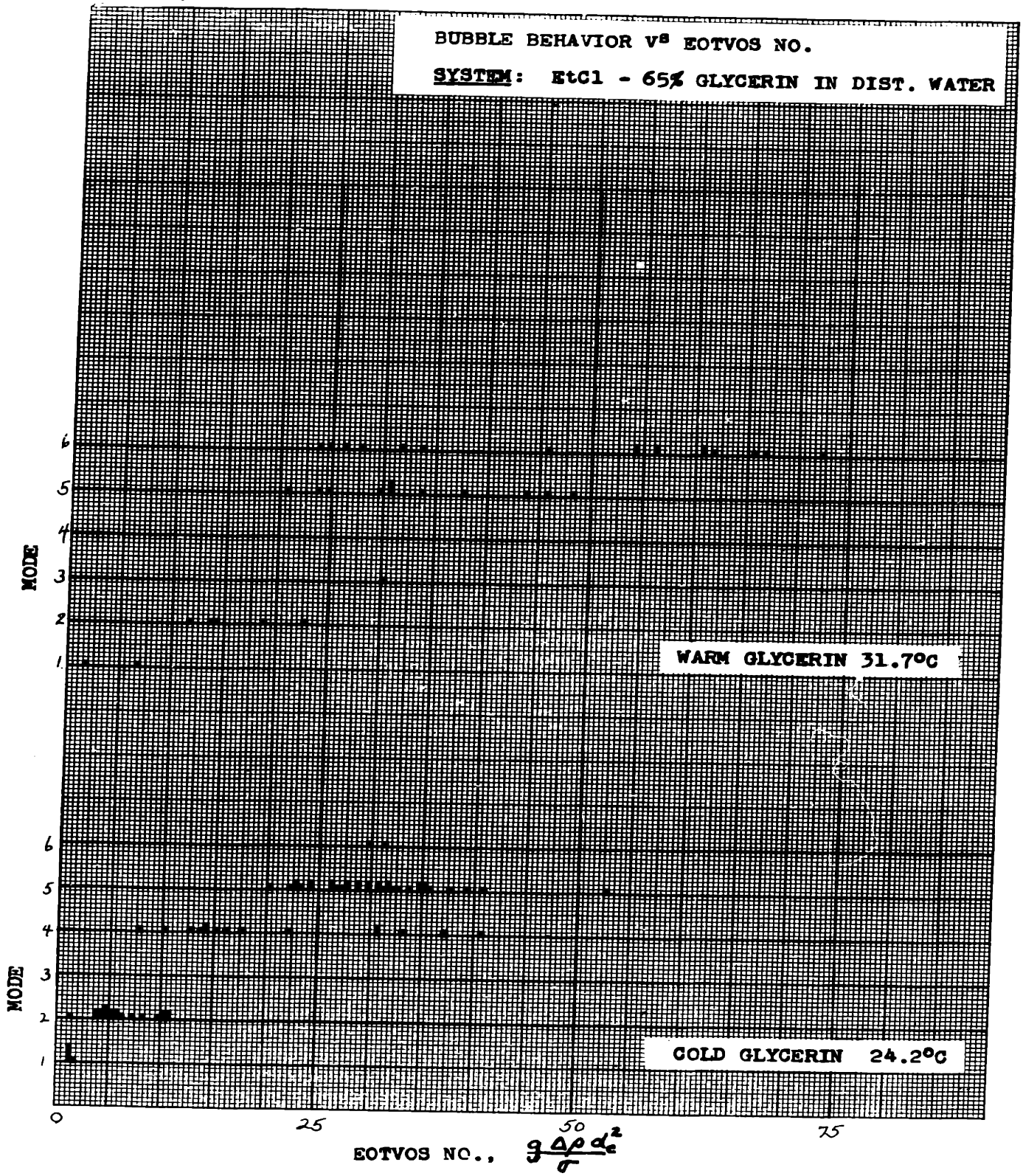
BUBBLE BEHAVIOR VS EOTVOS NO.
SYSTEM: EtCl - 65% GLYCERIN IN DIST. WATER
WARM GLYCERIN 31.7°C
COLD GLYCERIN 24.2°C
MODE
MODE
1
2
3
4
5
6
0
25
50
75
EOTVOS NO., $\frac{g \Delta\rho d_e^2}{\sigma}$

Figure 5-12

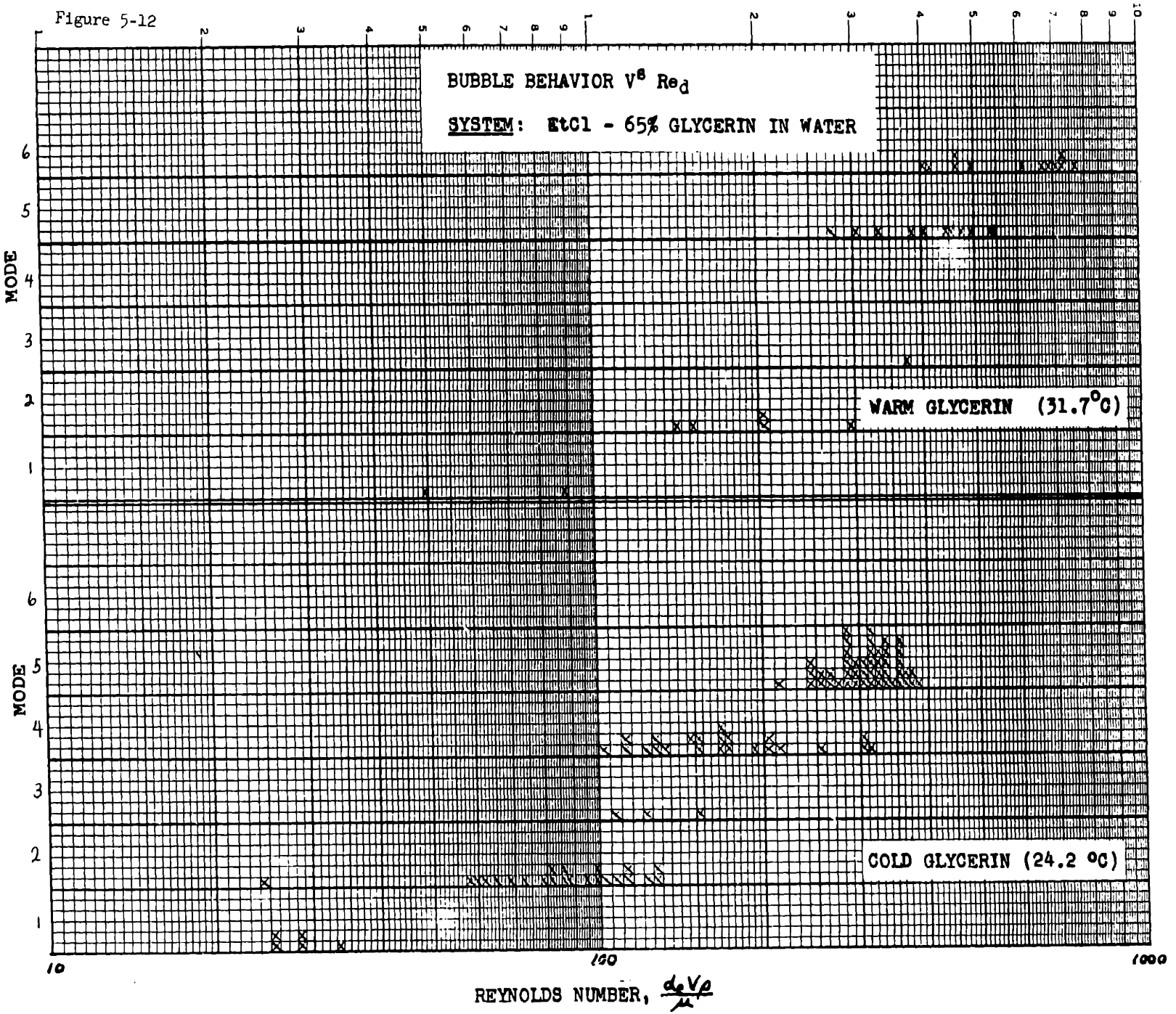
BUBBLE BEHAVIOR V^B Re_d
SYSTEM: EtCl - 65% GLYCERIN IN WATER
WARM GLYCERIN (31.7°C)
COLD GLYCERIN (24.2 °C)
MODE
MODE
10
100
1000
REYNOLDS NUMBER, $\frac{d_e V \rho}{\mu}$

surfactant molecules which stabilizes the surface temporarily against exhibiting the oscillation tendencies typical of modes 3 and 4.

3) The curves of Fig. 5.9 and 5.10 demonstrate that the deferring of mode changes does not appreciably effect the area available for heat transfer. This lends additional support to the conclusion already drawn from Fig. 5.6 that the interfacial area presented by a liquid puddle is not appreciably affected by minor changes in drop shape.

* Insert text 80A

C. Heat Transfer Coefficient

As pointed out in Chapter 1, the rate of a vaporization process can be limited by either the rate of heat transfer to the surface on the rate of molecular escape from the surface.

1) Surface Escape Limitation

Applying Langmuir's equation for the maximum rate of molecular escape to the experimental data, Run 14 (high ΔT, large drop size), we calculate an upper rate limitation of 4.4 gm./(cm.^{2})(sec.). Converting experimental rate measurements to the same basis we obtain .12 gm./(cm)^2(sec.) or 2.7% of the calculated maximum. As noted by Heideger and Boudart (39A) steric effects can cause maximum rates for many liquids to be limited to less than 1% of the Langmuir value. Thus it is conceivable that rates for the most favorable conditions studied could be approaching their absolute maximum. No positive conclusion can be reached on this point, however, without specific knowledge of the accommodation coefficient of ethyl chloride.

2) Heat Transfer Limitation

Although vapor escape rate can conceivably be setting the upper limit for vaporization rate in direct contact systems, most of the transfer rates measured in this work do not approach maximum levels and are more likely limited by the more conventional transfer limitations. At this point it is instructive to gain some feeling for the overall rates

(3) 65% Glycerol Continuous Phase

The use of index numbers to characterize shape transistions was also tested for the situation of a viscous continuous phase. Fluid Dynamic Modes are plotted versus Eötvos Number and Reynolds Number in Figs. 5.11 and 5.12. Characteristic ranges are listed in Table 5.6. Here the Reynolds Number becomes unsatisfactory as an index since the ranges are greatly different from those observed for the other conditions tested. The Eötvos number is seen to compare well with plain water for high values but higher than usual values are observed for the spherical and ellipsoidal range. This is because viscous forces have a strong effect in this region and the higher drag forces the shape to remain streamlined for a longer period. The behavior of spherical caps is independent of fluid viscosity so that shape history in that region is unaffected. Since it has already been shown that area is not a strong function of shape in the sphere-ellipsoid range, the effect of slight errors in shape prediction on overall rate is probably not great here either. Thus of the indexes examined the Eötvos number provides the best indication of shape transition for continuous phases of differing viscosity ranges.

Figure 5-11

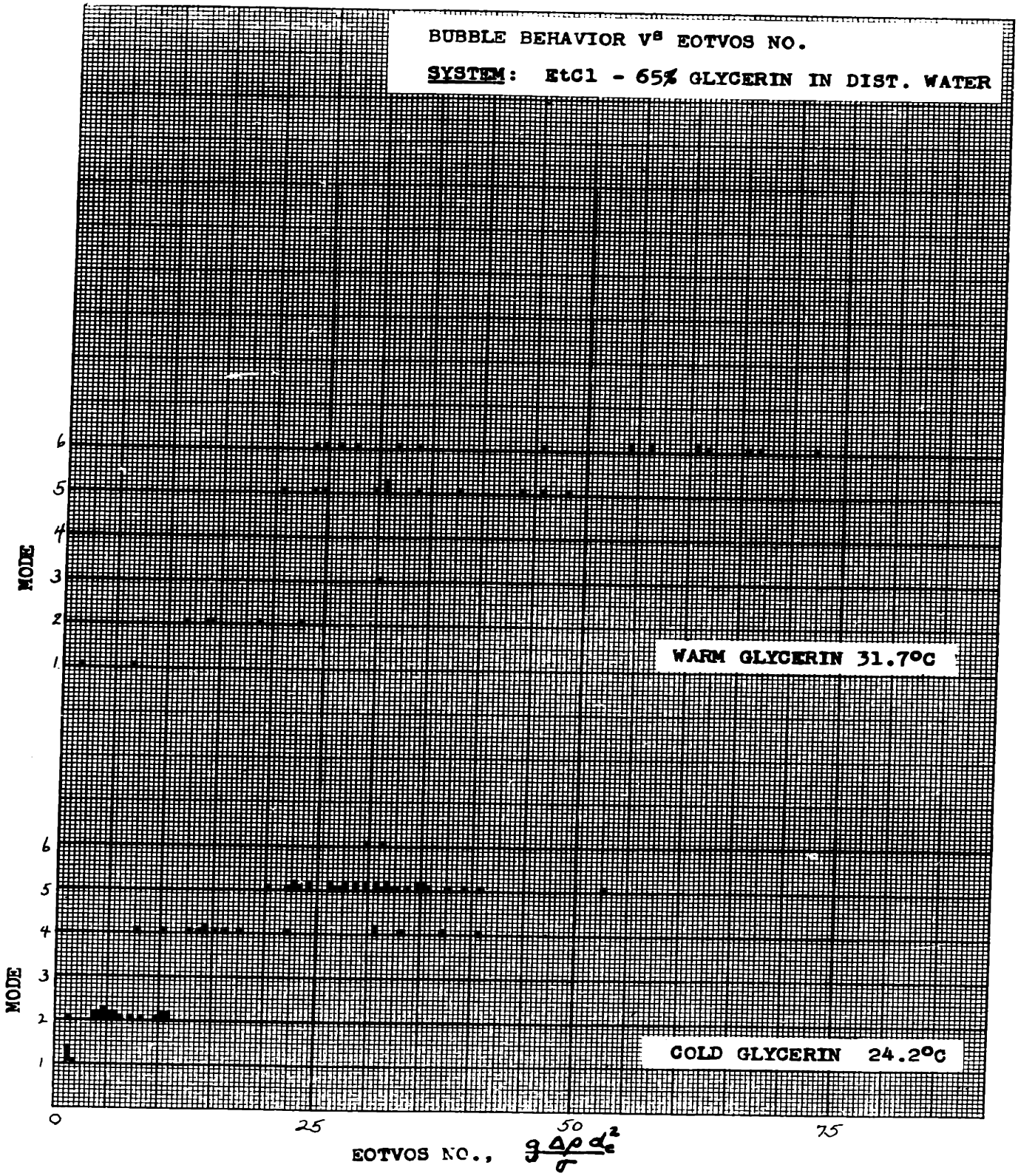
BUBBLE BEHAVIOR Vs EOTVOS NO.
SYSTEM: EtCl - 65% GLYCERIN IN DIST. WATER
WARM GLYCERIN 31.7°C
COLD GLYCERIN 24.2°C
MODE
MODE
1
2
3
4
5
6
0
25
50
75
EOTVOS NO., $\frac{g \Delta\rho d_e^2}{\sigma}$

Figure 5-12

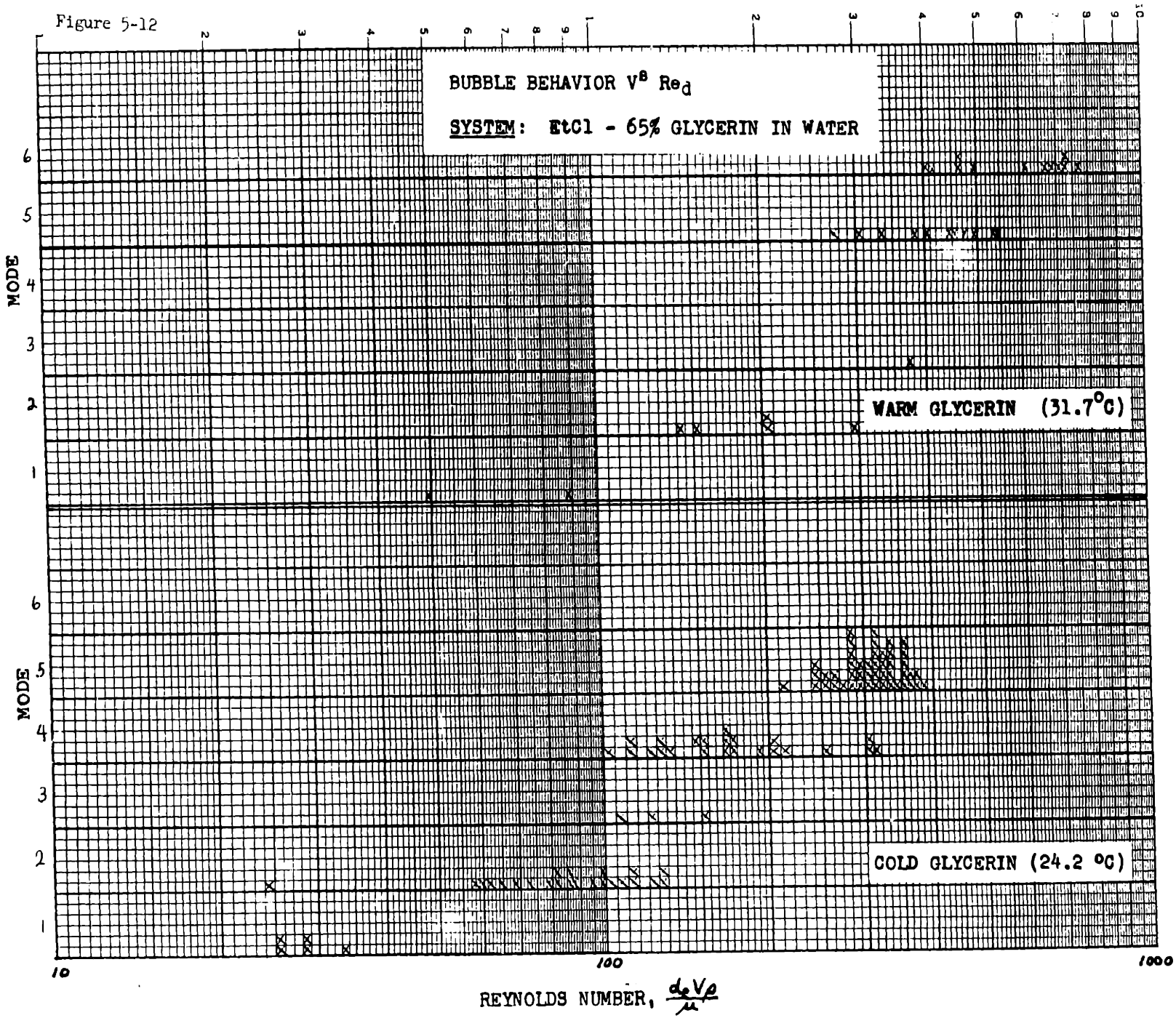
BUBBLE BEHAVIOR V^B Re_d
SYSTEM: EtCl - 65% GLYCERIN IN WATER
WARM GLYCERIN (31.7°C)
COLD GLYCERIN (24.2 °C)
MODE
MODE
10
100
1000
REYNOLDS NUMBER, $\frac{d_e V \rho}{\mu}$

involved relative to those for more conventional situations. This is done in Fig. 5.13 by plotting observed flux versus ΔT for various systems. It is gratifying to note that the system used in this work has a demonstrated flux capacity of almost two fold over the other non-mechanical systems with which it is compared.

The comparison also suggests reasons for this improvement. The effect of two major influences is illustrated: phase change and forced flow. The lowest rate is exhibited by data on natural convection to drops where neither influence is present. Garwin and Smith (26) achieved a significantly better rate by exploiting density differences between two immiscible liquids to achieve a moderate degree of forced counter flow in a liquid-liquid spray column. Related work by McDowell and Myers (56) on single drops established that the major heat transfer resistance in such a system lies in the dispersed phase even when circulation within the liquid drop is well developed. The rates reported by Garwin and Smith were surpassed many fold by Gordon et al (29) who caused a static organic phase to boil by floating it on heated mercury. Thus the presence of phase change apparently acts to reduce overall heat flow resistance by reducing the resistance offered by the internal phase.

The present work utilizing a dynamic system has added a strong interfacial shear to the process thereby converting the process from one of natural convection to one of largely forced convection. In this connection, Garner (25) states that free convection is significant over a range $1 < Re < 1000$ and forced convection entirely predominates above this range. By this rule, more than 95% of the vaporization cycle for all runs studied is in the forced convection region. Thus the gain observed for a rising boiling drop compared to the work of Graham et al can be attributed to a major reduction in external film resistance plus perhaps some further decrease in internal phase resistance due to the addition of some liquid circulation.

The only previously studied situation in which both phase change and forced flow are present is in studies made of boiling heat transfer

12-1N8

Figure 5-13

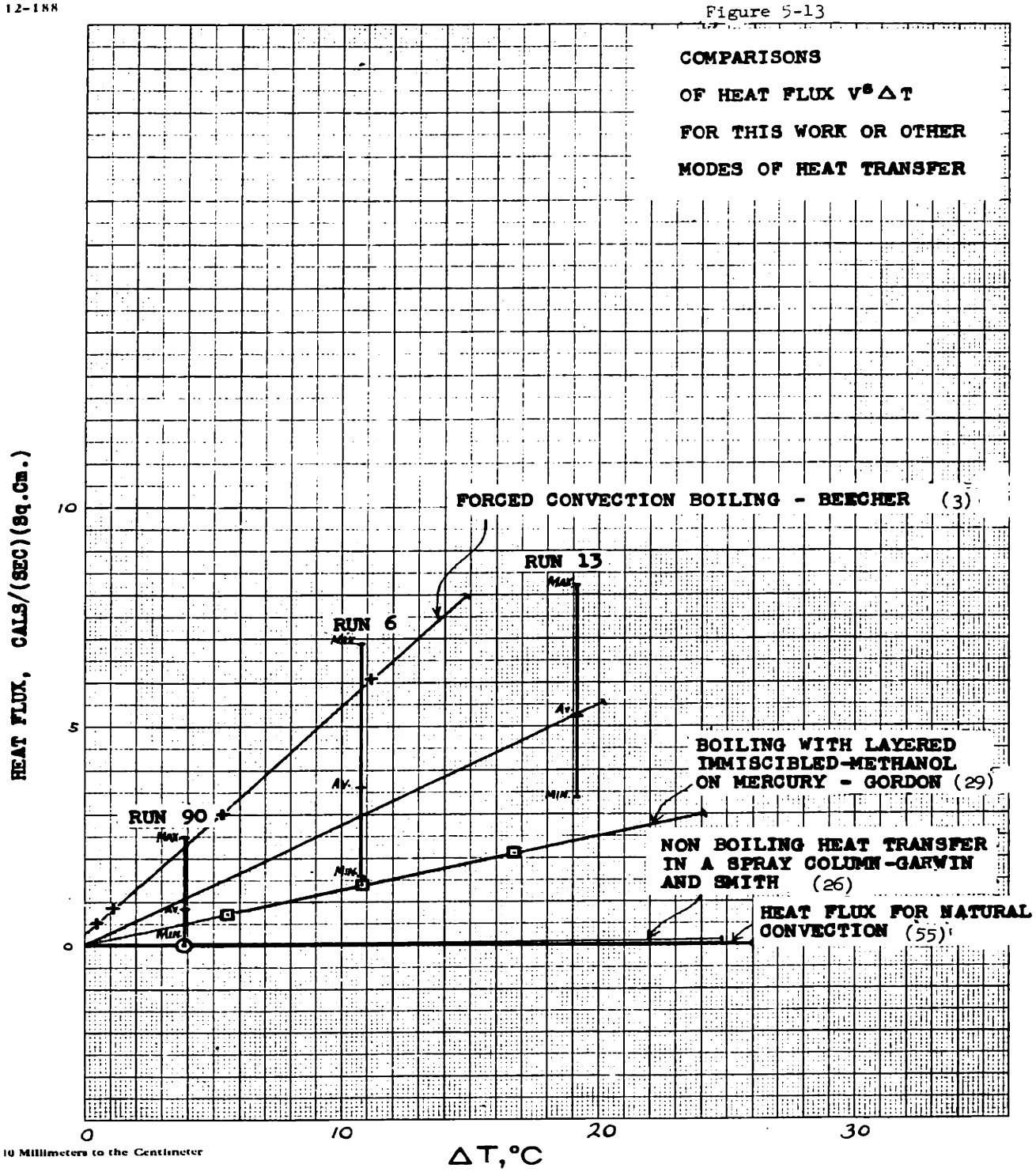

10 Millimeters to the Centimeter

involving forced flow past solid heating surfaces. Data from one such study by Beecher (3) predicts values which coincide with the uppermost values estimated from the present study. Beecher's results were gathered for a flow of 3 ft./sec. past a hot stainless steel tube of .050 inches diameter.

In describing the forced convection boiling of water McAdams (55) makes the following pertinent comments:

"In the temperature range, (2 - 9^{o}F ΔT), the liquid water is being superheated by natural convection and evaporation occurs only at the surface of the pool. ... For ΔT of less than 10^{o}F curves with and without imposed velocity are in agreement with the respective nonboiling correlations for forced convection and natural convection."

By analogy we may picture the present system as a pool of liquid which loses heat through evaporation at its upper surface and gains heat from a continuous phase which flows past its under surface in a forced convection regime.

As a further indication of the relative importance of the interior film it is instructive to compare observed heat transfer coefficients with those for transfer through a liquid puddle by pure conduction only. This is done in Figure 5. 14. Overall coefficients estimated from experimental data are plotted against fraction vaporized for several experimental conditions. In spite of the scatter of the data, the figure shows that the inside film coefficient for pure conduction is much lower than all estimates of the overall coefficients made from the data. Thus a considerable amount of mixing must be occurring in the internal phase. This is easy to accept since in addition to the obvious hydrodynamic shear there is the possibility of oscillation induced eddys such as described by Hughes and Gilliland (41) and thermal currents such as those studied by Spangenberg and Rowland (65).

Figure 5-14

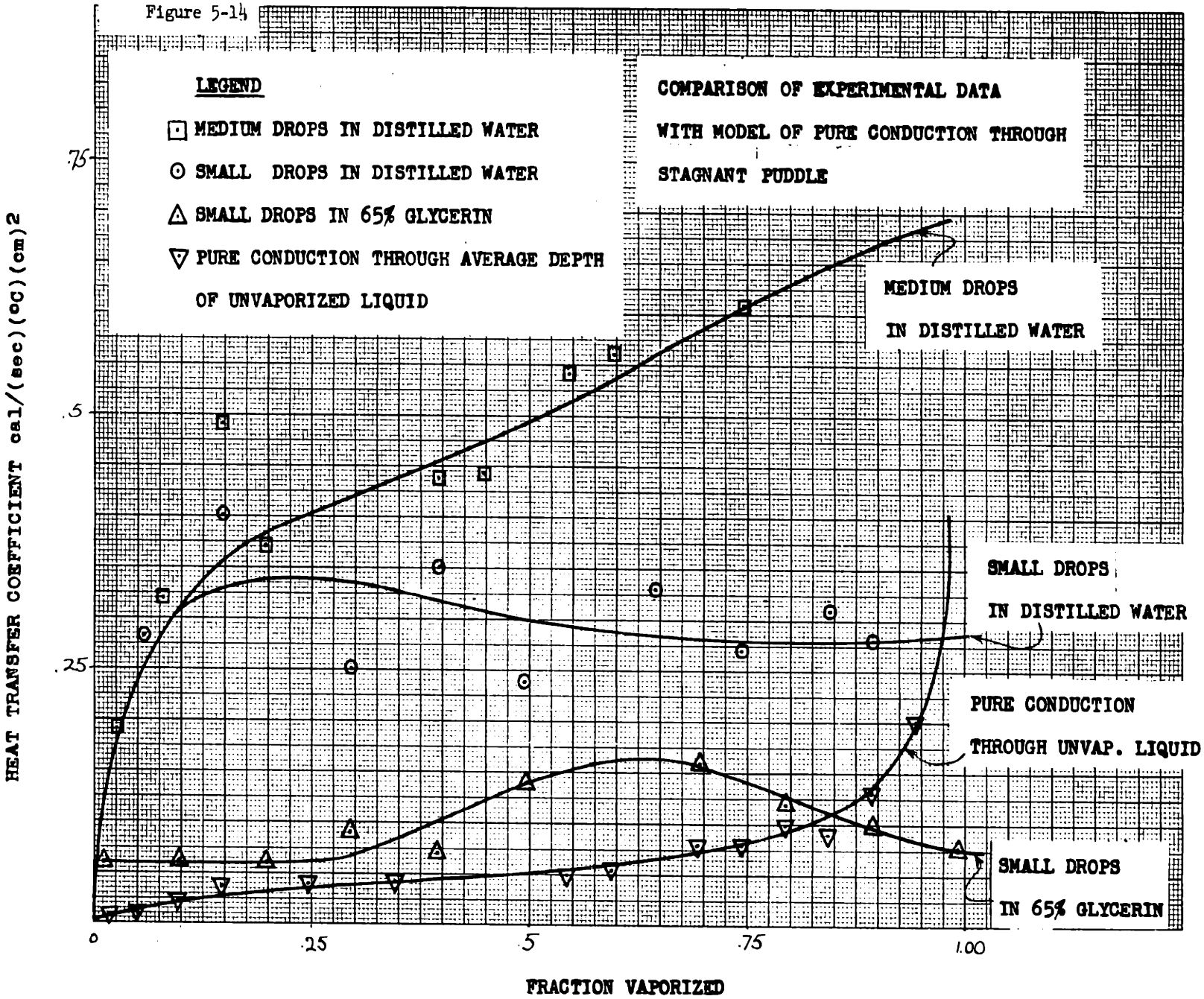
LEGEND
MEDIUM DROPS IN DISTILLED WATER
SMALL DROPS IN DISTILLED WATER
SMALL DROPS IN 65% GLYCERIN
PURE CONDUCTION THROUGH AVERAGE DEPTH OF UNVAPORIZED LIQUID
COMPARISON OF EXPERIMENTAL DATA WITH MODEL OF PURE CONDUCTION THROUGH STAGNANT PUDDLE
MEDIUM DROPS IN DISTILLED WATER
SMALL DROPS IN DISTILLED WATER
PURE CONDUCTION THROUGH UNVAP. LIQUID
SMALL DROPS IN 65% GLYCERIN
HEAT TRANSFER COEFFICIENT cal/(sec)(oC)(cm)2
.75
.5
.25
0
.25
.5
.75
1.00
FRACTION VAPORIZED

It has been shown already that much of the vaporization process occurs in a shape transition region where instabilities, which cause some shape oscillation are known to be present. Calderbank and Korchinski (9) have developed a summary of literature on drop behavior which shows that drop oscillation behavior in the Reynolds Number range 300 - 3000 can reduce the internal film resistance by 7 to 71 fold over that expected for pure conduction.

If thermal currents and oscillation both act to reinforce the effects of shear, a well mixed condition could easily be sustained in the unvaporized liquid puddle throughout the vaporization step. According to the ranges of Reynolds number and Rayleigh number which prevailed, this, in fact, does happen and the overall heat transfer coefficient should be almost entirely a function of exterior phase conditions from beginning to end.

3) Correlating Equation

To test the hypothesis that heat is transferred by a forced convection mechanism with external phase controlling, the data for both distilled water and 65% glycerin was ploted on coordinates of the Frossling type, $(Nu - 2)/Pr^{Z}$ Vs. Re. This was done in Fig. 5.15 and 5.16. In view of the number and scope of approximations which had to be made in calculating the parameters involved, correlation of the data is surprisingly good.

Of particular significance are comparisons of data regression lines with two well established correlations: the Ranz Marshall Model for transfer to a solid sphere over Re = 0 - 1000, and the Handlos Baron model for transfer to liquid droplets over the Reynolds number range 200 - 1000. As is clearly shown the slope of the data line is much steeper approximating 1.0 instead of 0.5 as found for the two models. The regression equation on Ranz Marshall coordinates is

$$(Nu - 2)/Pr^{1/3} = .096\ Re^{.93}.$$

TEST OF RANZ - MARSHALL

MODEL $Nu = 2. - .6\, Re^{\frac{1}{2}} Pr^{\frac{1}{3}}$

Figure 5-15

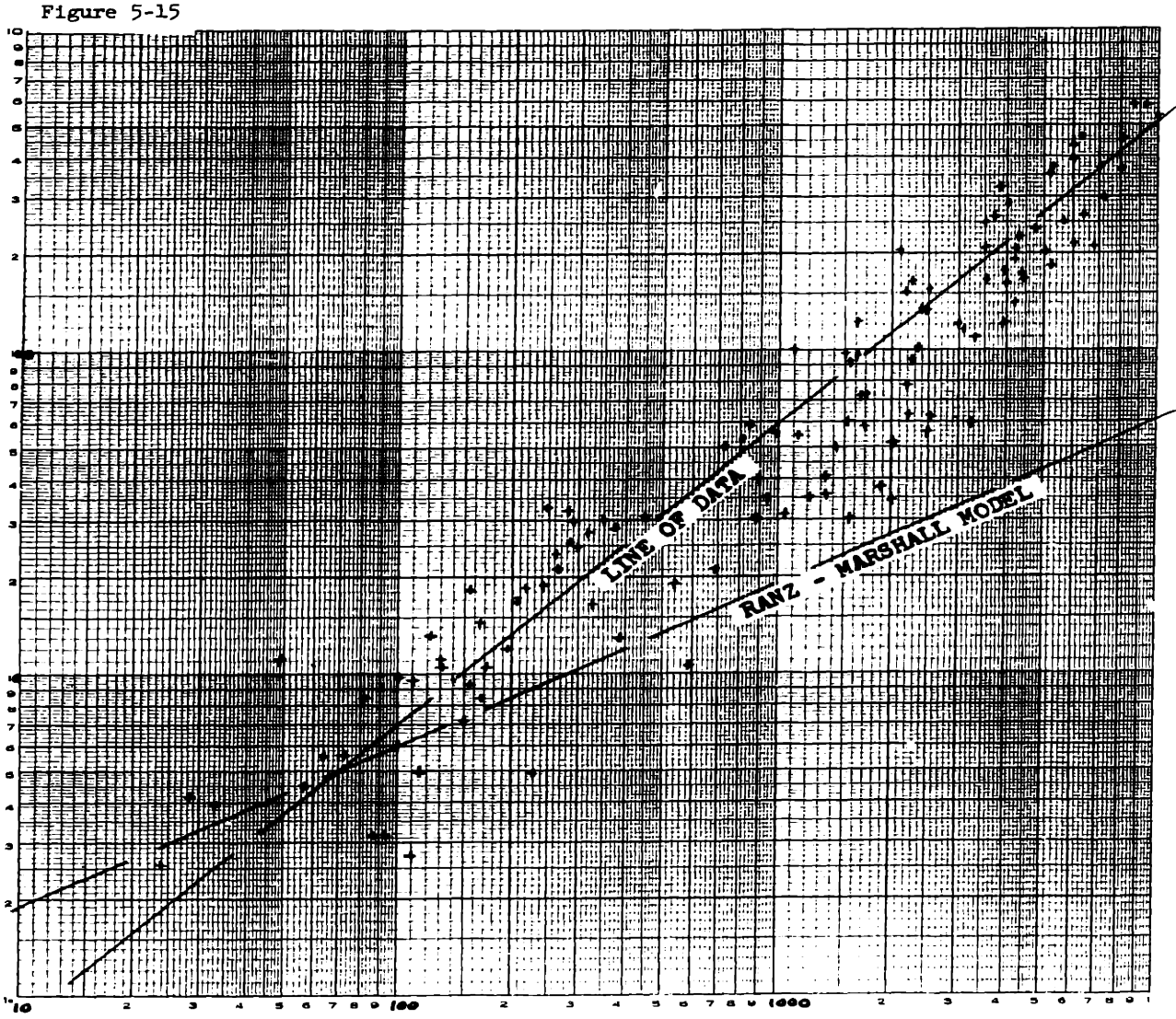

$(Nu - 2)/Pr^{\frac{1}{3}}$

RE_f (BASED ON FILM PROPERTIES AND EQUIVALENT SPHERICAL DIAMETER)

Figure 5-16 TEST OF HANDLOS - BARON MODEL $\left[Nu=1.13\ Re_f^{\frac{1}{2}}\ Pr_f^{\frac{1}{2}}\right]$

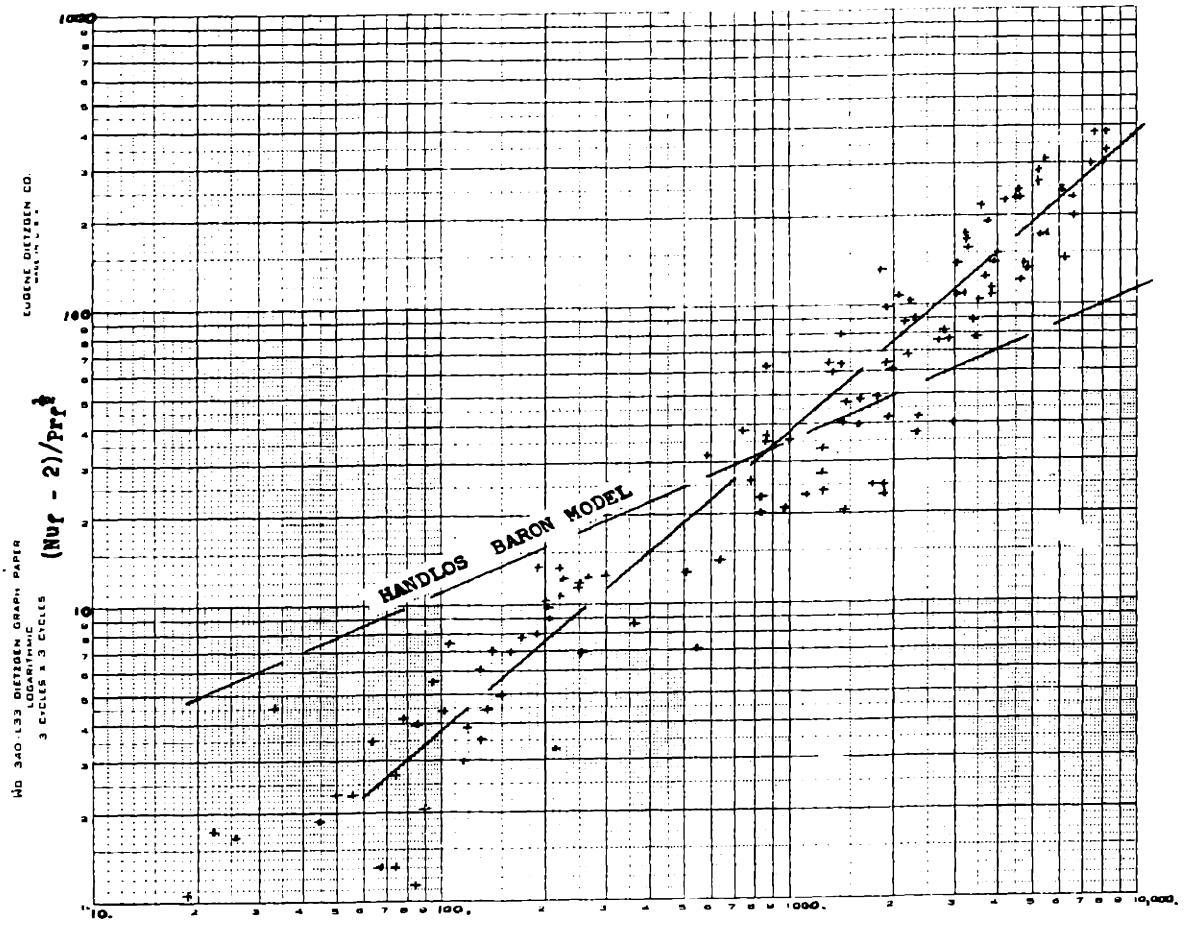

References cited in Chapter 1 (38, 67) tell of two other situations in which this strong a Reynolds number dependence has been reported: a) for transfer to a cylinder from the wake region at high Reynolds numbers and, b) for vapor bubbles whose growth is a power function of time. For the former an equation of

$$Nu - 2/_{Pr}{}^{1/3} = .016\ Re^{.93}$$

can be developed to fit data given in Jakob (44). For the latter, substitution of constants from the ethyl chloride - distilled water system at $\Delta T = 10^{o}C$ yields the formula, $Nu = .072\ Re\ Pr$.

One additional reference point is available through the calculation of a boundary layer thickness comparable to the values of overall coefficients observed. From Run #1 a measured U of .5 cal/(cm.)^2(sec.)(^{o}C) is equivalent to a film 3×10^{-3} cm. thick. Since laminar boundary layers are several orders of magnitude thicker than this, the evidence points to the presence of unusually high turbulence in the transfer region.

Comparisons of the results with the various models discussed leads to the conclusion that the main mechanism of heat transfer is one of turbulent transfer from the wake region. This hypothesis is the most logical in view of the fact that the bulk of the transfer apparently takes place into the puddle at the rear of the drop. Also, Reynolds number dependences are nearly identical with the model for wake region transfer to a cylinder. Differing values of the coefficients in the two situations are considered insignificant in view of the differing conditions under which the data were taken (air over a solid cylinder in one case, water over a gaseous bubble in the other).

The good agreement obtained with Zuber's equation for a growing bubble must be considered fortuitous in view of basic differences in the physical situations involved. No physical significance can be attached to this coincidence without additional work extending the range of the data, particularly that of the exterior phase Prandtl number.

4) The Effect of Surfactant

Although a general analysis of surfactant action has already been presented it is helpful to re-examine our results in terms of what we now know about the dynamic behavior of area and heat transfer coefficient.

In Chapter 4 the depression by surfactant of heat transfer rate in large bubbles was said to be due to a thickening of external film and a dampening of internal circulation. In Chapter 5 we have established that external boundary layer behavior is similar to that in forced convection past a solid surface. Thus minor changes in interfacial shear resistance would not be likely to effect it. It is more likely that the internal resistance which has been shown to be greatly reduced in the pure water - EtCl system is now offering a greater resistance due to the diminishing of shear-induced circulation currents.

The increase in transfer rate noted for small drops in a surfactant environment now becomes more difficult to explain. The hypothesis presented in Chapter 4 that rate increases were due to area increases and oscillation mixing is no longer tenable. In an earlier section we have established that the presence of a surfactant does not appreciably increase interfacial areas. Also, it was established that internal film resistance in a pure water system is insignificant; greater oscillation induced circulation could thus not act to make this resistance appreciably smaller. The only reasonable explanation must be found in terms of the external phase: photographs have shown that small drops do oscillate more vigorously in the presence of a surfactant. It is conceivable that this motion could cause an instability in the external film which would decrease its effective thickness and thereby reduce its resistance to heat transfer. Future studies should employ surfactants with varying capacities to reduce surface and interfacial tension to more precisely define the nature of the effects involved.

D. A Vaporization Model

To prove the internal consistency of this reasoning we may

now re-examine the plots of drop growth data presented early in Chapter 4 (Figures 4.3, 4.4 and 4.5). If the instantaneous coefficient can be expressed approximately as

$$\frac{hd_e}{k} = \frac{.1 d_e V \rho}{\mu} Pr^{\frac{1}{3}},$$

then h is proportional to V and transfer rate may be expressed as $q \sim VS\Delta T$. If S can be taken as roughly proportional to d_e^2 and V is set equal to 22.6 d_e, as can be done for spherical caps (33), $q = dv/dt \lambda \rho$ and we can substitute to give

$$\frac{dv}{dt} \lambda p \sim 22.6 (d_e)(d_e)^2 \Delta T.$$

For a single run ΔT is constant and this reduces to $\frac{dv}{dt}$ = const v. Integrating we get log v = at at + b. Thus a plot of q versus t should yield a nearly straight line on semilog coordinates as indeed it does for run 90 (low ΔT, big drop) in Figure 5.17. Some curvature at the upper end is of course to be expected since the assumption of $S \sim d_e^2$ becomes inadequate at the high end. Nevertheless the correspondence of data and model over the first one-third of the data gives strong support to the picture of mechanism which has been developed. It also shows that what appears to be sharp breaks in the original data curves are not significant in themselves, but merely the consequence of a smoothly developing logarithmic process.

Figure 5.17

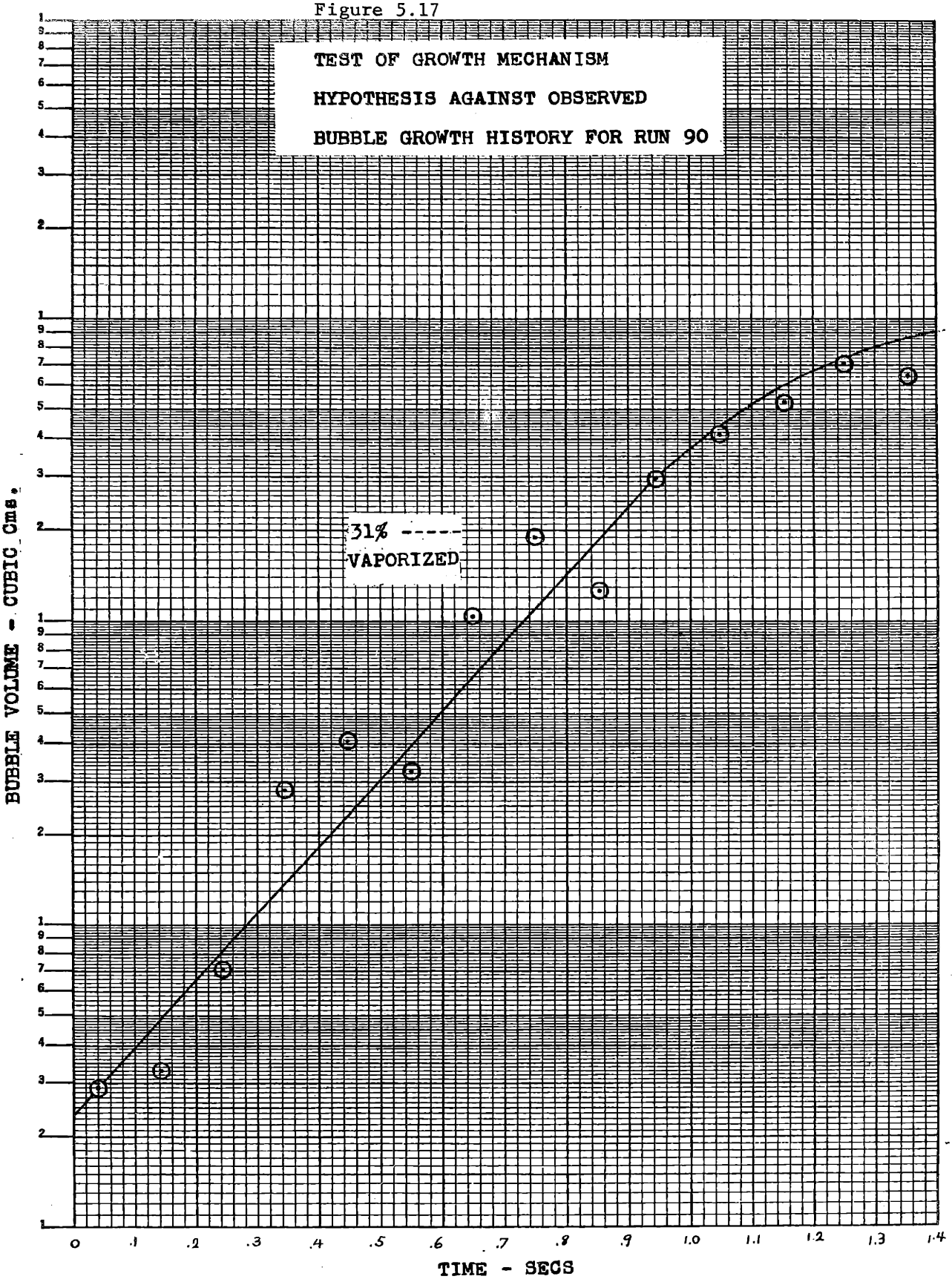
TEST OF GROWTH MECHANISM
HYPOTHESIS AGAINST OBSERVED
BUBBLE GROWTH HISTORY FOR RUN 90
31% -----
VAPORIZED
BUBBLE VOLUME - CUBIC Cms.
TIME - SECS
0
.1
.2
.3
.4
.5
.6
.7
.8
.9
1.0
1.1
1.2
1.3
1.4

CHAPTER 6 - LARGE SCALE UTILITY

I. Potential Capacity

Because of its similarity to gas absorption, the main limitation on commercial scale potential for direct-contact cooling would probably be imposed by gas phase entrainment. Using a formula given by Brown (8)

$$G = C\sqrt{\rho_d(\rho_c - \rho_d)}$$

where C is a function of interfacial tension and free space over the liquid. For an ethyl chloride - water system with high free space C = 730 yielding a G of 2320 lbs./hr./ft.^{2}. This is equivalent to a heat transfer rate of 382,000 Btu/(ft.)^2(hr.). This can be directly compared with peak values for fluxes to boiling liquids from submerged heaters (55) given in Chapter 1.

a) for boiling organics - 125,000 Btu/(ft.^{2})(hr.)
b) for boiling water - 400,000 Btu/(ft.^{2})(hr.)

This shows that the direct contact cooling process can yield flux rates that compare favorably to those for boiling from submerged tubes.

Knowledge of equipment volume requirements depends upon the contacting depth required. Katz and Schroeder have shown that seal heights H_s will vary with ΔT as

$$\Delta T = \frac{a(H_s + 318)^{2/3}}{H_s}$$

but were unable to define the constant, a for conditions other than those used in their experiments. At shallow depths, rates will be limited by channeling.

II. Advantages

The main advantage of a direct contact cooling system is that it offers sustained high rates under the normally adverse conditions of surface fouling and continuous phase freezing. In addition, capital cost for corrosive service should be greatly reduced. Although units will be less compact by virtue of the high free space requirements over the liquid, only the container must be built of costly alloy instead of tubes and container as well.

III. Disadvantages

The main disadvantage of a direct contact refrigeration system is refrigerant absorption by the continuous phase. Even at low solubility levels the cooling of large volumes could result in high loss rates and attendant problems of air or stream pollution. The normal problem of ice plugging due to the freezing of absorbed moisture in the lines would probably not be a problem with expansion taking place into a free space. Under some operating conditions, however, unsteady feed pressures might cause ice plugging of the feed nozzles.

Most of the above statements are at this point necessarily conjecture. An important future step will be the full scale testing of these hypotheses.

CHAPTER 7 - CONCLUSIONS AND RECOMMENDATIONS

I. Conclusions

A. General

1. The technique of studying the vaporization of an immiscible drop by hot wire nucleation and multiple exposure still photography is sufficiently accurate and reproducible to provide reliable and meaningful results.

B. Hydrodynamic Behavior

1. Unvaporized organic liquid in the bottom of a vapor bubble shows no tendency to distend the bubble surface or to separate from the vapor.

2. The vaporizing bubble exhibits behavior similar to that for ordinary gas bubbles. Velocities of rise for the growing bubbles lag corresponding terminal velocities by about 10%. Greater degrees of lag are found for heavy drops (inertial effect) and for viscous continuous phases.

C. Average Heat Transfer Rate

1. Heat transfer rate from distilled water to vaporizing drops of ethyl chloride depends on initial drop diameter and temperature driving force according to the model.

$$q_A = 2.84\, d_i^2\, \Delta T$$

2. Increasing viscosity in the continuous phase causes a drop in average rate but a meaningful correlation could not be developed.

3. The presence of a surfactant brings about a 30% gain in rate for small drops ($d_i = .239$ cm.) no change in medium sized drops ($d_i = .301$ cm.) and a 20% loss in large drops ($d_i = .379$ cm.).

D. Mechanism

1. The major portion of heat entering the drop is transferred from the wake region directly to the unvaporized liquid. Transfer through the gas phase is minor.

2. The unvaporized liquid sits as a flat puddle in the bottom of the vapor bubble. The prime transfer area is that of the interface between the puddle and the continuous phase. Area is primarily dependent on initial drop size and fraction vaporized. Oscillations, minor changes in bubble shape and liquid-upon-liquid spreading tendencies have little effect.

3. The internal phase is well mixed at all times offering no appreciable resistance to heat transfer.

4. Vaporization apparently occurs wholly by surface evaporation. Correlations of rate with temperature driving force show no signs of nucleate or film boiling behavior.

5. The external phase coefficient can be predicted by the equation , $Nu = 2 + .096\ Re^{.93} Pr^{1/3}$ for both the distilled water and glycerol systems.

6. Surfactants act to lower rate largely by repressing circulation and interfacial rippling. They increase rate by increasing oscillation tendencies.

E. Large Scale Potential

1. Direct contact vaporization can yield somewhat larger heat fluxes than can boiling from submerged tubes.

2. Equipment needed will be simpler and less expensive than for shell and tube exchangers but may be more bulky.

3. The ability to maintain high fluxes under conditions which normally lead to fouling is the systems main advantage; continuing loss of the refrigerant to the continuous phase is the major disadvantage.

II. Recommendations

A. Single Drop Data

1. In future work special care should be taken to insure saturation of the continuous phase. If possible fully vaporized bubbles should be caught and measured to provide an independent size value.

2. Back lighting and motion picture photography should be used to better define the disposition of the unvaporized liquid.

3. Additional data should be collected to test the validity of data from this work on ethyl chloride in 65% Glycerine and in distilled water at low temperature driving forces.

4. The findings of this study should be tested and extended by taking comparable data at high ΔT's, under higher pressures, using smaller drops.

5. Other dispersed phase materials should be studied which are heavier than water, have contrasting Prandtl numbers, are prone to drop break up.

6. Hydrodynamic behavior of air-oil bubbles should be studied to identify separately, aspects of behavior due to the presence of two phases in the bubble.

B. Bulk Contacting

1. Bulk contacting studies should be conducted to determine more accurately upper limits to the peak flux potential.

2. The natural tendency of commercial materials to nucleate should be studied along with the effect which dissolved air and system properties have on this.

3. The effect of mechanical agitation on transfer rates should be examined.

Section A. 1 Supplementary Details

1. Nucleation Using Ionizing Radiation

An attempt was made to eliminate liquid superheating in drops by exposing them to beta radiation from a Strontium 90 source of .5 millicuries strength. The source was sealed in a quartz tube and suspended as close as possible to the feed nozzle. Drops of the proper size were jarred loose to rise through the focus of the radiation field. Continuous phase temperature and temperature of the feed tube jacket water were varied and observations made of nucleation frequency. For the most part nucleation was infrequent and erratic at best. Less than 30% of the drops nucleated and to achieve this, such high jacket water temperatures were used that nucleation began to occur in the feed tube.

A second source representing a two fold increase in radiation strength was tried but without significant improvement. This approach was abandoned without further modification.

2. Photographic Techniques

Several lighting techniques were tried before sufficient contrast was achieved for obtaining clear multiple exposures. Back lighting was attempted using opal glass but no more than four images could be achieved by this method. Previous studies had shown that excellent outline definition was achieved by lighting from an angle of 135^{o} to the camera axis. This, too, was tried but with disappointing results. Six images were captured but definition was not improved. The adopted system of top lighting with a moving viewing window was considerably more effective than any of the others tried.

Some pictures were taken using Panatomic X film which was over-exposed and underdeveloped for high contrast. The resulting images were no better than those obtained on the Polaroid film with less delay and less effort.

TABLE A-1
SYSTEM PHYSICAL PROPERTIES

CONTINUOUS PHASE

	Temp °C	ρ gm/cc.	μ cp.	cp Cal (gm)(°C)	$k \times 10^6$ cal/(sec) (cm) (°C)	v.p. mm Hg.	Pr dim.	EtCl ρ_v gm/cc	EtCl Sol wt %	A-22 wt %	σ_s dyne-cm	σ_i dyne-cm	$\Delta\sigma_s$ dyne-cm	$\Delta\sigma_i$ dyne-cm	Runs Made
EtCl - Dist. Water	18.0	.999[b]	1.05[b]	1.000[b]	1418[b]	15.6[b]	7.45[h]	.00272[a]	.56[a]	0	73.0[b]	27.6	0	0	82-92
	24.6	.997[b]	.902[b]	.999[b]	1448[b]	23.2[b]	6.22[h]	.00278[a]	.44[a]	0	72.0[b]	-	0	0	1-7
	32.6	.995[b]	.759[b]	.999[b]	1477[b]	36.9[b]	5.13[h]	.00286[a]	.35[a]	0	70.8[b]	-	0	0	8-14
EtCl - 86%Gly	17.0	1.23	159.	.629	740	5.4	1351.[f]	.00271[a]	-	0	65.0	-	0	0	25-30
	24.1	1.22	98.3	.634	760	9.2	483.[f]	.00278[a]	-	0	64.6	-	0	0	31-36
	31.8	1.22	61.3	.660	780	14.5	307.[f]	.00286[a]	-	0	64.1	-	0	0	37-42
EtCl - 66% Gly	18.0	1.17	18.5	.713	1120	10.7	118.[f]	.00272[a]	-	0	67.3	-	0	0	49-58
	24.2	1.17	13.8	.720	1140	15.5	86.8[f]	.00278[a]	-	0	66.8	-	0	0	64-71
	31.7	1.16	10.0	.731	1150	24.2	63.6[f]	.00285[a]	-	0	66.2	-	0	0	72-81
EtCl - Ae 22	24.5	.997[b]	.904[b]	.999[b]	1448[b]	23.1[b]	6.24[h]	.00278[a]	-	.00525	66.2[e]	18.3[e]	6.4	9.0	93-102
	24.5	.997[b]	.904[b]	.999[b]	1448[b]	23.1[b]	6.24[h]	.00278[a]	-	.074	42.5[e]	9.2[e]	30.1	18.	103-109
	24.5	.997[b]	.904[b]	.999[b]	1448[b]	23.1[b]	6.24[h]	.00278[a]	-	.135	41.8[e]	9.2[e]	30.8	18.	110-118

EtCl PHYSICAL PROPERTIES AT 14.5°C

ρ^a	μ^a	Cp^a	k^c	Pr^c	sol of water in [a]
.902	.271	.389	274.5	3.17	.11 wt

Sources:
a) Kirk Othmer Encyclopedia
b) Perry's Handbook
c) Reid & Sherwood
d) McAdams
e) laboratory measurement
f) calculated

TABLE A-2

SUMMARY OF DATA AND CALCULATED VALUES

Image No.	A/B dim.	SHAPE MODE dim.	de cm.	Eo dim.	V cm./sec.	V/V_T dim.	Re_A dim.	Re_d dim.	S sq.cm.	H cal.	q cal./sec.	h_i cal./(sec)(cm^2)(°C)	U cal./(sec)(cm^2)(°C)	Nu dim.	Ra dim.
Run 1 - 1	1.39	2	.59	4.1	13.6	.65	981	884	.32	.023	.63	.006	.19	75.2	22300
2	2.18	2	.80	8.3	17.0	.75	2060	1500	.51	.063	1.7	.010	.31	170.5	3700
3	2.54	2	.98	12.7	19.3	.81	3040	2090	.63	.118	3.76	.013	.55	375	1680
4	2.25	4	1.48	29.5	22.4	.81	5080	3660	.94	.416	4.90	.028	.48	490	89.4
5	2.04	4	1.78	42.8	26.6	.89	6940	5240	.78	.724	4.72	.038	.56	692	38.8
6	2.45	5	1.92	49.6	29.6	.96	9010	6270	.71	.903	5.03	.055	.66	870	11.4
7	2.58	5	2.09	58.9	30.4	.94	10280	7020	.26	1.165	5.76	.178	2.07	-	.3
8	3.00	6	2.27	69.8	31.1	.92	11910	7790	.0	1.499	4.66	∞	-	-	.0
9	-	6	2.41	-	32.7	.94	13390	8700	-	1.793	.82	-	-		-
Run 2 - 1	1.47	3	.66	5.3	13.5	.66	1110	977	.35	.033	.85	.033	.23	103	14700
2	2.44	4	.83	8.9	17.5	.83	2300	1600	.56	.070	1.92	.070	.32	181	2700
3	2.22	4	1.13	16.9	20.0	1.13	3440	2490	.91	.181	3.62	.181	.37	288	216
4	2.11	5	1.48	29.4	22.8	1.48	5020	3730	.91	.414	4.30	.414	.44	445	104
5	2.05	5	1.79	43.1	26.3	1.79	6900	5190	.77	.732	4.44	.732	.53	652	37.1
6	2.21	5	1.83	45.5	29.1	1.83	8110	5890	.77	.792	4.76	.792	.57	727	24.5
7	2.58	5	2.14	61.9	29.9	2.14	10330	7060	.0	1.256	3.34	1.256	-	-	.00
8	2.88	6	2.14	61.9	29.9	-	10710	7080	-	1.253	-	1.253	-	-	-
9	-	6	2.18	-	31.0	-	11500	7460	-	1.319	-	-			-
10	-	6	2.33	-	-		-	-		-		-			
11		6	2.29		-		-	-		-					
12		6	2.28												
Run 3 - 1	1.91	2	.63	4.9	16.2	.75	1450	1130	.40	.029	.61	.029	.14	102.7	8800
2	2.57	2	.80	8.3	18.7	.83	2420	1650	.57	.063	1.52	.117	.25	136.5	2600
3	3.70	4	.98	12.6	19.9	.84	3410	2150	.78	.117	3.54	.168	.42	282	860
4	2.83	5	1.43	27.4	22.2	.82	5280	3500	1.07	.371	4.57	.299	.40	388	64.7
5	2.36	5	1.77	42.6	26.0	.87	7220	5100	.85	.719	4.92	.406	.54	659	28.7
6	2.49	5	1.83	45.3	29.1	.94	8770	6230	.82	.930	5.66	.458	.64	800	19.6
7	2.84	6	2.18	64.1	30.8	.94	11190	7420	.0	1.323	4.20	∞	-	-	.00
8	2.71	6	2.21	66.3	32.1	.97	11680	7840	-	1.387	1.54	-	-	-	-
9	-	6	2.23	-	33.0	.99	12580	8120	-	1.417	-	-			-
10	-	6	2.19	-	33.1	1.00	12580	8000		1.335	-				

TABLE A-2 (CONTINUED)

Image No.	A/B dim.	SHAPE MODE dim.	de cm	Eo dim.	V cm/sec.	V/V_T dim.	Re_A dim.	Re_d dim.	S sq.cm.	H cal.	q cal/sec.	h_i cal/(sec.)(cm²)(°C)	U cal/(sec.)(cm²)(°C)	Nu dim.	Ra dim.
									Ø			Ø			
Run 4- 1	1.48	2	.55	3.8	13.6	.65	950	832	.20	.020	.60	.010	.25	93.3	6230
2	2.30	2	.75	7.4	17.7	.79	2050	1464	.32	.053	1.23	.018	.31	162.	1130
3	3.00	2	.99	13.0	20.3	.85	3370	2206	.58	.122	1.60	.040	.22	148.	45.3
4	2.51	4	1.26	21.5	23.0	.89	4670	3218	.48	.259	1.24	.054	.19	163.	25.4
5	2.58	5	1.29	22.3	25.3	.97	5280	3601	.48	.273	1.15	.058	.17	153.	22.0
6	3.21	5	1.36	24.9	25.7	.96	5950	3848	.47	.320	1.20	.076	.17	158.	10.6
7	3.17	5	1.50	30.3	26.2	.95	6640	4333	.24	.431	.80	.171	.14	142.	4.3
8	2.94	5	1.47	29.2	28.2	1.03	6960	4577	.30	.406	-	.122	-	-	6.3
9	2.96	5	1.54	32.0	29.7	1.06	7690	5045	.0	.465	-	.0	-	-	3.4
10	-	5	1.55	32.5	30.2	1.08	7460	5175		-					
11	-	5	1.65	36.8	29.3	1.02	7590	5346		-					
									Ø			Ø			
Run 5- 1	-	2	.56	4.1	15.4	.72	1230	963	.23	.022	.68	.013	.23	89.3	-
2	-	2	.77	7.8	18.5	.82	2240	1568	.32	.057	1.45	.019	.36	189.	-
3	-	4	1.03	14.2	21.1	.87	3610	2396	.54	.139	2.04	.043	.28	199.	-
4	3.07	5	1.34	24.2	23.4	.88	5310	3461	.43	.308	1.55	.079	.22	204.	12.5
5	2.92	6	1.40	26.6	25.4	.94	5970	3929	.34	.354	1.14	.100	.18	170.	9.8
6	2.92	6	1.40	26.6	26.9	1.00	6320	4162	.35	.353	1.38	.099	.21	205.	9.9
7	3.27	6	1.57	33.3	27.7	.98	7450	4802	.0	.495	.62	.0	.13	140.	1.8
Run 6- 1	1.61	5	.62	4.1	13.7	.67	1110	940	.47	.024	.76	.005	.15	66.3	60400
2	2.41	5	.81	8.1	15.9	.71	2030	1420	.76	.062	1.39	.008	.17	94.6	9920
3	2.92	5	1.08	15.3	18.2	.75	3310	2180	1.45	.157	2.51	.015	.16	119.5	461
4	2.55	5	1.29	22.1	21.3	.82	4430	3040	1.49	.270	3.88	.016	.24	215.	406
5	2.45	5	1.64	36.1	24.0	.84	6260	4360	1.58	.563	4.68	.020	.27	310.	234
6	2.40	6	1.83	44.9	26.0	.86	7490	5250	1.56	.778	4.61	.022	.27	343.	170
7	2.54	6	2.03	55.6	28.0	.88	9160	6290	1.56	1.071	5.89	.027	.35	490.	94.6
8	2.93	6	2.10	59.6	29.9	.92	10550	6940	1.64	1.186	8.30	.031	.47	680.	59.2
9	3.10	6	2.49	83.7	31.1	.88	13120	8540	1.10	1.968	7.49	.059	.63	1080.	8.6
10	3.11	6	2.58	-	32.2	.90	14100	9170	.79	2.191	5.16	.087	.61	1080.	2.7
11	3.45	6	2.65	-	33.4	.92	15310	9780	.25	2.378	4.61	.331	1.71	-	.1
12	3.37	6	2.72		34.0	.92	15970	10250	-	2.579	-	-	2.11	-	-
13	-	6	2.82		34.3	.92	17010	10710	-	2.859	-	-	-		-

Ø Calculation based on observed volume not nominal

TABLE A-2 (CONTINUED)

Image No.	A/B dim.	SHAPE MODE dim.	de cm	Eo dim.	V cm./sec.	V/V_T dim.	Re_A dim.	Re_d dim.	S sq.cm.	H cal.	q cal./sec.	h_i cal./(sec.)(cm^2)(°C)	U cal./(sec.)(cm^2)(°C)	Nu dim.	Ra dim.
Run 7- 1	1.33	4	.50	2.1	11.5	.58	700	640	-	.010	.50	.004	-	90.6	155900
2	1.79	4	.73	6.4	11.5	.71	1560	1260	.58	.044	.73	.006	.18	113	25400
3	2.47	5	1.02	13.4	17.6	.74	2860	1990	1.29	.130	1.02	.013	.16	205	729.
4	2.67	5	1.19	18.6	19.5	.77	3800	2560	1.47	.210	1.19	.016	.25	309	446.
5	2.39	6	1.60	34.3	22.0	.78	5550	3900	1.55	.522	1.60	.019	.28	394	267.
6	2.26	6	1.84	45.6	25.2	.83	7100	5120	1.51	.796	1.84	.022	.31	567	189.
7	2.59	6	1.96	51.9	28.0	.90	8910	6070	1.60	.965	1.96	.026	.42	720	108.
8	3.18	6	2.22	-	29.6	.89	11220	7270	1.59	1.397	2.22	.036	.47	727	35.0
9	3.13	6	2.51	-	30.8	.87	13690	8550	1.04	2.024	2.51	.064	.42	190	6.7
10	3.15	6	2.51		32.0	.91	14190	8890	1.05	2.020	2.51	.064	.11	-	6.8
11	3.44	6	2.50		32.8	.93	-	-	1.12	2.003	2.51	.065	-	-	6.2
12	4.02	6	2.48		33.3	.95	-	-	1.39	1.947	-	.070	-		-
13	-	6	2.41		33.9	.98			1.59	1.791	-	-			-
14	-	6	2.37		34.5	1.00			-	1.690		-			
15		6	2.67		34.4	.94			-	2.412					
Run 8- 1	1.32	2	.84	9.4	12.0	.53	1450	1330	.67	.071	2.21	.008	.30	174	17900
2	2.07	2	1.08	15.6	18.3	.75	3440	2580	1.53	.151	4.59	.019	.28	208	510.
3	2.21	5	1.60	34.9	22.8	.80	6560	4770	1.64	.501	6.12	.031	.34	375	123.
4	2.13	5	1.92	50.9	26.6	.86	9090	6740	1.22	.879	5.49	.049	.42	556	30.6
5	2.68	6	2.11	60.9	29.3	.90	12020	8100	.57	1.151	3.70	.155	.60	673	1.0
6	2.65	6	2.17	64.9	30.6	.93	12890	8720	.0	1.264	.98	-	.00	-	.0
7	-	-	2.21	-	31.1	.94	14030	9020	-	1.325	-	-	-	-	-
8	-	-	2.02	-	31.6	.99	12480	8390	-	1.015	-		-		-
9			2.20		31.9	.96	14030	9210		1.308					
10			2.28		32.1	.95	12480	9630		1.460					
11			2.26		32.4	.96	14500	9620		1.418					

TABLE A-2

SUMMARY OF DATA AND CALCULATED VALUES

Image No.	A/B dim.	SHAPE MODE dim.	de cm	Eo dim.	V cm./sec.	V/V_T dim.	Re_A dim.	Re_d dim.	S sq.cm.	H cal.	q cal./sec.	h_i cal./(sec.)(cm²)(°C)	U cal./(sec.)(cm²)(°C)	Nu dim.	Ra dim.
Run 9 - 1	1.77	4	.53	3.3	9.2	.46	800	640	.34	.02	1.35	.007	.21	75.	31100.
2	1.80	5	.96	12.4	15.7	.66	2470	1980	.50	.11	2.55	.010	.27	175.	6723.
3	2.14	5	1.30	23.0	20.3	.78	4700	3470	.93	.27	3.90	.023	.22	193.	286.9
4	2.46	5	1.58	34.1	24.2	.86	7210	5000	.99	.48	4.74	.032	.25	267.	103.1
5	2.46	6	1.87	48.1	27.5	.90	9720	6750	.81	.81	4.11	.047	.26	328.	32.2
6	2.96	6	1.99	54.7	29.6	.94	11800	7750	.69	.98	3.19	.072	.24	322.	8.5
7	3.15	6	2.06	58.2	30.2	.94	12580	8160	.55	1.07	1.96	.100	.19	265.	3.1
8	3.62	6	2.17	64.8	30.1	.91	13550	8580	.00	1.26	.00	∞	∞	-	.00
9	-	6	2.05	-	30.2	.94	13030	8130		1.06	.00	-			-
10	-	6	1.89	-	30.7	1.00	12590	-		.83	-				
Run 10- 1		5	.77	7.8	11.1	.52	1560	1290	.42	.05	2.56	.008	.32	167.	13090.
2		5	1.10	16.4	17.7	.74	3400	2640	.84	.16	4.54	.019	.28	208.	570.
3		5	1.68	38.5	22.1	.84	6700	5130	.84	.58	5.28	.031	.33	375.	121.
4		6	1.82	45.4	25.1	.91	9300	6410	.87	.74	4.79	.044	.29	357.	40.4
5		6	2.10	60.3	26.4	.95	11430	7920	.36	1.13	2.89	.125	.42	596.	1.79
6		6	2.07	59.1	26.8	.97	12340	8200	.47	1.10	1.35	.108	.15	210.	2.70
7			2.12	61.5	27.6	.99	13550	8590	.32	1.16	.57	.209	.09	129.	.37
8			2.13	62.3	29.1	1.06	13630	8710	.21	1.18	.00	.370	.00	-	.12
9			2.09	59.8	29.1	1.01	14030	8500	.54	1.11	.00	.144			1.18
10			1.87		26.9	1.00			1.10	.80		.063			14.4

TABLE A-2 (CONTINUED)

Image No.	$\bar{A}/B$ dim.	SHAPE MODE dim.	de cm	Eo dim.	V $\frac{cm.}{sec.}$	V/V_T dim.	Re_A dim.	Re_d dim.	S sq.cm.	H cal.	q cal./sec.	h_i $\frac{cal.}{(sec.)(cm^2)(°C)}$	U $\frac{cal.}{(sec.)(cm^2)(°C)}$	Nu dim.	Ra dim.
									ø			ø			
Run 11- 1	1.29	4	.70	6.4	11.1	.52	1100	1020	.19	.040	1.36	.012	.30	177.	8720
2	2.01	5	.98	13.0	17.7	.74	2990	2270	.43	.114	2.22	.036	.31	179.	1384
3	2.20	5	1.31	23.6	22.1	.84	5240	3810	.34	.279	2.24	.071	.20	308.	51.5
4	2.32	5	1.49	30.3	25.1	.91	6870	4890	.0	.404	1.25	∞	.13	-	18.0
5	2.89	6	1.53	32.0	26.4	.95	8010	5280	.0	.439	.41	∞	.04	-	8.2
6	3.07	6	1.48	30.0	26.8	.97	7960	5190	-	.396	.17	∞	.02		11.2
7	3.14	6	1.54	32.4	27.6	.99	8580	5570	-	.445	-	∞	.05		6.6
8	2.80	6	1.48	30.2	29.1	1.06	8510	5660		.400	-	-	-		12.7
9	3.70	6	1.67	38.1	29.1	1.01	10100	6360		.566		-	-		.4
10	4.02	6	1.40	-	26.9	1.00	-	-		.332					11.3

ø Based upon observed size rather than nominal size

Run 12- 1	1.84	5	.73	7.2	12.7	.57	1540	1230	.31	.047	.876	.013	.147	72.7	3510.
2	2.47	5	.92	11.4	17.8	.76	3100	2150	.42	.094	.707	.019	.088	54.8	1050.
3	3.51	5	1.10	16.5	19.2	.78	4350	2770	.75	.163	.334	.026	.023	17.1	44.8
4	4.02	6	.95	12.2	19.2	.81	3930	2380	.57	.103	.549	.035	.050	32.2	400.
5	2.39	6	1.15	17.9	21.0	.84	4490	3150	.63	.184	.713	.039	.059	46.0	80.0
6	2.66	6	1.20	19.8	23.9	.94	5590	3780	.66	.214	.395	.041	.031	35.2	53.3
7	2.70	6	1.24	21.0	25.4	.98	6140	4120	.66	.233	-	.040	-		45.7
8	2.82	6	1.20	19.7	25.1	.98	5960	3960	.68	.212	-		-		48.1
9	3.90	6	1.04	14.9	24.1	.99	5350	3300	.80	.138					43.7
10	2.55	6	1.04	16.7	24.6	1.01	4910	3370	.66	.137					96.6

TABLE A-2 (CONTINUED)

Image No.	A/B dim.	SHAPE MODE dim.	de cm	Eo dim.	V cm/sec.	V/V_T dim.	Re_A dim.	Re_d dim.	S sq.cm.	H cal.	q cal/sec.	h_f cal./(sec.)(cm²)(°C)	U cal./(sec.)(cm²)(°C)	Nu dim.	Ra dim.
Run 13- 1	1.66	5	.61	4.0	9.1	.46	870	720	.47	.02	1.98	.005	.22	91.	109000
2	1.73	5	1.07	15.0	15.6	.64	2670	2180	1.10	.14	3.98	.011	.19	137.	2640.
3	1.87	5	1.50	30.7	21.0	.76	5270	4150	1.35	.41	6.23	.016	.24	243.	981.
4	2.16	6	1.83	45.6	24.9	.83	8130	5970	1.50	.75	8.72	.021	.30	371.	391.
5	2.17	6	2.19	65.5	28.1	.85	11000	8060	1.37	1.28	11.33	.028	.43	636.	160.
6	2.38	6	2.48	84.3	30.7	.87	14160	9970	1.06	1.87	11.31	.046	.55	921	34.6
7	2.33	6	2.80	107.4	32.2	.86	16620	11810	.00	2.69	7.18	∞	∞	-	.00
8	-	-	2.81	-	33.5	.89	18220	-		2.73	4.11				-
9	-	-	2.85	-	34.5	.92	20090	-		2.85	-				-
10			2.93		35.3	.92	21320			3.08	-				
11			2.86		35.6	.94	21230			2.87					
Run 14- 1	1.48	2	.79	7.8	12.2	.55	1450.	1270	.55	.06	2.54	.005	.24	128.	57600.
2	1.85	5	1.18	18.5	18.5	.74	3610	2850	1.21	.20	5.68	.013	.24	191.	1807.
3	1.87	5	1.63	36.3	23.0	.81	6260	4930	1.38	.53	9.90	.017	.38	418.	783.
4	2.13	6	2.12	61.4	27.0	.83	10130	7490	1.40	1.17	12.53	.026	.47	672.	204.
5	2.11	6	2.52	87.1	30.3	.86	13460	10010	.91	1.97	10.00	.048	.57	971.	32.5
6	2.15	6	2.73	102.4	32.3	.87	15690	11550	.00	2.50	6.45	∞	∞	-	.00
7	2.44	6	2.68	98.9	33.4	.91	-	-		2.37	5.72				-
8	2.63	6	2.91	116.6	34.7	.91	-	-		3.03	-				-
9	2.79	6	2.88	113.8	35.8	.95				2.92					
10	3.07	6	3.06	129.1	36.7	.94				3.52					
11	3.24	6	3.00	123.6	37.2	.96				3.29					

TABLE A-2 (CONTINUED)

Image No.	A/B dim.	SHAPE MODE dim.	de cm	Eo dim.	V cm/sec.	V/V_T dim.	Re_A dim.	Re_d dim.	S sq.cm.	H cal.	q cal./sec.	h_i cal./(sec)(cm²)(°C)	U cal./(sec)(cm²)(°C)	Nu dim.	Re dim.
Run 64- 1	1.03	1	.32	1.21	9.10	.88	25.	25	.15	.003	.11	.006	.070	19.6	65200.
2	-	2	.48	-	14.5	1.25	65.	59	.20	.012	.11	-	.053	22.3	-
3	1.98	2	.55	4.83	17.4	1.39	106.	81	.27	.019	.11	.01	.036	17.4	3210.
4	-	2	.54	-	18.5	1.47	108.	85	.26	.018	.17	-	.058	27.4	-
5	3.18	4	.66	7.12	18.7	1.40	161.	104	.41	.034	.22	.02	.049	28.4	828.
6	-	4	.70	-	18.7	1.36	174.	111	.44	.042	.28	-	.058	35.6	-
7	3.35	4	.79	10.4	19.1	1.30	199.	128	.46	.060	.46	.02	.090	62.3	511
8	-	4	.85	-	20.4	1.31	232.	148	.50	.077	.58	-	.107	79.8	-
9	4.02	4	1.02	17.8	23.0	1.31	331.	200	.82	.134	.56	.04	.062	55.5	27 2
10	-	4	1.02	-	25.3	1.42	331.	219	.68	.132	.97	-	.132	118.	-
11	2.46	4	1.14	22.3	26.2	1.38	367.	255	.63	.188	1.32	.04	.191	191.	42.2
12	-	4	1.36	-	26.3	1.26	476.	304	.69	.315	.80	-	.106	126.	-
13	3.22	4	1.34	30.8	26.6	1.28	469.	303	.68	.303	.55	.05	.075	88.1	12.0
14	-	4	1.35	-	27.3	1.30	485.	313	.68	.307	.49	-	.066	78.2	-
15	3.17	5	1.47	36.9	28.1	1.27	542.	351	.59	.397	.00	.07	.00		6.03
16	-	5	1.35	-	29.0	1.37	513.	333	.68	.306	.00	-	-		-
17	2.88	5	1.34	30.8	29.7	1.40	514.	339	--	.302	-	.05	-		14.9
18	-	5	1.38		30.1	1.40	536.	354	-	.328	-	-			-
Run 65- 1	1.30	1	.33	1.33	8.79	.86	26.8	25	.16	.003	.11	.006	.067	19.4	48300.
2	1.31	2	.50	3.89	14.4	1.24	66.4	61	.20	.014	.13	.008	.062	27.2	10400.
3	1.55	2	.53	4.39	17.5	1.41	91.2	78	.22	.017	.18	.009	.073	33.9	6310.
4	2.13	2	.62	6.31	18.6	1.42	132.	98	.31	.029	.22	.013	.067	36.4	2050.
5	2.81	2	.70	8.20	19.0	1.37	171.	114	.39	.042	.22	.017	.050	30.7	890
6	2.91	2	.75	9.55	19.2	1.33	187.	123	.42	.053	.26	.018	.058	38.2	712
7	3.17	4	.79	10.39	19.1	1.31	198.	128	.45	.060	.41	.020	.083	57.5	534
8	3.64	4	.91	13.9	19.4	1.22	236.	149	.72	.092	.83	.033	.106	84.6	41.1
9	4.02	4	.98	16.3	20.9	1.23	287.	174	.81	.118	1.34	.039	.152	131.	30.1
10	3.37	5	1.25	26.6	23.7	1.21	392.	252	.71	.244	1.11	.047	.142	155.	16.2
11	2.76	5	1.31	29.5	25.8	1.26	433.	289	.63	.286	.55	.047	.080	92.0	17.6
12	4.02	5	1.30	28.7	26.1	1.29	476.	288	.85	.274	.58	.060	.063	71.9	12.9
13	2.86	5	1.35	31.3	26.6	1.27	462.	306	.63	.311	.41	.050	.059	69.9	14.0
14	3.07	5	1.43	35.1	27.4	1.26	513.	334	.61	.369	.00	.060	.00	-	18.0

TABLE A-2 (CONTINUED)

Image No.	A/B dim.	SHAPE MODE dim.	de cm	Eo dim.	V $\frac{cm.}{sec.}$	V/V_T dim.	Re_A dim.	Re_d dim.	S sq.cm.	H cal.	q cal./sec.	h_1 $\frac{cal.}{(sec)\ (cm^2)\ (°C)}$	U $\frac{cal.}{(sec.)\ (cm^2)\ (°C)}$	Nu dim.	Ra dim.
Run 66- 1	1.10	1	.34	1.50	9.7	.93	29.0	28.	.15	.003	.126	.006	.076	20.3	65300.
2	1.65	2	.51	4.08	14.8	1.26	76.5	64.	.20	.015	.149	.009	.059	26.4	5910.
3	1.93	2	.55	4.91	17.5	1.40	106.	82.	.27	.020	.239	.011	.081	39.2	3350.
4	-	2	.63	-	18.7	1.41	148.	101.	.36	.031	.321	-	.082	45.6	-
5	2.78	2	.79	10.5	19.1	1.30	193.	129.	.42	.061	.327	.018	.071	49.2	663.
6	-	4	.79	-	19.4	1.31	216.	131.	.54	.062	.406	-	.069	48.1	-
7	4.02	4	.92	14.2	19.5	1.20	251.	152.	.82	.096	.469	.038	.053	42.6	41.8
8	-	4	.98	-	20.7	1.22	283.	172.	.88	.116	.547	-	.057	48.8	-
9	-	4	1.04	-	23.3	1.31	341.	206.	.88	.141	.796	-	.083	75.8	-
10	3.45	5	1.14	22.3	25.3	1.34	386.	246.	.74	.188	1.172	.042	.145	146.	22.4
11	-	5	1.26	-	26.2	1.31	436.	282.	.70	.254	.988	-	.130	144.	-
12	3.82	5	1.40	33.7	26.4	1.24	508	316.	.69	.348	.755	.063	.100	123.	6.4
13	-	5	1.30	-	26.0	1.28	474.	287.	.82	.273	1.061	-	.118	135.	-
14	3.88	5	1.54	40.5	26.4	1.17	558.	345.	.51	.456	.613	.090	.099	134.	2.3
15	3.51	5	1.48	37.6	27.9	1.26	552.	352.	.60	.408	-	.072	-		4.6
16	-	5	1.47	-	29.5	1.32	604.	370.	.66	.399	-	-	-		-
17	-	5	1.41	-	30.5	1.40	575.	365.	-	.347		-			-
18	3.37	5	1.43	35.1	30.8	1.39	584.	375.	-	.365		.062			7.1
Run 68- 1	1.90	2	.37	1.39	7.5	.79	30.4	24.	.29	.003	.128	.006	.041	13.4	34600
2	1.30	2	.50	3.48	13.6	1.21	62.1	57.	.27	.012	.145	.005	.050	21.7	47400
3	1.68	2	.60	5.54	17.2	1.37	106.	87.	.35	.024	.115	.007	.030	15.8	13600
4	1.90	2	.58	5.25	18.6	1.46	118.	93.	.38	.022	.128	.008	.031	15.9	10900
5	-	3	.66	-	19.1	1.42	154.	108.	.49	.034	.127	-	.024	14.0	-
6	3.26	4	.69	7.71	19.4	1.42	177.	114.	.60	.039	.254	.012	.039	23.7	2340
7	-	4	.71	-	20.0	1.43	188.	121.	.62	.042	.659	-	.097	60.6	-
8	4.02	4	.92	14.0	21.2	1.29	272.	165.	1.11	.094	1.01	.023	.083	66.6	115.
9	3.44	5	1.09	20.0	23.5	1.29	340.	218.	1.11	.159	1.06	.024	.088	83.8	103.
10	3.00	5	1.20	24.2	25.6	1.32	397.	260.	1.08	.213	1.19	.025	.101	106.	102.
11	3.41	5	1.27	27.6	26.1	1.30	442.	283.	1.16	.259	1.32	.029	.104	116.	68.7
12	3.00	5	1.43	34.8	26.8	1.24	498.	326.	1.11	.365	.73	.031	.060	75.2	59.2
13	3.32	5	1.45	35.9	27.1	1.24	519.	334.	1.16	.382	-	.033	-		47.3
14	2.83	5	1.38	32.6	26.3	1.25	467.	310.	1.09	.330	-	.029	-		75.1
15	3.06	5	1.38	29.6	27.1	1.28	487.	318.	1.14	.326		.030			66.4
16	2.85	5	1.32	31.9	29.2	1.40	494.	328.	-	.284		.027			87.0
17	3.25	5	1.37	27.8	30.4	1.42	549.	354.	-	.317		.030			61.5
18	3.65	5	1.28	29.7	30.6	1.48	528.	333.		.259		.029			62.0

TABLE A-2 (CONTINUED)

Image No.	A/B dim.	SHAPE MODE dim.	de cm	Eo dim.	V $\frac{cm.}{sec.}$	V/V_T dim.	Re_A dim.	Re_d dim.	S sq.cm.	H cal.	q cal./sec	h_j $\frac{cal.}{(sec)(cm^2)(^\circ C)}$	U $\frac{cal.}{(sec)(cm^2)(^\circ C)}$	Nu dim.	Ra dim.
Run 70- 1	1.04	1	.37	1.4	10.6	1.01	33.6	33	.24	.003	.16	.005	.060	19.4	110000.
2	1.61	2	.55	4.5	15.4	1.30	85.6	72	.32	.018	.19	.006	.055	26.5	19400.
3	1.95	2	.61	5.9	17.9	1.40	121.	94	.39	.026	.24	.008	.056	40.9	9000.
4	-	2	.68	-	18.8	1.39	149.	109	.46	.037	.37	-	.074	44.2	-
5	2.89	2	.79	10.3	19.0	1.31	194.	128	.61	.060	.46	.013	.069	47.8	2100.
6	-	3	.90	-	19.5	1.22	232.	150	.97	.090	.45	-	.042	33.2	-
7	3.89	4	.95	15.3	20.5	1.23	269.	166	1.09	.107	.56	.023	.047	39.2	109.
8	-	4	1.02	-	22.3	1.28	319.	193	1.18	.131	.79	-	.061	54.6	-
9	2.86	5	1.15	22.5	24.5	1.30	363	240	1.04	.191	.96	.024	.085	85.8	122.
10	-	5	1.22	-	25.2	1.29	398	263	1.07	.229	1.04	-	.090	96.2	-
11	2.94	5	1.34	30.7	25.7	1.25	447.	294	1.10	.303	.70	.028	.058	68.2	75.7
12	-	5	1.39	-	27.0	1.27	460	319	1.01	.334	.14	-	.013	15.9	-
13	2.94	5	1.34	30.7	27.3	1.31	473	311	1.10	.301	.04	.028	.029	34.1	76.9
14	2.82	5	1.35	31.3	26.9	1.29	468	311	1.09	.310	.27	.028	.022	26.1	80.8
15	-	5	1.37	-	27.9	1.32	502	327	1.15	.322	.59	-	.047	56.4	-
16	-	5	1.43	-	29.5	1.35	535	360	1.08	.365	.49	-	.00	-	-
17	-	5	1.50	-	29.8	1.32	581	380	1.13	.418	.00	-			-
18	2.68	5	1.42	34.5	28.9	1.33	520	350	1.08	.257	.76	.029			76.8
Run 71- 1	1.05	1	.35	1.0	9.4	.92	28.0	28	.25	.002	.14	.005	.051	15.6	85700.
2	-	2	.54	-	14.8	1.26	82.8	68	.33	.016	.15	-	.040	19.0	-
3	2.20	2	.57	5.0	17.5	1.40	117.	85	.41	.020	.22	.008	.050	25.0	8140.
4	-	2	.62	-	18.5	1.43	143.	98	.48	.027	.28	-	.054	29.4	-
5	3.69	2	.80	10.5	18.8	1.29	203	128	.70	.061	.23	.014	.030	21.1	1360
6	-	3	.74	-	19.1	1.36	185	121	.60	.049	.25	-	.039	25.3	-
7	3.45	4	.87	12.6	20.2	1.29	234.	150	.71	.080	.58	.015	.074	57.0	1260.
8	-	4	.88	-	21.9	1.36	272.	165	.79	.084	.94	-	.109	84.1	-
9	3.77	5	1.16	22.6	24.5	1.30	385.	241	1.18	.192	.85	.027	.066	67.2	74.6
10	-	5	1.17	-	26.1	1.36	378.	259	.99	.197	.76	-	.070	71.8	-
11	3.33	5	1.24	26.2	25.8	1.30	424.	272	1.14	.239	.60	.028	.048	52.2	77.1
12	-	5	1.33	-	26.4	1.28	438.	298	1.03	.293	.16	-	.014	16.3	-
13	2.68	5	1.26	27.0	26.8	1.34	426	287	1.04	.249	.05	.025	.044	48.6	111.
14	-	5	1.30	-	26.6	1.31	450.	294	1.13	.271	.15	-	.012	13.7	-
15	2.88	5	1.29	28.5	27.8	1.36	463.	306	1.10	.269	.01	.027	.001	1.13	90
16	-	5	1.33	-	29.1	1.39	476.	329	1.03	.290	.00	-	.00	0	-
17	3.39	5	1.25	26.4	29.7	1.47	492	315	1.18	.239	.00	.028	-		76.
18	2.87	5	1.20	24.2	29.7	1.50	457	302	1.09	.210	-	-			115.

TABLE A-2 (CONTINUED)

Image No.	A/B dim.	SHAPE MODE dim.	de cm.	Eo. dim.	V $\frac{cm.}{sec.}$	V/VT dim.	Rea dim.	Red dim.	S sq.cm.	H cal.	q cal/sec.	hi $\frac{cal.}{(sec)(cm^2)(^oC)}$	U $\frac{cal.}{(sec)(cm^2)(^oC)}$	Nu dim.	Ra dim.
Run 72- 1	1.08	1	.41	1.93	10.3	.92	49.6	49	.24	.005	.60	.005	.13	46.3	216000
2	1.82	2	.84	11.6	15.8	1.00	193.	154	.45	.069	.88	.009	.10	74.3	8710.
3	2.15	2	.92	14.1	19.4	1.14	280.	206	.79	.092	1.34	.017	.09	70.3	655.
4	2.41	2	1.15	22.6	22.0	1.13	420.	294	.94	.185	1.81	.022	.10	102.	298.
5	2.83	3	1.34	30.3	24.0	1.12	561.	372	1.05	.289	2.02	.027	.10	116.	145.
6	2.94	5	1.49	37.7	25.5	1.11	670.	440	1.07	.399	1.98	.032	.10	124.	92.8
7	2.94	5	1.60	43.9	26.6	1.10	753.	495	1.05	.501	1.35	.035	.07	93.5	66.9
8	2.86	5	1.68	48.4	27.4	1.09	807.	534	1.00	.579	.89	.038	.05	67.2	54.7
9	3.63	5	1.63	45.6	28.6	1.15	855.	541	1.15	.528	1.93	.040	.09	125.	42.5
10	3.58	6	1.78	54.2	29.8	1.12	969.	614	1.05	.683	2.74	.048	.14	209	25.4
11	3.87	6	1.96	65.9	30.5	1.08	1120.	693	.87	.913	1.08	.071	.06	105.	7.73
12	3.05	6	1.97	66.6	31.0	1.09	1090.	708	.76	.928	.09	.065	.06	105.	10.9
13	3.77	6	1.81	56.3	31.6	1.17	1060.	665	1.06	.720	.67	.051	.03	47.2	20.1
14	3.31	6	2.05	72.0	32.4	1.10	1200.	771	.63	1.04	0	.091	0	-	4.10
15	3.89	6	1.88	60.5	32.7	1.17	1160.	713	1.04	.799					
16	3.36	6	1.78	54.4	32.8	1.22	1060.	679	-	.680					
17	3.37	6	1.90	61.9	33.4	1.19	1150.	737		.823					
18	3.89	6	1.88	60.5	33.8	1.21	1190.	737		.794					
Run 81- 1	1.08	1	.64	6.8	11.9	.93	90.2	89	.20	.031	.45	.008	.11	64.3	14500
2	-	2	.73	13.7	16.8	1.13	194.	143	.34	-	.65	.024	.10	64.4	241.
3	1.98	2	.90	18.8	19.8	1.17	270.	207	.53	.088	.78	.030	.08	60.3	124.
4	2.20	5	1.05	20.7	22.3	1.20	373.	272	.58	.141	.69	.036	.06	56.6	63.4
5	2.83	5	1.10	23.5	23.7	1.23	457.	303	.67	.163	.84	.039	.07	62.3	50.6
6	2.84	5	1.17	30.5	24.5	1.22	503.	334	.67	.196	1.03	.051	.08	82.6	22.1
7	3.22	5	1.33	30.9	25.1	1.17	602.	389	.67	.289	.83	.050	.06	75.4	24.8
8	2.95	5	1.34	33.7	26.0	1.20	618.	406	.64	.296	.42	.055	.03	39.8	17.9
9	3.02	5	1.40	30.8	27.9	1.24	694.	454	.62	.336	0	.045	0	-	37.1
10	2.43	5	1.34	24.6	29.3	1.32	652.	455	.58	.292					
11	3.53	6	1.20	26.0	29.1	1.40	637.	405	.74	.209					
12	3.38	6	1.23	31.9	29.1	1.38	649.	417	-	.226					
13	2.97	5	1.37	29.2	30.1	1.34	727.	477		.308					
14	3.73	6	1.31	33.5	30.6	1.39	738.	464		.269					
15	3.30	6	1.40	27.9	30.5	1.34	769	495		.329					

TABLE A-2 (CONTINUED)

Image No.	A/B dim.	SHAPE MODE dim.	de cm	Eo dim.	V cm/sec.	V/V_T dim.	Re_A dim.	Re_d dim	S sq.cm.	H cal.	q cal./sec.	h_i cal./(sec.)(cm^2)(°C)	U cal./(sec.)(cm^2)(°C)	Nu dim.	Re dim.
									ø			ø			
Run 83- 1	1.57	2	.35	1.2	11.3	.53	443	379	.16	.004	.060	.006	.097	1.39	12300
2	.98	2	.43	2.1	16.7	.77	682	642	.16	.009	.110	.007	.172	1.80	10100.
3	1.79	3	.59	4.4	19.3	.88	1350	1090	.26	.026	.146	.011	.139	6.87	1220.
4	2.35	3	.68	6.0	20.1	.90	1860	1310	.34	.041	.248	.015	.180	13.4	488
5	3.61	4	.77	7.8	20.3	.89	2350	1490	.46	.060	.541	.021	.279	31.1	161
6	3.66	4	.99	12.9	21.2	.88	3160	1990	.51	.127	.851	.026	.405	51.5	89.1
7	3.29	4	1.23	20.3	22.9	.89	4180	2690	.64	.249	.772	.049	.271	165.	6.3
8	3.72	5	1.37	25.1	23.8	.89	4940	3100	.61	.340	.847	.067	.302	239.	2.7
9	4.02	5	1.36	24.6	23.9	.90	5110	3090	.69	.329	.841	.072	.262	282.	3.1
10	3.50	5	1.67	37.3	24.5	.85	6110	3890	.0	.614	.658	∞	∞	-	.00
11	2.59	5	1.44	27.6	25.0	.92	5030	3420		.389	.936	.058	.410		3.7
12	2.47	5	1.81	43.9	25.3	.84	6300	4360		.779	.577	∞	∞		.00
13	2.11	5	1.71	39.1	25.9	.89	5680	4220		.655	.258		-		.00
14	-	5	1.73	-	26.4	.90	6470	-		.674	-	-	-		-
15	-	5	1.56	-	26.2	.93	6360	-		.490	-	-			-

ø based on observed size not nominal size

Run 84- 1	1.39	2	.36	1.3	14.3	.64	544.	490	544.	.004	.106	.006	.176	44.5	16200.
2	1.40	2	.53	3.5	18.5	.85	1050.	940	1050.	.019	.170	.009	.204	76.6	2721.
3	1.71	2	.69	6.0	17.8	.80	1410.	1160	1410	.041	.270	.012	.246	118.7	986.
4	2.20	3	.78	8.0	17.9	.79	1830.	1340	1830	.062	.436	.015	.311	171.5	415.
5	3.24	4	.98	12.8	19.5	.81	2820.	1820	2820	.126	.642	.024	.324	224.	104.
6	3.83	4	1.12	16.7	20.6	.82	3530	2190	3530	.186	1.302	.043	.418	330.	7.1
7	2.89	4	1.31	23.0	21.8	.83	4140.	2730	4140	.300	1.756	.049	.682	630.	5.6
8	4.02	4	1.71	39.2	23.1	.79	6220.	3770	6620	.664	.964	∞	∞	-	00
9	2.19	5	1.67	37.3	24.6	.85	5350.	3910	5350	.615	.209	∞	-	-	.00
10	-	5	1.63	-	26.0	.84	6060.	4050	6060	.576	.567	-	-		-

TABLE A-2 (CONTINUED)

Image No.	A/B dim.	SHAPE MODE dim.	de cm.	Eo dim.	V cm./sec.	V/VT dim.	Rea dim.	Red dim.	S sq.cm.	H cal.	q cal/sec.	Hi cal./(sec)(cm^2)(°C)	U cal./(sec)(cm^2)(°C)	NU dim.	Ra dim.
Run 85- 1	1.11	2	.44	2.2	14.3	.67	612	599	.174	.010	.08	.007	.11	34.	7670.
2	1.37	2	.53	3.4	17.2	.80	955	864	.216	.018	.10	.008	.12	45.	2960.
3	1.83	3	.60	4.5	18.1	.83	1300	1040	.274	.027	.12	.011	.12	51.	1150.
4	2.23	3	.70	6.3	19.0	.84	1740	1260	.346	.044	.23	.014	.17	84.	528.
5	2.76	4	.76	7.5	19.9	.88	2150	1430	.413	.056	.54	.018	.33	177	273.
6	4.02	4	.99	13.1	20.1	.84	3140	1900	.803	.129	1.41	.039	.44	306	9.62
7	4.02	4	1.24	20.5	20.5	.80	4000	2430	.793	.252	1.79	.053	.55	480	4.53
8	3.24	4	1.72	39.6	21.8	.74	5520	3570	-	.673	1.27	∞	∞	-	.0
9	3.99	5	1.56	32.5	23.0	.82	5610	3410		.500	.89				
10	2.33	5	1.84	45.5	24.3	..80	6000	4260		.825	.59				
11		5	1.68		24.3	.84	6170	3910		.630	.68				
12		5	1.88		24.0	.78	7090	4300		.869	.84				
13		5	1.88		24.5	.80	6620	4400		.874	.46				
14		5	1.97		25.4	.81	7160	4760		.994	0				
Run 87- 1		2	.41	1.4	9.9	.49	409	385.	.253	.005	.09	.005	.09	27.3	34500.
2		4	.47	2.3	15.1	.72	864	681.	.315	.010	.15	.006	.13	43.5	8810.
3		4	.70	6.1	17.9	.82	1360	1200.	.367	.042	.20	.007	.14	69.6	4460.
4		4	.73	6.7	19.2	.86	2000	1330	.572	.048	.31	.011	.14	72.3	1010.
5		4	.90	10.4	19.6	.85	2640	1670.	.748	.092	.54	.015	.19	118.	412.
6		4	1.04	14.1	19.9	.82	3250	1970.	1.243	.145	.46	.027	.09	69.2	35.1
7		4	1.25	20.7	20.7	.80	4060	2460.	1.430	.256	.72	.035	.12	111.	33.5
8		5	1.05	14.4	22.2	.91	3200	2210	.982	.148	1.73	.022	.43	320.	64.2
9		5	1.65	36.3	24.2	.84	5430	3800	.925	.592	2.06	.035	.54	632.	16.8
10		5	1.75	41.0	25.2	.85	6870	4200	1.103	.709	1.51	.052	.33	406	4.37
11		5	1.91	49.1	26.0	.84	7580	4750	.843	.924	1.76	.071	.49	666	1.80
12		5	1.88	47.3	27.6	.90	7540	4940	.814	.872	2.37	.057	.67		3.71
13		6	2.26	68.5	28.9	.86	9570	6230	-	1.52	1.15	∞	-		0
14		6	2.18	63.5	29.8	.90	9440	6180		1.35	.45				

TABLE A-2 (CONTINUED)

Image No.	A/B dim.	SHAPE MODE dim.	de cm	Eo dim.	V $\frac{cm.}{sec.}$	V/V_T dim.	Re_A dim.	Re_d dim.	S sq.cm.	H cal.	q cal/sec.	h_i $\frac{cal.}{(sec)(cm^2)(°C)}$	U $\frac{cal.}{(sec)(cm^2)(°C)}$	Nu dim.	Ra dim.
Run 88- 1	1.55	2	.32	.32	9.1	.56	324	278	.27	.001	.05	.006	.05	10.	23300.
2	1.51	2	.40	1.3	14.8	.68	645	561	.24	.002	.09	.005	.09	24.	5790.
3	1.58	3	.59	4.2	18.1	.84	1200	1020	.32	.005	.14	.007	.10	39.	4370.
4	1.78	4	.60	4.2	19.3	.89	1360	1100	.35	.024	.33	.007	.23	93.	848.
5	2.67	4	.82	8.6	19.8	.87	2280	1540	.57	.025	.60	.012	.26	144.	31.6
6	3.91	4	1.05	14.5	20.5	.84	3330	2050	1.04	.069	.79	.026	.17	121.	29.7
7	4.02	4	1.21	19.5	20.7	.81	3940	2390	1.34	.151	.96	.032	.18	139.	22.4
8	4.02	4	1.38	25.2	21.3	.80	4610	2790	1.42	.234	1.35	.038	.23	214.	11.2
9	3.79	5	1.52	30.7	23.0	.83	5330	3330	1.22	.343	1.34	.038	.27	236.	6.33
10	3.06	5	1.78	42.1	25.3	.85	6560	4280	.97	.460	.71	.047	.18	216.	15.0
11	2.55	5	1.66	36.8	27.1	.94	6250	4280	.99	.738	.77	.037	.19	213.	5.3
12	3.32	5	1.79	42.9	27.3	.91	7250	4660	1.02	.601	1.74	.050	.41	495.	2.2
13	3.67	5	1.90	48.4	27.3	.89	7850	4950	.92	.755	2.24	.067	.59	758.	.00
14	3.38	5	2.17	63.3	28.3	.86	9120	5850	.00	.901	.86	∞	∞	-	
15	3.29	5	2.16	62.3	28.8	.88	9180	5920	-	1.34	.00				
16	-	-	1.98	-	29.1	.93	9060	5490	-	1.31					
17	-	-	1.94	-	29.7	.96	8350	5490							
Run 89- 1	.33	1	.30	.12	7.9	.73	187	278	.26	.000	.06	.005	.05	10.	371000.
2	1.20	2	.40	1.30	14.2	.66	567	541	.23	.005	.13	.005	.14	38.	34700.
3	1.28	3	.61	4.5	17.8	.83	1120	1040	.29	.027	.18	.006	.15	64.	8440.
4	1.91	3	.72	6.5	19.4	.87	1710	1330	.42	.046	.28	.009	.16	81.	2290.
5	2.69	3	.80	8.1	19.9	.88	2240	1510	.57	.064	.50	.012	.21	128.	861.
6	4.02	3	1.02	13.8	20.6	.85	3320	2010	1.15	.139	.53	.026	.11	79.	32.1
7	4.02	4	1.18	18.4	21.0	.83	3900	2360	1.23	.215	1.23	.029	.24	200.	23.0
8	4.02	4	1.17	18.0	21.6	.86	3970	2400	1.29	.208	1.76	.030	.33	272.	28.7
9	4.02	4	1.81	43.7	23.3	.78	6610	4010	1.13	.780	2.05	.062	.44	561.	3.9
10	4.02	5	1.51	30.3	24.5	.88	5810	3520	1.39	.452	2.61	.042	.46	490.	13.6
11	3.84	5	2.20	65.1	25.5	.77	8630	5360	.00	1.41	1.49	∞	∞	-	.00
12	4.02	5	1.95	50.9	27.3	.88	8370	5070		.973	1.51	-			-
13	4.02	5	2.13	60.7	29.0	.89	9700	5880		1.27	1.51	-			-
14	4.02	5	2.36	74.9	29.5	.86	10960	6640		1.73	.00				
15	4.02	5	2.04	-	29.8	.93	9440	-		1.11	-				

TABLE A-2 (CONTINUED)

Image No.	A/B dim.	SHAPE MODE dim.	de cm	Eo dim.	V cm./sec.	V/V_T dim.	Re_A dim.	Re_d dim.	S sq.cm.	H cal.	q cal/sec.	h_i cal./(sec.)(cm²)(°C)	U cal./(sec.)(cm²)(°C)	Nu dim.	Ra dim.
Run 90- 1	1.11	2	.39	.24	9.3	.68	350	342	.38	.000	.02	.004	-	-	43900.
2	1.24	2	.40	.45	15.2	.83	615	579	.39	.001	.13	.004	.08	23.	39300.
3	1.93	3	.51	2.2	18.2	.87	1140	886	.41	.011	.29	.004	.17	61.	31000.
4	1.69	3	.81	8.1	19.9	.89	1864	1540	.56	.065	.25	.006	.11	63.	8040.
5	2.24	4	.92	10.5	21.2	.92	2550	1840	.74	.095	.36	.008	.12	78.	3200.
6	4.02	4	.85	8.9	21.0	.93	2805	1700	1.03	.075	1.03	.011	.24	144.	1230.
7	4.02	4	1.25	20.3	21.0	.82	4120	2500	1.83	.251	1.08	.020	.14	123.	83.1
8	4.02	4	1.53	30.9	22.0	.79	5270	3190	1.95	.466	.89	.024	.11	118.	43.3
9	3.85	4	1.33	23.2	23.4	.89	4780	2960	1.82	.303	1.94	.020	.26	244.	68.0
10	3.48	4	1.78	42.0	25.3	.85	6100	4280	2.00	.734	2.78	.026	.35	438.	36.1
11	4.02	5	1.98	52.5	26.8	.85	8350	5060	2.50	1.02	3.00	.041	.29	404.	41.8
12	4.02	5	2.14	61.4	27.7	.85	9340	5660	1.91	1.29	2.62	.039	.33	497.	11.0
13	4.02	5	2.36	74.3	29.7	.87	11010	6670	1.62	1.71	1.70	.052	.25	415.	4.7
14	3.59	5	2.29	70.3	32.8	.97	11290	7160	1.65	1.57	2.50	.043	.36	580.	8.3
15	4.02	6	2.46	80.8	33.9	.97	13120	7940	1.40	1.93	3.05	.065	.51	883.	2.5
16	4.02	6	2.68	96.4	33.7	.92	14210	8610	.00	2.51	1.61	∞	∞	-	.00
17	4.02	6	2.62	91.8	33.2	.92	13670	8280	-	2.32	.24	-			.2
Run 91- 1		4	.40	-	10.6	.61	446	403	.40	.001	.05	.005	.03	8.0	-
2	1.73	4	.42	.82	15.6	.75	770	630	.43	.003	.15	.005	.08	24.	23400.
3	2.10	4	.62	4.1	18.9	.89	1500	1120	.52	.025	.24	.005	.11	48.	10700.
4	1.77	4	.80	7.7	20.9	.94	1960	1590	.57	.060	.33	.006	.14	79.	7680.
5	3.13	5	.87	9.4	21.3	.94	2720	1770	.89	.081	.68	.009	.18	110.	1856.
6	2.69	5	1.06	14.5	21.5	.89	3230	2170	1.33	.153	1.09	.014	.20	149.	208.
7	3.87	5	1.36	24.5	21.8	.82	4570	2830	1.80	.330	1.33	.021	.18	173.	61.3
8	3.68	5	1.48	29.0	22.4	.82	5010	3160	1.83	.423	1.78	.022	.23	240.	55.9
9	3.15	5	1.70	38.3	24.5	.84	6110	3970	1.77	.641	2.56	.023	.34	407.	49.6
10	3.51	5	1.91	48.7	26.8	.87	7660	4880	1.86	.917	4.00	.029	.51	686.	26.5
11	2.84	6	2.16	62.4	28.4	.87	8830	5850	1.57	1.32	6.09	.033	.92	1400.	19.6
12	3.12	6	2.53	85.5	29.7	.84	11020	7160	.93	2.12	5.06	.074	1.29	2300.	1.71
13	3.41	6	2.83	107.6	31.4	.84	13240	8480	.00	2.98	2.32	∞	∞	-	.00
14	3.29	6	2.59	90.1	33.4	.93	12810	8250	-	2.28	2.54				-
15	4.02	6	2.91	113.4	34.2	.90	15650	9480	-	3.20	2.76				-
16	4.02	6	2.89	111.6	33.9	.89	15390	9320		3.12	2.77				
17	-	6	3.00		37.7	.97				3.51	3.35				

TABLE A-2 (CONTINUED)

Image No.	A/B	SHAPE MODE	de	Eo	V	V/V_T	Re_A	Re_d	S	H	q	h_i	U	Nu	Ra
	dim.	dim.	cm.	dim.	cm./sec.	dim.	dim.	dim.	sq.cm.	cal.	cal/sec.	cal./(sec)(cm^2)(^{o}C)	cal./(sec)(cm^2)(^{o}C)	dim.	dim.
Run 92- 1	1.50	2	.38	.18	12.9	1.01	538.	470	.42	.000	.08	.004	.06	16.	23200.
2	1.78	3	.53	2.5	17.6	.84	1100.	884	.39	.012	.16	.004	.10	37.	39600.
3	1.34	4	.66	4.9	19.7	.91	1360.	1250	.43	.032	.30	.005	.17	79.	25000.
4	1.97	4	.80	7.7	20.5	.93	2040.	1560	.62	.061	.44	.007	.17	96.	5910.
5	2.90	4	1.01	13.1	21.1	.89	3090.	2040	1.32	.132	.49	.014	.09	71.	199.
6	3.55	4	1.09	15.4	21.2	.87	3470.	2210	1.52	.166	.68	.016	.10	77.	121.
7	2.53	4	1.21	19.2	22.3	.88	3760.	2580	1.41	.235	1.65	.015	.28	238.	178.
8	3.21	5	1.42	26.7	23.8	.88	5000.	3230	1.70	.375	2.69	.020	.38	380.	79.3
9	4.02	5	1.88	47.2	25.2	.83	7472.	4530	2.02	.876	1.91	.031	.23	304.	22.1
10	3.44	5	1.98	52.2	26.8	.86	7910.	5060	1.82	1.02	1.26	.030	.16	223.	23.4
11	4.02	5	1.86	46.2	28.5	.94	8350.	5060	2.20	.843	3.32	.032	.36	471.	29.2
12	3.46	5	2.21	65.5	30.7	.92	10140.	6480	1.70	1.42	5.59	.038	.78	1221.	11.9
13	3.61	6	2.56	87.4	32.1	.90	12360.	7820	.91	2.18	6.32	.091	1.66	2990.	.92
14	3.94	6	2.77	102.9	32.6	.88	14030.	8610	--	2.77	7.24	∞	--		.00
15	4.02	6	3.00	120.4	32.9	.85	15530.	9400	--	3.50	7.55				
16		6	3.27		33.2	.82	17090.	10350			4.84				
Run 93- 1	1.15	1	.68	5.79	12.7	.63	990.	957	.44	.034	.52	.004	.11	52.6	84800.
2	2.11	2	.80	8.44	17.0	.78	2004.	1490	.69	.059	1.21	.007	.17	93.7	13600.
3	3.07	4	.93	12.0	18.8	.82	2960.	1930	.96	.098	2.99	.010	.30	192.	4370.
4	2.53	5	1.34	25.9	20.8	.79	4460.	3070	1.51	.305	4.00	.017	.25	231.	368.
5	2.49	5	1.70	42.1	24.3	.84	6580.	4550	1.59	.628	4.61	.021	.28	328.	197.
6	2.47	5	1.74	44.3	27.8	.94	7680.	5320	1.60	.677	7.34	.021	.44	528.	184.
7	2.34	5	2.13	66.4	30.6	.94	10100.	7180	1.43	1.24	12.21	.028	.82	1200.	82.9
8	2.42	5	2.41	85.5	31.9	.92	12100.	8480	1.13	1.81	15.24	.044	1.29	2130.	22.7
9	2.12	5	2.87	121.1	32.0	.85	13600.	10120	.00	3.04	11.60	∞	∞		.00
10	2.75	5	2.97	129.7	33.6	.87	16400.	10990	--	3.36	5.30				
11	--	5	2.99	--	35.0	.91	17200.	11560	--	3.44	2.75				
12	--	5	2.98	--	35.8	.93	17500.	11760		3.39	3.07				
13		5	3.07		36.7	.94	18900.	12430		3.70	2.97				
14		5	3.09		37.1	.94	19600.	12640		3.77	2.74				
15		5	3.13		37.4	.95	19800.	12910		3.91	4.72				
16		5	3.18		38.3	.96	20800.	13410		4.09	2.74				
17			3.34		38.6	.95	23200.	14200		4.73	.00				
18			3.05		37.5	.96	20200.	12610		3.62					

TABLE A-2 (CONTINUED)

Image No.	A/B dim.	SHAPE MODE dim.	de cm.	Eo dim.	V $\frac{cm.}{sec.}$	V/V_T dim.	ReA dim.	Re_d dim.	S sq.cm.	H cal.	q cal/sec.	h_1 $\frac{cal.}{(sec)(cm^2)(^oC)}$	U $\frac{cal.}{(sec)(cm^2)(^oC)}$	Nu dim.	Ra dim.
Run 94- 1	1.29	1	.57	3.43	12.3	.64	832.	771	.39	.017	.48	.004	.118	46.4	226000.
2	1.87	2	.73	6.83	16.5	.77	1690.	1330	.59	.043	1.04	.006	.167	84.	22800.
3	2.49	4	.93	11.9	18.6	.82	2750.	1900	.85	.096	2.69	.009	.303	194.	6600.
4	2.97	4	1.22	21.3	20.3	.80	4160.	2730	1.56	.227	4.73	.017	.289	243.	335.
5	2.32	5	1.69	41.6	22.9	.79	6000.	4260	1.54	.616	6.21	.020	.285	332.	232.
6	2.09	5	1.88	51.8	26.3	.86	7300.	5450	1.44	.856	7.96	.022	.526	681.	198.
7	2.26	5	2.20	71.2	29.4	.89	9950.	7160	1.35	1.38	9.28	.030	.656	995.	69.0
8	2.38	5	2.44	87.3	30.0	.86	11500.	8070	1.06	1.86	10.08	.046	.903	1520.	20.0
9	2.49	5	2.63	102.2	30.2	.83	12700.	8770	.32	2.36	9.77	.191	2.93	5320.	.33
10	2.66	5	2.85	119.6	33.7	.89	15700.	10570	0	2.98	5.49	∞	∞		.00
11	2.99	5	2.91	124.6	35.8	.94	17500.	11480	--	3.16	2.34	--	--		
12	--	-	2.81	--	35.9	.96	17200.	11120		2.84	2.06	--	--		
13	--	-	3.00	--	37.1	.96	19200.	12240		3.45	.00				
14			2.84		37.7	1.00	18800.	11810		2.94	--				
15			2.80		37.6	1.00	18100.	11620		2.81	--				
16			2.77		37.8	1.02	18600.	11540		2.72	--				
Run 95- 1	1.35	1	.56	3.32	12.0	.62	814.	741	.40	.016	.44	.004	.106	41.0	206000.
2	1.64	2	.77	7.76	16.6	.77	1680.	1410	.57	.052	.78	.006	.132	70.1	26900.
3	2.06	2	.84	9.55	18.6	.84	2290.	1720	.71	.070	2.20	.007	.298	173.	12400.
4	3.31	4	1.15	18.8	20.1	.81	3950.	2540	1.61	.189	4.45	.017	.268	213.	318.
5	2.02	5	1.59	36.8	22.8	.81	5270.	4000	1.43	.514	5.90	.017	.398	436.	383.
6	2.40	5	1.88	51.9	26.0	.85	7680.	5390	1.58	.859	7.70	.023	.472	611.	146.
7	2.40	5	2.09	63.9	28.6	.89	9360.	6570	1.50	1.17	9.69	.028	.625	901.	88.2
8	2.66	5	2.46	89.2	29.6	.85	11900.	8040	1.08	1.93	10.78	.052	.961	1630.	12.9
9	2.78	5	2.59	98.8	30.5	.85	13000.	8720	.66	2.24	9.62	.095	1.41	2520.	2.01
10	2.91	5	2.89	123.3	32.7	.86	15800.	10430	0	3.12	5.54	∞	∞	--	.00
11	2.80	5	2.81	116.3	35.0	.93	16300.	10830	--	2.85	4.66				
12	--	-	2.92	--	36.7	.96	18200.	11840		3.21	3.62				
13	--	-	3.04	--	37.3	.96	19500.	12510		3.61	.00				
14			2.88		37.1	.98	18500.	11790		3.07	.49				
15			2.93		37.4	.98	19600.	12070		3.21	3.66				
16			3.06		38.0	.97	21200.	12850		3.67	1.64				
17			3.06		38.5	.98	21400.	12980		3.66	.00				
18			2.97		38.0	.99	2600.	12470		3.35	--				

TABLE A-2 (CONTINUED)

Image No.	A/B dim.	SHAPE MODE dim.	de cm.	Eo dim.	V $\frac{cm.}{sec.}$	V/V_T dim.	Re_A dim.	Re_d dim.	S sq.cm.	H cal.	q cal/sec.	h_i $\frac{cal.}{(sec)(cm^2)(^oC)}$	U $\frac{cal.}{(sec)(cm^2)(^oC)}$	Nu dim.	Ra dim.
Run 96- 1	.97	1	.31	.178	8.13	.65	270.	275	.25	.000	.41	.005	.155	33.1	83900.
2	1.22	2	.63	5.21	13.7	.67	1000.	948	.31	.029	.60	.006	.184	80.0	23300.
3	2.13	2	.88	11.1	16.9	.74	2220.	1650	.52	.086	1.27	.011	.229	139.	3080.
4	2.41	4	.86	10.6	19.4	.85	2640.	1850	.57	.081	3.28	.012	.548	325.	2450.
5	2.04	4	1.40	28.7	22.2	.83	4550.	3430	.90	.354	4.73	.025	.500	482.	132.
6	1.72	4	1.73	44.0	25.8	.88	6000.	4920	.74	.669	4.22	.032	.544	650.	68.2
7	1.98	5	1.88	51.9	28.6	.93	7730.	5930	.67	.857	3.78	.045	.536	695.	22.8
8	2.63	5	1.95	55.9	30.3	.97	9610.	6510	.68	.956	3.79	.064	.534	718	6,93
9	2.22	5	2.15	68.1	31.4	.96	10300.	7440	0	1.28	3.05	∞	∞	-	.00
10	2.98	5	2.16	68.4	32.1	.98	11600.	7640	-	1.29	2.40				
11			2.26		33.1	.99	12600.	8240		1.48	1.56				
12			2.27		33.7	1.00	13500.	8440		1.50	.04				
13			2.27		34.1	1.01	13600.	8530		1.50	.56				
14			2.19		34.4	1.04	13300.	8300		1.35	1.75				
Run 97- 1	-	1	.66	-	12.0	.59	916.	1420	-	.034	-	-	-	-	-
2	-	4	.79	-	16.2	.73	1780.	1950	-	.061	-	-	-	-	-
3	-	4	.95	-	18.7	.80	2840.	3260.	.62	.106	3.11	-	.483	317.	-
4	-	4	1.37	-	21.7	.82	4340.	4780	.90	.328	5.07	-	.533	503.	-
5	-	5	1.71	-	25.4	.87	6490.	6140	.85	.641	5.19	-	.585	690.	-
6	2,28	5	1.98	57.6	28.1	.90	8560.	6430	.57	1.00	4.26	.066	.716	972.	6.6
7	2.41	5	1.99	58.3	29.3	.93	9180.	7360	.56	1.02	5.29	.072	.892	1220.	5.2
8	2,53	5	2,20	71.6	30.3	.91	10700.	8560	0	1.38	6.13	∞	∞	-	.00
9	2.71	5	2,41	85.3	32.3	.93	12700.	9170		1.80	3.59				
10			2.46		33.8	.97	13700.	8930		1.92	.89				
11			2,38		34.1	.99	13800.	9290		1.73	.03				
12			2.45		34.3	.98	14700.	8920		1.90	.00				
13			2.35		34.4	1.00	14700.	8870		1.67	-				
14			2.31		34.7	1.02	14000.	9460		1.59	-				

TABLE A-2 (CONTINUED)

Image No.	A/B dim.	SHAPE MODE dim.	d_e cm.	Eo dim.	V $\frac{cm.}{sec.}$	V/V_T dim.	Re_A dim.	Red dim.	S sq.cm.	H cal.	q $\frac{cal.}{sec.}$	h_i $\frac{cal.}{(sec)(cm^2)(^oC)}$	U $\frac{cal.}{(sec)(cm^2)(^oC)}$	Nu dim.	Ra dim.
Run 98- 1	1.02	1	.26	-	7.6	.35	217.	218	.27	-	.34	.005	.117	19.2	47200.
2	1.47	2	.66	5.79	13.2	.64	1080.	955	.35	.033	.60	.007	.165	75.2	14300.
3	2.44	2	.77	8.23	16.5	.75	2010.	1400	.54	.056	1.89	.011	.333	177.	3060.
4	2.92	4	.99	14.2	18.9	.80	3140.	2070	.99	.124	4.03	.021	.389	266.	163.
5	2.04	4	1.54	34.8	22.0	.79	4950.	3740	.88	.472	5.23	.028	.564	599.	90.2
6	2.09	5	1.78	46.5	25.9	.87	6800.	5080	.78	.728	5.41	.038	.657	807.	35.5
7	2.28		2.00	58.9	28.8	.91	8860.	6350	.52	1.03	5.09	.073	.929	1280.	4.9
8	2.33		2.14	67.4	29.6	.91	9870.	7000	0	1.27	4.94	∞	∞	-	.00
9			2.25		30.5	.91	11200.	7590	-	1.48	4.70				
10			2.40		32.2	.93	13300.	8530		1.79	2.71				
11			2.44		33.7	.96	14000.	9060		1.87	.00				
12			2.38		34.3	.99	14600.	9020		1.74	-				
13			2.29		34.2	1.01	14100.	8640		1.55	-				
14			2.38		33.6	.97	14600.	8840		1.74	-				
Run 100-1	-	1	.40	-	10.8	.53	481.	474	.16	.007	.62	-	.363	100.	-
2	-	2	.76	-	15.7	.71	1650	1310	.31	.055	1.39	-	.427	224.	-
3	2.30	2	.97	13.7	18.9	.80	2820.	2010	.59	.117	2.78	.028	.446	298.	78.0
4	2.32	4	1.32	25.6	21.9	.84	4490.	3190	.57	.298	4.06	.044	.682	620.	22.6
5	2.02	5	1.64	39.4	25.4	.89	6050.	4590	.19	.568	3.21	.144	1.58	1790.	.73
6	2.61	5	1.82	49.0	27.7	.92	8200.	5570	0	.786	.76	∞	∞	-	.00
7	-		1.70	-	27.4	.94	7740.	5150	-	.640	.00	-			-
8			1.69		27.6	.95	7730.	5140		.622	.00				
9			1.75		28.8	.97	8400.	5550		.692					
10			1.63		28.4	.99	8130.	5120		.561					
11			1.72		28.5	.97	8540.	5430		.661					

TABLE A-2 (CONTINUED)

Image No.	A/B dim.	SHAPE MODE dim.	de cm.	Eo dim.	V cm./sec.	V/V_T dim.	Re_A dim.	Re_d dim.	S sq.cm—	H cal.	q cal/sec.	h_i cal./(sec)(cm²)(°C)	U cal./(sec)(cm²)(°C)	Nu dim.	Ra dim.
Run 101-1	1.02	1	.44	2.51	10.2	.51	497.	498	.17	.010	.56	.007	.316	95.8	23700.
2	2.10	2	.71	7.14	15.5	.71	1630.	1210	.33	.044	1.23	.014	.357	175.	1542.
3	2.22	4	.96	13.6	18.9	.80	2770.	2010	.58	.115	2.72	.028	.445	294.	85.0
4	2.18	5	1.25	22.9	22.2	.86	4180.	3060	.57	.253	3.23	.038	.539	464.	35.0
5	2.24	5	1.67	40.9	25.2	.87	6420	4640	0	.601	3.35	∞	∞		.00
6	2.44	5	1.53	34.4	27.3	.98	6610.	4600	-	.463	3.69				.485
7	2.84	5	2.02	60.4	27.6	.87	9300.	6170		1.07	1.73				.00
8			1.81		27.4	.91	8690.	5470		.761	.12				
9			1.93		27.8	.90	9280.	5920		.927	.17				
10			1.82		28.6	.95	9200.	5720		.771	.00				
11			1.95		29.1	.93	9840.	6260		.954					
12			1.48		28.5	1.04	700	4660		.417					
Run 102-1	1.12	1	.27	.42	7.9	.44	242.	236	-	.000	-	.006	-	-	40200
2	1.41	2	.61	5.17	13.7	.66	1030.	918	.23	.028	.53	.010	.218	91.8	5290.
3	1.96	4	.73	7.58	17.1	.78	1790.	1380	.32	.049	1.11	.014	.330	166.	1650.
4	3.04	4	.96	13.3	20.2	.86	3260.	2130	.68	.112	1.62	.032	.227	150.	46.7
5	2.53	5	1.24	22.4	23.4	.91	4640.	3190	.62	.244	2.01	.040	.308	263.	26.9
6	3.23	5	1.31	25.3	25.2	.96	5640.	3650	.68	.292	2.55	.051	.360	325.	12.4
7	3.03	5	1.58	36.5	26.6	.94	7060.	4610	.40	.506	1.49	.099	.352	383.	1.73
8	3.30	5	1.66	40.8	27.3	.95	7780.	5010	.10	.595	1.13	.560	1.08	1240.	02
9	3.02	5	1.45	31.0	27.9	1.02	6830.	4460	.57	.395	3.07	.064	.512	512.	6.49
10	3.16	5		53.6	28.6	.93	9290.	6020	0	.894	2.02	∞	∞		.00
11					28.7	.93	9400.	6050	-		1.10				
12					28.9	.98	8420.	5570			3.98				
13					27.6	.85	10700.	6490			2.26				
14					27.9	.84	11300	6870			.00				

TABLE A-2 (CONTINUED)

Image No.	A/B dim.	SHAPE MODE dim.	de cm.	Eo dim.	V $\frac{cm.}{sec.}$	V/V_T dim.	Re_A dim.	Re_d dim.	S sq.cm.	H cal.	q $\frac{cal/}{sec.}$	h_i $\frac{cal.}{(sec)(cm^2)(^oC)}$	U $\frac{cal.}{(sec)(cm^2)(^oC)}$	Nu dim.	Ra dim.
Run 103-1	1.00	1	.30	1.14	7.5	.45	248.	250	.15	.002	.34	.006	.211	43.7	63800.
2	1.54	2	.66	9.67	13.4	.70	1140.	79	.26	.036	.63	.011	.232	106.	3630.
3	2.66	4	.76	12.86	16.9	.81	2090.	1410	.40	.055	1.81	.017	.433	227.	806.
4	2.93	4	1.02	23.7	19.2	.83	3270.	2160	.68	.136	3.37	.034	.473	332.	41.3
5	2.31	4	1.50	51.4	22.3	.82	5160.	3680	.45	.435	3.18	.063	.674	698.	7.43
6	2.39	5	1.65	62.8	25.0	.87	6500.	4570	.14	.587	2.22	.261	1.55	1760.	.13
7	2.70	5	1.67	63.8	26.6	.92	7300.	4900	0	.600	1.53	∞	∞	-	.00
8	3.60	5	1.81	75.4	27.4	.91	8640.	5470	-	.770	.09				
9	3.87	5	1.72	67.7	27.4	.94	8400.	5200		.654	.00				
10	2.96	5		63.2	28.2	.98	7876.	5160		.589	.00				
11	4.02	5		59.2	29.2		8540.	5170		.534					
Run 105-1	.94	1	.36	2.17	8.9	.54	343.	353	.15	.004	.54	.006	.339	84.2	97500
2	1.70	2	.77	13.1	14.6	.70	1500.	1230	-	.057	.95	-	-	-	236000
3	2.28	4	.89	17.8	17.8	.81	2420	1740	.59	.089	1.35	.027	.218	134.	108.1
4	2.50	4	1.16	30.9	20.2	.83	3750	2590	.63	.204	2.49	.037	.377	302.	35.7
5	3.00	4	1.25	35.7	22.2	.89	4780.	3060	.67	.252	2.79	.045	.395	341.	18.4
6	2.58	5	1.71	67.4	24.4	.83	6750.	4600	0	.652	1.84	∞	∞	-	.00
7	2.74	5	1.45	48.1	26.7	.99	6360.	4260	-	.393	2.64				
8	3.60	5	1.82	76.3	27.9	.92	8850.	5700		.784	2.26				
9	3.82	5	1.89	81.7	28.5	.93	9530	5930		.868	.00				
10	-	5	1.78		29.2	.98	8770.	5720		.722	.00				
11	-	5	1.71		30.4	1.04	8770.	5720							

TABLE A-2 (CONTINUED)

Image No.	A/B dim.	SHAPE MODE dim.	de cm.	Eo dim.	V $\frac{cm.}{sec.}$	V/V_T dim.	Re_A dim.	Re_d dim.	S sq.cm.	H cal.	q cal/sec.	h_i $\frac{cal.}{(sec)(cm^2)(^oC)}$	U $\frac{cal.}{(sec)(cm^2)(^oC)}$	Nu dim.	Ra dim.
Run 106-1	1.65	2	.47	4.49	11.7	.68	729.	609.	.22	,012	.673	.008	.291	94.4	7130.
2	2.06	2	.77	13.2	16.1	.77	1810.	1360.	.51	.057	1.62	.022	.301	160.	178.
3	2.95	4	1.01	23.2	18.4	.80	3130.	2050.	.68	.132	2.62	.034	.367	255.	42.0
4	2.58	4	1.40	44.8	21.0	.80	4750.	3240.	.56	.354	2.92	.053	.495	478.	12.2
5	2.41	5	1.53	53.4	24.0	.87	5760.	4040.	.43	.460	2.96	.071	.659	695.	5.17
6	2.66	5	1.70	66.5	26.2	.90	7280.	4920.	0	.639	2.66	∞	∞	-	.00
7	2.82	5	1.81	75.6	27.1	.90	8170.	5420.		.774	.954				
8	3.11	5	1.86	79.2	28.5	.93	9000.	5830.		.828	.0				
9	2.82	5	1.67	64.2	30.2	1.05	8390.	5600.							
10	3.82	5	1.81	74.9	30.9	1.03	9890.	6150.							
11	-	5	1.70	-	31.5	1.08	9470.	5900.							
Run 107-1	1.20	1	.58	6.64	11.2	.64	748.	711.	.29	.021	.736	.006	.241	96.5	31300.
2	1.92	2	.91	18.2	15.9	.72	2050.	1590.	.76	.093	.831	.016	.108	67.8	480.
3	1.97	2	.95	20.2	18.5	.83	2530.	1940.	.79	.108	1.61	.017	.194	127.	408.
4	2.31	2	1.13	28.6	20.6	.86	3580.	2550.	.93	.182	3.35	.021	.344	268.	192.
5	2.52	4	1.48	50.1	22.5	.83	5340.	3680.	1.0	.419	4.70	.030	.446	455.	67.9
6	2.62	5	1.77	71.6	24.9	.84	7150.	4860.	.90	.715	4.69	.043	.498	608.	23.1
7	2.58	5	1.95	87.4	27.2	.87	8570.	5850.	.66	.963	4.50	.064	.649	872.	6.91
8	2.87	5	2.05	96.2	28.9	.90	9850.	6520.	.45	1.11	5.42	.114	1.15	1630.	1.25
9	2.79	5	2.24	115.1	30.8	.92	11400.	7620.	0	1.45	3.74	∞	∞	-	.00
10	2.99	5	2.41	133.0	32.4	.93	13100.	8590.		1.80	0				
11	-	-	2.19	-	32.8	.99	12200.	7900.							
12			2.23		33.0	.99	12500.	8120.							
13			2.04		33.6	1.05	11800	7550.							

TABLE A-2 (CONTINUED)

Image No.	A/B dim.	SHAPE MODE dim.	d_e cm.	L_o dim.	V $\frac{cm.}{sec.}$	V/V_T dim.	Re_A dim.	Re_d dim.	S sq.cm.	H cal.	q cal/sec.	h_j $\frac{cal.}{(sec)(cm^2)(^oC)}$	U $\frac{cal.}{(sec)(cm^2)(^oC)}$	Nu dim.	Ra dim.
Run 108-1	1.01	1	.53	5.46	10.6	.63	618.	622.	.26	.016	.586	.005	.213	77.8	57700
2	1.59	2	.77	12.8	15.6	.75	1560.	1320.	.40	.056	1.11	.008	.264	140.	8110.
3	2.47	2	.96	20.5	18.2	.81	2770.	1920.	.89	.111	2.25	.019	.240	159.	245.
4	2.53	4	1.23	34.1	20.5	.83	4040.	2780.	1.0	.236	4.22	.024	.403	342.	126.
5	2.74	5	1.56	55.9	23.5	.84	6040.	4050.	1.02	.494	4.40	.034	.408	440.	45.2
6	2.51	5	1.90	83.1	26.1	.85	7940.	5480.	.73	.894	2.27	.055	.298	391.	11.1
7	2.55	5	1.78	72.9	28.2	.95	8120.	5560.	.88	.733	2.24	.043	.244	300.	22.6
8	2.61	5	1.91	83.4	29.3	.95	9070.	6160.	.75	.896	4.55	.056	.582	767.	10.2
9	3.17	5	2.09	100.	29.6	.92	10500.	6830.	.24	1.18	4.36	.256	1.70	245.	.135
10	2.61	5	2.31	123.	31.4	.92	11800.	8010.	0	1.59	.344	∞	∞	-	0
11	2.58	5	2.18	109.	33.3	1.01	11700.	8010.		1.33	0				
12	3.07	5	2.05	96.3	33.5	1.05	11600.	7570.		1.10					
13	3.92	5	2.29	121.	32.7	.97	13500.	8290.		1.55					
Run 109-1	1.18	2	.53	5.40	12.3	.71	750.	718.	.27	.016	.806	.005	.279	102	42900.
2	1.99	2	.86	16.5	16.4	.76	2040	1560.	-	.081	1.31	-	-	-	-
3	3.03	4	1.04	24.3	18.4	.79	3220.	2110.	-	.143	2.05	-	-	-	-
4	3.05	4	1.28	37.0	20.4	.81	4400.	2880.	-	.267	3.03	-	-	-	-
5	2.11	5	1.51	96.0	23.5	.86	5200.	3900.	.92	.440	3.50	.028	.364	379	96.3
6	2.79	5	1.74	96.0	26.1	.89	7480	4900.	.95	.675	2.92	.042	.293	352	23.6
7	2.93	5	1.82	96.5	27.4	.91	8360	5500.	.90	.779	3.20	.049	.338	424	14.3
8	2.98	5	1.88	96.6	28.9	.95	9180	6020	.83	.863	4.35	.057	.499	647	9.41
9	2.57	5	2.14	96.9	31.2	.95	10700	7350.	0	1.26	3.90	∞	∞	-	.00
10	3.31	5	2.20	96.9	32.8	.99	12300	7970		1.37	2.68				
11	-	6	2.26	-	32.9	.98	12900	8180		1.48	1.65				
12	-	6	2.30		32.5	.96	13100	8240		1.57	.294				
13		6	2.27		33.1	.98	12800.	8310.		1.51	0				
14		6	2.25		34.0	1.02	13400.	8430.		1.46	-				

TABLE A-2 (CONTINUED)

Image No.	A/B dim.	SHAPE MODE dim.	de cm.	Eo dim.	V cm./sec.	V/V_T dim.	Re_A dim.	Red dim.	S sq.cm.	H cal.	q cal/sec.	h_i cal./(sec)(cm^2)($^\circ$C)	U cal./(sec)(cm^2)($^\circ$C)	Nu dim.	Ra dim.
Run 110-1	1.51	2	.41	2.47	.785	.51	407.	354.	.26	.005	.287	.005	.105	29.7	63800.
2	1.34	2	.68	9.92	13.4	.70	1100.	1000.	.34	.037	.492	.007	.139	65.2	16000.
3	1.43	2	.69	10.3	17.0	.85	1460.	1290.	.35	.039	1.07	.007	.287	136.	13200.
4	2.53	2	.99	22.2	18.6	.82	2950.	2030	.92	.122	2.14	.020	.222	152.	216.
5	3.03	2	1.21	33.7	20.4	.83	4160.	2720.	1.09	.226	5.45	.026	.479	574.	93.5
6	2.41	5	1.54	55.1	23.8	.86	4760.	4040.	.97	.472	7.63	.031	.750	797.	63.0
7	1.69	5	2.16	108.	26.8	.82	7710.	6380.	0	1.30	4.57	∞	∞	-	0
8	2.83	5	2.07	99.8	28.1	.88	9670.	6420.		1.14	1.79				
9	2.60	5	2.12	105.	29.2	.90	100000.	6840.		1.23	1.99				
10	-	5	2.15	-	30.3	.92	10900.	6180.		1.29	3.57				
11	3.40	5	2.27	120	30.9	.92	12100.	7730.		1.51	5.09				
12	-	5	2.45	-	31.9	.91	13400.	8610.		1.88	3.90				
13	3.88	6	2.53	149.	33.2	.93	15000.	9260.		2.08	.834				
14	-	6	2.49	-	34.1	.97	14600.	9340.		1.97	0				
15	-	6	2.44	-	34.4	.99	15300.	9240.		1.85					
16	4.02	6	2.27	120.	34.6	1.03	14300.	8660.		1.50					
Run 112-1	1.63	2	.79	14.0	13.7	.66	1430.	1200.	.64	.062	.590	.013	.088	47.9	939.
2	2.36	2	.90	18.1	17.1	.78	2390.	1690.	.84	.090	.647	.018	.073	45.3	312.
3	3.08	2	.90	18.2	18.7	.86	2850.	1860.	.96	.091	2.11	.020	.209	130.	185.
4	3.13	2	1.15	30.6	21.1	.87	4130.	2680.	1.20	.196	4.01	.025	.353	280.	99.8
5	2.54	5	1.62	61.2	24.6	.87	6420.	4400.	.97	.552	4.31	.035	.424	474.	43.4
6	2.90	6	1.78	73.8	27.2	.91	8100.	5350.	.93	.729	3.66	.046	.373	458.	18.0
7	3.22	6	1.92	85.8	29.3	.95	9580.	6190.	.80	.912	3.84	.064	.456	603.	6.3
8	2.90	6	2.00	93.4	30.8	.97	10300.	6790.	.59	1.04	4.16	.083	.668	922.	3.0
9	2.99	6	2.21	113.	30.1	.91	11200.	7340.	0	1.39	3.11	∞	∞	-	.00
10	3.16	6	2.23	116.	30.2	.91	11400.	7410.		1.42	2.84				
11	3.20	6	2.28	121.	31.8	.94	12400.	8000.		1.52	3.26				
12	3.52	6	2.42	137.	32.8	.94	13800.	8760.		1.83	.02				
13	3.82	6	2.42	136.	33.4	.96	14300.	8890.		1.81	0				
14	4.02	6	2.12	105.	33.8	1.04	13100	7900		1.22					
15	-	6	2.19		34.0	1.03	13600	8240		1.35					

TABLE A-2 (CONTINUED)

Image No.	A/B dim.	SHAPE MODE dim.	de cm.	Eo dim.	V $\frac{cm.}{sec.}$	V/V_T dim.	Re_A dim.	Re_d dim.	S sq.cm.	H cal.	q cal/sec.	h_i $\frac{cal.}{(sec)(cm^2)(^oC)}$	U $\frac{cal.}{(sec)(cm^2)(^oC)}$	Nu dim.	Ra dim.
Run 113-1	1.00	1	.43	2.98	10.3	.64	486.	490.	.24	.007	.529	.005	.207	62.3	168000.
2	1.61	2	.81	14.5	15.6	.74	1650.	1390.	.65	.065	.654	.013	.097	54.3	916.
3	2.00	2	.85	16.1	18.4	.86	2250.	1720.	.74	.075	1.30	.015	.165	96.8	512.
4	2.20	4	1.03	24.4	19.7	.86	3090.	2250.	.87	.140	2.95	.019	.322	229.	264.
5	2.49	5	1.36	42.9	21.9	.84	4750.	3280.	1.01	.324	4.37	.027	.414	388.	94.9
6	2.05	5	1.71	68.0	25.2	.86	6310.	4750.	.82	.646	4.59	.034	.531	626	49.9
7	2.13	5	1.86	80.8	27.8	.91	7720.	5720.	.72	.834	5.28	.045	.700	898	21.6
8	2.37	5	2.03	95.8	29.2	.92	9240.	6520.	.47	1.08	5.40	.087	1.10	1540	2.91
9	2.68	5	2.28	121.	29.8	.88	11100.	7500.	0	1.53	4.80	∞	∞	-	0
10	2.16	5	2.25	18.	31.2	.93	10500.	7740		1.47	4.88				
11	-	5	2.51	-	32.6	.92	14000.	9010.		1.95	4.22				
12	3.13	5	2.48	143.	33.2	.94	14000.	9070.		2.33	1.46				
13	4.02	6	2.63	161.	34.0	.94	16300	9850		1.67	0				
14	-	6	2.51	-	34.7	1.01	13900	9010.		2.02					
15	-	6	-	-	35.2	.99	15100	9740.		1.51					
Run 115-1	1.02	1	.54	4.18	10.2	.61	510.	512.	.17	.010	.388	.007	.216	80.5	22200.
2	1.95	2	.72	11.7	15.3	.75	1560.	1210.	.32	.047	.552	.013	.166	82.5	1720.
3	1.96	2	.78	13.8	18.0	.85	2010.	1540.	.50	.060	1.52	.022	.289	155.	1920.
4	2.90	4	.99	22.6	20.0	.88	3310.	2180.	.67	.124	2.82	.033	.399	272.	46.2
5	2.32	5	1.44	48.1	22.9	.86	5100.	3630.	.39	.385	3.33	.054	.630	625.	11.8
6	2.48	5	1.56	56.8	26.0	.93	6470	4480.	0	.493	2.51	.084	.614	660.	3.18
7	1.94	5	1.78	74.2	27.9	.93	7090	5480.		.734	.879	∞	∞	-	0
8	3.71	5	1.63	62.1	28.9	1.01	8280	5200.		.562	.191				
9	3.23	5	1.74	70.5	29.7	1.01	8820	5700		.678	0				
10	3.88	6	1.66	64.1	29.6	1.03	8760	5420		.587					

TABLE A-2 (CONTINUED)

Image No.	A/B dim.	SHAPE MODE dim.	de cm.	Eo dim.	V $\frac{cm.}{sec.}$	V/V_T dim.	Re_A dim.	Re_d dim.	S sq.cm.	H cal.	q cal/sec.	h_1 $\frac{cal.}{(sec)(cm^2)(^oC)}$	U $\frac{cal.}{(sec)(cm^2)(^oC)}$	Nu dim.	Ra dim.
Run 116-1	1.38	2	.62	8.43	12.0	.65	901.	814.	.23	.029	,655	.009	.269	115.	5360.
2	1.95	2	.76	13.1	16.0	.77	1740.	1340.	.49	.055	1.40	.021	.271	142.	206.
3	3.62	4	1.03	24.4	18.0	.78	3220.	2040.	.75	.139	2.31	.038	.294	209.	27.9
4	2.31	4	1.32	40.7	21.1	.82	4330.	3080.	.56	.300	2.91	.044	.491	447.	22.4
5	2.07	5	1.51	53.2	22.0	.80	4890.	3660.	.41	.447	2.70	.062	.626	652.	8.38
6	2.54	5	1.70	67.3	23.3	.80	6360.	4360	0	.635	1.30	∞	∞	-	0
7	3.60	5	1.70	67.1	29.2	1.00	8640.	5470.		.632	.704				
8	3.38	5	1.64	62.7	31.2	1.09	8800.	5640.		.570	1.50				
9	2.98	5	1.82	77.3	29.4	.97	8990	5890.		.777	1.87				
10	3.15	6	1.84	79.0	28.9	.95	9050.	5870.		.803	1.86				
Run 117-1	1.34	2	.71	11.2	13.1	.67	1120.	1020.	.24	.044	.660	.010	.258	126.	4150.
2	2.08	2	.83	15.8	16.8	.78	2050	1530.	.53	.073	1.36	.024	.243	139.	145.
3	3.10	4	.99	22.7	18.9	.83	3180	2070.	.69	.125	2.97	.034	.408	279.	40.5
4	1.87	5	1.37	43.8	21.8	.83	4180	3290.	.48	.334	4.03	.042	.792	748.	28.2
5	2.09	5	1.68	66.2	24.9	.86	6180	4620.	0	.619	3.28	∞	∞	-	0
6	2.60	5	1.80	75.3	27.6	.92	8040	5470.		.751	1.37				
7	2.97	5	1.82	77.6	28.1	.93	8630	5660.		.784	.439				
8	3.62	5	1.73	69.8	27.9	.95	8420	5330.		.669	1.63				
9	3.45	5	1.88	82.8	28.5	.93	9260	5920.		.862	2.41				
10	3.69	6	2.00	93.7	28.7	.91	10100.	6340.		1.04	1.15				
11	-	6	2.02		28.8	.91	10000.	6400.		1.06	0				
12	-	6	1.94	-	28.7	.92	9810.	6160.		.946	-				
13	-	6	1.81	-	29.3	.97	8920.	5860.		.764	-				

TABLE A-3
SUMMARY OF DATA AND CALCULATED VALUES
SYSTEM: EtCl - DISTILLED WATER

Run No.	Depth Above Nozzle cms	Feed T °C	t_o sec	Δt sec	Nucleation energy cals	H_T cals	Obs H_T cals	Calc V_T cm/sec	Surf Wt%	PrNo dim.	Vap time sec.	q_A cal/sec	T_c °C	$\Delta T_{Av.}$ °C
1	99.	-	.053	.05	.0057	1.2	1.59	-	0	6.22	.432	3.68	24.6	10.8
2	99.	-	.049	.05	.0057	1.2	1.40	32.8	0	6.22	.393	3.57	24.6	10.8
3	99.	-	.058	.05	.0057	1.2	1.36	33.0	0	6.22	.370	3.66	24.6	10.8
4	99.	-	.046	.05	.0057	.6	.47	29.7	0	6.22	.377	1.24	24.6	10.8
5	99.	-	.058	.05	.0057	.6	.46	-	0	6.22	.342	1.36	24.6	10.8
6	99.	-	.063	05	.0057	2.4	2.63	35.6	0	6.22	.606	4.33	24.6	10.8
7	99.	-	.036	.05	.0057	2.4	1.95	34.4	0	6.22	.453	4.31	24.6	10.8
8	99.	-	.04	.05	.0010	1.2	1.28	32.2	0	5.13	.256	5.02	32.6	19.2
9	99.	-	.05	.05	.0010	1.2	.98	31.1	0	5.13	.301	3.30	32.6	19.2
10	99.	-	.05	.05	.0010	1.2	.95	30.9	0	5.13	.208	4.55	32.6	19.2
11	99.	-	.038	.05	.0086	.6	.39	27.3	0	5.13	.180	2.16	32.6	19.2
12	99.	-	.035	.05	.0086	.6	.14	-	0	5.13	.117	1.19	32.6	19.2
13	99.	-	.029	.05	.0086	2.4	2.84	36.8	0	5.13	.347	8.15	32.6	19.2
14	99.	-	.035	.05	.0086	2.4	3.03	37.1	0	5.13	.321	9.44	32.6	19.2
83	94.5	3.0	.030	.10	.0144	.6	.56	26.0	0	7.45	.944	.590	18.1	4.0
84	94.5	3.1	.060	.10	.0144	.6	.66	27.1	0	7.45	.775	.848	18.1	3.9
85	94.5	3.1	.105	.10	.0144	.6	.78	25.4	0	7.45	.862	.905	18.1	4.0
87	94.5	3.0	.030	.10	.0134	1.2	1.45	31.0	0	7.45	1.300	1.12	18.1	4.1
88	94.5	3.0	.025	.10	.0134	1.2	1.07	29.5	0	7.45	1.271	.842	18.1	4.1
89	94.5	3.1	.020	.10	.0134	1.2	1.30	29.8	0	7.45	1.080	1.21	18.1	4.1
90	94.5	3.0	.040	.10	.0134	2.4	2.37	33.5	0	7.45	1.564	1.52	18.1	4.2
91	94.5	3.0	.057	.10	.0134	2.4	3.31	33.6	0	7.45	1.667	2.43	18.1	4.2
92	94.5	3.1	.080	.10	.0134	2.4	4.05	33.2	0	7.45	1.530	2.16	18.1	4.2
					SYSTEM: EtCl - 65% GLYCERIN-WATER									
64	59.7	2.9	.020	.05	.0081	.6	.324		0	86.8	.615	.527	24.1	10.8
65	59.7	3.3	.020	.05	.0072	.6	.327		0	86.8	.605	.540	24.1	10.8
66	59.7	3.2	.026	.05	.0072	.6	.422		0	86.8	.655	.645	24.1	10.8
68	59.7	3.2	.090	.05	.0072	1.2	.359		0	86.8	.670	.536	24.1	10.8
70	59.7	3.2	.040	.05	.0072	1.2	.339		0	86.8	.585	.580	24.1	10.8
71	59.7	3.2	.025	.05	.0072	1.2	.263		0	86.8	.545	.482	24.1	10.8
72	59.7	3.1	.034	.05	.0072	1.2	.843		0	63.6	.545	1.55	31.7	19.2
81	59.7	3.1	.036	.05	.0060	.6	.284		0	63.6	.372	.763	31.7	19.2

TABLE A-3 (CONTINUED)
SUMMARY OF DATA AND CALCULATED VALUES
SYSTEM: EtCl-WATER/AEROSOL 22

Runs No.	Depth Above Nozzle cms	Feed T °C	t_o sec	Δt sec	Nucleation energy cals	H_T cals	Obs H_T cals	Calc V_T cm/sec	Surf Wt.%	PrNo dim.	Vap time sec.	q_A cal/sec	T_c °C	$\Delta T_{Av.}$ °C
93	94.6	3.0	.053	.05	.0081	2.4	3.994		.00575	6.24	.559	7.15	24.5	10.7
94	94.6	3.0	.046	.05	.0081	2.4	2.949		.00575	6.24	.504	5.85	24.5	10.7
95	94.6	3.0	.046	.05	.0081	2.4	3.495		.00575	6.24	.552	6.33	24.5	10.7
96	94.6	3.0	.018	.05	.0081	1.2	1.434		.00575	6.24	.453	3.17	24.5	10.7
97	94.6	3.0	.050	.05	.0081	1.2	1.638		.00575	6.24	.436	3.76	24.5	10.7
98	94.6	3.0	.020	.05	.0081	1.2	1.576		.00575	6.24	.429	3.67	24.5	10.7
100	94.6	3.0	.029	.05	.0081	.6	.708		.00575	6.24	.262	2.70	24.5	10.7
101	94.6	3.0	.020	,05	.0081	.6	.828		.00575	6.24	.297	2.79	24.5	10.7
102	94.6	3.0	.015	.05	.0081	.6	1.008		.00575	6.24	.566	1.78	24.5	10.7
103	94.6	3.0	.020	.05	.0081	.6	.635		.074	6.24	.308	2.06	24.5	10.7
105	94.6	3.0	.015	.05	.0081	.6	.705		.074	6.24	.307	2.30	24.5	10.7
106	94.6	3.0	.025	.05	.0081	.6	.707		.074	6.24	.296	2.39	24.5	10.7
107	94.6	3.0	.035	.05	.0081	1.2	1.424		.074	6.24	.435	3.27	24.5	10.7
108	94.6	3.0	.030	.05	.0081	1.2	1.469		.074	6.24	.538	2.73	24.5	10.7
109	94.6	3.0	.045	.05	.0081	1.2	1.410		.074	6.24	.515	2.74	24.5	10.7
110	94.6	3.0	.025	.05	.0098	1.2	1.598		.135	6.24	.597	2.68	24.5	10.7
112	94.6	3.0	.057	.05	.0098	1.2	1.497		.135	6.24	.507	2.95	24.5	10.7
113	94.6	3.0	.025	.05	.0098	1.2	1.732		.135	6.24	.503	3.44	24.5	10.7
115	94.6	3.0	.03	.05	.0098	.6	.836		.135	6.24	.369	2.27	24.5	10.7
116	94.6	3.0	.047	.05	.0098	.6	1.096		.135	6.24	.346	3.17	24.5	10.7
117	94.6	3.0	.049	.05	.0098	.6	.611		.135	6.24	.260	2.35	24.5	10.7

SECTION A-3

SAMPLE CALCULATION

(With Run #1 as example)

1. Calculation of fineness ratio A/B

$$\frac{A}{B} = \frac{\bar{A}' \times XF}{\bar{B}' \times XF}$$

for image 6

Where XF is the photographic scale factor and $\bar{A}'$, $\bar{B}'$ are profile dimensions from projected images.

$\bar{A}' = 90.5$ mm.

$\bar{B}' = 37.$ mm.

$XF = .0034 \frac{cm}{image\ mm.}$

$$\frac{A}{B} = \frac{(90.5)\ (.0034)}{(37.)\ (.0034)}$$

$$\frac{A}{B} = 2.45$$

2. Calculation of bubble volume, v

$$v = w\ (A)^3$$

Where the empirical coefficient, $w = 1.23 - .94\ A/B + .28\ (A/B)^2 - .028\ (A/B)^3$

for image 6

$w = .21$

$A = 2.72$

$v = .21\ (2.72)^3 = 4.23$ cc.

3. Calculation of equivalent spherical diameter, d_e

$$d_e = \sqrt[3]{\frac{6v}{\pi}}$$

for image 6 $v = 4.23$ cm.^{3}

$$d_e = \sqrt[3]{\frac{6\ (4.23)}{\pi}} = 1.92 \text{ cm.}$$

4. System pressure on bubble, p

$p = p_{amb} + \rho_{mercury}$ (liquid depth - bubble dist. from nozzle) - partial pressure of water

for image 6

partial pressure of water = 23.2 mm. Hg
p_{amb} = 759.2 mm Hg.
$\rho_{mercury}$ = 13.51 gms./cm^3
tank depth - 99. cm.
bubble dist. from nozzle = 6.38 cm.

$p = 759.2 + 13.51\ (99 - 6.38) - 23.2$
$p = 804.$ mm. Hg

5. Latent heat generated, H

vapor mass, m. $= (v - v_i)\ \rho_g \quad \frac{p}{760} \times \frac{273}{T}$

$H = (\lambda)\ (m)$

for image 6

$v = 4.23$ cm^3
$v_i = .0143$ cm^3
$\rho_g = .0028$ gm/cm^3
$p = 804$ mm.
$T = 297.6°K$
$v = 91.3$ cal/gm

$m = (4.23 - .01)\ .0028\ \frac{804}{760}\ \frac{273}{297.6} = .01$ gms.

Heat content (H) $= (.01)\ (91.3) = .903$ cal.

6. Density difference, $\Delta\rho$

$\Delta\rho = \rho_c - m/v$

applying this to run Number 6

$\rho_c = 1.0$ gm/cm^3
$m = .01$ gms.
$v = 4.23$ cc

$\Delta\rho = 1.0 - .01/4.23 = 1.0$ gm/cm^3

7. Eotvos Number, Eo

$$Eo = \frac{g \Delta\rho \, d_e^2}{\sigma}$$

for image 6

$g = 980.2 \text{ cm/sec}^2$
$\Delta\rho = 1.0 \text{ gm/cm}^3$
$d_e = 1.92 \text{ cm.}$
$\sigma = 72. \text{ dgne-cm.}$

$$Eo = \frac{(980.2)(1.0)(1.92)^2}{72} = 49.6$$

8. Fraction Vaporized, f

$$f = \frac{H}{H_T}$$

Where H_T is the nominal heat content of a fully vaporized drop.

for image 6

$H = .903 \text{ cal.}$
$H_T = 1.2 \text{ cal.}$

$$f = \frac{.903}{1.2} = .75$$

9. Velocity of rise, V

This is defined as the rate of movement of the bubble center of gravity whose position at time, t is W

$$W = Y - s.f. (B/2) - (1-f)(B/2 - s.f. B/2)$$

where Y is the vertical midpoint of the image.

and the empirical s.f. = 0 for Eo < 13
= .38 (Eo-13)/27 for 13 > Eo < 40
= .38 for Eo > 40

for image 6

$Y = 6.38 \text{ cm.}$
$s.f. = .38$
$B = 1.12 \text{ cm}$
$f = .75$

$W = 6.38 - .38 (1.12/2) - (1-.75)(1.12/2 -(.38)(1.12/2)$
$W = 5.30 \text{ cm.}$

using standard numerical differentation with second order differences

$V = 29.6 \text{ cm/sec}$

10. Reynolds numbers, Re_A and Re_d

$$Re_A = \frac{AV\rho}{\mu}; \quad Re_d = \frac{d_e V \rho}{\mu}$$

For image 6

$A = 2.72$ cm.
$d_e = 1.92$ cm.
$V = 2.96$ cm.
$\rho = 1.0$ gm/cm^3
$\mu = .009$ poises

$$Re_A = \frac{(2.72)(29.6)(1.0)}{.009} = 9010$$

$$Re_d = \frac{(1.92)(29.6)(1.0)}{.009} = 6270$$

11. Terminal Velocity, V_t

$$V_t = \sqrt{\frac{4g \Delta\rho d_e}{3 C_D \rho_c C^*}}$$

Where Cd = drag coeff for solid sphere from Perry
C^* = correction factor from Harmathey (37)

For image 6

$$V_t = \sqrt{\frac{4}{3}\frac{(980.2)(1.0)(1.92)}{(.44)(1.0)(6.22)}}$$

$V_t = 30.8$ cm/sec.

$g = 980.2$ cm/sec.
$\Delta\rho = 1.0$ gm/cm^3
$d_e = 1.92$ cm.
$C_D = .44$
$\rho c = 1.0$ gm/cm^3
$C^* = 6.22$

12. Volume of unvaporized liquid, v_l

$$v_l = v_i (1 - f)$$

applying to image 6

$v_i = .0143$ cm^3
$F_v = .75$

$v_l = .0143 (1 - .75)$

$v_l = .0036$ cm^3

13A. Depth of unvaporized liquid puddle, l

Formulas were given in the body of the text (p 77) relating liquid volume and puddle depth for various drop shapes

For Eo > 40

$$v_l = \frac{\pi A^2 l^2}{.48B^2} \qquad (.6B-1)$$

Newton's method of iterative solution was used to find l

for image 6 $A = 2.72$ cm.

$v_l = .0036$ cm^3

$B = 1.12$ cm

$$.0036 = \frac{\pi (2.72)^2 l^2 (.6)(1.12)-1)}{(.48)(1.12)^2}$$

$$l = .0051 \text{ cm.}$$

13B. Interfacial area, S

As above for Eo>40

$$S = \pi A l \left[2 - \frac{2.5\, l}{B} \sqrt{1 + \frac{A^2}{6B^2}}\right]$$

$$S = \pi (2.72)(.0051) \left[2 - \frac{2.5\,(.0051)}{1.12} \sqrt{1 + \frac{(2.72)^2}{.6\,(1.12)^2}}\right]$$

$$S = .71 \text{ cm}^2$$

14. Effective heat transfer coefficient for conductive puddle, h_i

$$h_i = \frac{k}{l}$$

for image 6 $k = 2.75 \times 10^{-4}$ cal/(sec.)(°C)(cm)

$l = .0051$ cm.

$$h_i = \frac{2.75 \times 10^{-4}}{.0051} = 0.055 \text{ cal/(sec)(cm)}^2(°C)$$

15. Time to full vaporization t_v

t_v was evaluated by standard linear curve fitting techniques using data from the approximately linear portions of Figures 4-3, 4-4, and 4-5.

16. Observed size of fully vaporized bubble, H_T

H_T in calories was evaluated by averaging all values of H for each bubble beyond $t = t_v$.

17. Average rate, Q_A

$$q_A = \frac{H_T}{t_v}$$

for Run No. 1 $\quad H_T = 1.59 \pm .30$

$t_v = .432$ sec.

$$q_A = \frac{1.59}{.432}$$

$$q_A = 3.68 \text{ cal/sec}$$

18. Dispersed phase boiling point, T_d

From literature data on p vs T for EtCL.

$T_d = 3052 / (17.3 - \ln p)$

for image 6 $\quad p = 804$ mm. mercury

$T_d = 3052/(17.3 - 2.93)$

$T_d = 296.8°C.$

19. Differential rate of heat transfer q

$$q = \frac{dH}{dt}$$

Using values calculated for H (see calc.No.5) q was evaluated by standard numerical differentitation methods using second order differences.

20. Overall heat transfer coefficient, U

$$U = \frac{q}{S\Delta T}$$

for image 6

$$U = \frac{5.03}{(.71)(10.8)}$$

$$U = .66 \text{ cal/(sec.)(°C)(cm}^2\text{)}$$

$S = .71 \text{ cm}^2$
$\Delta T = 10.8 \text{ °C}$
$q = 5.03 \text{ cal/sec}$

21. Nusselt Number, Nu

$$Nu = \frac{U\, d_e}{k}$$

for image 6

$$Nu = \frac{(.66)(1.92)}{1.45 \times 10^{-3}}$$

$$Nu = 870$$

$U = .66 \text{ cal/(sec.)(°C)(cm}^2\text{)}$
$d_e = 1.92 \text{ cm}$
$k = 1.45 \times 10^{-3}$

22. Rayleigh Number, Ra

$$Ra = g \alpha \Delta T l^4 / k \nu$$

for image 6

$$Ra = (980)(1.61 \times 10^{-3})(10.8)(.0051)^4/(2.74 \times 10^{-4})(.301 \times 10^{-2})$$

$$Ra = 11.4$$

$\alpha = 1.61 \times 10^{-3} \text{ 1/°C}$
$g = 980.2 \text{ cm/sec}^2$
$\Delta T = 10.8 \text{ °C}$
$l = .0051 \text{ cm}$
$k = 2.75 \times 10^{-4} \text{cal/(sec)(°C)(cm)}$
$\nu = .301 \times 10^{-2} \text{(cm)}^2\text{/sec}$

Section A 4 TABLE OF NOMENCLATURE

Symbol	Definition	Units
A	Horizoltal dimension of bubble	cms
A'	Diameter at the top of a truncated cone (model of a spherical cap)	cms
a	Constant in Frossling equation	dimensionless
$\bar{A}$	Horizontal dimension of bubble image	cms
B	Vertical dimension of bubble	cms
Bn	Coefficient in the Vermeulen equation	dimensionless
b	Coefficient of Reynolds and Prandtl number in Frossling equation	dimensionless
$\bar{B}$	Vertical dimension of bubble image	cms
C	Flooding coefficient	dimensionless
C_D	True drag coefficient	dimensionless
C_{Do}	Drag coefficient under steady motion	dimensionless
C_p	Specific heat at constant pressure	cal/(gm)(^oC)
C_s^{-1}	Reciprocal compressibility modulus for interfacial film	dimensionless
D	Molecular diffusivity	
D_v	Diameter of the vessel	cms
d	Diameter of a spherical shape	cms
d_c	Critical equivalent diameter at which drop circulation starts	cms
d_e	Diameter of sphere of same volume	cms
d_i	Equivalent spherical diameter of starting drop	cms

Symbol	Definition	Units
E	Fractional approach to equilibrium in interphase transfer process	dimensionless
E_f	Combined end effect on efficiency $E_{f_1} + E_{f_2} - E_{f_1} \times E_{f_2}$	dimensionless
E_{f_1}	Entry effect where dispersed phase enters	dimensionless
E_{f_2}	Entry effect where dispersed phase leaves	dimensionless
E_o	Eotvos number, $\frac{g \Delta \rho d^2}{\sigma}$	dimensionless
E_t	Total Transfer efficiency	dimensionless
ϵ	Coefficient of surface viscosity	dimensionless
F_D	Drag Force	lbs. Force
f	Fraction vaporized	dimensionless
G	Mass flow rate of vapor phase	gms/sec.
g	The acceleration of gravity	(cms/sec)/sec.
H	Latent heat content of disperse phase vapor	cals.
ΔH_V	Enthalpy of vaporization	Cal./gm.-mole
h_c	Individual outside film coefficient of heat transfer	Cal./(cm^2)(sec)(^oC)
h_d	Individual inside film coefficient of heat transfer	cal/(cm^2)(sec)(^oC)
j	An integer in the Vermeulen equation	dimensionless
k	Thermal conductivity	cal/(cm^2)(sec)^oC/cm
k_{af}	Thermal conductivity of air at the film temperature	cal/(cm^2)(sec)^oC/cm
k_{vf}	Thermal conductivity of vapor at the film temperature	cal/(cm^2)(sec)^oC/cm

Symbol	Definition	Units
L	Distance from vessel bottom	cms
l	Depth of liquid puddle of unvaporized liquid	cms
l'	Height of conical bottom in spherical cap model	cms
M	Molecular Weight	
m	Mass	gms
N_p	Physical property group $\frac{\sigma^3 \rho_c^2}{g \mu_c^4 \Delta\rho}$ from Hu and Kintner (40)	dimensionless
Nu	Nusselt number, $\frac{h\ d}{k}$	
n	Frequency of eddy release in a Karmen street	eddies/sec
P	Rate of energy input required to sustain circ.	dyne-cm/sec
P_c	Critical pressure of boiling liquid	atm
Pe	Peclet Number, (Re)(Pr)	dimensionless
Pe_d	Modified Peclet number for the dispersed phase $(Pr_d)(Re_d)/(1+\mu_d/\mu_c)$	dimensionless
Pr	Prandtl number $\frac{C_p \mu}{k}$	dimensionless
p	Local system pressure	mm. Hg.
pamb	Ambient barometric pressure	mm. Hg.
p_v	Saturated vapor pressure against a flat surface at any given temperature, T	mm. Hg.
q	Overall heat transfer rate at time, t.	cal/sec
Q	Total heat transfered	cal.
q_A	Average heat transfer rate, Q/t	cal/sec

Symbol	Definition	Units
R	Gas constant	cm^3-atm/(gm-mole)(^oK)
Ra	Rayleigh number, $\alpha g \Delta T l^4 \rho / k \mu$	dimensionless
Re_d	Reynolds number based upon equivalent sphere diam. $\frac{d_e V \rho}{\mu}$	
Re_A	Reynolds number based upon projected diameter $\frac{AV\rho}{\mu}$	dimensionless
Re_x	Reynolds number based upon boundary layer length $\frac{xV\rho}{\mu}$	dimensionless
r	Radius to a given point from the sphere center	cms
r_e	Radius of sphere with equivalent volume	cms
ro	Radius of a drop	cms
S	Liquid-Liquid Interfacial Surface Area	cms^2
s	Distance between centers of interacting particles	cms
Sc	Schmidt Number, $\mu/\rho d$	dimensionless
S_p	Spreading coefficient	dyne-cm
St	Stanton number $\mu/C_p V_A$	dimensionless
Str	Strouhal Number nd/V_A	dimensionless
T	Absolute temperature	^oK
T	Temperature driving force	^oC
T_b	Temperature of boiling point	
t	Time from release (i.e. contact time)	sec.
t_f	Drop formation time	sec.
U	Overall Heat transfer coefficient at time, t,	cal/(cm^2)(sec)(^oC)
U'	Empirical average heat transfer coefficient	cal/(cm^2)(sec)(^oC)
u	Local fluid velocity	cms/sec

Symbol	Definition	Units
u_i	Tangential velocity at the interface	cms/sec
u_∞	Free stream velocity at infinite distance	cms/sec
u_r	Tangential velocity at the radius	cms/sec
V	Velocity of rise (measured)	
V_a	Average stream velocity	cms/sec
V_t	Terminal velocity of rise (calculated)	cms/sec
v	Volume of dispersed phase entity	$cms.^3$
v_i	Volume of initial drop	cm^3
v_l	Volume of unvaporized liquid	cm^3
We	Weber Number, $\rho V_A^2 d/\sigma$	dimensionless
w	Volume factor for computing bubble volume from profile measurements	dimensionless
X	Diffusivity multiplier factor (R in ref. 46c)	dimensionless
x	Boundary layer length from point of initiation	cms.
y	Exponent of Reynolds number in Frossling equation	dimensionless
z	Exponent of Prandtl number in Frossling equation	dimensionless

Symbol	Definition	Units
α	Coefficient of cubic expansion	$(\frac{cm^3}{cm^3})/(°C)$
β	Thermal diffusivity $\frac{k}{\rho C_p}$	$cm^2/sec.$
$\gamma_{v/a}$	Interfacial tension vapor in aqueous phase	dyne-cm.
$\gamma_{o/a}$	Interfacial tension organic phase and vapor	dyne-cm.
$\gamma_{o/w}$	Interfacial tension organic phase and aqueous phase	dyne-cm.
$\Delta\gamma_i$	Interfacial pressure	dyne-cm.
λ_v	Latent heat of vaporization	cal/gm
λ	Eigenvalue	
μ_d	Viscosity of dispersed phase fluid	centipoises
μ_c	Viscosity of continuous phase fluid	centipoises
π	Pi = 3.1416	
ρ_{Hg}	Density of mercury	gm/cm^3
ρ_d	Average density of the dispersed phase	gm/cm^3
ρ_c	Density of the continuous phase	gm/cm^3
	$\rho_c - \rho_d$	gm/cm^3
ρ_v	Density of the vapor phase	gm/cm^3
ρ_l	Density of the boiling liquid phase	gm/cm^3
σ_c	Surface tension, continuous phase Vs air	dyne/cm
δ	Thickness of the boundary layer	cms
ν	Kinematic Viscosity	cm^2/sec
∇	del, differential vector operator	dimensionless
θ	polar coordinate of a point	degrees

LITERATURE CITATIONS

1. Adamson, A. W., "Physical Chemistry of Surfaces," 107-113, New York, Interscience, 1960

1A. Andrada, E. N. da C. "Encyclopedia Britannica," Vol. 23, 638, Chicago, Encyclopedia Britannica, Inc., 1945

2. Baird, M. H. I., and Hamielec, A. E., Can. J. of Chem. Eng., 40, 119 (1962)

2A. Baird, M. H. I., and Davidson, J. F., Chem. Eng. Sci., 17, 87 (1962)

3. Beecher, N., S. M. Thesis, Chem. Eng., M.I.T., (1948)

4. Benzing, W. C., S. M. Thesis, Chem. Eng., M.I.T. (1948)

5. Berinstein, M. L., and Khetani, B. N., S. B. Thesis, Chem. Eng., M.I.T. (1960)

6. Bond, W. M., and Newton, D. A., Phil. Mag., 5, 794 (1928)

6A. Boussinesq, J., Ann. de Chimie et de Phys., 29, 364 (1913)

7. Bowman, C. W., Johnson, A. I., Can. J. Chem. Eng., 40, 139 (1962)

8. Brown, G. G., and Assoc., "Unit Operations," 72-84, New York, Wiley, 1950

9. Calderbank, P. H., and Korchinski, I.J.O., Chem.Eng. Sci., 6, 65 (1956)

10. Calderbank, P. H., and Moo-Young, M.B., Chem. Eng. Sci., 16, 39 (1961)

11. Cary, J. R., Trans. Amer. Soc. Mech. Eng., 75, 483 (1953) cited in ref. 25.

12. Conkie, W. R. and Savic, P., Mech. Eng. Report #23, National Res. Coun. Can. (Oct., 1953)

13. Coppock, P. D., and Meiklejohn, G. T., Trans. Inst. Chem. Engrs., 29, 75 (1959)

14. Coulson, J. W., and Richardson, J. F., "Chemical Engineering," Vol. II, 486-489, New York, McGraw-Hill, 1955

15. Davies, J. T., and Rideal, E. K., "Interfacial Phenomenon," 314-325, New York, Academic Press, 1961

16. Davies, R. M., and Taylor, G. I., Proc. of Royal Society, A-200, 375. (1950)

16A. Denbigh, K. G., J. Soc. Chem. Ind. (London), 65, 61 (1946) as cited in ref. 60A.

16B. Drew, T. B., and Ryan, W. P., Ind. Eng. Chem., 23, 945 (1931); Trans. Am. Inst. Chem. Engrs., 26, 118, (1931) as cited in Ref. 55.

17. Elzinga, E. R., and Banchero, J. T., Chem. Eng. Prog. Symp., Ser. No. 29, 55, 149 (1959)

18. Elzinga, E. R., and Banchero, J. T., A.I.Ch.E. Journal, 7, 394 (1961)

19. Farmer, W. S., Report ORNL 1950, 635, Oak Ridge National Laboratories as cited in ref. 23.

20. Foust, A. S., et. al, "Principles of Unit Operations," 159-165, New York, Wiley, 1960

21. Frankel, J., "Kinetic Theory of Liquids," 366-381, New York, Dover, 1955

22. Fuginawa, K., Nakaike, Y., and Kurihara, T., Kagaku Kogaku, 22, 920 (1958)

23. Garner, F. H., and Hale, A. R., Chem. Eng. Sci., 2, 157 (1953)

24. Garner, F. H., and Hammerton, D., Chem. Eng. Sci., 3, 1 (1954)

25. Garner, F. H., Jenson, V. G., and Keey, R. B., Trans. Inst. of Chem. Engs., 37, 191 (1959)

26. Garwin, L., and Smith, B. D., Chem. Eng. Prog., 49, 591 (1953)

27. General Radio Co., "Catalogue P," Cambridge, Mass., 1959

28. Gordan, K. F., and Sherwood, T. K., paper presented at A.I.Ch.E. Meeting, Toronto, 1953, 29, as cited in ref. 23.

29. Gordon, K. F., Singh, T., and Weisman, E. Y., Int. J. Heat Mass Trans., 3, 90 (1961)

30. Gorring, R. L., and Katz, D. L., A. I. Ch.E. Journal, 8, 123 (1962)

31. Griffith, R., ScD. Thesis, Chem. Eng., Univ. of Wisconsin (1958) as cited in ref. 38.

32. Grover, S. S., and Knudsen, J. G., "Heat Transfer - St. Louis" A.I.Ch.E. Symp. No. 17, 71 (1956)

32A. Gunn, R., J. Geophysic. Research, 54, 383 (1949) as cited in ref. 18.

33. Haberman, W. L., and Morton, R. K., Taylor Model Basin, Report 802 U. S. Navy Dept. (1953)

34. Hadamard, J., Comptes Rendus, 152, 1735 (1911) as cited in ref. 33.

35. Hamielec, A. E., and Johnson, A. I., Can. J. of Chem. Eng., 40, 41 (1962)

36. Handlos, A. E., and Baron, T., A.I.Ch.E. Journal, 3, 127 (1957)

36A. Happel, J., and Pfeffer, R., A.I.Ch.E. Journal, 6, 129 (1960)

37. Harmathy, T. F., A.I.Ch.E. Journal, 6, 281 (1960)

38. Harriott, Peter, Can. J. of Chem. Eng., 40, 60 (1962)

39. Hayworth, C. B., and Treybal, R. E., Ind. Eng. Chem. 42, 1174 (1950)

39A. Heideger, W. J., and Bondart, M., Chem.Eng. Sci., 17, 1 (1962)

40. Hu, S., and Kintner, R. C., A.I.Ch.E. Journal, 1, 42 (1955)

41. Hughes, R. R., and Gilliland, E. R., Chem. Eng. Prog., 48, 497 (1952)

42. Hunsacker, J. C., and Rightmire, B. G., "Engineering Applications of Fluid Mechanics," 182-204, New York, McGraw Hill, 1947

43. Ingebo, R. D., National Advisory Council Aerouant, Tech. Note 2368 (July, 1951) as cited in ref. 18.

44. Jakob, Max, "Heat Transfer," 614-652, New York, Wiley, 1949

45. Johnson, A. I., and Braida, L., Can. J. Chem. Eng., 35, 165 (1957)

46. Johnson, A. I., and Hamielec, A. E., A.I.Ch.E. Journal, 6, 145 (1960)

47. Johnson, A. I., Minard, G. W., et.al., A.I.Ch.E. Journal, 3, 101 (1957)

48. Katz, G., and Schroeder, G., S. B. Thesis, Chem. Eng., M.I.T. (1959)

49. Kavesh, S., S. B. Thesis, Chem. Eng., M.I.T. (1957)

50. Kintner, R. C., Horton, T. J., Grammann, R. E., and Amberkar, S., Can. J. Chem. Eng., 39, 235 (1961)

51. Kramers, H., Physica, 12, 61 (1946) as cited in ref. 25.

52. Kronig, R., and Brink, J. C., Appl. Sci. Res., A2, 142 (1951)

52A. Ladenberg, R., Ann. Phys., 23, 447 (1927) as cited on 489 of ref. 14.

53. Lautman, L., and Droege, W. C., Air Material Command, AIRL, A6118, 50-15-3 (8/50) as cited in ref. 55.

53A. Licht, W., and Narasimhamurty, G.S.R., A.I.Ch.E. Journal, 1, 366 (1955) as cited in ref. 37.

53B. Lohrisch, W., for Schangsarb. a. d. Geb. d. Ingenieurwes, 322, 46 (1929) as cited p. 607, ref. 44.

53C. Lewis, J. B., Chem. Eng. Sci., 3, 248, 260 (1954) as cited in ref. 66A.

53D. ibid. 8, 295 (1958) as cited in ref. 66A.

54. Lyakhovsky, D. N., J. Tech. Phys., Moscow, 10, 999 (1940) as cited in ref. 25.

55. McAdams, "Heat Transmission," New York, McGraw Hill, 1950

56. McDowell, R. V., and Myers, J. E., A.I.Ch.E. Journal, 2, 384 (1956)

57. Moore, G. R., A.I.Ch.E. Journal, 5, 458 (1959)

58. Pierce, R. D., Dwyer, O. E., and Martin, J. J., A.I.Ch.E.-Journal, 5, 257 (1959)

58A. Prandtl, L. Über Flüssigkeitsbewegung bei sehr kleiner Reibung. Proceedings 3rd. Intern. Congr. Heidelberg, 1904. Reprinted in "Vier Abhandlungen zur Hydrodynamik and Aerodynamik." Göttingen 1927; NACA TM 452 (1928) as cited in ref. 67.

58B. Pearcey, T., and Hill, G. W., Australian J. Phys., 9, 19, (1956) as cited in ref. 18.

59. Rayleigh, Lord, Phil. Mag., 32, 529 (1916)

60. Ranz and Marshall Chem. Eng. Prog., 48, 141, 173 (1952)

60A. Reid, R. C., and Sherwood, T. K., "The Properties of Gases and Liquids," 261, New York, McGraw Hill, 1958

61. Robinson, C. S., and Gilliland, E. R., "Elements of Fractional Distillation," 393, New York, McGraw Hill, 1954

62. Rosenberg, B., Taylor Model Basin, Report 727, U. S. Navy Department (1950)

62A. Ruckenstein, E., Chem. Eng. Sci., 10, 22 (1959) as cited in ref. 38.

62B. Rybczynski, W., Bull. Acad. de Sci. de Cracovie, A, 40 (1911) as cited in ref. 33.

63. Savic, P., Report MT-22, National Research Council of Canada (July 1953)

64. Shlichting, H., "Boundary Layer Theory," 4th Ed., 24-41, McGraw Hill, New York, 1960

65. Spangenberg, W. G., and Rowland, W. R., Physics of Fluids, 4, 743 (1961)

66. Spells, K. E., Proc. Phys. Soc., 64B, 541 (1952)

66A. Sternling, C. V., and Scriven, L. E., A.I.Ch. E. Journal, 5, 514 (1959)

66B. Steinberger, R. L., and Treybal, R. E., A.I.Ch.E. Journal, 6, 227 (1960) as cited in ref. 38.

67. Strenge, P. H., and Orell, A., and Westwater, J. W., A.I.Ch.E. Journal, 7, 578 (1961)

68. Tang, Y. S., Duncan, J. M., and Schweyer, H. E., Tech. Notes in Adv. Comm. Aero., Washington 1953, No. 2867 as cited in ref. 25.

69. Thorsen, G., and Terjesen, S. G., Chem. Eng. Sci., 17, 137 (1962)

69A. Torobin, L. B., and Gauvin, W. H., A.I. Ch.E. Journal 7, 615 (1961)

70. Vermeulen, T., Ind. Eng. Chem., 45, 1664 (1953)

71. Vyroubov, D. J., Tech. Phys. Leningr, 9, 1923 (1939) as cited in ref. 25.

72. Warshay, W., Bogus, E., Johnson, M., and Kintner, R. C., Can. J. Chem. Eng., 37, 29 (1959)

73. Weaver, Robert, Sc.D. Thesis, Chem. Eng., Princeton University (1958)

73A. Wei, J. C., Thesis, Chem. Eng., M.I.T. (1955) as cited in ref. 66A.

74. Zuber, N., Tribus, M., and Westwater, J. M., ASME, Pt. 2, Colorado (1961) p. 230

27A. Gilliland, E. R., Personal Communication, March 22, 1963

THE ORIGINAL DATA IS LOCATED AT THE DEPARTMENT OF CHEMICAL ENGINEERING AT THE MASSACHUSETTS INSTITUTE OF TECHNOLOGY

BIOGRAPHY

Early in the 1880's my grandfather changed the course of family history by throwing over the traditional medical career to join a chemical firm. In his turn my father, Kenneth Klipstein, continued the trend so that by the time I was born in 1930 there was a well-worn path to follow.

After the usual preliminaries I began to find my own interest in chemistry at Lawrenceville School and subsequently chose a chemical engineering major at Princeton. After graduation I began work for Lederle Laboratories Division of American Cyanamid Company, first as a production engineer and later as a research engineer working on design and process development for a semi-works fermentation mash refining plant. Here I became increasingly aware that my undergraduate training was insufficient to the technical problems which I was encountering and so entered M.I.T. in the fall of 1954 for graduate work.

After a year at Cambridge I took a summer job in process development with Johns-Manville before going to Oak Ridge, Tennessee, for a fall term in the Engineering Practice School. Also, during that summer I was married to Jane Gade Koven on June 10, 1955.

The term at Oak Ridge was a most valuable one. Under the encouragement of Director R. C. Reid I improved my engineering facility, began working on my first professional publication and resolved to start working toward a doctorate. The final fruition of these events was the publication of "Two Phase Flow Through Large Diameter Pipes"* in the A.I.Ch.E. Journal and my successful passage through the doctorate qualifying exams in 1957. Ten days after the exams my first child, Constance, was born and not to be outdone I had my appendix removed.

After appropriate recuperation and deliberation I chose the subject of the present thesis with Professor E. R. Gilliland as advisor and began work in March 1957. This continued until July of 1958 when I temporarily put aside the thesis to establish a new practice school station at the American Cyanamid Organic Chemicals Division Plant in Bound Brook, New Jersey. A full summer was spent preparing facilities and developing problems for the first student group which arrived as scheduled on September 1958. Also as scheduled, twelve hours later my wife gave birth to our second child, Kenneth Hampton Klipstein II.

* Reid, R. C., Klipstein, D. H., et. al., A. I. Ch. E. Journal, 3, 321 (1957).

The two years spent as a Practice School Director were invaluable. Our groups worked in every department from basic research to sales utilizing broadly all available service functions even including outside consultants. This was further enriched for me by the administrative and managerial responsibilities of directorship. This is certainly the best training M.I.T. has to offer.

Unfortunately, little progress was made on the thesis during this period although it became apparent that the direction of my earlier work was not a fruitful one. Thus in June 1960, a fresh start was made using equipment and facilities in the Practice School Station. This effort was pursued steadily until the thesis was submitted last June with only minor interruptions while our third and fourth children, Pamela and David, were born and while I took the first steps toward a career in New Products Marketing with Union Carbide Chemicals Company. With the thesis at last complete I am now pursuing this career with undivided enthusiasm and living with my wife and children in Far Hills, New Jersey.